NGT-21-002-080
NGT-80001

UCLA

NASA/USRA ADVANCED AERONAUTIC

DESIGN PROJECT

HYPERSONIC DRONE DESIGN:

A MULTIDISCIPLINARY EXPERIENCE

SCHOOL OF ENGINEERING AND APPLIED SCIENCE

JUNE 1988

UCLA

NASA/USRA ADVANCED AERONAUTIC DESIGN LABORATORY REPORT

Submitted To

University Space Research Association

June 1988

SCHOOL OF ENGINEERING AND APPLIED SCIENCE

HYPERSONIC DRONE VEHICLE DESIGN: A MULTIDISCIPLINARY EXPERIENCE

UCLA'S Advanced Aeronautic Design group focussed their efforts on design problems of an unmanned hypersonic vehicle. It is felt that a scaled hypersonic drone is necessary to bridge the gap between present theory on hypersonics and the future reality of the National Aerospace Plane (NASP) for two reasons: (1) to fulfill a need for experimental data in the hypersonic regime, and (2) to provide a testbed for the scramjet engine which is to be the primary mode of propulsion for the NASP.

The group concentrated on three areas of great concern to NASP design: **propulsion, thermal management,** and **flight systems**. Problem solving in these areas was directed towards design of the drone with the idea that the same design techniques could be applied to the NASP.

A seventy degree swept double delta wing configuration, developed in the 70's at NASA Langley, was chosen as the aerodynamic and geometric model for the drone. This vehicle would be air-launched from a B-1 at Mach 0.8 and 48,000 feet, rocket boosted by two internal engines to Mach 10 and 100,000 feet, and allowed to cruise under power of the scramjet engine until burnout. It would then return to base for an unpowered landing. Preliminary energy calculations based upon the flight requirements give the drone a gross launch weight of 134,000 lb. and an overall length of 85 feet.

PROPULSION GROUP

Group Members:
John Beltran
Susan Durlak
Lura Kern
Mark Lin
Peter Waschak
Jerry Yen

Faculty Advisor:
Professor R.E. Kelly

Table of Contents

1. Introduction

1. Introduction

The efforts of the Advanced Aeronautics Propulsion Design group have been directed towards developing tools to analyze the effects of aircraft geometry and freestream conditions on scramjet performance. Specifically, the group has been concerned with the shock structure, boundary layer growth and inlet geometry of a Mach 10 drone research vehicle, and the impact of these parameters on the efficiency and thrust of the scramjets.

The tools used to analyze the flowfield have primarily consisted of pre-existing computer software. Six programs (STUB, INLET, CPIPE, SEAGULL, SCRAM, and EDDYBL) were used to evaluate different components of the drone's underbody and scramjet engines. SCRAM is a one-dimensional program for the estimation of scramjet performance of a hypersonic vehicle. SCRAM begins with the geometry of the vehicle and calculates gross estimates of thrust, efficiency, and other engine parameters. It is used by our group as a check for the more detailed analysis. SEAGULL calculates inviscid conical shock structures and freestream conditions for axisymmetric geometries. SEAGULL is used to calculate the shock structures over the drone forebody. EDDYBL is a two-dimensional/axisymmetric, compressible, turbulent boundary layer program, and is used in conjunction with SEAGULL to simulate the viscous flow conditions along the forebody. Using the freestream conditions from SEAGULL, EDDYBL is used to calculate the boundary layer growth along the vehicle. INLET uses an inviscid analysis to design hypersonic engine inlets. For given inlet conditions and desired combustor entrance conditions, INLET calculates the cowl geometry required. Data from SEAGULL and EDDYBL will be used to generate inlet conditions for use with INLET.

2. Hypersonic Cruise Vehicle(HCV) Configuration

Finally, CPIPE is a one-dimensional code for the analysis of scramjet combustor performance. CPIPE will use the output conditions from INLET to calculate the combustor efficiencies. An overall momentum balance on the engine should give the actual thrust of the scramjet engine configuration. The use of these codes allows a detailed analysis of scramjet engine performance from nose to tail of the vehicle.

An initial application of these codes was performed on a five-degree half-angle cone with two five-degree compression ramps leading into the inlet. Boundary layer and flow properties were determined for the forebody, and an inlet configuration was generated.

Analysis of this initial design revealed that greater forebody compression was required to produce an acceptable inlet design. Therefore, the design was altered by placing one additional five and two additional three-degree ramps between the nose of the vehicle and the two five-degree ramps leading into the inlet. The location of the three-degree ramps were varied to maximize static pressure gains. The final design provided sufficient thrust to maintain level flight at design condition.

2. Hypersonic Cruise Vehicle (HCV) Configuration

It was determined early in Winter Quarter 1988 that the Advanced Aeronautics Design Group (AAD) needed a unifying concept for the design of the hypersonic drone. This was accomplished by choosing a configuration that had been researched extensively at NASA Langley Research Center in the late 1970's. The advantage of a single tested configuration for the entire class is clear: each group would base their designs on the same vehicle, with the same restrictions applying to all three groups, thereby forcing greater interaction among the groups.

The configuration chosen by the AAD students was a 70 degree swept delta wing design conceived by NASA Langley engineers. It was a hypersonic research airplane concept, and has been dubbed the Hypersonic Cruise Vehicle (HCV) by the AAD students. Figure 1 shows the HCV as it was originally conceived. The HCV was designed to be air-launched from a B-52 at Mach 0.8 and rocket-accelerated up to a cruise speed of Mach 7 by four liquid hydrogen rocket motors mounted in the base. At this point, the scramjets would be ignited and the vehicle would cruise until burn-out, at which point it would return to base for an unpowered landing. A detailed description of the HCV's configuration is given in Figure 2. In developing the HCV design, a wind tunnel model was built, and performance characteristics of the model were collected and tabulated in Reference 1. The geometric characteristics of the model are tabulated in Table 1. The scaling for the model was 0.021 of the size conceived for the actual HCV.

The first step in adapting the HCV for the purpose of a hypersonic drone was to size it according to the needs of the class. This included calculating the amount of fuel required to go from the air-launch speed to cruise speed. From that, size and weight necessary for the fuel requirements were determined . In order to do this, it became necessary to determine a means of air-launch. The B-52 has size and weight constraints consisting of a 24-ft. wing span limit, a 9-foot fuselage

height limit, and a gross weight restriction of 70,000 pounds. This limits the size of the drone considerably and, in order to reach Mach 10, it was found that the weight limit was exceeded. Alternatives were then examined. The 747 and B-1 aircraft were determined to be viable options for the air-launch.

Therefore, the HCV is a basis upon which each group can build their design. It gives the Flight Systems group the geometry and spacing of the vehicle so that they can determine which sensors and how many are required in certain places. This would result in a more detailed and more exact design. The Thermal Management group can determine critical areas on the HCV that would require cooling. They can change the design within certain reasonable limits to satisfy their cooling system design. A definite configuration for the the drone gives the Propulsion group a starting point on the design of the underbelly for the vehicle; that is, a first iteration could be performed from which they refined their design to achieve an optimum configuration.

3. Program Applications

The group explored pre-existing computer programs, as well as devising others as needed, as a method of analyzing the merits of various designs because of the time savings afforded and the ability to calculate complex flowfields that are inherent to hypersonic design. Figure 3 shows the areas of application of each of the codes in analyzing the drone. A brief description of each program follows, while a more detailed description fo the workings of each code may be found in Appendix A.

SCRAM

The program SCRAM is a one-dimensional airframe-integrated scramjet simulation program. It is currently being used by NASA on the National Aerospace Plane (NASP) project as a first iteration on scramjet performance calculations. It is available to the AAD (Advanced Aeronautics Design) students on IBM PC computers and has already been run successfully using the HCV geometry as inputs (see Appendix A1 for a description of the program and a sample case).

The inputs to SCRAM include freestream conditions, scramjet geometry, and other parameters necessary for calculating the flowfield properties such as kinetic energy efficiency, which approximates momentum losses due to shocks, and temperatures along the surfaces. SCRAM calculates the flowfield characteristics for five stages of the scramjet: freestream, forebody, inlet, combustor, and nozzle. It outputs the flow conditions at the end of each stage, as well as boundary layer thicknesses. It then calculates the engine cycle performance parameters and outputs them in an overall summary.

SCRAM was used in two ways for the Hypersonic Drone concept. First, it was used to help determine the sizing of the engine. By developing a scaled drone instead of a full-sized, piloted hypersonic vehicle, there

was a concern that the scramjet engine will not be large enough to produce sufficient thrust. SCRAM can be run at the smallest size limit of the drone to determine feasibility of the design. Since SCRAM generates values that are optimistic for the engine performance, it offers a means of evaluating relative worth of designs. That is, if SCRAM's output shows that a design is not feasible, then the design will be certain not to work, and further study into that configuration would probably not be worthwhile.

STUB

The flow behind the detached bow shock structure generated by a hypersonic blunt body contains regions of both subsonic and supersonic flow. Since SEAGULL is restricted to the case of flow that is purely supersonic after a shock, there arises a need for an analysis of the shock structure and flow properties at the nose of the hypersonic drone studied by the Advanced Aeronautics Design class. The shock structure and flow properties then become inputs for the SEAGULL and EDDYBL programs.

STUB is a written program that utilizes the time-dependent technique to generate the detached bow shock structure off a hypersonic blunt body. Details of the method used by the program can be found in References 2, 3, and 4, and the governing equations in Appendix A2. The program is also listed in Appendix A2.

Briefly, the time-dependent technique employs a numerical calculation of flow properties through time steps, using the unsteady Navier-Stokes equations as the governing equations. Although the introduction of time appears to be an added complication for a steady-state flow, it becomes a necessary simplification to the problem of hypersonic blunt bodies. There currently exists no uniformly valid, steady state technique that can handle the mixed supersonic and subsonic

region behind the bow shock (Ref. 2).

Although STUB was written to analyze two-dimensional blunt bodies, an extension to axisymmetric or three-dimensional asymmetric blunt bodies could be made in the same manner as References 4 and 5. The two-dimensional nature of this analysis, however, does mean that relieving effects and other three-dimensional, axisymmetric effects for a spherically-tipped nose (as should be modelled for the hypersonic drone) are neglected. This then became a severe limitation of the program.

SEAGULL

SEAGULL is a code designed for the analysis of a two-dimensional or axisymmetric supersonic inviscid flow of an ideal gas. For the purposes of the Advanced Aeronautics Propulsion Design Group, SEAGULL was used to model the external compression along the forebody of a scramjet engine. SEAGULL provides only an inviscid solution for the forebody flowfield and shock structure, and thus the boundary layer code EDDYBL was used with SEAGULL to iteratively solve for a viscous flowfield solution.

The resulting flowfield properties calculated using SEAGULL (and EDDYBL) were used as inputs for the program INLET. One limitation of SEAGULL is that it models both an upper and lower wall; thus, the flow properties that SEAGULL outputs are for internal compression. This causes the flow on the body downstream of the shock to slow, whereas for purely external flow, it would remain constant. The slowing effect is minimized, however, by placing the walls far apart.

EDDYBL

EDDYBL is a fully compressible, two-dimensional or axisymmetric computer program for the calculation of boundary layer properties. The program accounts for mass flux at the body surface, heat flux, pressure and temperature gradients, and both transverse and longitudinal body curvature. The program does not, however, account for the effects of shock-boundary layer interaction or separated flow. EDDYBL is currently a fully operational program and has been run for supersonic cases. For a more complete description of the program EDDYBL and sample output parameters, see Appendix A4.

For the purposes of the Advanced Aeronautics Propulsion Design group, EDDYBL was used in conjunction with the program SEAGULL, which performed an inviscid analysis on the forebody of the scramjet. Provided with upstream conditions and geometry from SEAGULL, EDDYBL output the boundary layer characteristics of the flow field. The boundary layer thickness was used to redefine the geometry, thus creating a new inviscid input geometry for SEAGULL. This will alter the shock structure calculated for the forebody, and thus will alter the upstream conditions used for EDDYBL. This iterative procedure was used until the flowfield properties converged on a viscous solution.

EDDYBL was helpful in determining the overall performance of a given scramjet configuration by calculating the boundary layer growth at the inlet entrance (or cowl lip), and thus determining the effective mass flow entering the engine (Fig. 4). Overall, using EDDYBL in conjunction with the inviscid codes SEAGULL and INLET will provide a more realistic evaluation of the performance of a given scramjet configuration.

INLET

INLET was the code used in designing the internal cowl and centerbody geometries of the scramjet. It is a two dimensional inviscid code that uses the method of characteristics to determine the internal geometry of the inlet (see Appendix A5 for a description of the program and sample inputs and outputs). Given the conditions at the entrance to the inlet and the desired combustor entrance conditions, INLET calculates the cowl and centerbody geometries required to minimize total pressure loss across the inlet. Although the distinction between the forebody and inlet can be nebulous, the propulsion group decided to use SEAGULL mainly for external compression and INLET for internal compression. Thus, the main benefit of using INLET is that it determines the cowl and centerbody geometries for the scramjet engine. However, it was necessary to meet the desired combustor entrance requirements, as well as the upstream entrance conditions (acquired from SEAGULL). Therefore, it was necessary to iteratively use INLET and CPIPE (combustor code) to determine whether INLET could provide reasonable cowl and centerbody geometries for the combustor requirements.

CPIPE

CPIPE is a one dimensional real gas analysis of the combustion of hydrogen in air in a supersonic channel. Given the initial upstream conditions and geometry definition, CPIPE outputs the downstream one dimensional flow properties (see Appendix A6 for a description of the program and required inputs).

CPIPE was used to model the combustor region of the scramjet engine. CPIPE is a relatively simple analysis of the combustor since it uses only one dimensional conservation equations to calculate the

downstream conditions. However, more complicated analyses of the supersonic combustor are rare and tend to concentrate on the flow structure in specific areas of the combustor (i.e. directly behind a flameholding structure or fuel injection area). In addition, CPIPE has several useful features such as (1) possibilities for several fuel injection points at a variety of angles, (2) estimates of ignition and flameholding likelihood, and (3) estimates of heat flux, given temperature distribution. Thus, CPIPE served the purpose of scramjet performance analysis without being unnecessarily complex.

Since CPIPE is one dimensional it was necessary to average the flowfield values obtained from INLET in order to input the appropriate values in CPIPE.

References 10, 11, and 12, which contain temperature and pressure distributions for various combustor designs that were tested in Langley's supersonic combustor test facility, could be used to validate CPIPE. This valdation was not completed due to time constraints; however, CPIPE has been used satisfactorily at NASA Langley to simulate scramjet combustor designs.

4. Preliminary Design

SCRAM was used as a first iteration on the scramjet design for the drone. It was primarily used to determine whether an engine small enough to fit onto the HCV would produce enough thrust to overcome the total aircraft drag. One of the primary weaknesses of SCRAM, however, is it's dependance on wise choices of abstract efficiency parameters. Such parameters define the overall kinetic energy efficiency of the design, the pressure loss coefficients across the various shocks and through the combustors, and have a large impact upon the overall thrust delivered.

When SCRAM was run with the HCV's geometry and flight condition as input, it was found that the scramjet could supply the required thrust. With a nozzle efficiency of 1.0, SCRAM predicted a total thrust force of 43,000 pounds. This value was as low as 30,000 pounds with a nozzle efficiency of 0.96. Using information given from wind tunnel tests on the HCV configuration, [13], the total drag at Mach 10 and 100,000 feet was found to be 26,600 pounds, for an excess thrust of 3,400 pounds with 96% nozzle efficiency.

The vehicle nose was modelled as a two-dimensional, five degree ramp, with a rounded, one-inch radius nosetip. Initial guesses for the shock structure and flow properties were inputted into STUB, and final converged values were computed. These values for the shock structure and flow properties were made available too late for use, but would have served as inputs for SEAGULL and EDDYBL. As it was, the vehicle was modeled as having a sharp nose, compared to the one-inch radius nose of the actual vehicle. The next step, then, would have been to proceed through one iteration using STUB outputs.

The group began to analyze the merits of various forebody geometries. For the following forebody geometries presented, two opposing constraints were considered. Static compression of the flow by the forebody had to be attained with maximum efficiency and minimal total pressure loss. At the

same time, the flow had to be slowed sufficiently prior to the inlet so that the cowl would be made as short as possible.

The first geometry analyzed was a simple five degree cone and also acted as verification for SEAGULL. (Appendix A3). The cone did not compress or slow the flow sufficiently and required a cowl length of 150 feet to compress the flow from Mach 9 ahead of the inlet ramps to the maximum combustor speed of Mach 4.

The second geometry consisted of two ramps in addition to the basic five degree cone. (Fig. 5). The first ramp is five degrees and is located fifteen feet from the nose. A second, three degree ramp is located twenty-four feet from the nose for a total turning angle of thirteen degrees. This design resulted in a total pressure loss of 22%, and a static pressure increase of 8.97 before the inlet ramps. The Mach at the entrance to the inlet was 7.51. (Table 2).

The third geometry moved the ramps of the second design three feet further from the nose (Fig 6). This resulted in a decrease of total pressure loss at the inlet and an increase in static pressure. (Table 2). These changes improved the performance of the forebody as a compression surface. The last geometry added another three degree ramp thirty-one feet from the nose. This resulted in a total pressure loss of 23%, but a static pressure increase of 14.6. (Table 1). This geometry was the one chosen for the final design. (Fig 7).

Boundary layer properties were computed for a variety of geometries in the early stages of the design. The simplest case run was for the five degree cone which was modeled as having a sharp nose, unlike the rounded nose of the drone. This approximation introduces error in the downstream flowfield, but was necessary because of a lack of freestream data in that region. The surface rougness of the vehicle was set to .001 in., the default value of EDDYBL, which is a very smooth surface. Lacking any data for high

altitude atmospheric turbulence, the freesteam turbulence intensity was set to 2 %, which is what could be expected from a well designed wind tunnel [14].

The results of the computations are presented in Figures 8 and 9. Note first the "blips" that occur for the boundary layer thickness. These are points where the program converged on an incorrect thickness, but with the next step corrected itself and converged on the correct value. Communication with the author of EDDYBL indicates that these points are stations that have difficulty converging due to the grid representation of the flowfield which result in numerical errors. The automatic addition of grid points by the program can cause EDDYBL not to converge for that station, but generally converges to the correct solution with the next step.

Note also the trend of the lower left corners of the curves to have a slight lip. This is also caused by convergence errors of the program. EDDYBL calculates the stagnation properties from input free stream conditions and uses these initial starting conditions to predict the boundary layer properties at the next step. If that prediction is incorrect and the program does not converge after twenty iterations, the program will proceed to the next station. To say that the program does not converge does not mean that the calculations diverged, merely that the solution did not converge fast enough. After several stations, however, the program begins to make to make correct predictions and the solution converges. Extrapolation of the curves, shown by dotted lines in Figures 8 and 9 shows that the computed boundary layer values are close to zero at the stagnation point, as they should be.

The shape of the curves in Figure 9 suggests that transition does not occur and that the flow is entirely laminar. Literature shows that transition on 10 degree cones occurs at an arc-length Reynolds number of approximately ten million, while EDDYBL shows that transition has not yet

occured at Reynolds numbers of 48 million.[15, pp 39, 59,61]. The data presented in the literature, however, is for cones with roughness heights of .015 in., and unknown freestream turbulence intensity, both of which have an impact on transition to turbulence and are different than those used for this case.

Figure 10 shows the heat flux at the surface of the vehicle as a function of axial distance, with the surface maintained at 1000 degrees Rankine. (A misunderstanding occured between the thermal management and propulsion groups as to the temperatuure that the wall would be maintained at. The thermal management group specified 1000 degrees *Kelvin*, which is higher than the 1000 degrees Rankine used here. The heat flux could thus be expected to be somewhat lower than that indicated.) The portion of the curve to the left of point A of Figure 10 is incorrect, suffering from the same convergence problems near the stagnation point as the boundary layer properties of Figures 8 and 9. The heating rates shown have been determined to be acceptable by the thermal management group. Active cooling would be required to maintain the skin temperature but would be within the capabilities of the cooling system.

Figures 11 through 14 show the effect of boundary layer suction at the wall. The mass removal began 31 feet from the nose at a rate of .0005 slugs/ft^2*s. (Figure 13). Figures 11 and 12 show the effects of the mass removal on boundary layer thickness. The impact is seen to be primarily on displacement, and is caused because the fluid that is being removed is the slowest and has the largest impact on displacement thickness. (Recall that displacement thickness is a measure of the mass flow rate along the body that is lost due to the slowing of the flow in the boundary layer.)

The mass removal has a profound effect on heat flux. Figure 14 shows that, although the suction has a small effect on boundary layer thickness, the heating rate at the wall was increased to a value comparable to the heating rates experienced in the first few feet of the forebody. Increased

boundary layer suction might therefore lead to unacceptably high heating rates, which would put an upper limit on the amount of boundary layer control that could be obtained through suction.

Finally, several hand-calculations were performed to estimate the total mass removed. (Appendix B). The results indicate that, for the five degree cone, the mass removal rate per unit width over the last five feet of the forebody directly before the inlet ramps would be .00425 slugs/sec*ft. Assuming a depth of 7 feet, (the width of the forebody at the inlet ramps), the total mass flow rate would be .0298 slugs/sec. The average velocity of the removed mass would be 57.2 ft/sec, thus removing 400 ft^3/sec over the 35 square foot area, which would be a large volume of air to dispose of.

Another calculation was made to determine the removal rate that would be required to remove the same amount of boundary layer as displacement thickness over 7 square feet of the forebody. The required mass flow rate would be .208 slugs/sec, with an average velocity of 400 ft/sec, and a total volume of 2795 ft^3/sec. Such a high mass removal rate would be unacceptably large.

At the outset of the Spring quarter, it was still the intention of the Propulsion group to use INLET as an axisymmetric code when designing and analyzing the scramjet inlet geometry. However, an error in the code prevented the group from utilizing INLET's axisymmetric feature. This turned out to benefit the group since the actual nature of each scramjet module is more closely represented by a two-dimensional geometry because of its location far aft of the nose (see Figure 2) . Once the attention of the group was turned to a two-dimensional analysis of the scramjet modules, a test case was run using an inlet Mach number of 2.5, two ramps of five degrees each, and an exit Mach number of 1.3. The ouput of this result was the same as that calculated using the shock relations

5. Final Design

from Reference [2]. With the program running correctly, the first inlet geometry case was run.

The first inlet geometry case was actually a dual case. Since problems were experienced running other computer codes, it was thought that the flow could only be slowed to Mach 9.3 at the starting point where INLET calculations would begin. Hence, INLET was run for two cases: a Mach 9.3 to Mach 3 case and a Mach 9.3 to Mach 4 case. The results of these cases are shown in Figures 15 to 22. The output generated was not favorable. Inlet plane area to exit plane area ratios were 0.075 for the Mach 9.3 to Mach 3 case and 0.173 for the Mach 9.3 to Mach 4 case. This means that for an inlet area of 2 feet, the outlet area would be 1.8 inches for the Mach 3 exit condition and 4.14 inches for the Mach 4 exit condition. These small areas would not allow enough flow through the combustor to produce the thrust required to propel the drone at Mach 10 for 5 minutes. Not only was the area for these cases a problem, but the total pressure losses were enormous due to normal shock waves within the inlet. The total pressure recovery for the Mach 9.3 to 4 case was 0.09 and 0.02 for the Mach 9.3 to Mach 3 case mainly because of the normal shock wave within the inlet. From these results, it was apparent that the free stream Mach number needed to be reduced to obtain a reasonable scramjet engine design.

The solution to the problem was to recompute upstream Mach numbers. After correcting an operational error with SEAGULL, a free stream Mach number of 7.0 could be obtained in order to use as input to INLET. The final inlet geometry was generated for a Mach 7 to Mach 4 compression. The results are presented in the design section of this report.

The forebody geometry consists of three ramps: one five degree and two three degree ramps, as previously mentioned and shown in Figure 7. This resulted in 23% loss of total pressure but an increase of 14.23 in static pressure. Furthermore, the shocks lie sufficiently close to the body so that the inlet capture area is 7.1 times the width of the cowl inlet, and there is no spillage for on-design conditions. (Figure 23).

Difficulties encountered in EDDYBL resulted from the lack of shock-boundary layer modeling in the program. (Figures 24 and 25). The problem is that the boundary layer properties are discontinuous across the shock and it is difficult to determine the correct starting conditions to compute properties downstream of the shock. As seen from Figures 25 and 26, the arc-length Reynolds number increases discontinuously across the shock, despite a discontinuous *decrease* in freestream Mach number. However, at the second shock, the Reynolds number decreases with a decrease in Mach number, as it should. The result of these variations is reflected in the boundary layer properties. The trend in compressible boundary layers is for increasing boundary layer thickness with increasing Mach number. [2, p. 538]. This agrees with the first discontinuity of Figure 24, but not with the second. Furthermore, shock-boundary layer interaction is not modeled in EDDYBL. Although the computed flow is laminar, experiments have shown, very generally speaking, that turbulent boundary layers at Mach 7 experience a 10% increase in thickness across a shock. [16, p. 7501-A-1]. Note that the computed boundary layer decreased in thickness across the shock, showing that EDDYBL is not applicable to shock-boundary layer interactions. (Figure 24).

With the program unable to predict boundary layer properties across shocks, quantitative analysis of the design is impossible. Qualitatively,

however, a number of results may be postulated based upon the results of the single five degree cone case.

Knowing that the boundary layer is .15 ft thick at the first ramp location downstream of the nose , boundary layer control will probably be required for efficient engine operation. In addition, the boundary layer will probably undergo transition *prior* to entering the inlet, due to traversing three shocks and increasing pressure. Forestalling transition, either by boundary layer diverson or suction will therefore be a necessity due to both heating and engine performance considerations.

Control of the boundary layer presents a major problem. Boundary layer diversion, as opposed to boundary layer suction, was discarded due to the high cooling expected to be required on the sharp edge of the splitter plate. Experience with the five degree cone, however, indicates that large cooling rates will be required for boundary layer suctiuon over a very large area due to the large removal rates required. This may make splitter plates more practical than boundary layer diversion because of it's simplicity. Both methods of control would require high cooling rates, as well as a large rate and volume of fluid diverted or ingested. The splitter plate would accomplish this task without pumps and other active removal devices required in boundary layer suction.

The final configuration for the inlet geometry of the scramjet was obtained by running the program INLET for a two-dimensional case by specifying a Mach number of 7.0 for the "free-stream" velocity and a Mach nubmer if 4.0 for the exit velocity, "free-stream" meaning the flow conditions after the initial ramp compressions on the forward underbody of the drone but before the two five degree ramps on which INLET constructs the flow field. Three internal isentropic compression sections were used and the ouptut from INLET is summarized in Figure 27 thru 32.

Figure 27, Inlet Area vs. Horizontal Distance, shows the inlet cross-sectional area measured axially from the cowl lip postion. If the graph is scaled by setting the initial area equal to 1.07 square feet,

assuming a 1.0 foot depth because it is a two-dimensional case, then 0.36 on the nondimensional scale is 1.07 feet on the actual drone. This 1.07 feet dimension is the approximate inlet length shown in Figure 2. This scaling will allow the discussion of the results to be related to the actual dimensions of the drone. Using the scale 0.36 = 1.07 feet, it can be seen in Figure 27 that the inlet area contracts rapidly from 1.07 feet (0.36) to 0.456 feet (0.154) in a distance of 3.2 feet (1.08). This sharp decrease in area then tapers off and the final inlet area is 0..394 feet (0.133) which occurs 20.0 feet (6.75) aft of the initial spike tip. Note that the area is approxiately 0.394 square feet (0.133) from a distance of 19.1 (6.44) to 20.0 (6.75) feet. This 0.9 feet is needed to ensure uniform properties across the exit plane give an area contraction of 2.7 times, meaning that the area at the entrance plane is 2.7 times greater than the exit plane area.

The relative locations of the five degree ramps and the cowl lip can be seen in Figure 28. Again, using a scale of 0.36 = 1.07 feet it can be seen that the intersections of the two five degree ramps is at 6.87 feet (2.32) behind the spike tip of the first ramp and the cowl lip is located 14.2 feet (4.78) aft of the spike tip of the first ramp. The intersection of the two five degree ramps was calculated by INLET so that the shock waves generated by the two ramps intersect at the cowl lip. Placing both shock waves at the cowl lip minimizes flow spillage and increases engine efficiency. Figure 28 also shows that the minimum cross-sectional area of the inlet occurs at 18.4 feet (6.2) along the axis of the drone and remains constant up to the exit plane at 10.0 feet (6.75).

Mach number and pressure distributions on the cowl contour are shown in Figures 29 and 30, respectively. The magnitude of the Mach number can be traced in the output from INLET from the spike tip of the first five degree ramp to the exit plane of the inlet. The "free-stream" Mach number is 7.0. Behind the shock wace generated from the first five degree ramp the Mach number is 6.106. The Mach number after the second

es shock wave originating at the intersection of the two five degree ramps is 5.401. These results can be calculated using the Prandtl-Meyer oblique shock relations found in reference [2]. The shock wave originating from the cowl lip further reduces the Mach number to 4.267. This Mach number remains constant because INLET assumes that the cowl contour is a straight wall for the first 1.73 feet (0.583) for the geometry calculated. At 15.88 feet (5.359), the cowl contours change from being a straight wall to being an isentropic compression surface and assumes an appropriately curved shape. The flow is compressed from a Mach number of 4.267 at 15.88 feet (5.359) to a Mach number of 4.00 at 17.63 feet (5.950). From Figure 30 it can be seen that the pressure increases as Mach number decreases. The static pressure ratio increases from 14.9 at the entrance of the inlet to 21.2 at the exit plane of the inlet which means that approximately one-third of the compression is taking place internally.

An extremely important feature of all supersonic flow engines is the total pressure loss, which dictates the efficiency of the engine. High total pressure loss indicates a low engine efficiency while a low total pressure loss indicates high engine efficiency. The total pressure ratio along the centerbody contour is plotted in Figure 31 and the total pressure ratio along the cowl contour is plotted in Figure 32. It can be seen that the total pressure ratio along the centerbody contour behind the first shock drops to 95% of its initial value behind the second shock. Past the second shock, the flow along the centerbody contour encounters no other shock waves because the flow is compressed isentropically, which means no further total pressure loss occurs. Behind the oblique shock wave at the cowl lip the total pressure is only 77% of it's "free-stream" value. Because the cowl lip shock wave is cancelled at the centerbody by INLET, there are no internal shock reflections. Since the flow is compressed isentropically internally, the total pressure along the cowl surface is constant. Since the

total pressure ratio along both the centerbody and cowl contours is 77% at the exit plane, the overall total pressure recovery for the scramjet from Mach 7 at the spike tip of the first ramp to Mach 4 of the exit plane is 77% for the geometry generated.

The configuration used for the combustor is illustrated in Figure 33. It is a two dimensional box combustor with an entrance height of 5 inches, and a constant width of 11.2 inches (the combustor length is 10.0 feet). There are two fuel injection points, at 3.75 ft. and 5.0 ft. respectively in the axial direction. Information regarding the injectors is given in Table 3. The temperature distribution as a function of axial distance is given in Figure 34. There is a steady rise in temperature until the location of the first injector, after which it levels off and even begins to decrease. This corresponds to a leveling off of the combustor efficiency (see Figure 35) at a value near 0.95 after the first injector. This gradual rise in combustion efficiency starting at the entrance to the combustor is due to the manner in which CPIPE "distributes" the reacted fuel equivalence ratio over the combustor. Thus, by the time the flow reaches the first injector, a large fraction of the fuel injected at that point has started combustion. After the first injector, there is a constant level of reaction. This explains the drop in static pressure (Figure 36) after the first fuel injection point. The pressure due to the combustion process is constant while the area of the combustor continues to increase. The Mach number displays a similar behavior (Figure 37), stabilizing at a constant value after the first injector. The exit Mach from the combustor is approximately 2.3.

With the combustor exit properties analyzed by the program CPIPE, the flow field inside the nozzle was modeled using the method of characteristics. Reference [2] provides the algorithm used to implement the computer code. In applying the method of characteristics, the flow

field is assumed to be irrotational, inviscid and adiabatic. In addition, the characteristic lines are determined to a first order appoximation.

Once the nozzle exit velocity was determined to be 11,000 ft/sec, a momentum balance was performed to determine the thrust. The control volume used for the momentum balance was defined by the equivalent inlet capture area under the nose of the HCV and the vertical nozzle exit plane. There was no spillage for the on-design condition; hence, it was not included in the momentum balance.

The thrust available with the nozzle design illustrated in Figure 28 was calculated to be 7646 lbs. per unit span, which is approximately 8.99% of the thrust available in isentropic expansion. Enthalpy losses due to heat flux and viscous effects at the upper nozzle wall, as well as plume drag, which was not accounted for, are expected to further reduce the efficiency of the nozzle although there should still be adequate thrust.

Note that a certain errors are propagated in locating the mesh points with the first order approximation. Reference 17 provides the thrust coefficient measured on a similar model tested at Mach 10. The thrust coefficient for this design is calculated to be 0.36, which falls between 0.1 and 0.92, the range of thrust coefficients presented in reference 2.

6. Conclusion

6. Conclusion

Various forebody geometries were evaluated for their ability to efficiently compress free stream flow prior to ingestion by scramjet inlets. Also, boundary layer growth on these forebodies was investigated, and boundary layer control, in the form of surface suction, was found to be somewhat effective. Inlet geometry design was investigated, and it was found that inlet speeds greater than Mach 7 would not allow sufficient capture area for the compression required.

A final design for the forebody consisted of a five-degree half-angle cone with a five degree compression ramp placed 18 feet aft of the nose, and two additional compression ramps placed at 27 and 31 feet. The Mach number entering the inlet was 7.2, and an inlet geometry was designed using two pre-inlet five degree compression ramps. The cowl geometry was generated to yield an isentropic compression to Mach 4 at the entrance to the combustor. The total length of the two pre-inlet ramps and cowl was twenty feet.

Although EDDYBL was not able to compute shock-boundary layer interaction and was therefore unable to calculate flow properties accurately at the shocks generated at the three degree ramps, results from the single five degree half-cone were used to obtain trends in boundary layer growth on the forebody. Boundary layer suction was found to require high suction velocities and large volumes of fluid ingested, accompanied by severe increases in surface heating.

CPIPE was used to compute combustor performance of the combustor, and the method of characteristics was used to roughly compute the expansion in the nozzle. Finally, a momentum balance was performed and the thrust generated by the design was calculated to be 58,000 lb, which was slightly higher than the values output by SCRAM, and was sufficient to propel the drone at a Mach 10 cruise speed.

FIGURES

AND

TABLES

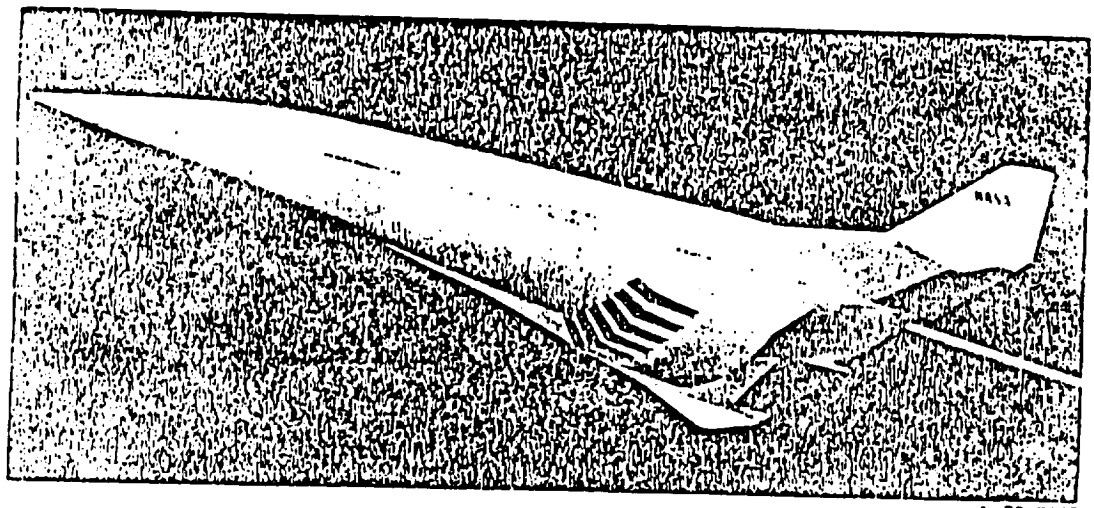

Configuration model.

L-72-9146

FIGURE 1: HCV Configuration

ORIGINAL PAGE IS
OF POOR QUALITY

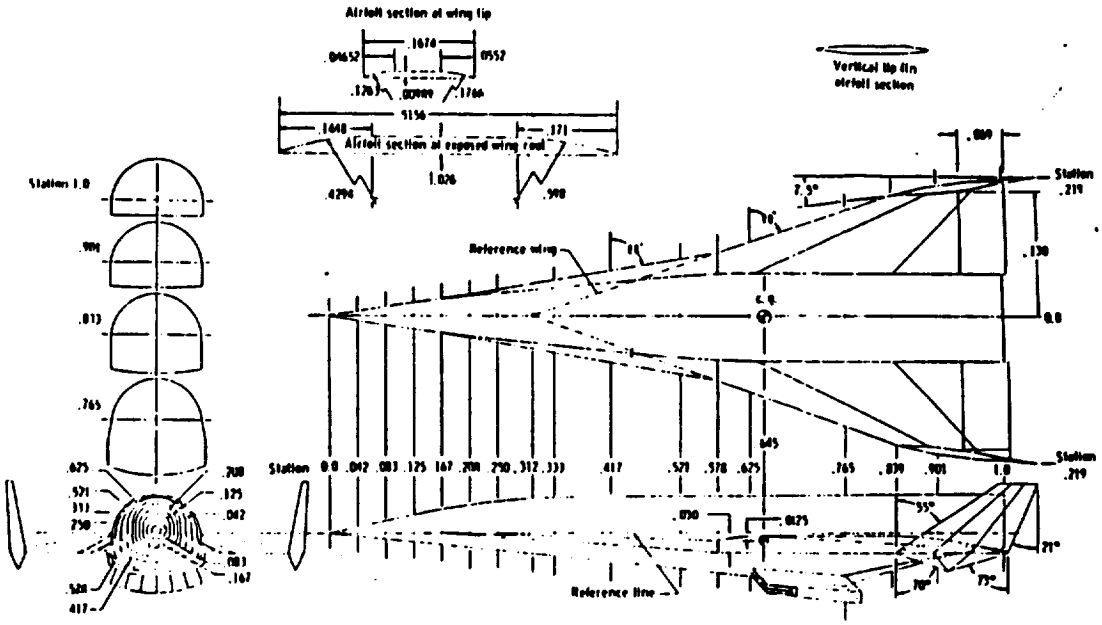

(a) Base-line configuration.

FIGURE 2 .- Model general dimensions. All dimensions have been normalized by the body length (ℓ = 50.8 cm).

TABLE I.- GEOMETRIC CHARACTERISTICS OF MODEL

Wing:		
Area, reference (includes fuselage intercept), m^2 (in^2)	0.043	(67.200)
Area, exposed, m^2 (in^2)	0.023	(36.121)
Area, wetted, m^2 (in^2)	0.047	(72.242)
Span, m (in.)	0.217	(8.542)
Aspect ratio		1.086
Root chord, at fuselage center line, m (in.)	0.353	(13.896)
Tip chord, m (in.)	0.085	(3.355)
Taper ratio		0.241
Mean aerodynamic chord, m (in.)	0.248	(9.779)
Sweepback angles:		
Leading edge, deg		70
25-percent-chord line, deg		64
Trailing edge, deg		0
Dihedral angle, at airfoil mean line, deg		-3.64
Incidence angle, deg		0
Airfoil section		(See fig. 5(a))
Airfoil thickness ratio:		
Exposed root		0.05
Tip		0.06
Leading-edge radius at -		
Fuselage-line chord, m (in.)	5.08×10^{-4}	(0.020)
Tip, m (in.)	5.08×10^{-4}	(0.020)
Area of both elevons, m^2 (in^2)	0.005	(7.161)
Forward delta wing:		
Area exposed, outside of fuselage, forward of wing leading edge, m^2 (in^2)	0.002	(3.394)
Leading-edge sweep, deg		80
Tip fin:		
Area, each, m^2 (in^2)	0.004	(5.848)
Span, m (in.)	0.069	(2.730)
Aspect ratio		1.274
Root chord, m (in.)	0.086	(3.383)
Tip chord, m (in.)	0.029	(1.135)
Taper ratio		0.336
Mean aerodynamic chord, m (in.)	0.062	(2.445)

Scale for original HCV = 0.021

TABLE I.- Concluded

Sweepback angles:		
Leading edge, top, deg		55.0
Leading edge, bottom, deg		70.1
Trailing edge, top, deg		21.3
Toe-in angle, deg		7.5
Airfoil section:		
Leading-edge radius, m (in.)	5.08×10^{-4}	(0.020)
Center vertical tail:		
Area, exposed, m^2 (in^2)	0.007	(11.492)
Span, exposed, m (in.)	0.086	(3.380)
Aspect ratio of exposed area		0.994
Root chord, at fuselage surface line, m (in.)	0.128	(5.040)
Tip chord, m (in.)	0.045	(1.760)
Taper ratio		0.349
Mean aerodynamic chord of exposed area, m (in.)	0.093	(3.664)
Sweepback angles:		
Leading edge, deg		55.0
Trailing edge, deg		24.6
Airfoil section:		
Thickness ratio at -		
Tip		0.106
Root		0.106
Leading-edge radius, m (in.)	5.08×10^{-4}	(0.020)
Fuselage:		
Length, m (in.)	0.508	(20.000)
Maximum height, m (in.)	0.071	(2.782)
Maximum width, m (in.)	0.073	(2.866)
Fineness ratio of equivalent round body		6.822
Planform area, m^2 (in^2)	0.026	(40.445)
Wetted area, m^2 (in^2)	0.083	(128.460)
Wetted area, with wing on, m^2 (in^2)	0.078	(120.695)
Wetted area, with both delta wings on, m^2 (in^2)	0.077	(118.747)
Base area, m^2 (in^2)	0.002	(3.726)
Complete model, with both delta wings:		
Planform area, m^2 (in^2)	0.052	(79.960)
Aspect ratio of planform		0.913

Scale for original HCL = 0.021

FIGURE 3

CODE APPLICATION

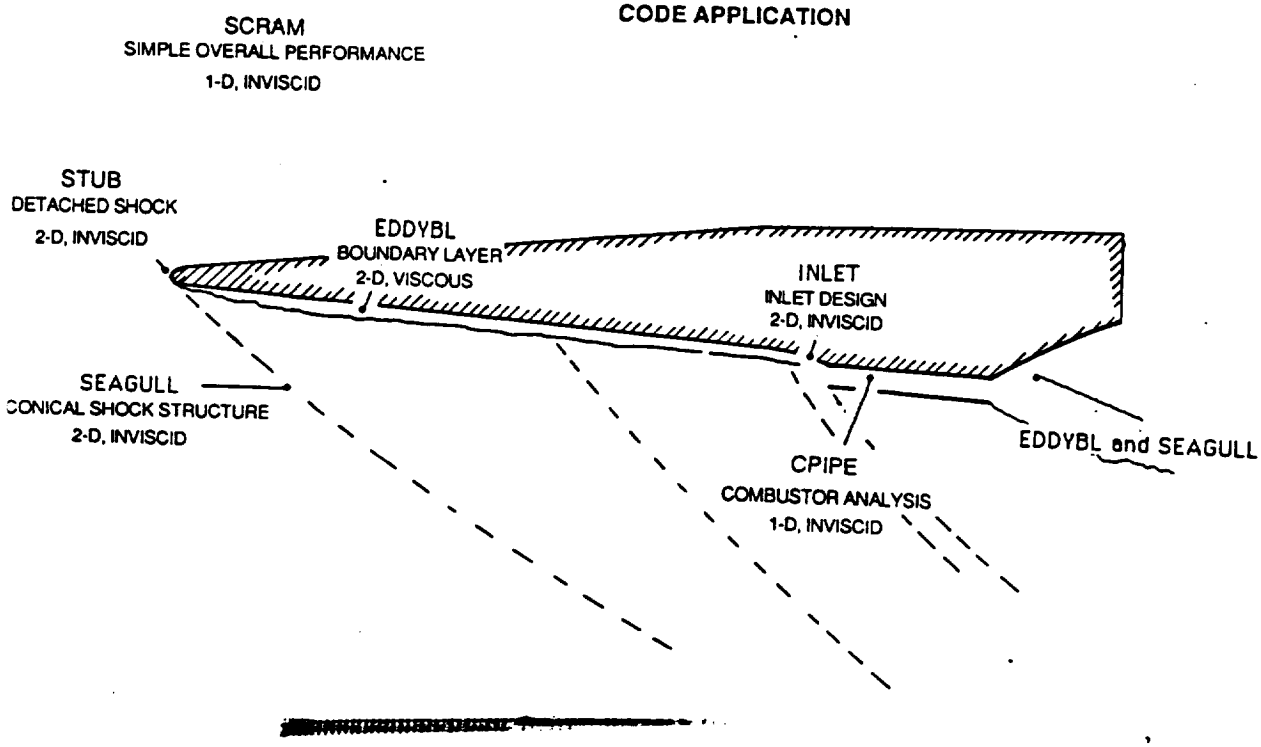

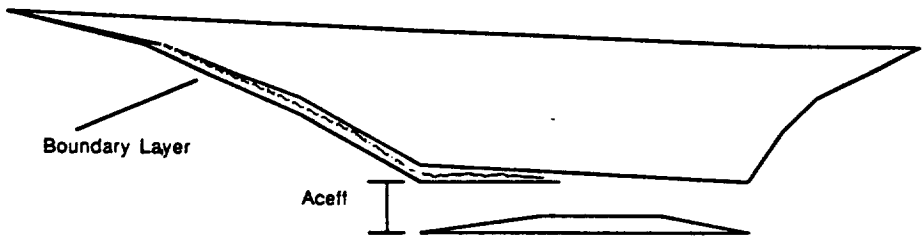

Aceff = Effective Capture Area

FIGURE 4 - Effective Mass Flow entering engine.

Table 2: Forebody Compressive Qualities

Forebody	$P_{t2}/P_{t\infty}$	M_2	P_2 / P_∞
#1	.7829	7.51	8.97
#2	.8798	7.85	9.17
#3	.7780	7.33	14.63

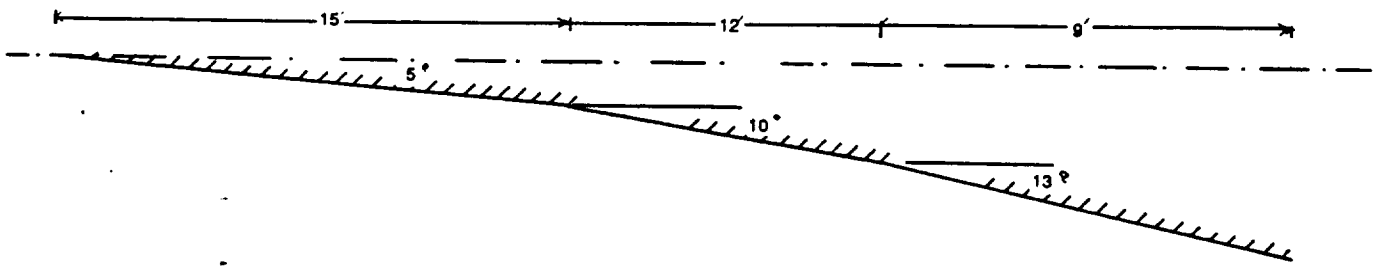

FIGURE 5: Design #1

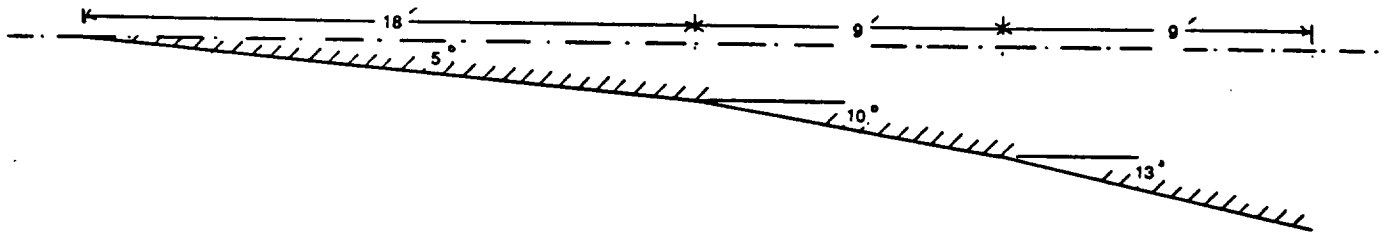

FIGURE 6: Design #2

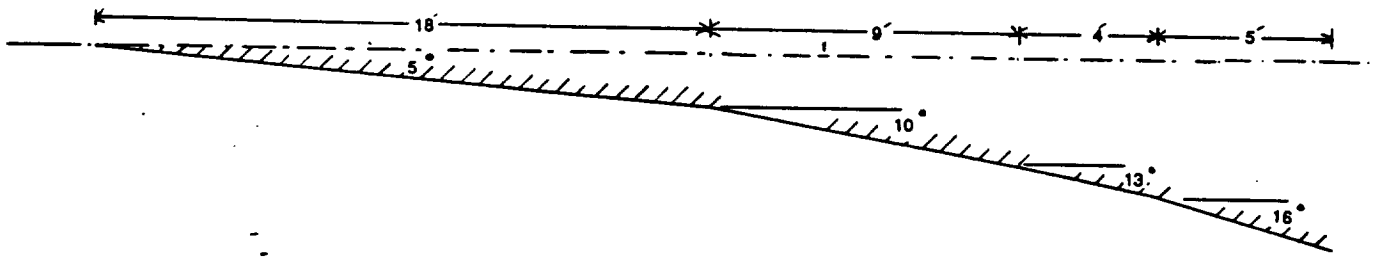

FIGURE 7: Final Forebody Geometry

FIGURE 8: Boundary Layer Growth vs. Axial Distance on Five Degree Cone

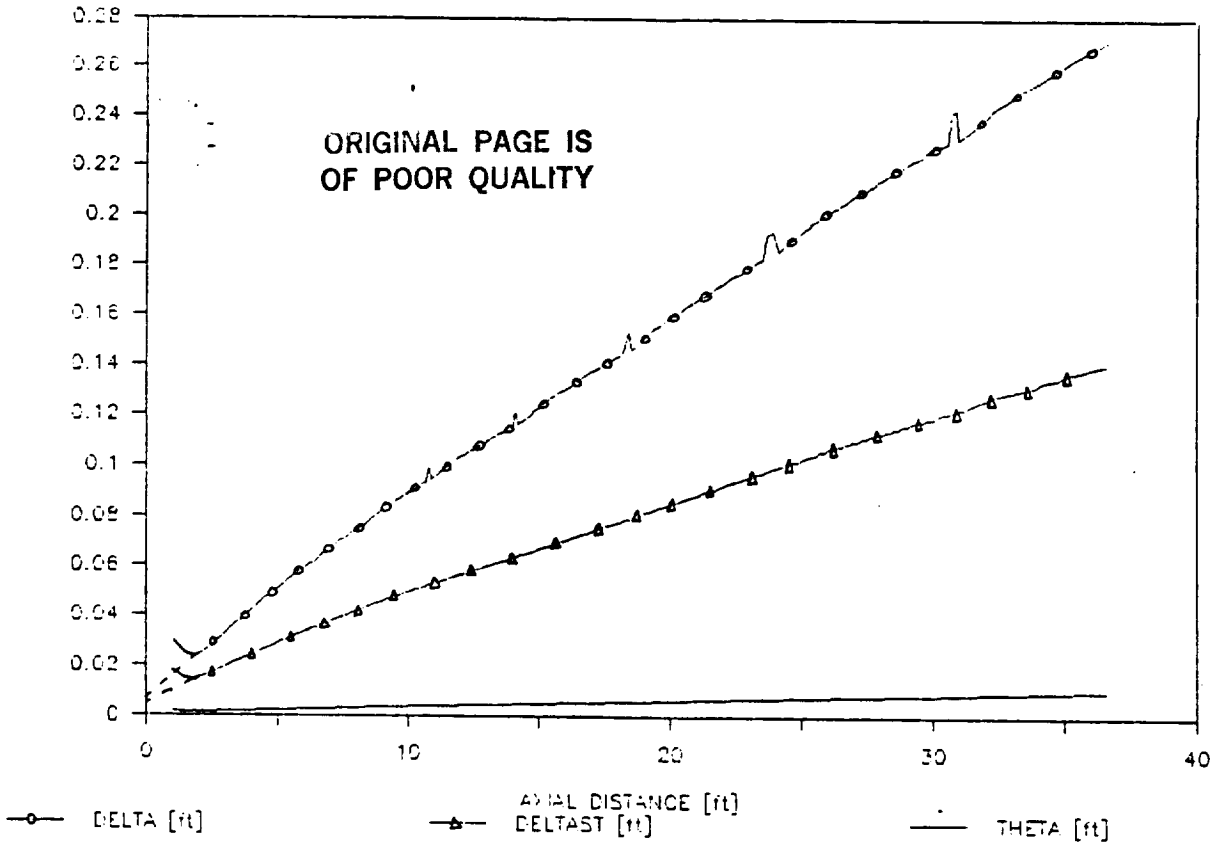

FIGURE 9: Boundary Layer Growth vs. Reynolds Number on Five Degree Cone

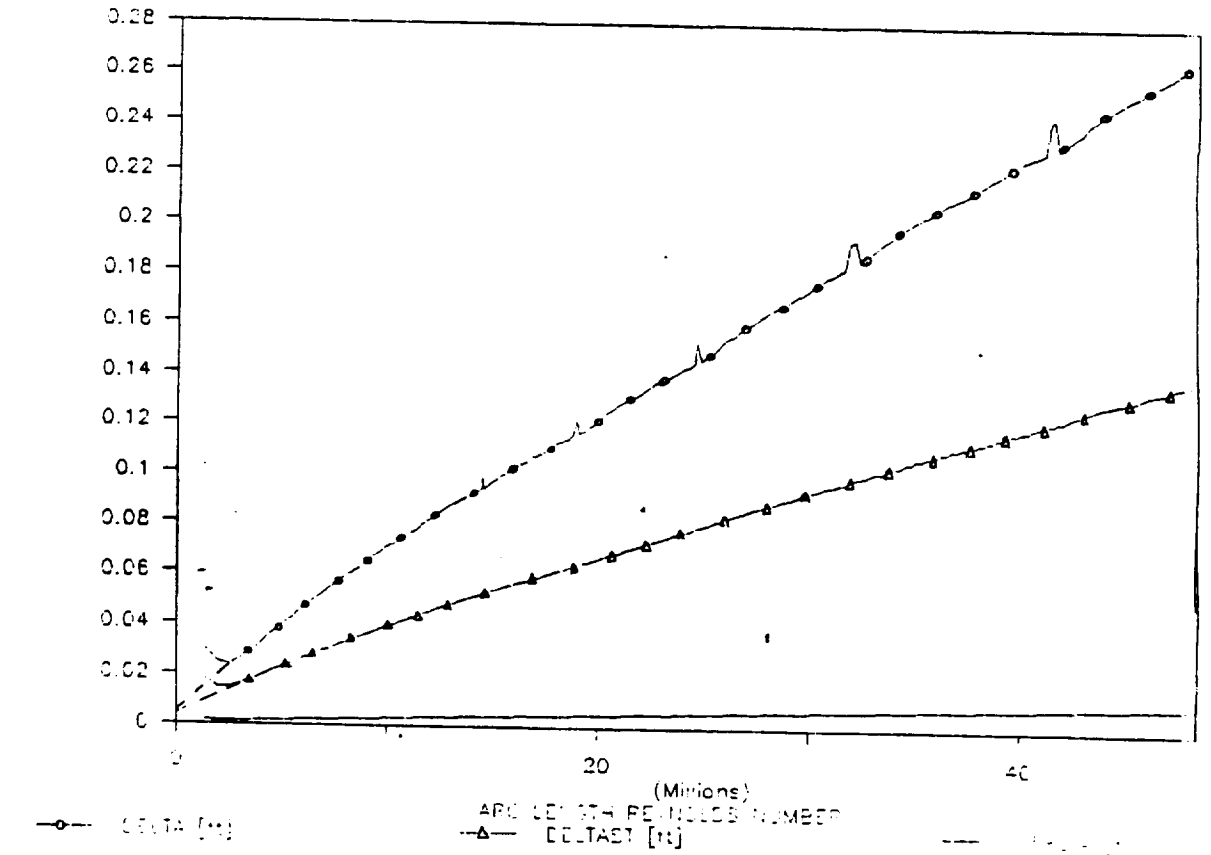

FIGURE 10: Heat Flux on Five Degree Cone

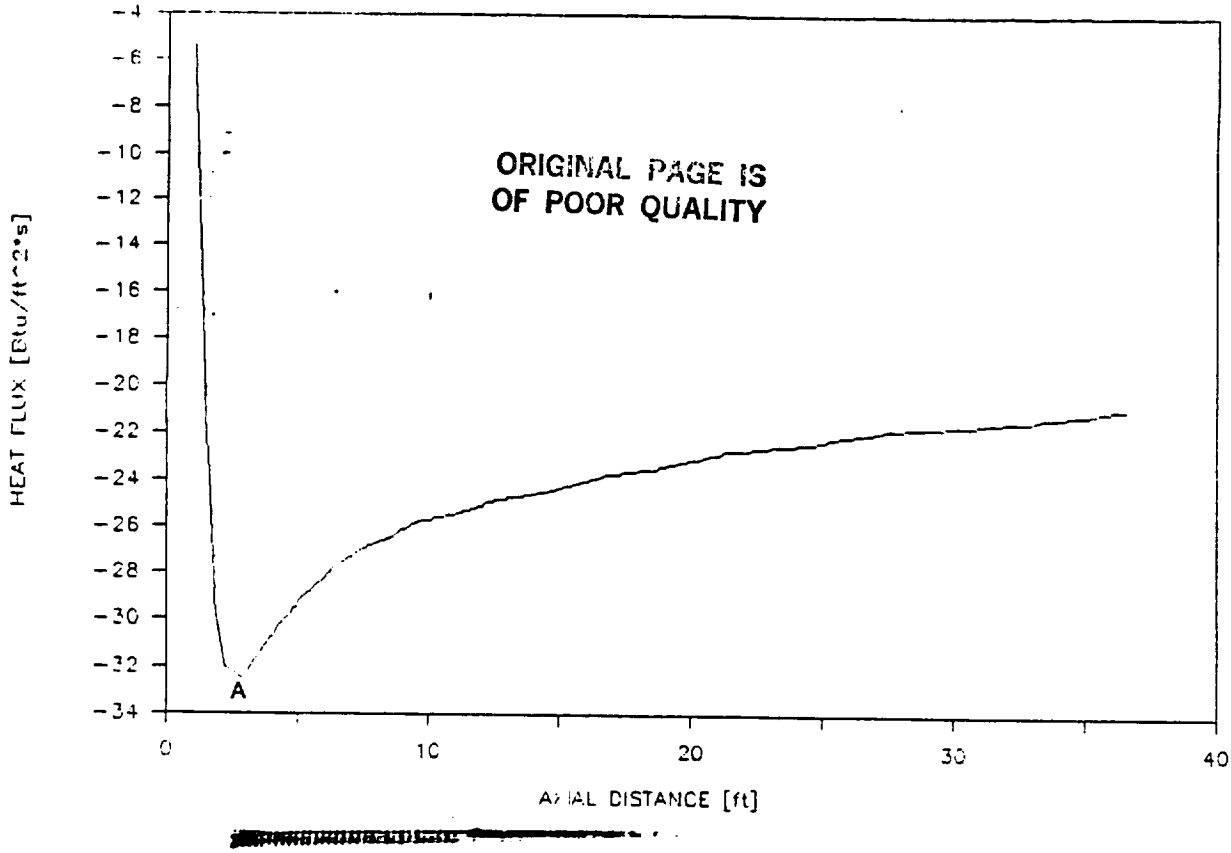

FIGURE 11: Boundary Layer Growth vs. Axial Distance on Five Degree Cone With Suction

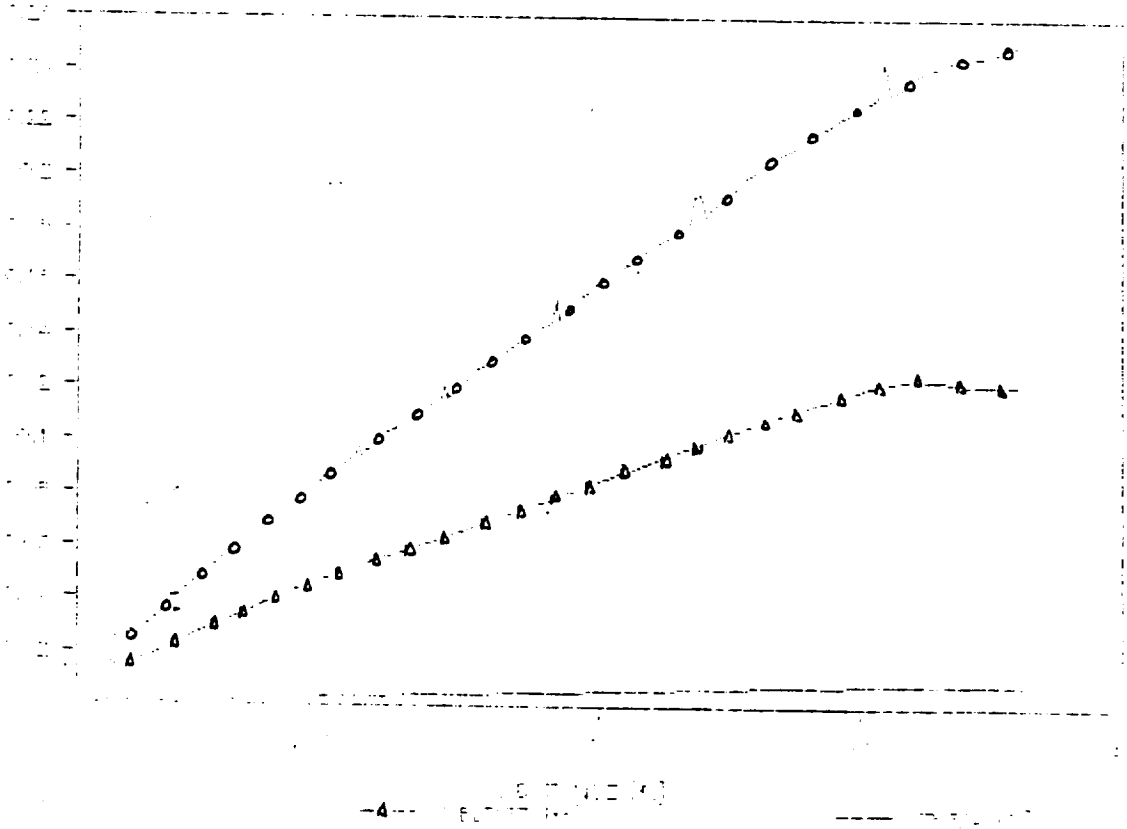

FIGURE 12: Boundary Layer Growth vs. Reynolds Number on Five Degree Cone With Suction

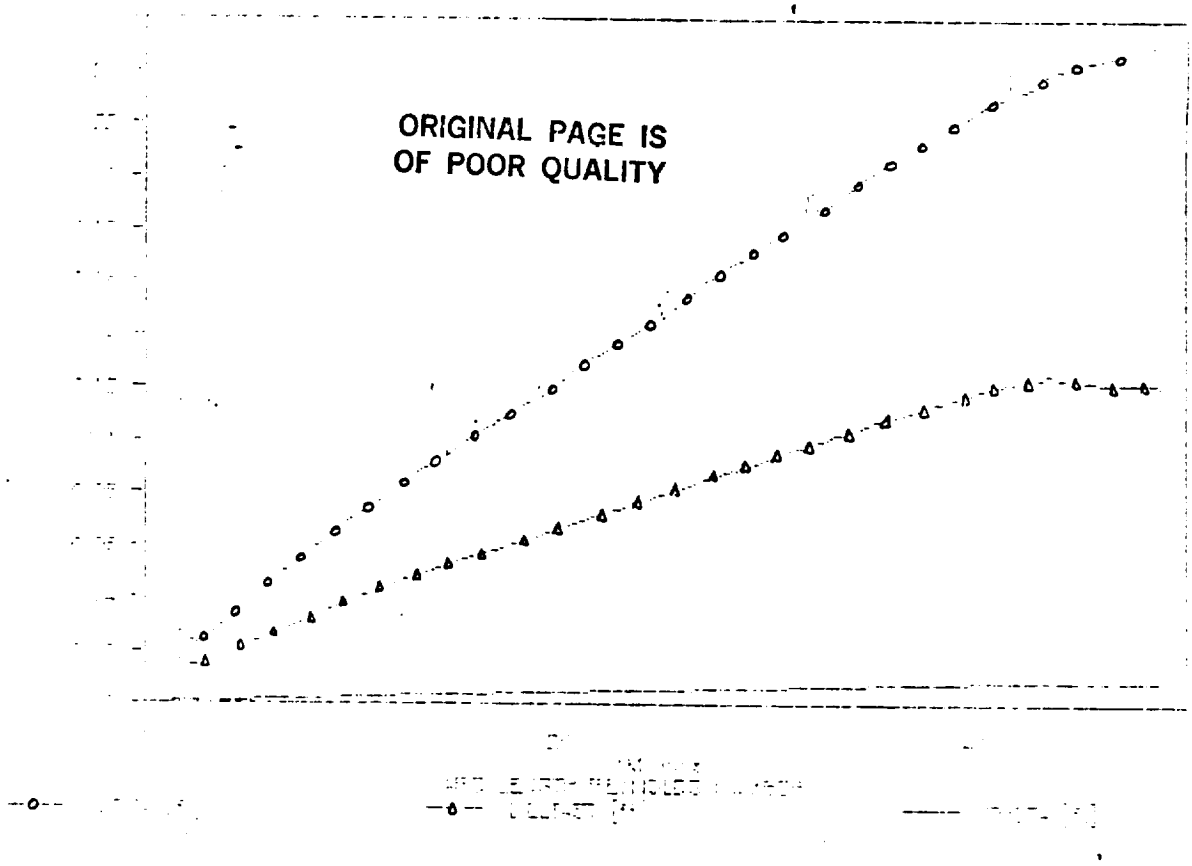

FIGURE 13: Mass Flux on Five Degree Cone

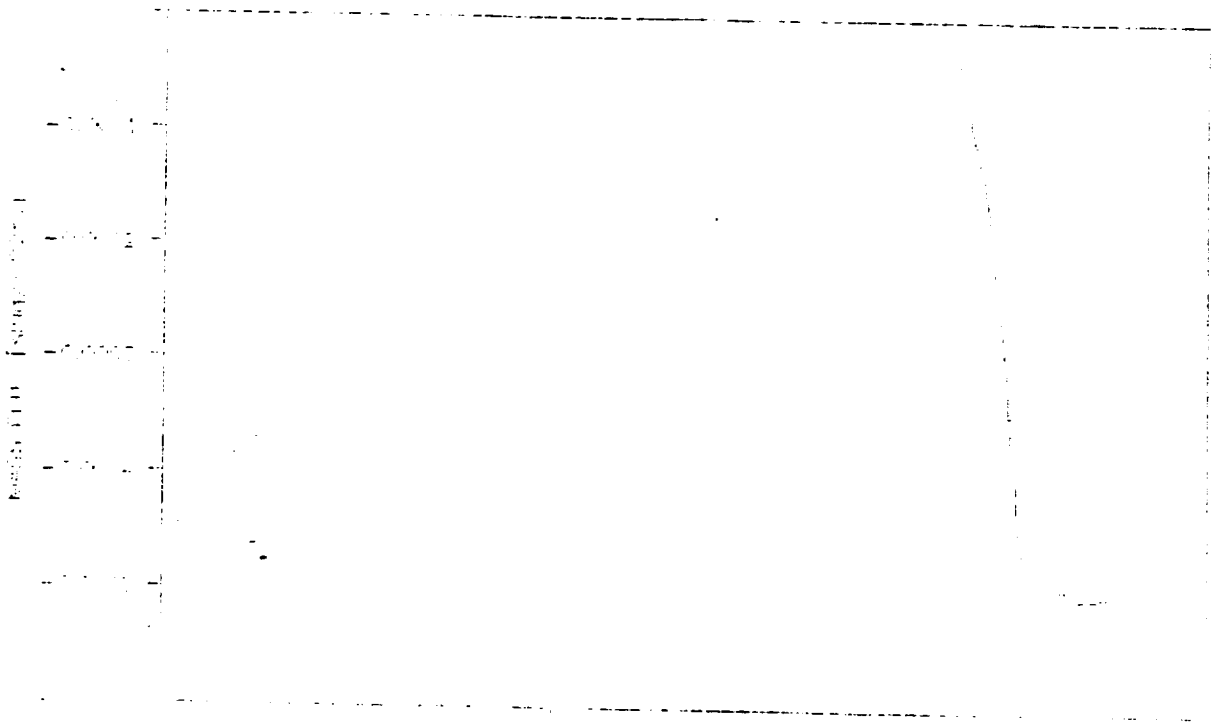

FIGURE 14: Heat Flux on Five Degree Cone With Suction

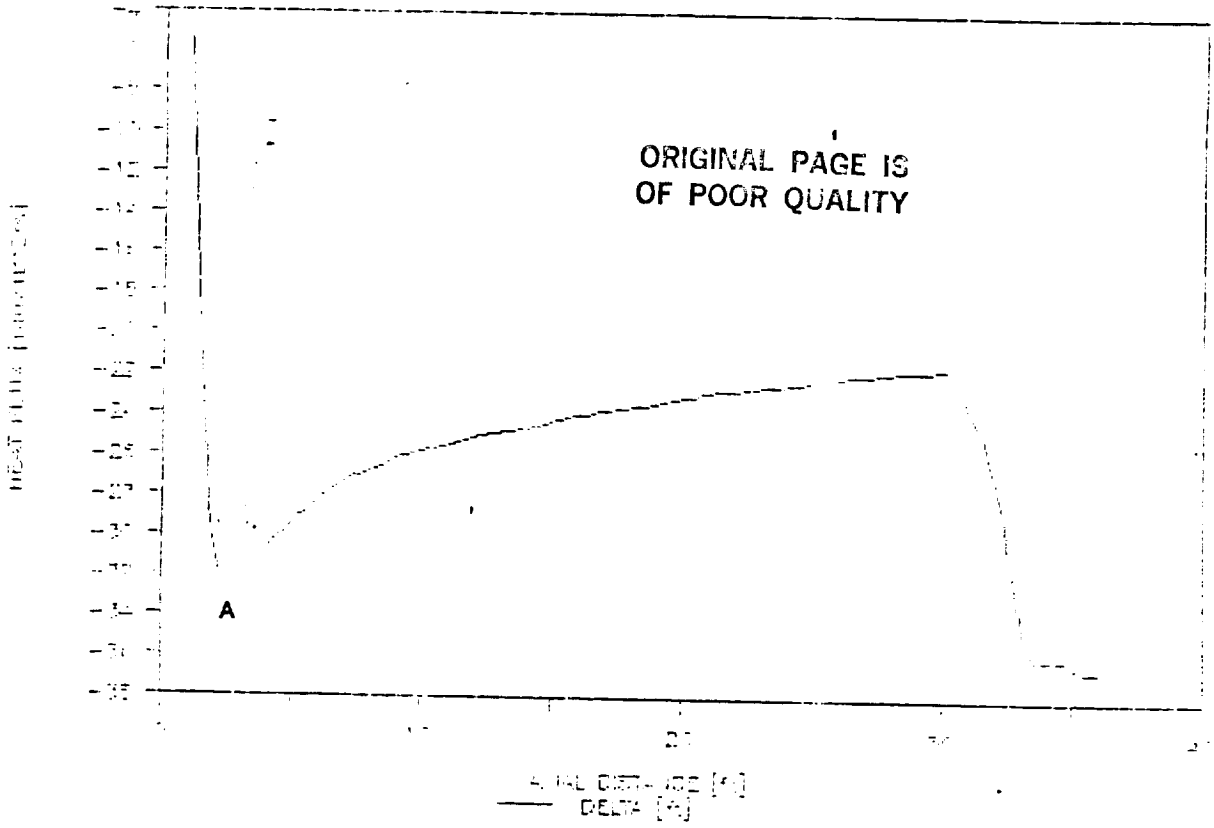

FIGURE 15

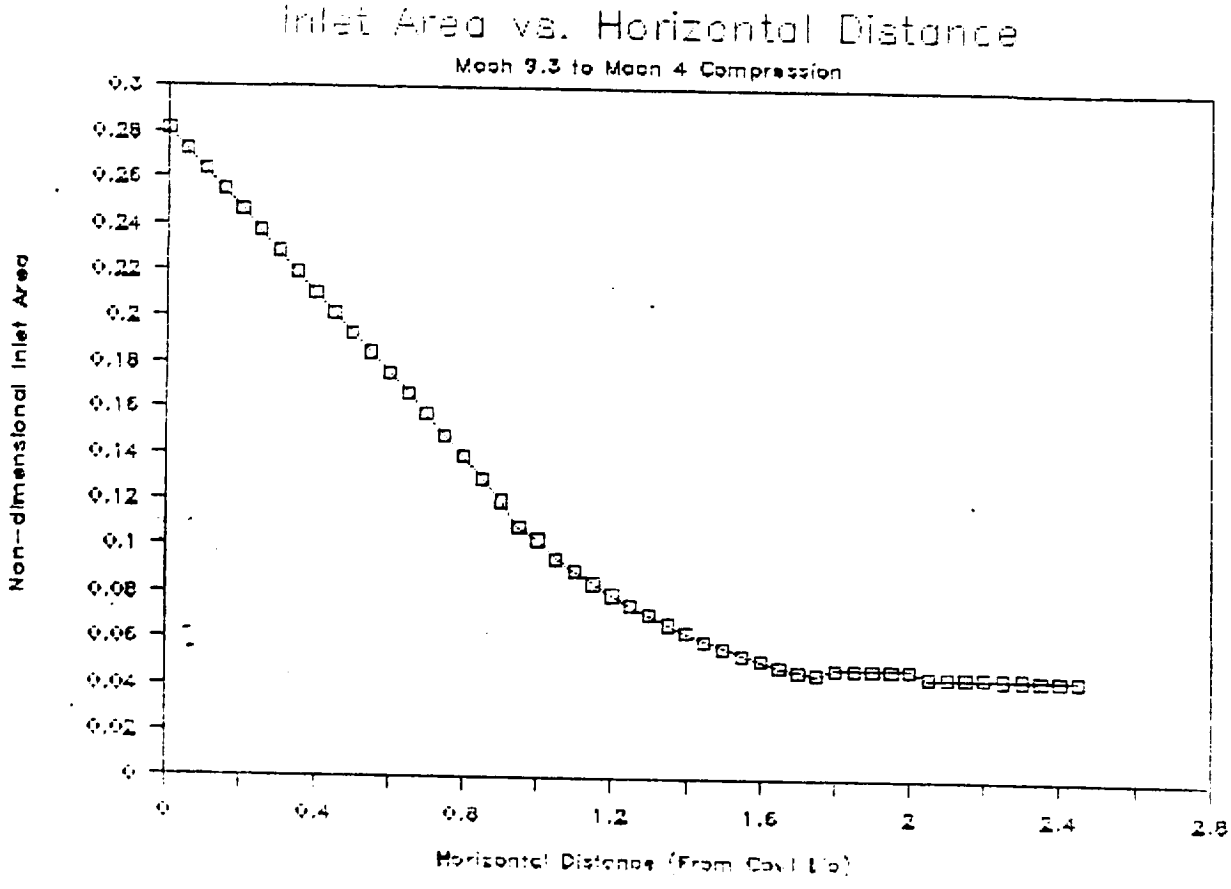

FIGURE 16

Cowl and Centerbody Contours

Mach 9.3 to Mach 4 Compression

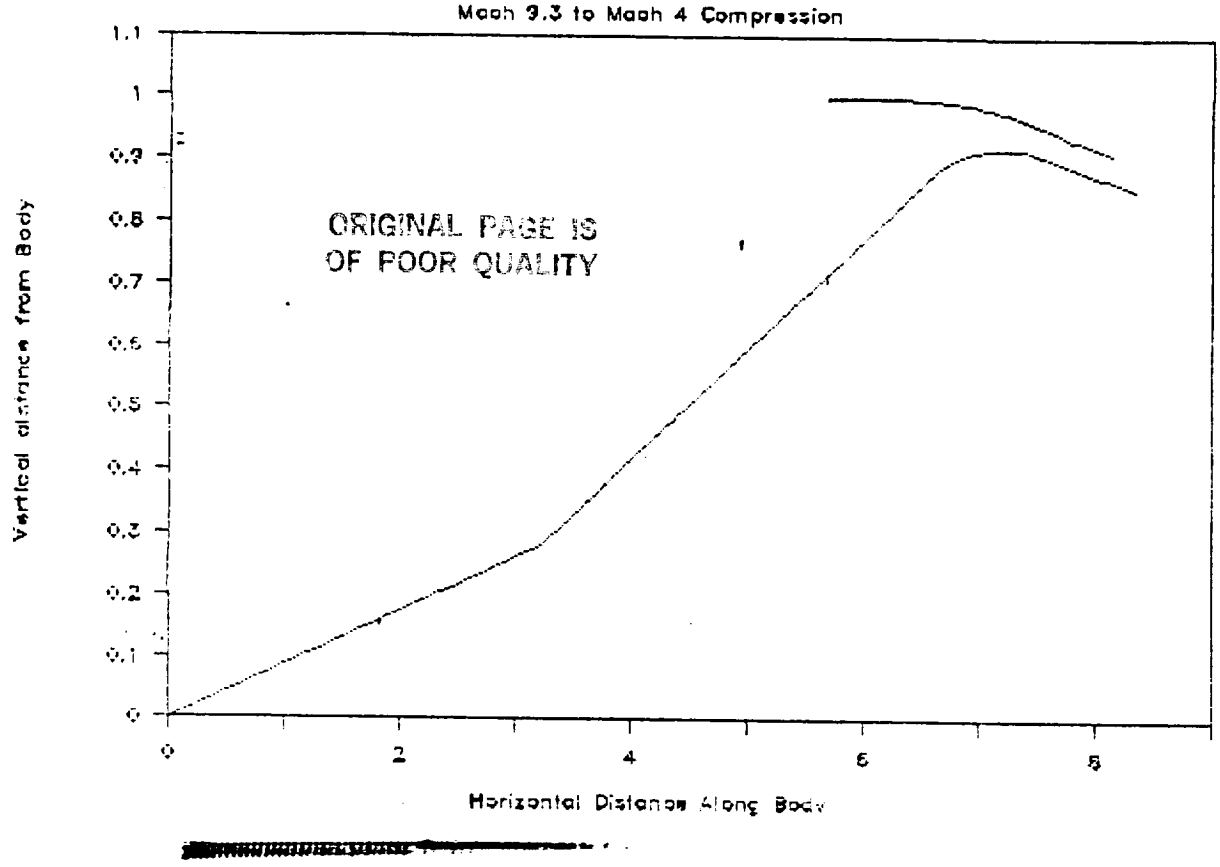

FIGURE 17

Mach Number on Cowl Surface

Mach 9.3 to Mach 4 Compression

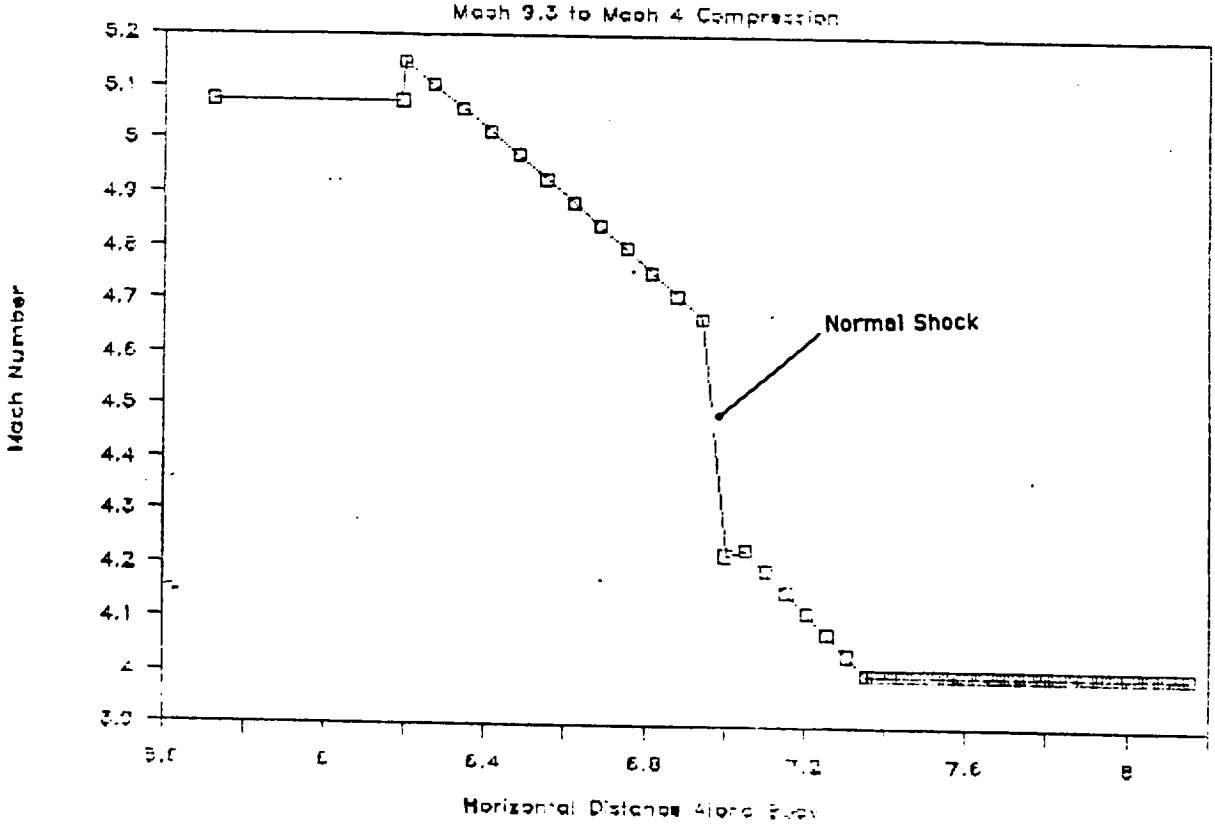

FIGURE 18

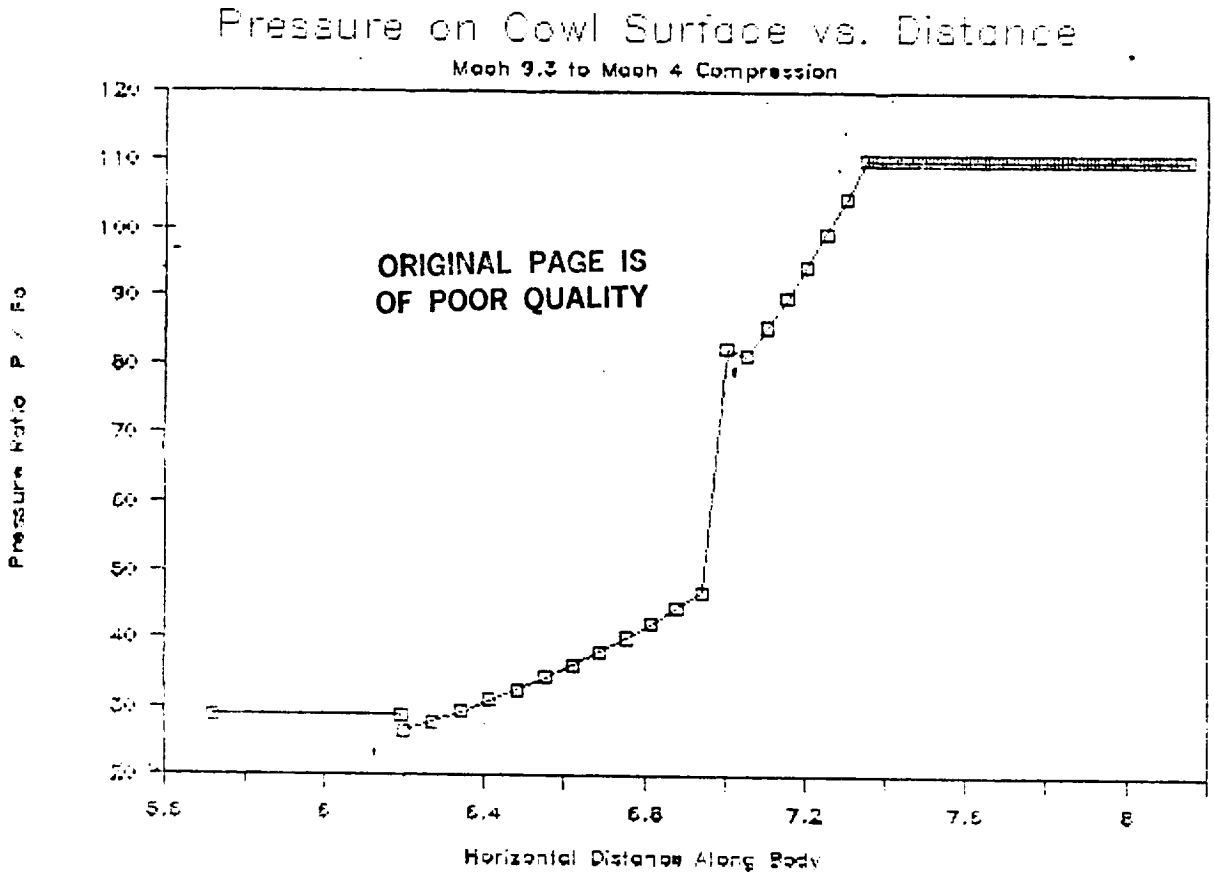

FIGURE 19

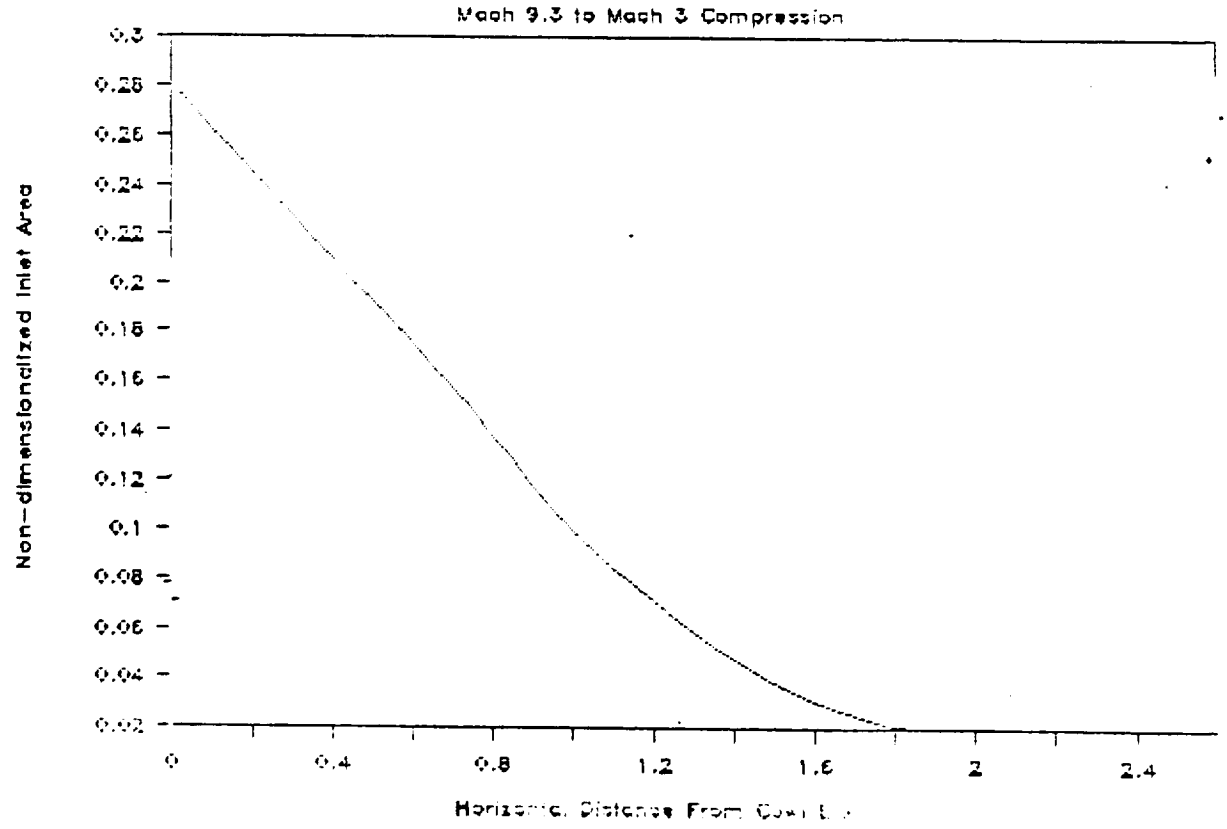

FIGURE 20

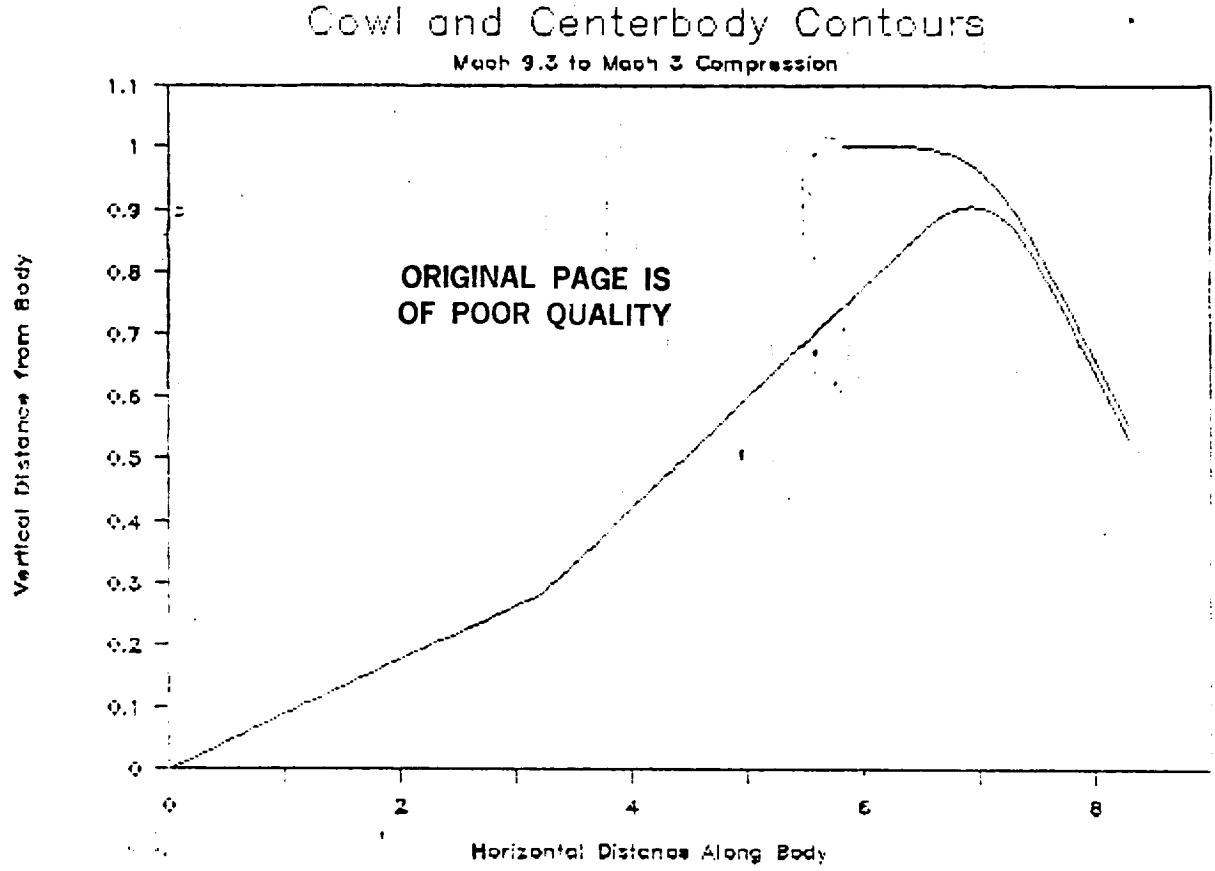

FIGURE 21

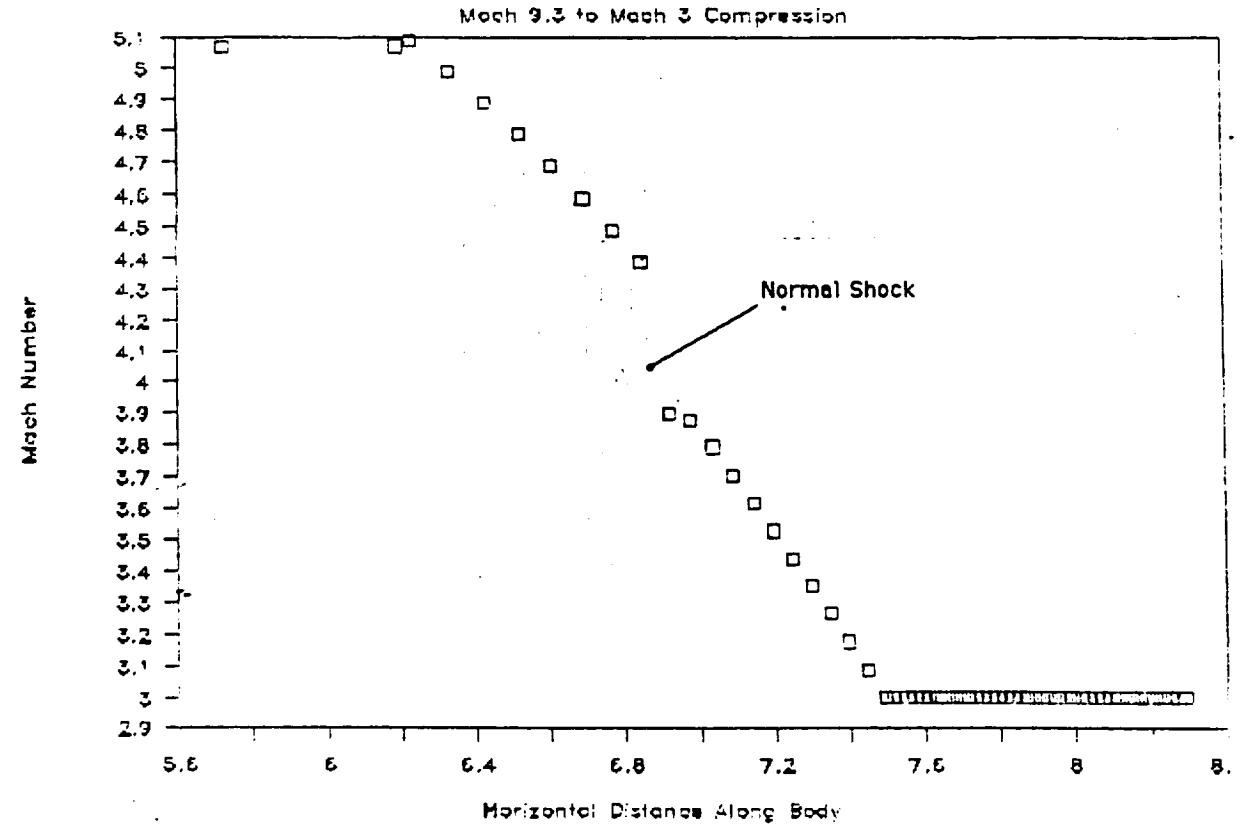

FIGURE 22

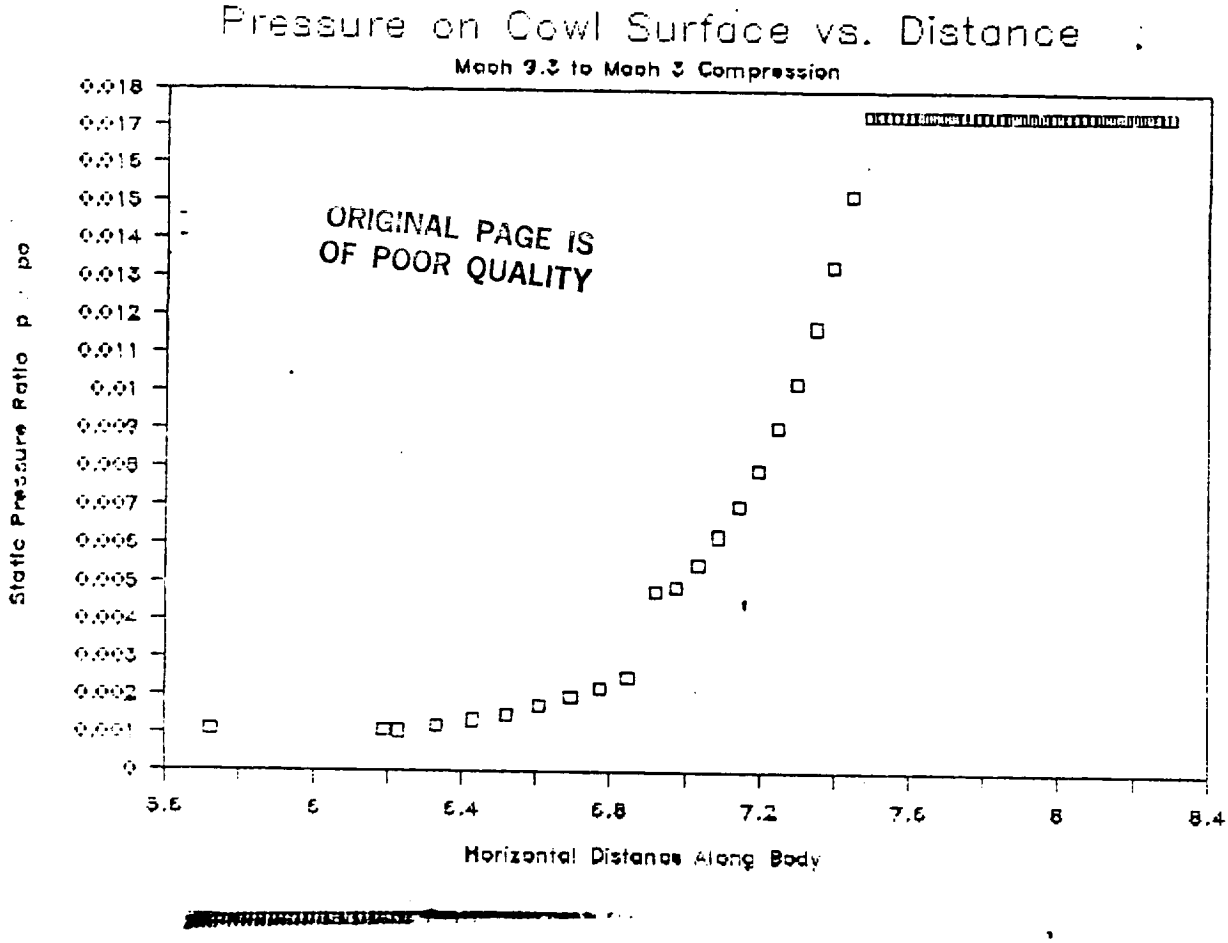

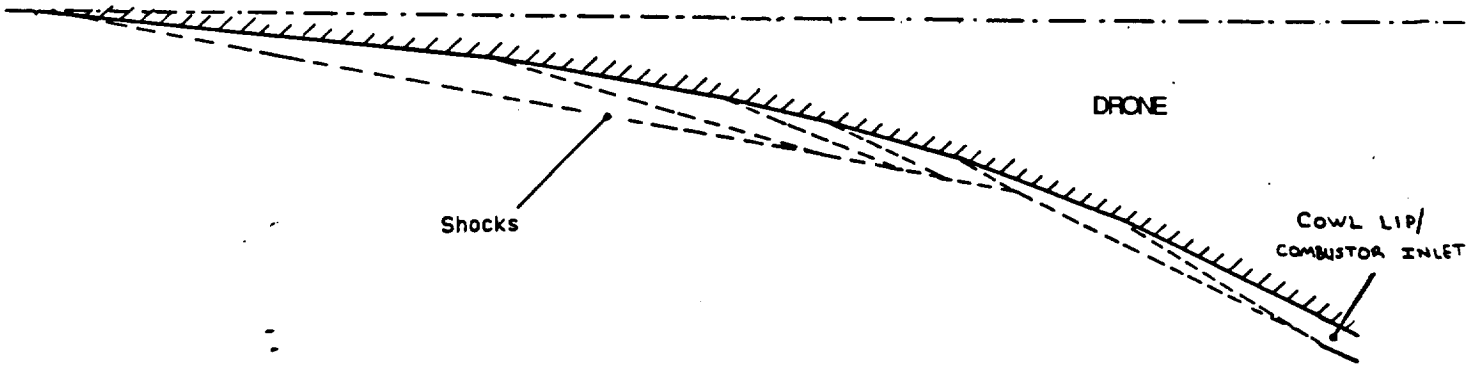

FIGURE 23: Shock Structure on Final Design

FIGURE 24: Boundary Layer Growth vs. Axial Distance on Final Design

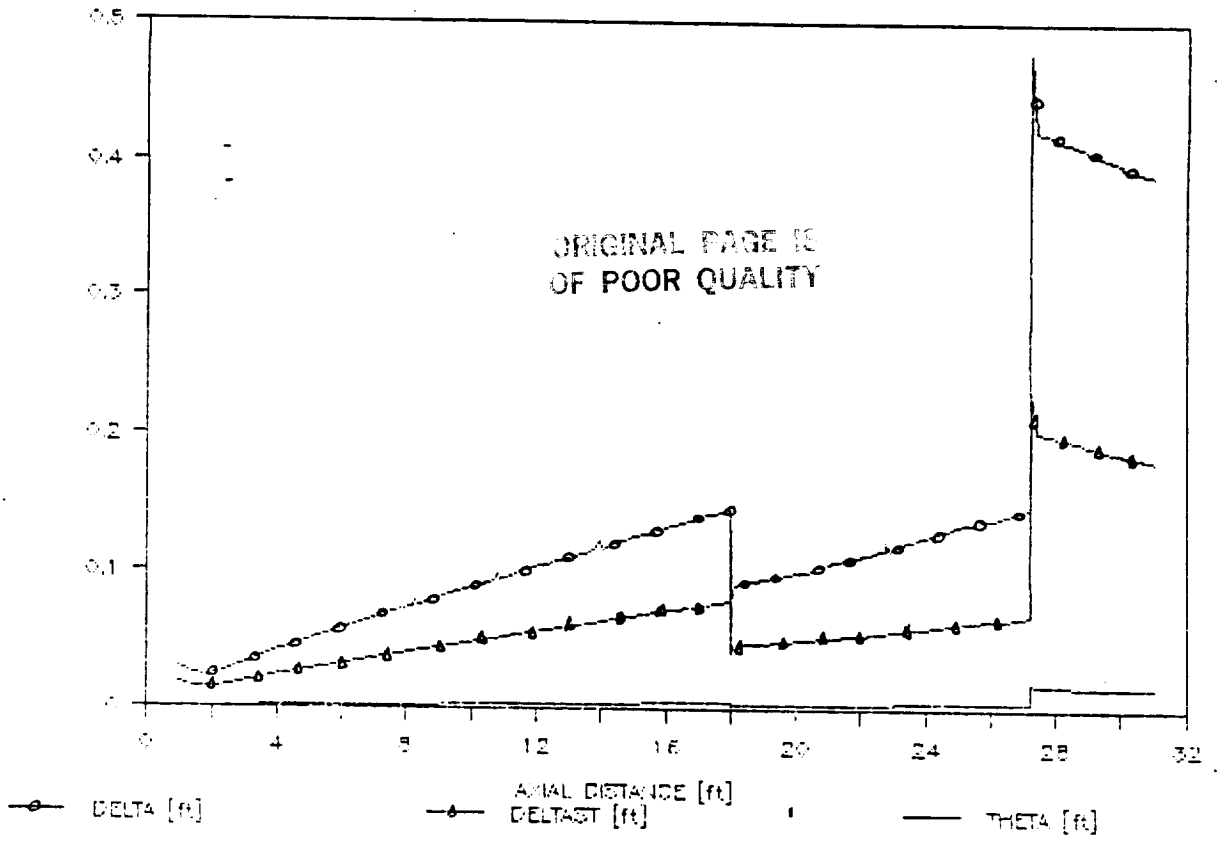

FIGURE 25: Reynolds Number vs. Axial Distance on Final Design

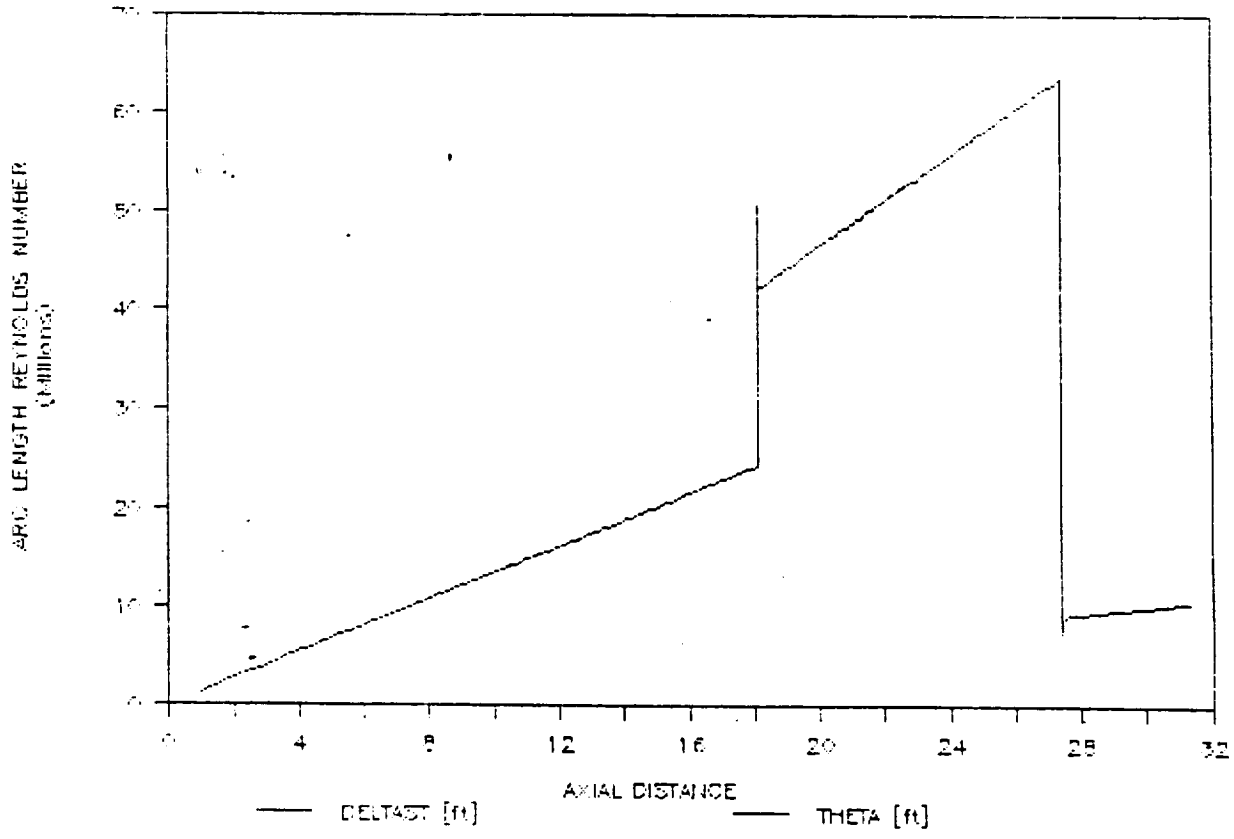

FIGURE 26: Mach Number vs. Axial Distance on Final Design

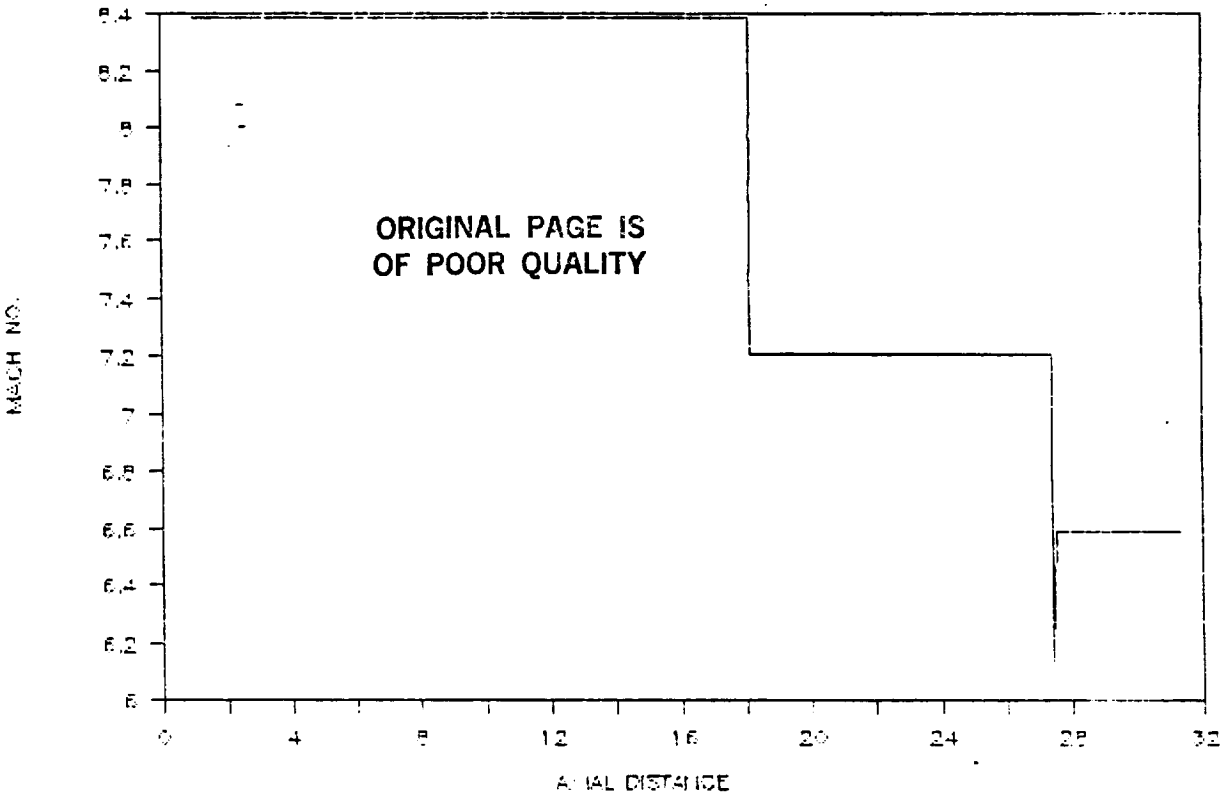

FIGURE 27

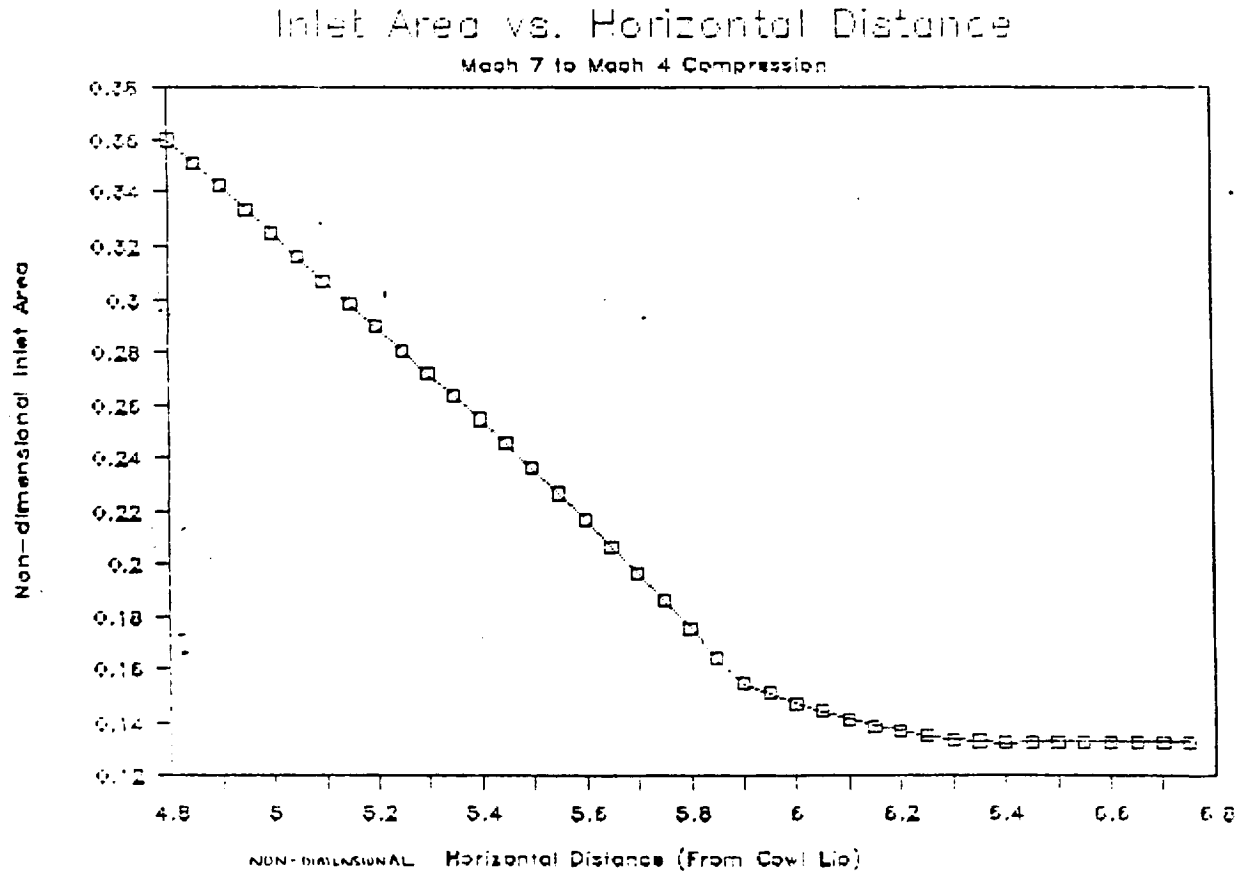

FIGURE 28

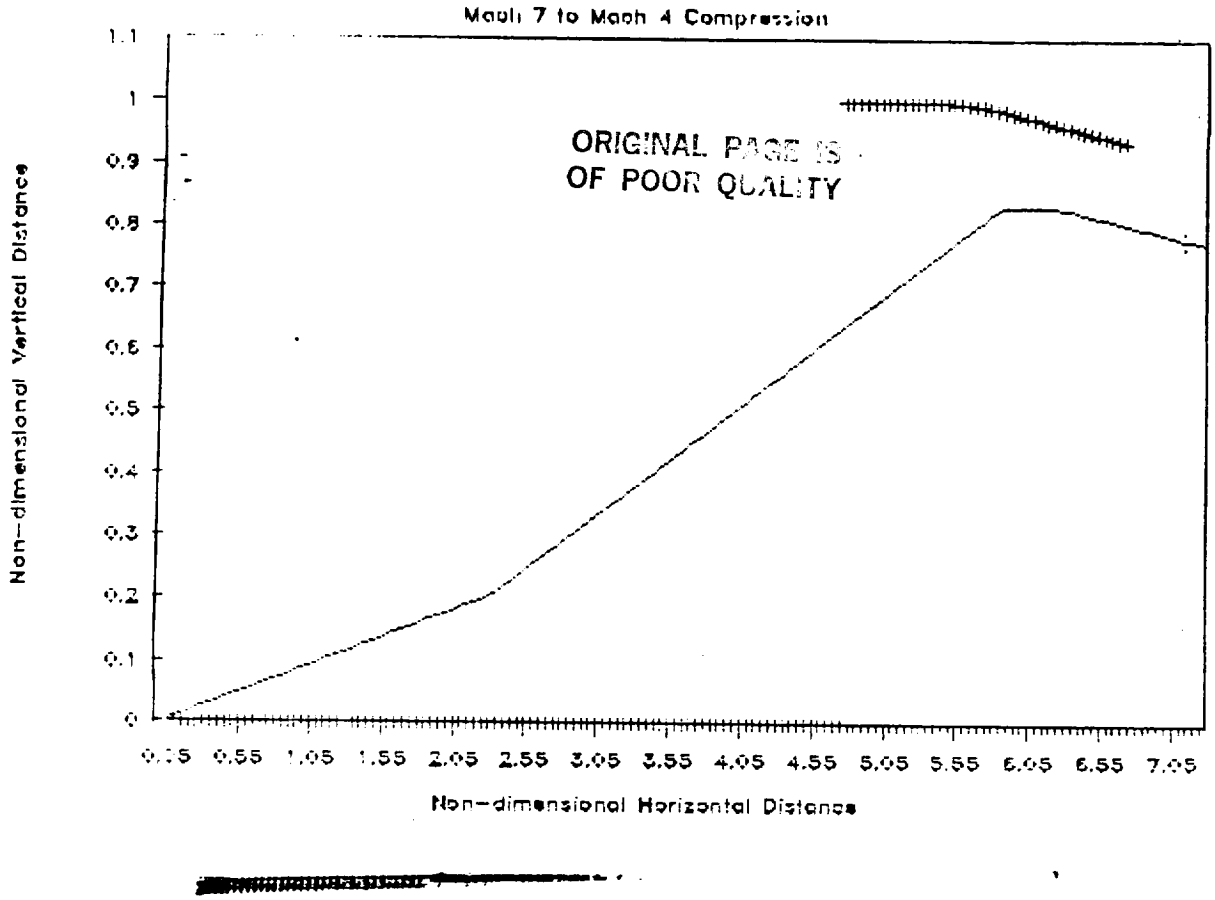

FIGURE 29

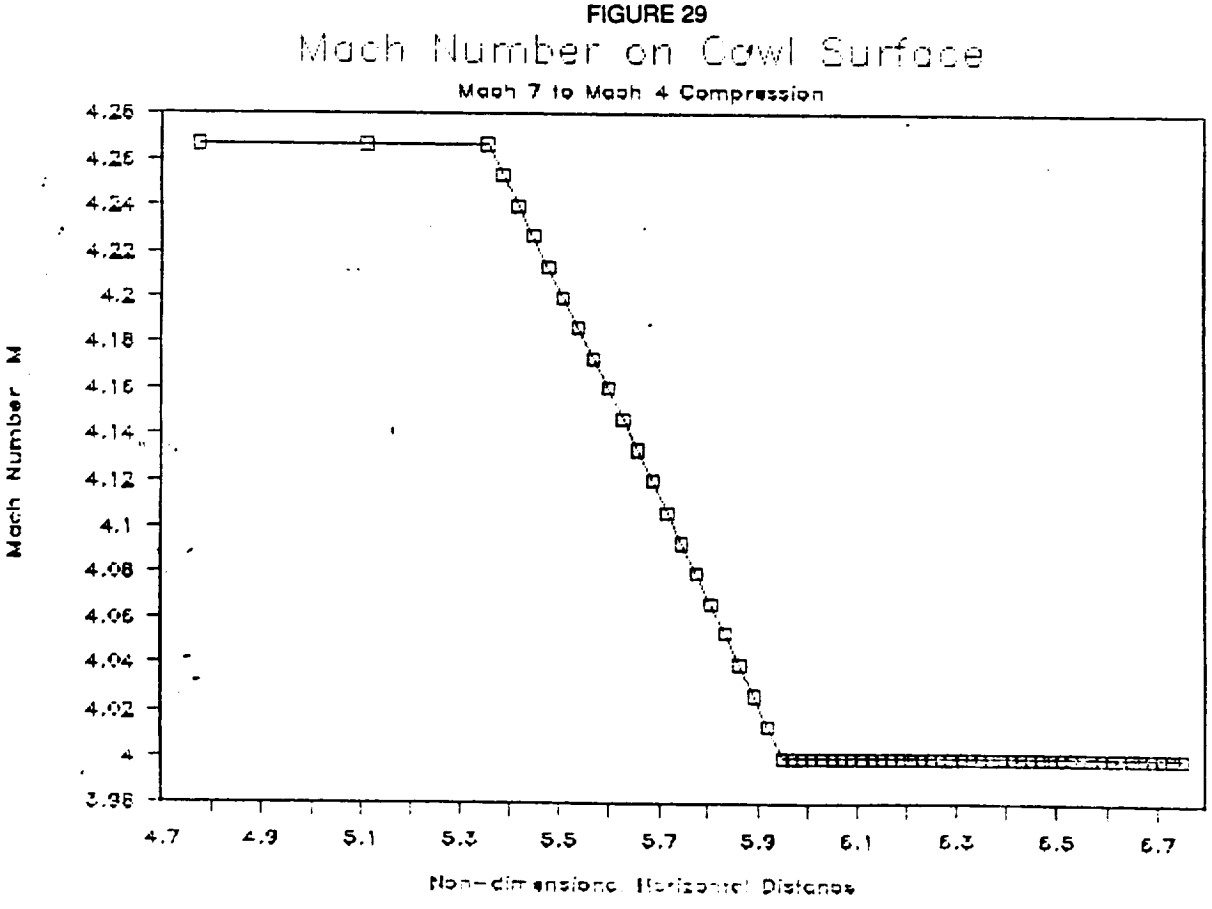

FIGURE 30

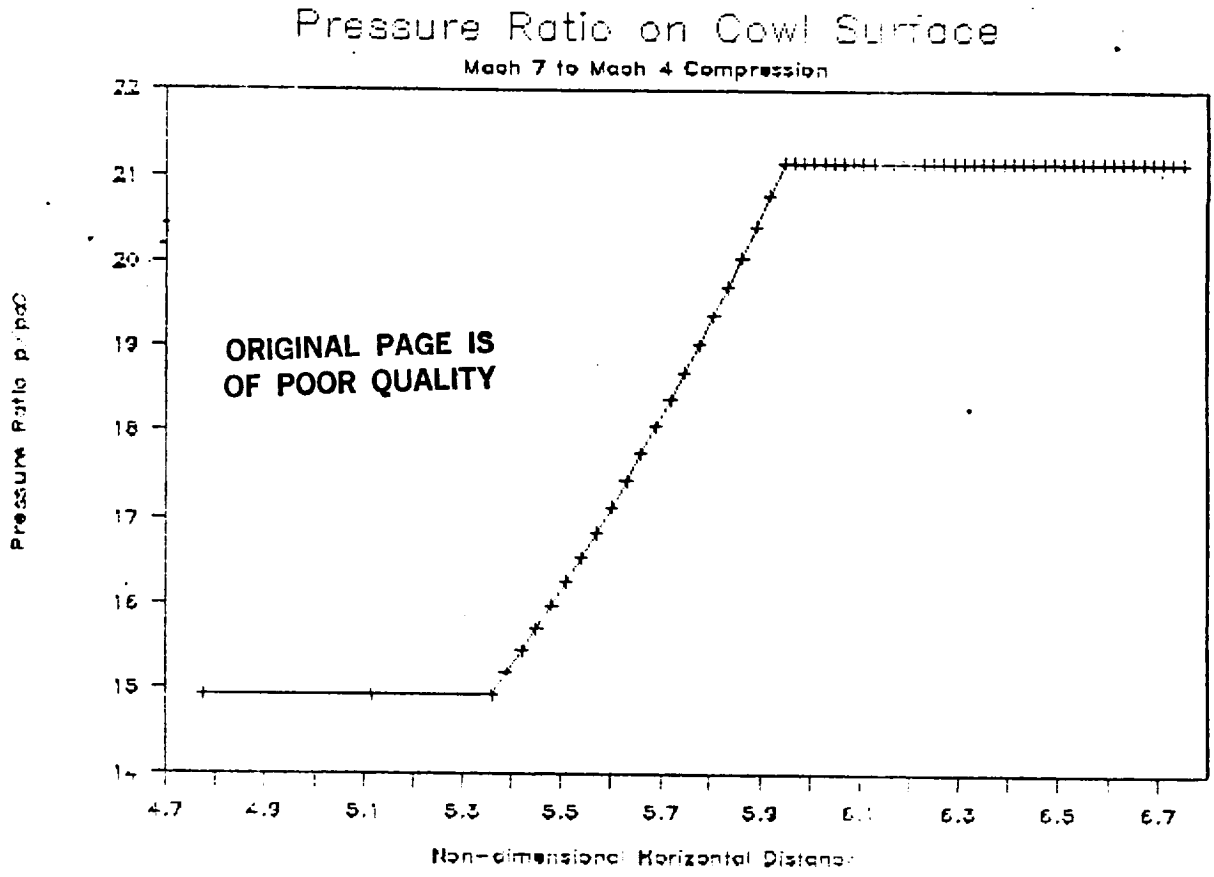

FIGURE 31

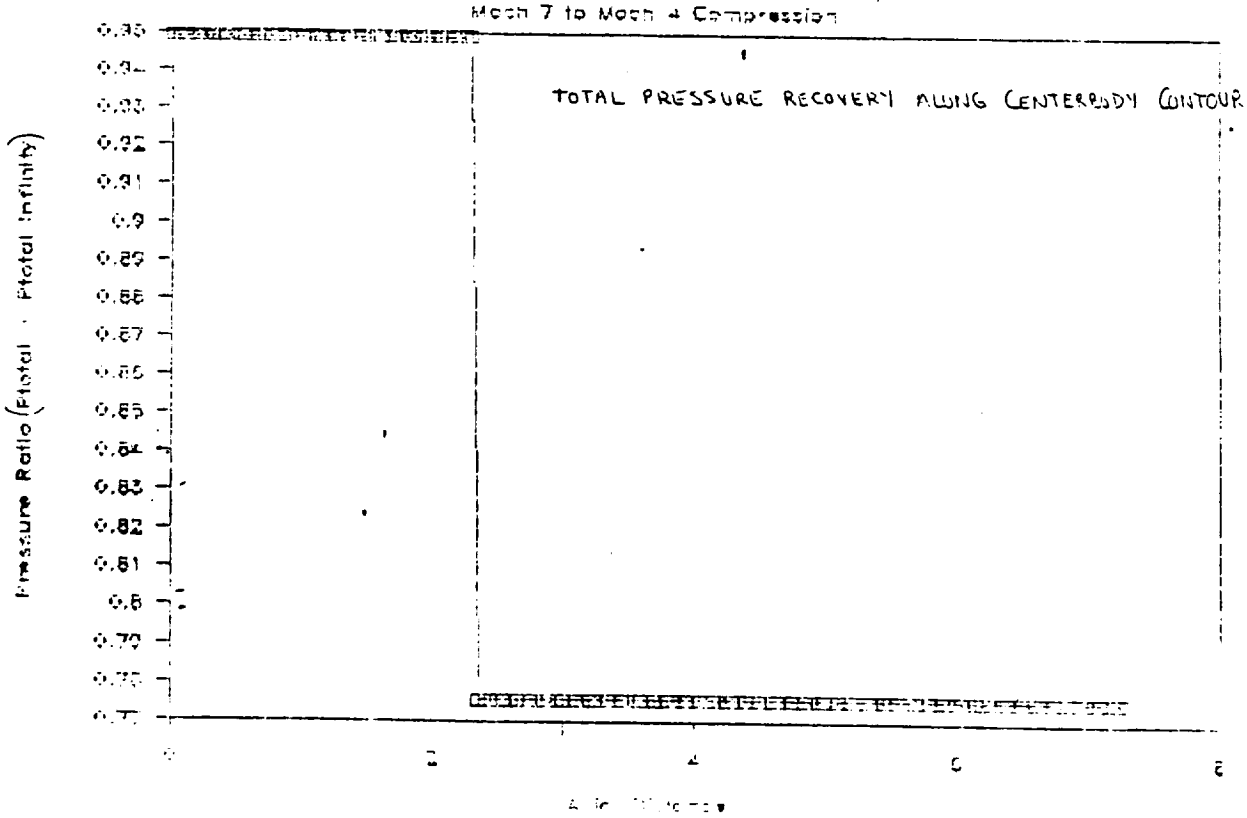

FIGURE 32

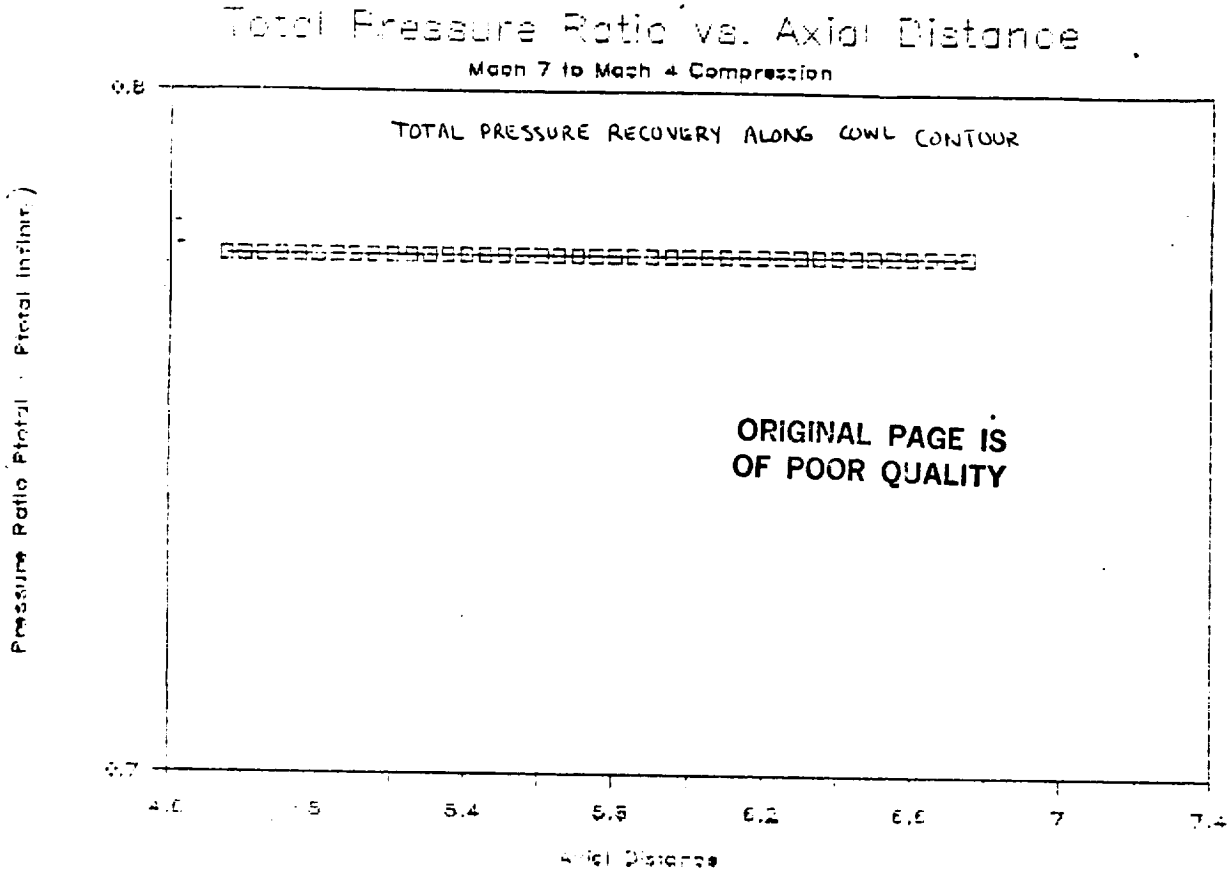

FIGURE 33 Geometry of the Combustor

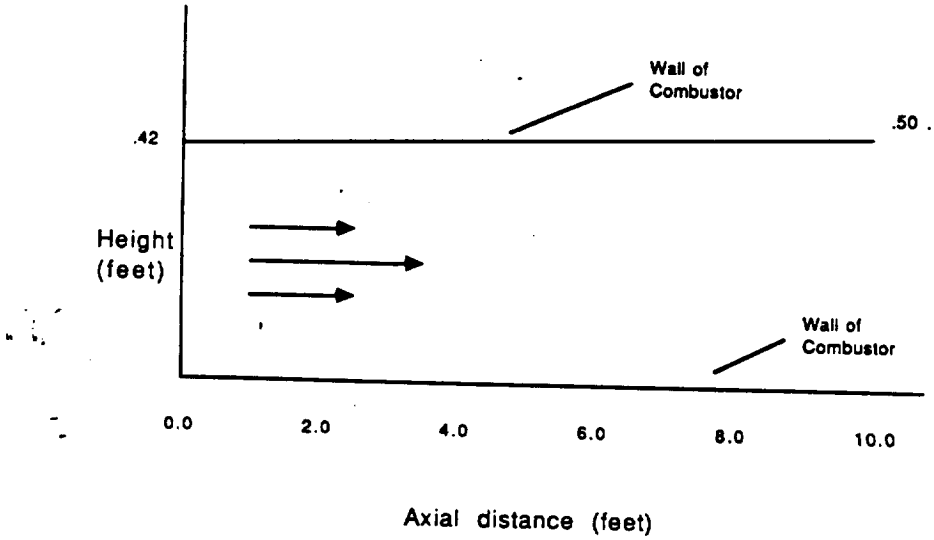

TABLE 3 Information on Injectors

	Injector #1	Injector #2
Axial Distance	3.75 ft.	5.0 ft
Fuel stagnation Temperature	1000 K	1000 K
Fuel stagnation Pressure	4758000.0 N/m2	4758000.0 N/m2
Mach Number	1.0	3.0
Injector angle from horizontal	0.78 Radians	0.0 Radians
Wall angle at injector	0.0 Radians	1.57 Radians

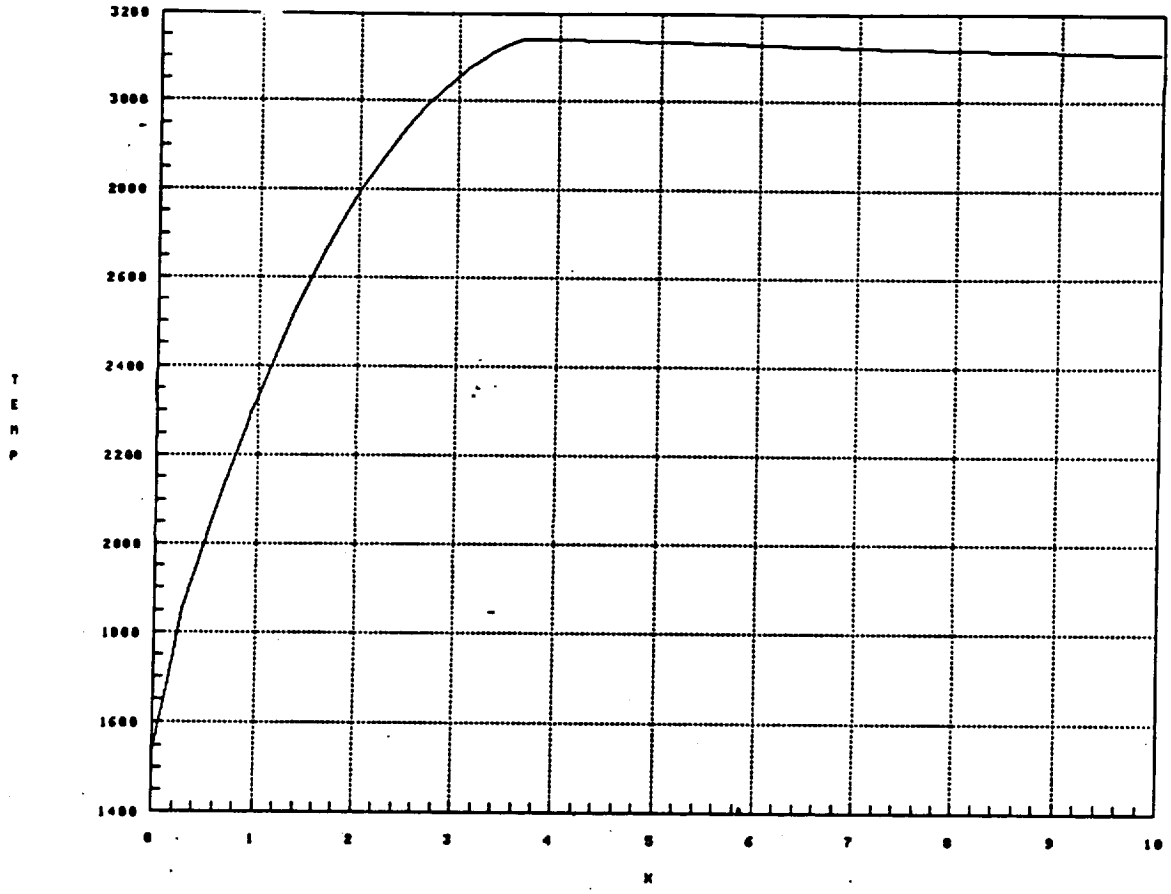

FIGURE 34: Combustor Temperature vs. Combustor Axial Distance

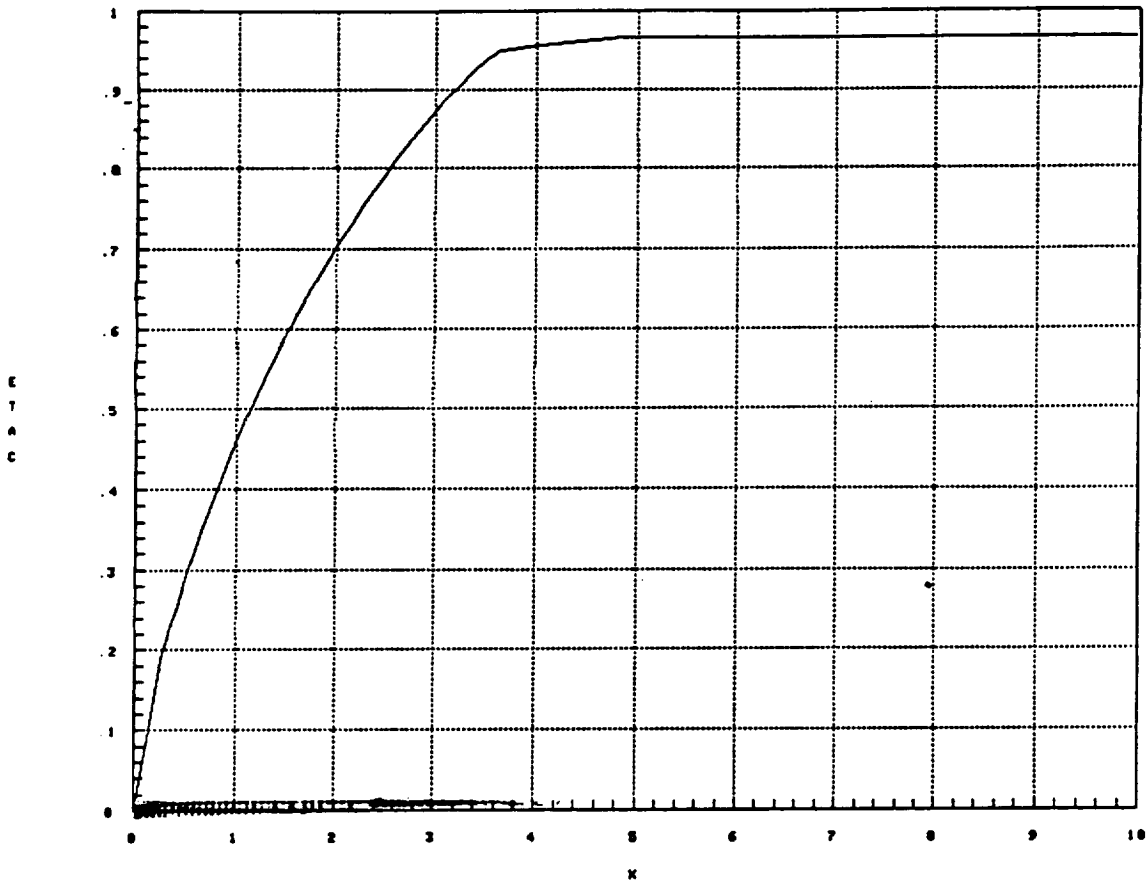

FIGURE 35: Combustor Efficiency vs. Combustor Axial Distance

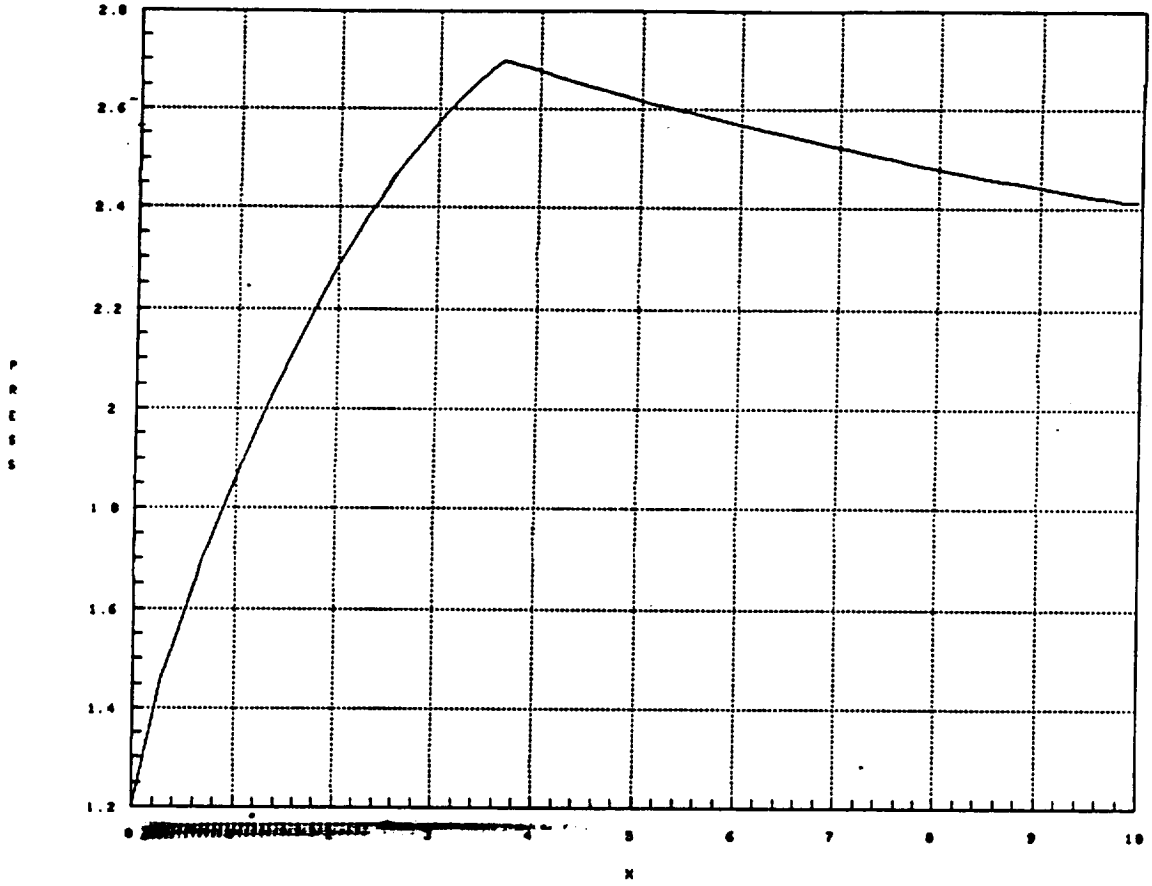

FIGURE 36: Combustor Pressure vs. Combustor Axial Distance

ORIGINAL PAGE IS
OF POOR QUALITY

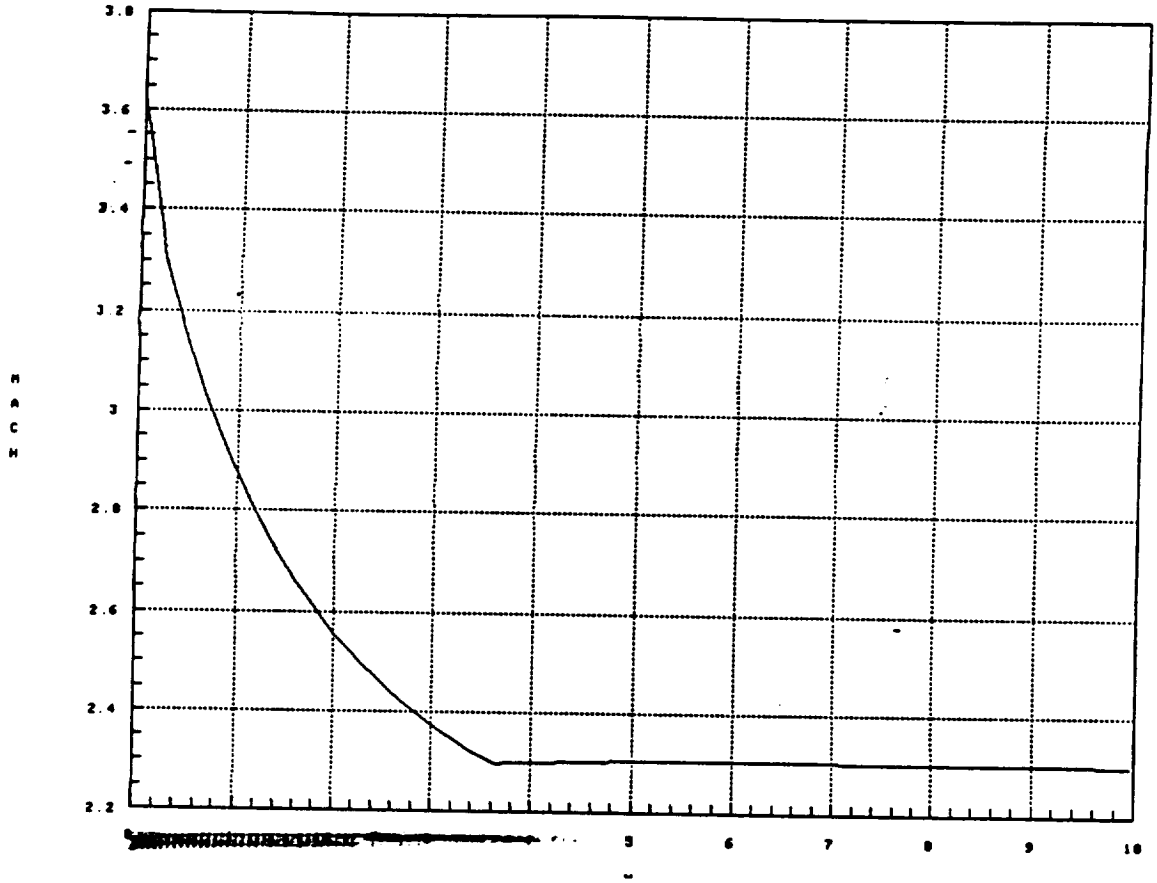

FIGURE 37: Combustor Mach No. vs. Combustor Axial Distance

FIGURE 38 - ISOLATED LIFT DRAG AND MOMENT COEFFICIENTS

NOTES:

1. "A" Point of application of forces.
2. Free stream pressure has been subtracted from all surfaces prior to integrations.

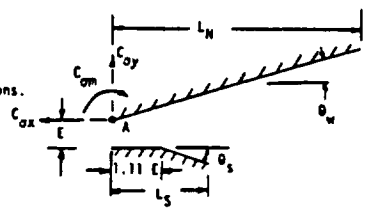

$C_{oy} = \frac{Lift}{q_\infty A_c}$

$C_{ox} = \frac{Thrust}{q_\infty A_c}$

$C_{om} = \frac{Moment}{q_\infty A_c L_N}$

$M_\infty = 4$

δw	L_N/E	θ_s	L_s/E	ϕ	C_{oy}	C_{ox}	C_{om}	P_∞/q
6.52	18.54	6.00	3.12	0.	-.536	-.015	.352	.0893
				1.0	1.966	.823	-.559	
12.02				0.	-1.021	-.1406	.547	
				1.0	1.033	.994	-.272	
19.8		0.		0.	-1.467	-.358	.655	
				1.0	-.044	1.107	.149	
		6.0	1.50	0.	-1.353	-.412	.737	
				1.0	.172	.802	.090	
			3.12	0.	-1.442	-.397	.744	
				1.0	-.138	1.065	.009	
			4.50	0.	-1.465	-.394	.747	
				1.0	-.325	1.113	.010	
		12.0	3.12	0.	-1.347	-.418	.752	
				1.0	-.090	1.041	.085	

$M_\infty = 6.0$

δ	L_N/E	θ_s	L_s/E	ϕ	C_{oy}	C_{ox}	C_{om}	P_∞/q
6.52	18.54	6.0	3.12	0.	.157	.076	.061	.0397
				1.	2.740	.777	-1.077	
12.02				0.	-.338	.022	.108	
				1.	1.643	1.043	-.775	
19.6		0.		0.	-.934	-.129	.269	
				1.	.186	1.183	-.631	
		6.	1.50	0.	-.645	-.169	.270	
				1.	.795	.944	-.468	
			3.12	0.	.771	-.128	.284	
				1.	.371	1.203	-.524	
			4.50	0.	-.871	-.114	.300	
				1.	-.054	1.241	-.497	
		12.0	3.12	0.	-.657	-.138	.275	
				1.	.280	1.167	-.420	

$M_\infty = 10$

δw	L_N/E	θ_s	L_s/E	ϕ	C_{oy}	C_{ox}	C_{om}	P_∞/q
6.52	18.54	6.00	3.12	0.	.431	.103	-.244	.0143
				1.5	2.260	.575	-1.069	
12.02				0.	-.062	-.075	.083	
				1.5	1.217	.757	.838	
14.83	27.02		1.50		1.565	.706	-.605	
			3.12		.996	.864	-.862	
			4.50		.556	.928	-.687	
19.8	18.54	0	3.12	0.	-.656	-.0338	.109	
				1.5	-.090	.796	-.705	
		6.0	1.50	0.	-.329	-.0336	-.0771	
				1.5	.703	.644	-.563	
			3.12	0.	.443	-.0192	.087	
				1.5	.102	.811	-.607	
			4.50	0.	-.545	-.008	.108	
				1.5	-.351	.845	-.501	
		12.0	3.12	0.	-	-	-	
				1.5	.208	.761	.475	
28.66	34.26	6.0	1.50		-.228	.462	-.395	
			3.12		-1.047	.548	-.219	
			6.50		-1.470	.592	-.074	

Appendix A1: SCRAM

Description

SCRAM is a one-dimensional airframe-integrated scramjet engine simulation program. It was written at the NASA Langley Research Center to give a first-order estimate of scramjet performance. SCRAM performs a real gas analysis for a five-stage model. These stages include the freestream, the vehicle forebody, the inlet, the combustor, and the exhaust nozzle. Once the flow for each stage is analyzed, the overall performance is calculated and a summary is given.

SCRAM is capable of analyzing: (1) oxygen, hydrogen, and air injection into the inlet and combustor; (2) axisymmetric or planar forebodies; (3) mixed combustion; (4) the boundary layer for a flat plate; (5) multistage perpendicular or parallel injection; (6) equilibrium or frozen flow referenced by area ratio in the combustor; (7) several internal hydrogen fuel mixing models; (8) a swept, symmetric wedge inlet, calculating inviscid real gas performance. The program only works for started inlets, and flow must be supersonic through the inlet and nozzle portions of the code. In addition, SCRAM is not usable if the combustor flow becomes subsonic. It is currently configured to handle two-dimensional engines only.

The freestream flowfield is calculated in Subroutine FSC1, where, given altitude, Mach number, and other parameters, it computes static temperature and pressure from a table based on the 1979 Standard Atmospheric Table. The other freestream flow properties are calculated from subroutines which find the real gas composition and the dynamic state variables.

The forebody flow properties are calculated in Subroutine FLOWF2. This subroutine accounts for forebody shocks, forebody boundary layer heat transfer, and friction losses, given the freestream conditions and forebody parameters. It utilizes a specified forebody kinetic energy efficiency that approximates engine capture flow momentum losses due to

the forebody shock system. Boundary layer properties and heat transfer through the boundary layer are calculated iteratively.

Subroutine INLET1 computes the flow properties for the inlet. It models flow through the inlet as supersonic flow undergoing a one-dimensional compression process with heat transfer and friction losses. Area ratio, length, and kinetic energy efficiency are the required inputs. INLET1 also is capable of handling oxygen/hydrogen mass flow injection.

The flow through the combustor is analyzed in Subroutine COMBUST. COMBUST uses perpendicular hydrogen fuel injection for up to seven injector stations; one of these stations can also be set for parallel injection. It approximates shock losses with the use of the kinetic energy efficiencies input by the user. Flow is initially assumed to be in equilibrium, but provisions can be made for frozen flow to occur. Regenerative cooling may also be taken into account.

Subroutine NOZZLE1 describes a one-dimensional expansion process simulating gas expansion for a scramjet nozzle. It computes boundary layer properties for freestream Mach numbers greater than 6.0, but neglects them for freestream Mach numbers less than 6.0.

Finally, subroutine SCRAP1 computes engine cycle performance parameters. It utilizes conservation of momentum equations applied to the engine as a whole, using engine geometry and flow properties computed by the component routines as inputs. It outputs thrust, specific impulse, and the coefficient of thrust as the scramjet performance parameters.

```
B   1    4  [10 DEG INLET, CRG=5.5, MO=7, (HPB RECIPE)]---> #4
    0
33863.2     7.0000     1.0303     0.0000    -8.8888    -888.88     200.01     7.000
2.5594     -8.8888     0.9990     0.1955    -1.0000     0.027266   555.55     4.000
    3    1 0.0000     4.4100    -1.0000
5.5000     -8.8888    555.55     0.0000     0.345719   10.000     -0.35287   0.514
0.0000     -888.88    0.0000    -8.8888    -888888.8   10.000     30.000    -8.888
5.5000     -8.8888    0.10581    0.94401    0.0271018
1.0000      1.0000    1.0000     496077.7   144117010.   14.000    0.0271018
0.0001      0.1000    1.0000     1.0000     1.0000     1.0000     1.0000
0.0100      0.0550    0.0804     0.1489     0.1820     0.2201     0.2582
0.0100      0.0677    0.09945    0.09945    0.06135    0.0423     0.06135
1.0000      200.00    555.55     00000.     00000.     00000.     200.00     5.400
-88888.8   -8888.8   -88888.8   -888.88    -8.8888
    1    3    2    2   -1       1.0000     0.0000     30.000     10.000     0.000
-.8888      1.0000    555.55     0.0000     0.12192    0.149098   2.0000        1
0.0000      0.0000    0.0000     0.0000     0.0000     0.0000     0.0000
```

---------scram.in--File: scram.in----Top---------

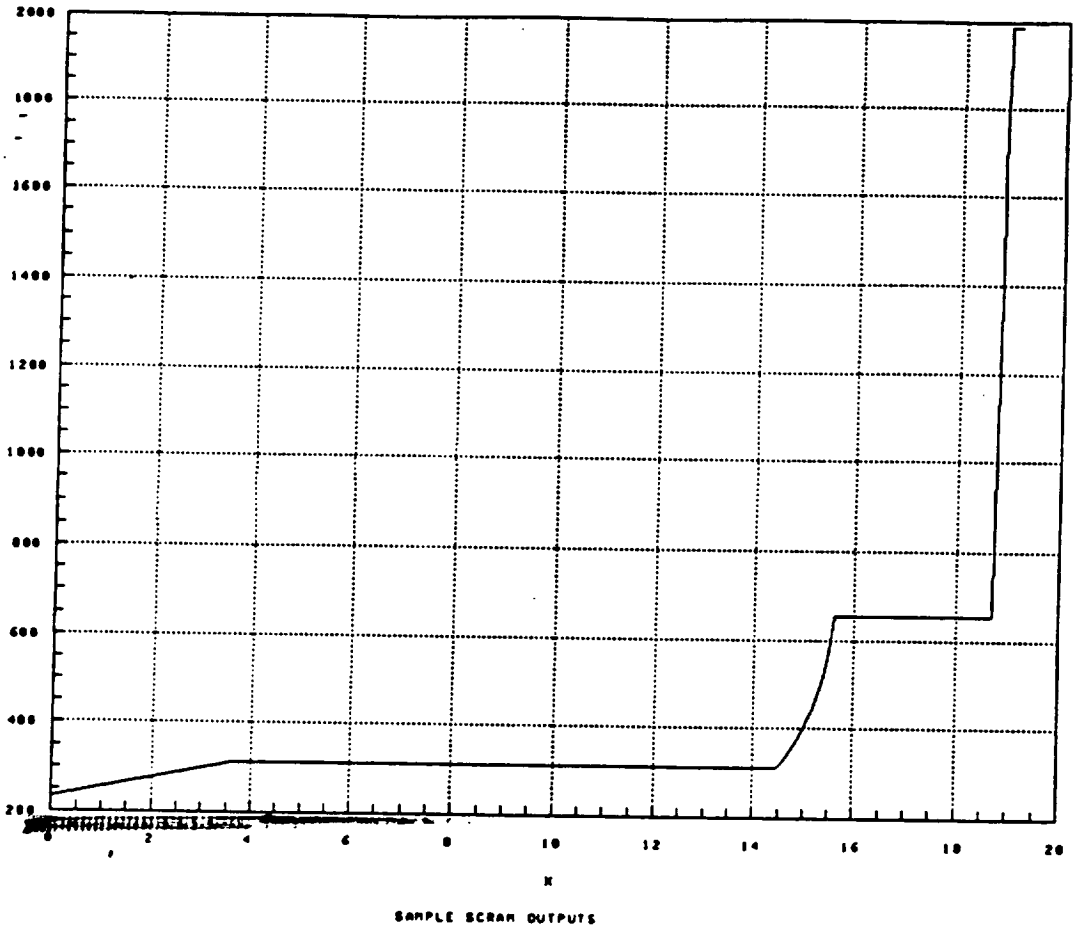

°K

SAMPLE SCRAM OUTPUTS

ORIGINAL PAGE IS
OF POOR QUALITY

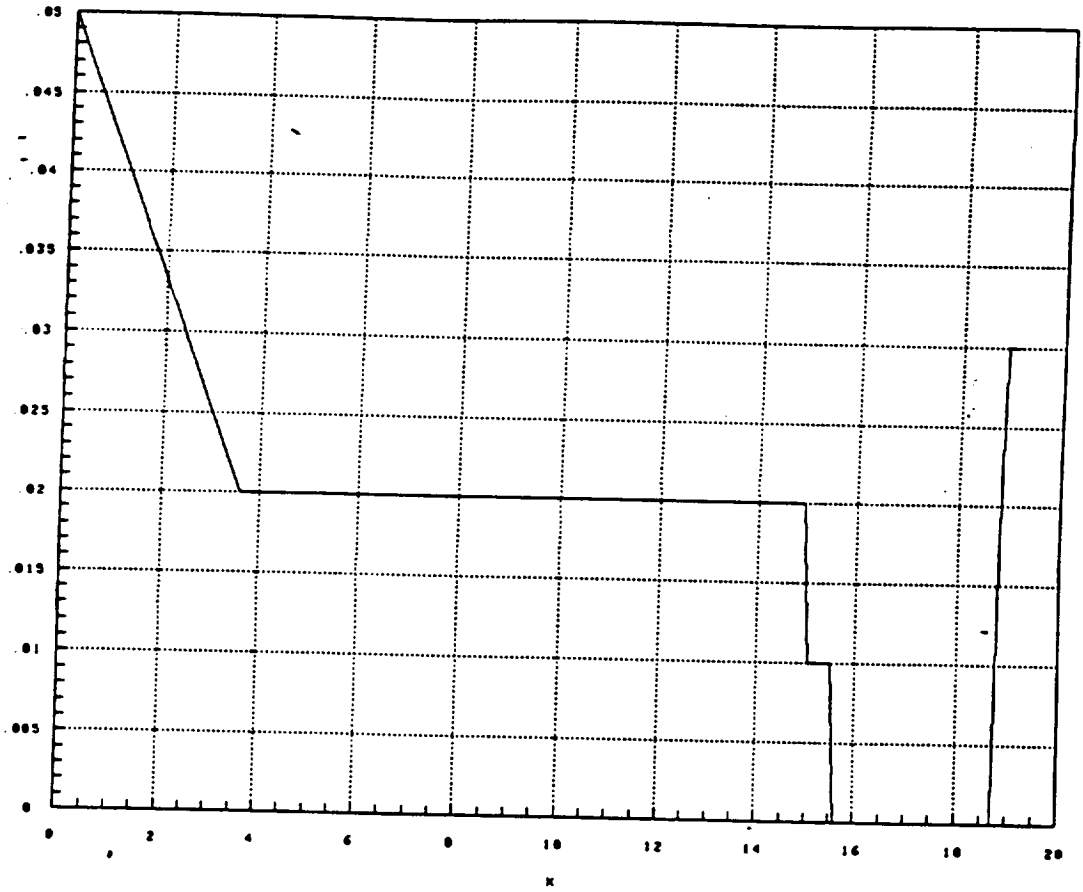

m^2 AREA

SAMPLE SCRAM OUTPUTS

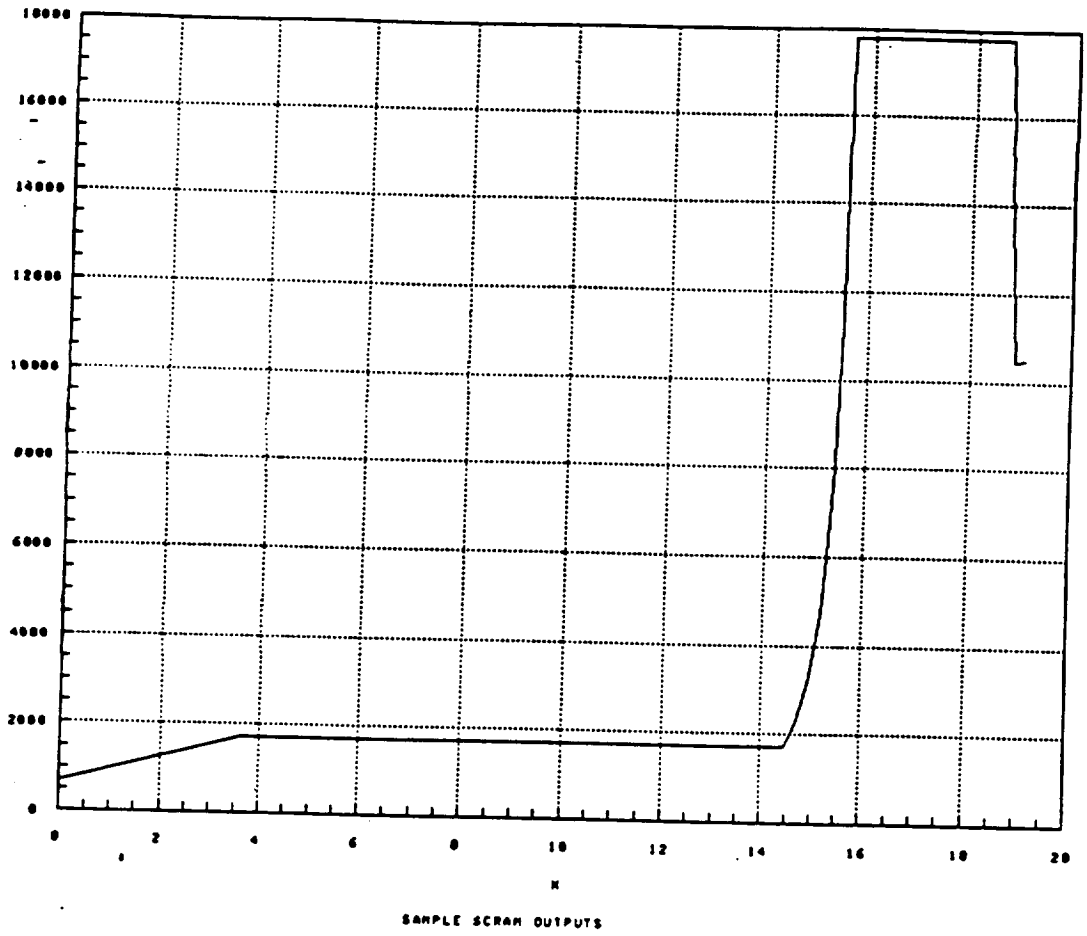

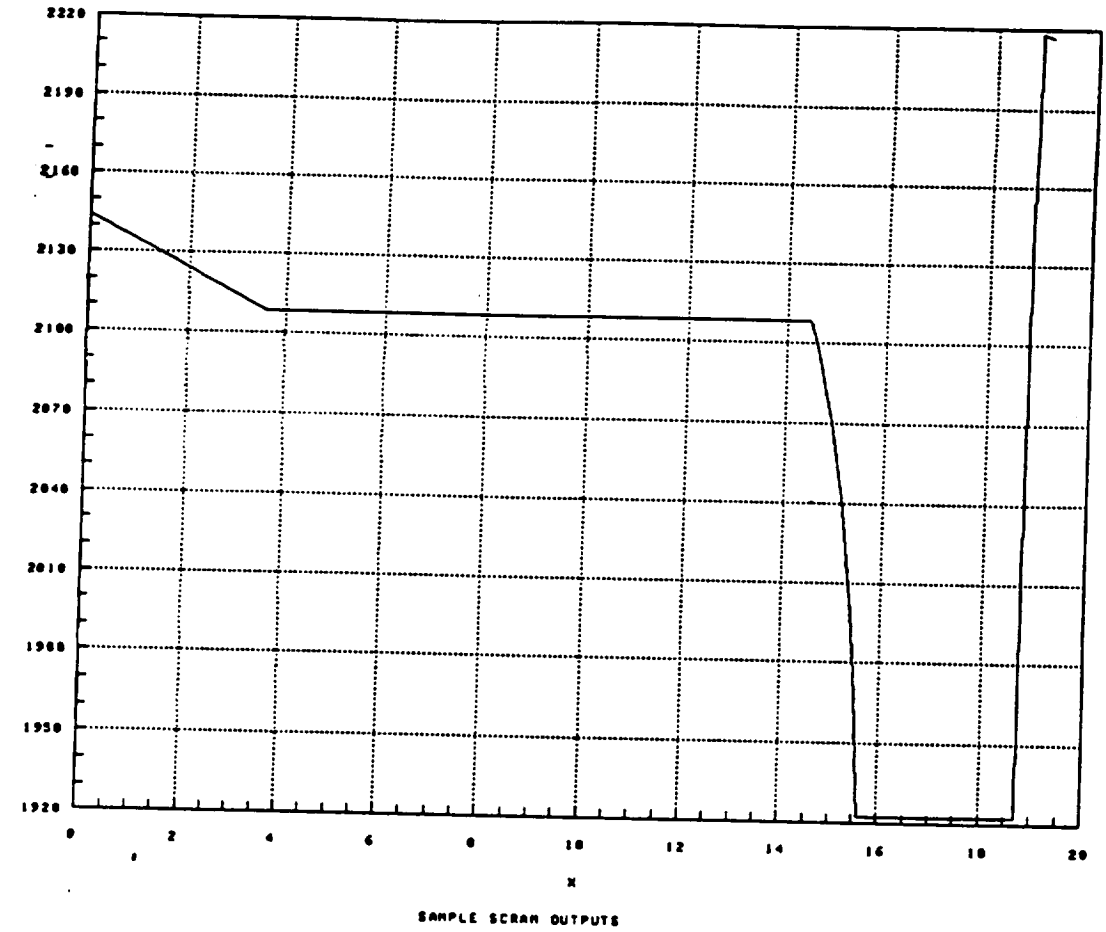

SAMPLE SCRAM OUTPUTS

ORIGINAL PAGE IS
OF POOR QUALITY

APPENDIX A2: STUB

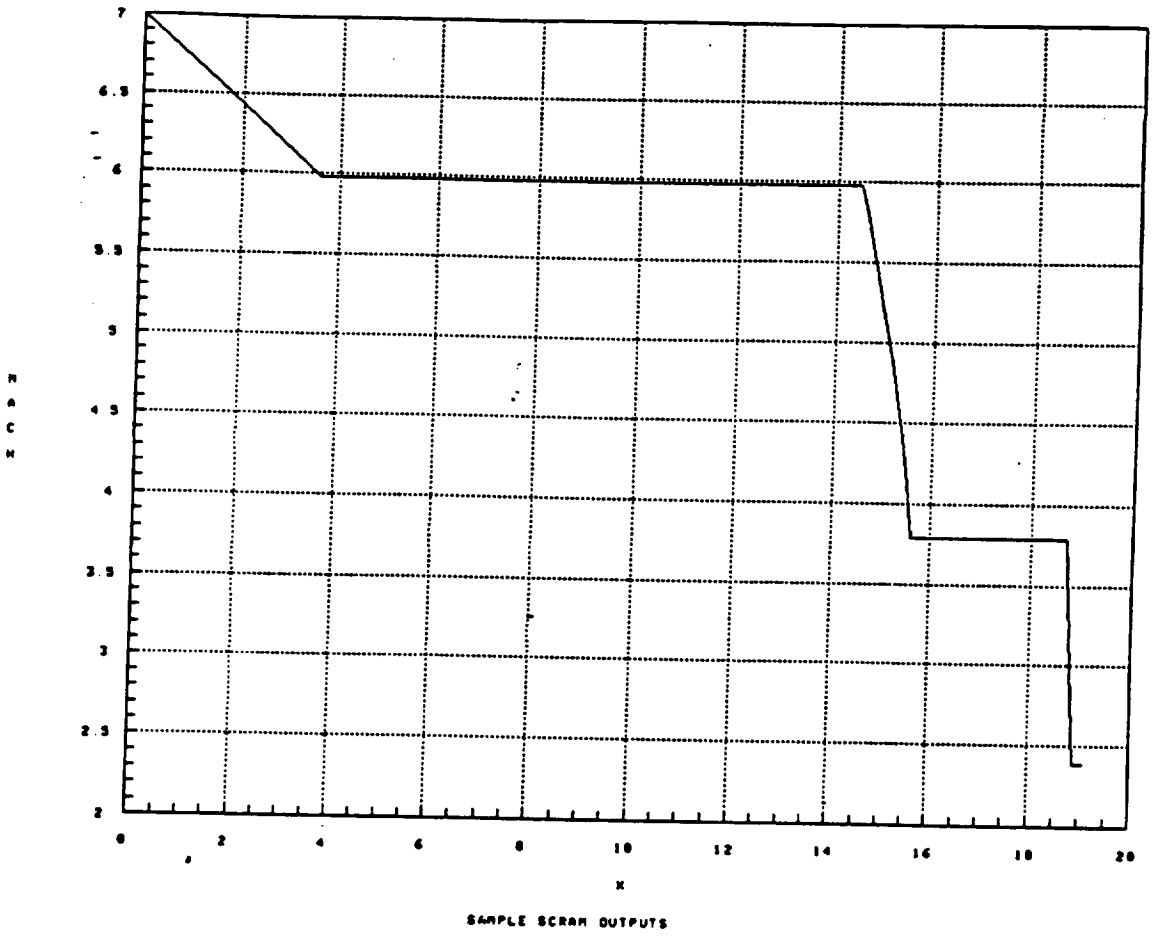

ORIGINAL PAGE IS
OF POOR QUALITY

INTRODUCTION

Since steady supersonic flow fields are governed by hyperbolic differential equations, whereas steady subsonic flow fields are described by elliptic differential equations (Reference 2), the mixed region behind the detached bow shock structure cannot be handled by any steady-flow technique. However, the unsteady Navier-Stokes conservation equations become hyperbolic with time, irregardless of the sonic nature of the flow. Therefore, the time-dependent technique becomes a simplified means through which the steady-state solution is attained.

Program Description

Details of the time-dependent technique are given in References 2, 3, and 4, and only a brief description is outlined here.

The flow field was covered with a mesh and transformed into a system of rectangular coordinates. Initial guesses for the shock structure and flow properties were inputted and non-dimensionalized. The flow field was divided into four regions and treated separately: [1] the shock, treated as a discontinuity; [2] the body, examined in the same manner as the shock; [3] the inner points between the shock and body, analyzed by the unsteady conservation equations; and [4] the upper boundary of the inner points, computed through linear extrapolation and restricted to lie beyond the sonic line. Time steps were taken in accordance to the CFL stability criterion outlined in References 2 and 3.

First, the shock was analyzed for each time step. At a particular time step, an initial guess for the shock velocity was made (the shock will

"move" through time until it converges onto its "steady-state" location), and the new shock location was found. Flow properties at the shock were determined by the Rankine-Hugoniot relations, presented in Reference 3.

A quasi-one-dimensional characteristic line was then drawn from this new shock location through time to an old inner point. Flow properties were obtained, and the characteristic line was computed. The information obtained was used in the compatibility equation given in Reference 3, and flow field variables obtained from the compatibility equation were then compared to values obtained from the Rankine-Hugoniot equations. A new shock velocity was guessed until these flow field variables converged. Thus, an iterative process was established: properties based on a given shock velocity were obtained from the Rankine-Hugoniot equations; different values were obtained from a characteristics approach and were determined independently by a compatibility equation; another shock velocity was guessed, and the process was repeated until flow field properties at the shock converged. Finally, another time step was taken, and the entire process was repeated.

A similar computaiton was performed for the body. The process was simplified, since the body points did not move with time.

The governing equations utilized for the inner points between the shock and body are presented in the form given in Reference 3.

The spatial derivatives on the right-hand side were evaluated using finite differences. MacCormack's predictor-corrector technique was utilized in determining the flow field properties after a given time step, and details of the procedure can be found in Reference 2.

Finally, for an upper boundary condition beyond the sonic line, the flow is supersonic. That is, any information obtained there will not affect properties lying below the sonic line, and upper boundary values may then

simply be linearly extrapolated

All flow field properties were therefore computed in this manner for each time step taken.

```
C
C     Program STUB          Jerry Yen
C     Version 5.28.88
C
C          This program will utilize the time-dependent technique to construc
C     the shock structure generated by a supersonic blunt body.
C
C          Limitations:
C               First-order accuracy for spatial derivatives
C               2 - D analysis
C
C        NOTE:  M,N = 8,8
C
C
        PROGRAM STUB
          COMMON pi,gamma,vinf,pinf,roinf,ainf,k,
     .           u(8,8),v(8,8),p(8,8),ro(8,8),sp(8,2),bp(8,2),b(8),
     .           dbdy(4)
C
C     Need to input actual numbers for m,n in ALL COMMON blocks
C        Also, need m,n for REAL block below
C
          Real pi,gamma,vinf,pinf,roinf,ainf,k,
     .           u,v,p,ro,sp,bp,b,dbdy,
     .           epss,epsb,epst,delx,dely,delt,wt0(4),theta(4),
     .           capc(8,8),capp(8,8),capr(8,8),capb(8,8),psi(8,8),
     .           zeta(4),del(4),pause,delzet
          Integer m,n,step,ichoice,jk,tt
          print* , ' Please input number of grid points (n,m):  '
          read* , n,m
          print* ,' Please input number of time steps:  '
          read* , step
          call INDAT(m,n,epss,epsb,epst)
          call START(m,n,delx,dely,delt)
        Do 10 j = 1, m
   10     wt0(j) = 0.
        Do 50 jk = 1, step
          call ATSHK(wt0,delt,epss,theta)
          call ATBODY(m,n,dely,delt,epsb)
          call CAP(m,n,theta,delx,wt0,capc,capp,capr,capb,psi,
     .           zeta,del)
          call ATINTR(capc,capp,capr,capb,psi,dely,delzet,del,delt)
          call BNDRY(m,n)
          pause = step/jk
          if (pause.ge.0.25.and.pause.lt.0.5) then
                print* ,' Number of time steps:  ',jk
                print* ,' Do you want to continue? '
                print* ,'     [1] Yes  [2] No'
                read* ,ichoice
                if (ichoice.eq.1) then
                   call OP(m,n,jk)
                else
                   goto 60
                endif
          elseif (pause.ge.0.5.and.pause.lt.0.75) then
                print* ,' Number of time steps:  ',jk
                print* ,' Do you want to continue? '
                print* ,'     [1] Yes  [2] No'
                read* ,ichoice
                if (ichoice.eq.1) then
                   call OP(m,n,tt)
```

```
            elseif (pause.ge.0.75.and.pause.lt.0.9) then
                print* ,' Number of time steps:  ',jk
                print* ,' Do you want to continue? '
                print* ,'     [1] Yes  [2] No'
                read* ,ichoice
                if (ichoice.eq.1) then
                   call OP(m,n,tt)
                else
                   goto 60
                endif
            endif
 50    continue
 60     Print* ,'          END OF PROGRAM  '
        Print* ,'  Number of time steps = ',jk
        call OPFIN(m,n,step)
        stop
        end

C
C================================================
C           SUBROUTINE INDAT
C================================================
C
        Subroutine INDAT(m,n,epss,epsb,epst)
          COMMON pi,gamma,vinf,pinf,roinf,ainf,k,
     .           u(8,8),v(8,8),p(8,8),ro(8,8),sp(8,2),bp(8,2),b(8),
     .           dbdy(4)
          integer m, n
          Real pi,gamma,vinf,pinf,roinf,ainf,k,u,v,p,ro,sp,bp,b,
     .         epss,epsb,epst,arg,dbdy
          open(3,file='shock.dat')
C
C       Upstream conditions and number of grid points are inputted
C         (m refers to the total number of y points, n refers to the
C         total number of x points); k refers to axisymmetric geometry
C
          read(3,*) vinf,pinf,roinf,gamma,k,epss,epsb,epst

          arg = gamma*pinf/roinf
          ainf = SQRT(arg)
C
C       j refers to the y location; inputted are the x locations for
C         the given j (y location); thus, the arrays contain a set of 2
C         numbers:  the x and y location for the body and shock in
C         the physical plane
C
          Do 20 j = 1, m
             read(3,*) (bp(j,i),i=1,2),(sp(j,i),i=1,2),dbdy(j)
 20       continue
C
C       Initial guesses for u, p, and ro are inputted; i and j refer
C         to points in the physical plane equidistant from each other;
C         thus, the arrays contain one number:  the value of the property
C         at the location x,y (i,j)
C
          Do 40 j = 1, m
            Do 30 i = 1, n
              read(3,*) u(j,i),v(j,i),p(j,i),ro(j,i)
 30         continue
 40       continue
          close(3)
          return
          end
```

```
C
      Subroutine START(m,n,delx,dely,delt)
        COMMON pi,gamma,vinf,pinf,roinf,ainf,k,
     .          u(8,8),v(8,8),p(8,8),ro(8,8),sp(8,2),bp(8,2),b(8),
     .          dbdy(4)
        Real pi,gamma,vinf,pinf,roinf,ainf,k,u,v,p,ro,sp,bp,b,
     .    -    dbdy,
     .    -    delx(m),dely(m),delt,deltx,delty,arg,a
        Integer n,m
        delt = 1000.0
        Do 20 j = 1, m
          delx(j) = (1.0/FLOAT(n-1))*(sp(j,1)-bp(j,1))
          dely(j) = bp(m,2)/FLOAT(m-1)
          b(j) = bp(j,2)
          Do 10 i = 1, n
            p(i,j) = p(i,j)/pinf
            ro(i,j) = ro(i,j)/roinf
            u(i,j) = u(i,j) * SQRT(roinf/pinf)
            v(i,j) = v(i,j) * SQRT(roinf/pinf)
            arg = gamma*p(i,j)/ro(i,j)
            a = SQRT(arg)
            deltx = delx(j)/(u(j,i) + a)
            delty = dely(j)/(v(j,i) + a)
            if (deltx.lt.delty.and.deltx.lt.delt) then
                delt = deltx/1.5
            elseif (delty.lt.deltx.and.delty.lt.delt) then
                    delt = delty/1.5
            endif
 10       continue
 20     continue
        return
        end
```

ORIGINAL PAGE IS
OF POOR QUALITY

```
C
C=============================================
C          SUBROUTINE CAP
C=============================================
C
      Subroutine CAP(m,n,theta,delx,w,capc,capp,capr,capb,psi,
     .          zeta,del)
      COMMON pi,gamma,vinf,pinf,roinf,ainf,k,
     .          u(8,8),v(8,8),p(8,8),ro(8,8),sp(8,2),bp(8,2),b(8),
     .          dbdy(4)
      Real pi,gamma,vinf,pinf,roinf,ainf,k,
     .     u,v,p,ro,sp,bp,b,dbdy,
     .     theta(m),delx(m),w(m),capc(m,n),capp(m,n),capr(m,n),
     .     capb(m,n),psi(m,n),zeta(m,n),del(m)
      Integer m,m1,n,n1
      m1=m-1
      n1=n-1
      Do 20 j = 1, m
        Do 10 i = 1, n
          del(j) = sp(j,1) - bp(j,1)
          zeta(j,i) = (i-1)*delx(j)
          capc(j,i) = (zeta(j,i)-1.0)*dbdy(j) - (zeta(j,i)/
     .                TAN(theta(j)))
          capp(j,i) = ALOG(p(j,i))
          capr(j,i) = ALOG(ro(j,i))
          capb(j,i) = (u(j,i)-w(j)*zeta(j,i)+v(j,i)*capc(j,i))/
     .                (sp(j,i)-bp(j,i))
```

```
      20    continue
            return
            end
```

ORIGINAL PAGE IS
OF POOR QUALITY

```
C
C=============================================================
C
C       This is good for converting inner point parameter values into
C         values at a certain location
C
C            Subroutine OP(
C
C             x and y locations
C
C             bp(j,2) = y location (at j)
C             bp(j,1) = x location for given y location (j)
C              n1 = n-1
C             x location of particular grid point at y ( = bp(j,2)):
C              Do 20 j = 1, m
C                y(j) =
C                dx = (1.0/(FLOAT(n1)) * (sp(j,1) - bp(j,1))
C                 Do 10 i = 1, n
C  10             x(j,i) = (n-i) * dx  +  bp(j,1)
C  20            continue
C
C          Thus, the value at that x and y location is:
C                u(j,x)
C          The shock's x value at a given j/y location is:
C                sp(j,1)
C                return
C             end
C
C
C
C
C
C=============================================
C            SUBROUTINE ATSHK
C=============================================
C
          Subroutine ATSHK(wt0,delt,epss,theta)
           COMMON pi,gamma,vinf,pinf,roinf,ainf,k,
     .             u(8,8),v(8,8),p(8,8),ro(8,8),sp(8,2),bp(8,2),
     .             dbdy(4)
            Real pi,gamma,vinf,pinf,roinf,ainf,k,u,v,p,ro,sp,bp,dbdy,
C
C****** NOTE:  The next two lines require m's actual value
C
     .             spnew(8,2),wguess(4),ushk0(4),pshk0(4),roshk0(4),
     .             vshk0(4),
     .             theta(m),arg,wt0(m),delt,epss,ushk,pshk,roshk,vshk,
     .             dedt,ptap(2),pta(2),dely,delz,incry,incrz,
     .             ypos1,ypos2,zpos1,zpos2,uy1,uy2,vy1,vy2,py1,py2,roy1,
     .             roy2,ua1,va1,ua,va,pa,roa,aa,ptap1(2),compx,compy,
     .             rhsa1,rhsa2,rhsa3,rhsa,rhshk1,rhshk2,rhshk3,rhshk,rhs,
     .             ucmpat,diff
            Integer j,jj,jjj,ii,m,n,m1,n1,ichoice
C
C       The shock point is moved, according to wt0, and at the same y
C          location; also found is theta, the angle between the tangent
C          to the shock and the x-axis
C
            Do 10 j=1,m
              spnew(j,1) = wt0(j) * delt + sp(j,1)
```

```
            if (jjj.eq.1) then
              theta(1) = pi/2.
               go to 5
            elseif (jjj.eq.m) then
              jjj = m - 1
            endif
            arg = (spnew(jjj+1,2) - spnew(j-1,2))/(spnew(jjj+1,1)
                  - spnew(j-1,1))
            theta(j) = ATAN(arg)
  5         call EOSHK(wt0(j),theta(j),ushk0(j),pshk0(j),roshk0(j),
                  vshk0(j))
 10       continue
C
C       The Rankine-Hugoniot equations are used to determine u, p, and
C          ro on the shock
C
          wguess(j) = 1.0
         Do 20 j = 1, m
100       call EOSHK(wguess(j),theta(j),ushk,pshk,roshk,vshk)
          arg = gamma*pshk/roshk
          ashk = SQRT(arg)
C
C       A characteristic is drawn from the new shock point to a point A,
C          and u, p, and ro are interpolated at A(t0)
C
          dedt = ushk - ashk
          ptap(1) = spnew(j,1) + dedt*delt*SIN(theta(j))
          ptap(2) = spnew(j,2) - dedt*delt*COS(theta(j))
110       pta(1) = (ptap(1) - bp(j,1))/(spnew(j,1) - bp(j,1))
          pta(2) = ABS(ptap(2))
          m1 = m - 1
          n1 = n - 1
          ii = 1
          jj = 1
          dely = bp(m,2)/float(m1)
          delz = 1.0/float(n1)
120       incry = pta(2)/(dely*jj)
          if (incry.ge.1.) then
               jj = jj + 1
               go to 120
          else
130            incrz = pta(1)/(delz * ii)
               if (incrz.ge.1.) then
                       ii = ii + 1
                       go to 130
               endif
          endif
          ypos1 = dely * jj
          ypos2 = dely * (jj-1)
          zpos1 = delz * ii
          zpos2 = delz * (ii-1)
        jj = jj + 1
        ii = ii + 1
        if (jj.gt.m.or.ii.gt.n) then
           print* ,' THERE IS A PROBLEM IN ATSHK '
           print* ,' Please begin with a new w '
           go to 1150
        endif
         call INTERP(zpos1,zpos2,pta(1),u(jj,ii),u(jj,ii-1),uy1)
         call INTERP(zpos1,zpos2,pta(1),v(jj,ii),v(jj,ii-1),vy1)
         call INTERP(zpos1,zpos2,pta(1),p(jj,ii),p(jj,ii-1),py1)
         call INTERP(zpos1,zpos2,pta(1),ro(jj,ii),ro(jj,ii-1),roy1)
         call INTERP(zpos1,zpos2,pta(1),u(jj-1,ii),u(jj-1,ii-1),uy2)
         call INTERP(zpos1,zpos2,pta(1),v(jj-1,ii),v(jj-1,ii-1),vy2)
```

```
      C                 ypos1,ypos2,pta(2),uy1,uy2,ua1)
            call INTERP(ypos1,ypos2,pta(2),vy1,vy2,va1)
            ua = ua1 * SIN(theta(j)) - va1 * COS(theta(j))
            va = ua1 * COS(theta(j)) + va1 * SIN(theta(j))
            call INTERP(ypos1,ypos2,pta(2),py1,py2,pa)
            call INTERP(ypos1,ypos2,pta(2),roy1,roy2,roa)
            arg = gamma * pa/roa
            aa = SQRT(arg)
C
C     A new characteristic slope is computed, and A locations are
C        evaluated and compared, and iterated until convergence
C
            dedt = (dedt + (ua - aa))/2.
            ptap1(1) = spnew(j,1) + dedt*delt*SIN(theta(j))
            ptap1(2) = spnew(j,2) - dedt*delt*COS(theta(j))
            compx = ABS(ptap1(1) - ptap(1))
            compy = ABS(ptap1(2) - ptap(2))
            if (compx.gt.epss.or.compy.gt.epss) then
                  ptap(1) = ptap1(1)
                  ptap(2) = ptap1(2)
                  go to 110
            else
                  pta(1)=(ptap1(1)-bp(j,1))/(sp(j,1)-bp(j,1))
                  pta(2) = ABS(ptap1(2))
            endif
C
C     The right side of the compatibility equation is computed at
C        A and at the new shock point
C
           rhsa1 = (va*aa/gamma)*((py1-py2)/dely)*SIN(theta(j))
           rhsa2 = aa*((uy1*COS(theta(j))+vy1*SIN(theta(j)))-(uy2*
          .          COS(theta(j))+vy2*SIN(theta(j))))*SIN(theta(j))/dely
           rhsa3 = va*((uy1*SIN(theta(j))-vy1*COS(theta(j)))-(uy2*
          .          SIN(theta(j))-vy2*COS(theta(j))))*SIN(theta(j))/dely
           rhsa = -1.0*(rhsa1+rhsa2-rhsa3)
           jjj = j
           if (jjj.eq.1) then
              rhshk = 0.
              go to 500
           elseif(jjj.eq.m) then
                  jjj = m - 1
           endif
           rhshk1 = (ashk*vshk0(j)/gamma)*(pshk0(jjj+1)-pshk0(jjj-1))*
          .          SIN(theta(j))/dely
           rhshk2 = ashk*(vshk0(jjj+1)-vshk0(jjj-1))*SIN(theta(j))/del
           rhshk3 = vshk*(ushk0(jjj+1)-ushk0(jjj-1))*SIN(theta(j))/del
           rhshk = -1.0*(rhshk1+rhshk2-rhshk3)
  500      rhs = 0.5 * (rhsa + rhshk)
C
C*       WGUESS is evaluated and a new guess is inputted if desired
C
            ucmpat = (ashk*ALOG(pshk/pinf) - aa*ALOG(pa/pinf))/gamma
          .        + ua - ( rhs ) * delt
            diff = ABS(ucmpat - ushk)
            write(*,1000) ushk, ucmpat, diff
 1000       format(//,' U from Rankine-Hugoniot =  ',E10.6,/,
          .          ' U from compatibility    =  ',E10.6,//,
          .          ' Difference              =  ',E10.6,//)
            print* ,' '
            print* ,'   CONTINUE ITERATION ([1] YES; [2] NO)?'
            read* , ichoice
            if (ichoice.eq.1) then
                write(*,1100) wguess(j)
 1100           format(//,' Most recent guess for w =   ',E10.6,/)
```

```
            read* , wguess(j)
            go to 100
          else
            call EOSHK(wguess(j),theta(j),ushk,pshk,roshk,vshk)
            u(j,n) = vshk*COS(theta(j)) + ushk*SIN(theta(j))
            v(j,n) = vshk*SIN(theta(j)) - ushk*COS(theta(j))
            p(j,n) = pshk
            ro(j,n) = roshk
            wt0(j) = wguess(j)
            sp(j,1) = spnew(j,1)
            sp(j,2) = spnew(j,2)
          endif
 20     continue
          return
          end
```

ORIGINAL PAGE IS
OF POOR QUALITY

```
C
C=================================================
C           SUBROUTINE ATBODY
C=================================================
C
      Subroutine ATBDY(m,n,dely,delt,epsb,phi,capp,capr,capv)
        COMMON pi,gamma,vinf,pinf,roinf,ainf,k,
     .          u(8,8),v(8,8),p(8,8),ro(8,8),sp(8,2),bp(8,2),
     .          dbdy(4)
        Real pi,gamma,vinf,pinf,roinf,ainf,k,u,v,p,ro,sp,bp,dbdy,
     .          phi(m),capp(m),capr(m),capv(m),dely,dpdy,drdy,drdt,
     .          dvdy,v1,diff,delt,epsb
        Integer m,n,jjj
        Do 10 j = 1, m
          jjj = j
          if (jjj.eq.1) then
            phi(1) = pi/2.
            go to 5
          elseif (jjj.eq.m) then
            jjj = m - 1
          endif
          arg = (sp(jjj+1,2) - sp(j-1,2))/(sp(jjj+1,1)
     .                - sp(j-1,1))
          phi(j) = ATAN(arg)
 5        capp(j) = ALOG(p(j,1))
          capr(j) = ALOG(ro(j,1))
          capv(j) = v(j,1)/SIN(phi(j))
 10     continue
C
C       J = 1 is evaluated already
C
        Do 20 j = 2, m1
          p(j,1) = p(1,1)-(roinf*vinf*vinf)+(roinf*vinf*vinf*
     .          COS(phi(j))**2)
          dpdy = (capp(j+1)-capp(j-1))/(dely*2.0)
          drdy = (capr(j+1)-capr(j-1))/(dely*2.0)
 15       drdt = (1.0/gamma)*(dpdy-gamma*drdy)*v(j,1)
          dvdy = (capv(j+1)-capv(j-1))/(dely*2.0)
          capr(j) = capr(j) + drdt*delt
          ro(j,1) = (2.718281828)**capr(j)
          dvdt = -v(j,1)*dvdy-(p(j,1)/ro(j,1))*dpdy*SIN(phi(j))
          v1 = (capv(j) + dvdt*delt)*SIN(phi(j))
          diff = ABS(v(j,1)-v1)
          if (diff.gt.epsb) then
            v(j,1) = v1
            go to 15
          else
```

```
                v(j,1) = v1
                u(j,1) = v(j,1)*TAN(phi(j))
              endif
   20       continue
            return
            end
```

ORIGINAL PAGE IS
OF POOR QUALITY

```
C
C=================================================
C          SUBROUTINE ATINTR
C=================================================
C
C         ATINTR calculates interior point properties:
C            capr(i,j), u(i,j), v(i,j), psi(i,j)
C
C
C
C     Note that input values need to be transferred to subroutine;
C          also, variable(m,n) needs to have m and n transferred;
C          don't forget that (m,n) refers only to INTERIOR points
C
        Subroutine ATINTR(capc,capp,capr,capb,psi,dely,delzet,del,
     .           delt)
          COMMON pi,gamma,vinf,pinf,roinf,ainf,k,
     .            u(8,8),v(8,8),p(8,8),ro(8,8),sp(8,2),bp(8,2),
     .            dbdy(4)
           Real pi,gamma,vinf,pinf,roinf,ainf,k,u,v,p,ro,sp,bp,dbdy,
     .           capc(m,n),capp(m,n),capr(m,n),capb(m,n),psi(m,n),
     .           delzet,dely,del(m),delt,drdz,drdy,dudz,dudy,dvdz,dvdy,
     .           dpsidz,dpsidy,dpdz,dpdy,
C
C*******NOTE:  The next 3 line require m's actual value
C
     .           dudt(8,8),dvdt(8,8),dpsidt(8,8),drdt(8,8),rbar(8,8),
     .           ubar(8,8),vbar(8,8),psibar(8,8),pbar(8,8),caprnw(8,8),
     .           unew(8,8),vnew(8,8),psinew(8,8),
     .           dudt1,dvdt1,dsdt1,drdt1,drdtav,dudtav,dvdtav,dsdtav
          Integer n,m,n1,m1
          n1 = n - 1
          delzet = 1.0/FLOAT(n1)
          m1 = m - 1
          Do 20 j = 1, m1
            Do 10 i = 2, n1
C
C       For all interior (i,j), spatial derivatives are calculated
C
              call FWD(capr(j,i),capr(j+1,i),delzet,drdz)
              call FWD(capr(j,i),capr(j,i+1),dely,drdy)
              call FWD(u(j,i),u(j+1,i),delzet,dudz)
              call FWD(u(j,i),u(j,i+1),dely,dudy)
              call FWD(v(j,i),v(j+1,i),delzet,dvdz)
              call FWD(v(j,i),v(j,i+1),dely,dvdy)
              call FWD(psi(j,i),psi(j+1,i),delzet,dpsidz)
              call FWD(psi(j,i),psi(j,i+1),dely,dpsidy)
              call FWD(p(j,i),p(j+1,i),delzet,dpdzeta)
              call FWD(p(j,i),p(j,i+1),dely,dpdy)
              call EOMOT(j,i,capc(j,i),capp(j,i),capr(j,i),capb(j,i),
     .           psi(j,i),del(j),drdz,dudz,dvdz,dpdz,dudy,dvdy,drdy,
     .           dpdy,dpsidz,dpsidy,dudt(j,i),dvdt(j,i),dpsidt(j,i),
     .           drdt(j,i))
              rbar(j,i) = capr(j,i) + (drdt(j,i) * delt)
```

```
                vbar(j,i) = v(j,i) + (dvdt(j,i) * delt)
                psibar(j,i) = psi(j,i) + (dpsidt(j,i) * delt)
                pbar(j,i) = psibar(j,i) + gamma*rbar(j,i)
   10         continue
   20       continue
C
C         J = 1 is first analyzed;  the rest are analyzed accordingly
C
          Do 15 i = 2, n1
             call REAR(rbar(1,i),rbar(1,i-1),delzet,drdz)
             call REAR(rbar(1,i),rbar(2,i),dely,drdy)
             call REAR(ubar(1,i),ubar(1,i-1),delzet,dudz)
             call REAR(ubar(1,i),ubar(2,i),dely,dudy)
             call REAR(vbar(1,i),vbar(1,i-1),delzet,dvdz)
             call REAR(vbar(1,i),vbar(2,i),dely,dvdy)
             call REAR(psibar(1,i),psibar(1,i-1),delzet,dpsidz)
             call REAR(psibar(1,i),psibar(2,i),dely,dpsidy)
             call REAR(pbar(1,i),pbar(1,i-1),delzet,dpdzeta)
             call REAR(pbar(1,i),pbar(2,i),dely,dpdy)
             call EOMOT(1,i,capc(1,i),capp(1,i),capr(1,i),capb(1,i),
     .          psi(1,i),del(1),drdz,dudz,dvdz,dpdz,dudy,dvdy,drdy,
     .          dpdy,dpsidz,dpsidy,dudt1,dvdt1,dsdt1,drdt1)
             drdtav = 0.5 * (drdt(1,i) + drdt1)
             dudtav = 0.5 * (dudt(1,i) + dudt1)
             dvdtav = 0.5 * (dvdt(1,i) + dvdt1)
             dsdtav = 0.5 * (dpsidt(1,i) + dsdt1)
             caprnw(1,i) = capr(1,i) + (drdtav * delt)
             unew(1,i) = u(1,i) + (dudtav * delt)
             vnew(1,i) = v(1,i) + (dvdtav * delt)
             psinew(1,i) = psi(1,i) + (dsdtav * delt)
   15      continue
           Do 40 j = 2, m1
              Do 30 i = 2, n1
             call REAR(rbar(j,i),rbar(j,i-1),delzet,drdz)
             call REAR(rbar(j,i),rbar(j-1,i),dely,drdy)
             call REAR(ubar(j,i),ubar(j,i-1),delzet,dudz)
             call REAR(ubar(j,i),ubar(j-1,i),dely,dudy)
             call REAR(vbar(j,i),vbar(j,i-1),delzet,dvdz)
             call REAR(vbar(j,i),vbar(j-1,i),dely,dvdy)
             call REAR(psibar(j,i),psibar(j,i-1),delzet,dpsidz)
             call REAR(psibar(j,i),psibar(j-1,i),dely,dpsidy)
             call REAR(pbar(j,i),pbar(j,i-1),delzet,dpdzeta)
             call REAR(pbar(j,i),pbar(j-1,i),dely,dpdy)
             call EOMOT(j,i,capc(j,i),capp(j,i),capr(j,i),capb(j,i),
     .          psi(j,i),del(j),drdz,dudz,dvdz,dpdz,dudy,dvdy,drdy,
     .          dpdy,dpsidz,dpsidy,dudt1,dvdt1,dsdt1,drdt1)
             drdtav = 0.5 * (drdt(j,i) + drdt1)
             dudtav = 0.5 * (dudt(j,i) + dudt1)
             dvdtav = 0.5 * (dvdt(j,i) + dvdt1)
             dsdtav = 0.5 * (dpsidt(j,i) + dsdt1)
             caprnw(j,i) = capr(j,i) + (drdtav * delt)
             unew(j,i) = u(j,i) + (dudtav * delt)
             vnew(j,i) = v(j,i) + (dvdtav * delt)
             psinew(j,i) = psi(j,i) + (dsdtav * delt)
   30        continue
   40      continue
         Do 105 j = 1,m1
            Do 90 i = 2, n1
               u(j,i) = unew(j,i)
               v(j,i) = vnew(j,i)
               ro(j,i) = (2.718281828)**(caprnw(j,i))
               arg = psinew(j,i) + gamma*caprnw(j,i)
               p(j,i) = (2.718281828)**arg
   90       Continue
  105    Continue
```

```
      end
```

ORIGINAL PAGE IS
OF POOR QUALITY

```
C
C=================================================
C           SUBROUTINE BNDRY
C=================================================
C
      Subroutine BNDRY(m,n)
        COMMON pi,gamma,vinf,pinf,roinf,ainf,k,
     .         u(8,8),v(8,8),p(8,8),ro(8,8),sp(8,2),bp(8,2),
     .         dbdy(4)
        Real pi,gamma,vinf,pinf,roinf,ainf,k,u,v,p,ro,sp,bp,dbdy
        Integer m,n
          Do 10 i = 1, n
            u(m,i) = ((u(m-1,i)-u(m-2,i))/u(m-2,i))*
     .               u(m-1,i) + u(m-1,i)
            v(m,i) = ((v(m-1,i)-v(m-2,i))/v(m-2,i))*
     .               v(m-1,i) + v(m-1,i)
            p(m,i) = ((p(m-1,i)-p(m-2,i))/p(m-2,i))*
     .               p(m-1,i) + p(m-1,i)
            ro(m,i) = ((ro(m-1,i)-ro(m-2,i))/ro(m-2,i))*
     .               ro(m-1,i) + ro(m-1,i)
   10       Continue
      return
      end

C
C=================================================
C           SUBROUTINE FWD
C=================================================
C
C       FWD generates the forward spatial derivative at (i,j):
C           dvardxij
C

      Subroutine FWD(varij,varilj,dx,dvardxij)
        Real varij,varilj,dx,dvardxij
          dvardxij = (varilj - varij)/dx
      return
      end


C
C=================================================
C           SUBROUTINE REAR
C=================================================
C
C       REAR generates the rearward spatial derivative at i,j:
C           dvdxij1
C

      Subroutine REAR(varij,varimlj,dx,dvdxij1)
        Real varij,varimlj,dx,dvdxij1
          dvdxij1 = (varij - varimlj)/dx
      return
      end

C
C=================================================
```

```
C          SUBROUTINE INTERP
C=================================================
C
C       INTERP interpolates for a value answer
C
        Subroutine INTERP(row1,row2,mid,col1,col2,answer)
          Real row1,row2,mid,col1,col2,answer
            answer = ((mid-row2)*(col1-col2))/(row1-row2) + col2
        return
        end

C
C=================================================
C          SUBROUTINE EOMOT
C=================================================
C
C       EOMOT computes values for time derivatives of the
C          equations of motion at (i,j):
C          drdt, dudt, dvdt, dpsidt
C

        Subroutine EOMOT(j,i,capc,capp,capr,capb,psi,del,drdz,dudz,
     .             dvdz,dpdz,dudy,dvdy,drdy,dpdy,dpsidz,dpsidy,dudt,dvdt,
     .             dsdt,drdt)
          COMMON pi,gamma,vinf,pinf,roinf,ainf,k,
     .             u(8,8),v(8,8),p(8,8),ro(8,8),sp(8,2),bp(8,2),
     .             dbdy(4)
           Real pi,gamma,vinf,pinf,roinf,ainf,k,u,v,p,ro,sp,bp,dbdy,
     .             capc,capp,capr,capb,psi,del,drdz,drdy,dudz,dudy,dvdz,
     .             dvdy,dpsidz,dpsidy,dpdz,dpdy,dudt,dvdt,dpsidt,drdt,y
          Integer i,j,m,n
           y = 1.0
           drdt = -((capb * drdz) + (dudz/del) +
     .       ((capc/del) * dvdz) + dvdy + (v(j,i)*drdy) +
     .       (k*(v(j,i)/y)))
           dudt = -((capb*dudz)+(v(j,i)*dudy)+((p(j,i)/(ro(j,i)*del))
     .          * dpdzeta))
           dvdt =-((capb*dvdz)+(v(j,i)*dvdy)+(((p(j,i)*capc)/(ro(j,i)*
     .          del)) * dpdzeta) + ((p(j,i)/ro(j,i)) * dpdy))
           dpsidt = -((capb * dpsidz) + (v(j,i) * dpsidy))
        return
        end

C
C=================================================
C          SUBROUTINE EQSHK
C=================================================
C
C       Rankine-Hugoniot relations
C

        Subroutine EQSHK(w,theta,ushk,pshk,roshk,vshk)
          COMMON pi,gamma,vinf,pinf,roinf,ainf,k,
     .          u(8,8),v(8,8),p(8,8),ro(8,8),sp(8,2),bp(8,2),
     .          dbdy(4)
           Real pi,gamma,vinf,pinf,roinf,ainf,k,u,v,p,ro,sp,bp,dbdy,
     .          w,theta,une1,ushk,pshk,roshk,vshk
         une1 = (gamma-1.)*((vinf-w)*SIN(theta))**2+2.*ainf*ainf
         ushk = une1/((gamma+1.)*(vinf-w)*SIN(theta))+w*SIN(theta)
         pshk = (2.*((vinf-w)*SIN(theta))**2-(gamma-1.))/(gamma+1.)
         roshk = ((gamma+1.)*pshk+(gamma-1.))/((gamma+1.)+
     .          (gamma-1.)*pshk)
         vshk = vinf * COS(theta)
        return
        end
```

```
C=======================================================
C           SUBROUTINE OP
C=======================================================
C
C       OP outputs values in the physical plane
C
        Subroutine OP(m,n,tt)
          COMMON pi,gamma,vinf,pinf,roinf,ainf,k,
     .          u(8,8),v(8,8),p(8,8),ro(8,8),sp(8,2),bp(8,2),
     .          dbdy(4)
           Real pi,gamma,vinf,pinf,roinf,ainf,k,u,v,p,ro,sp,bp,dbdy,
C
C******** NOTE:  the next line requires actual m,n values
C
     .          x(8,5),y(8),dx
           Integer tt
           Open(4,file='shock.out')
                write(4,1000) tt
 1000           format(//,'  TIME STEP NUMBER:  ',I4,//)
                write(4,1020)
 1020           format(///,'              OUTPUT FROM STUB      ',///,
     .          '    PHYSICAL LOCATIONS OF GRID POINTS: ',//)
                write(4,1040)
 1040           format(5X,'   I       X         J       Y ',/)
           Do 20 j = 1, m
              y(j) = bp(j,2)
              dx = (1.0/(FLOAT(n-1)))*(sp(j,1)-bp(j,1))
              Do 10 i = 1, n
                x(j,i) = (n-i) * dx + bp(j,1)
                write(4,1050) i,x,j,y
 1050           format(5X,I4,2X,F8.4,2X,I4,2X,F8.4)
   10         continue
   20      continue
           write(4,1060)
 1060      format(//,'   PHYSICAL LOCATIONS OF SHOCK AND BODY POINTS:',
     .     //,' (Note that x coordinates are presented for a given y)',
     .     5X,'    Y        X locations:   SHOCK        BODY   ',/)
           Do 40 j = 1, m
                write(4,1080) y(j),sp(j,1),bp(j,1)
 1080           format(5X,F8.4,16X,F8.4,3X,F8.4)
   40      continue
                write(4,1100)
 1100           format(//,'       PHYSICAL LOCATIONS AND VALUES OF FLOW
     .PROPERTIES:',//)
           Do 60 j = 1, m
              write(4,1150) y(j)
 1150         format(//,'       Y LOCATION:  ',F8.4,//)
              write(4,1175)
 1175  format(5X,'    X          U          V          P          RO   ',/)
              Do 50 i = 1, n
                write(4,1200) x(j,i),u(j,i),v(j,i),p(j,i),ro(j,i)
 1200           format(5X,F8.4,2X,4(F8.4,2X))
   50         continue
   60      continue
           Close(4)
           return
           end

C
C=======================================================
C           SUBROUTINE OPFIN
C=======================================================
C
C       OP outputs values in the physical plane
C
```

```
     .           u(8,8),v(8,8),p(8,8),ro(8,8),sp(8,2),bp(8,2),
     .           dbdy(4)
          Real pi,gamma,vinf,pinf,roinf,ainf,k,u,v,p,ro,sp,bp,dbdy,
C
C******** NOTE:  the next line requires actual m,n values
C
     .           x(8,8),y(8),dx
          Integer tt
          Open(2,file='shock.fin')
               write(2,1000) tt
 1000          format(//,'  TIME STEP NUMBER:  ',I4,//)
               write(2,1020)
 1020          format(///,'              OUTPUT FROM STUB      ',///,
     .          '    PHYSICAL LOCATIONS OF GRID POINTS: ',//)
               write(2,1040)
 1040          format(5X,'   I       X         J        Y ',/)
          Do 20 j = 1, m
             y(j) = bp(j,2)
             dx = (1.0/(FLOAT(n-1)))*(sp(j,1)-bp(j,1))
             Do 10 i = 1, n
               x(j,i) = (n-i) * dx + bp(j,1)
               write(2,1050) i,x,j,y
 1050          format(5X,I4,2X,F8.4,2X,I4,2X,F8.4)
   10        continue
   20      continue
          write(2,1060)
 1060     format(//,'   PHYSICAL LOCATIONS OF SHOCK AND BODY POINTS:',
     .     //,' (Note that x coordinates are presented for a given y)',
     .     5X,'    Y        X locations:   SHOCK        BODY    ',/)
          Do 40 j = 1, m
               write(2,1080) y(j),sp(j,1),bp(j,1)
 1080          format(5X,F8.4,16X,F8.4,3X,F8.4)
   40     continue
               write(2,1100)
 1100          format(//,'       PHYSICAL LOCATIONS AND VALUES OF FLOW
     .PROPERTIES:',//)
          Do 60 j = 1, m
             write(2,1150) y(j)
 1150        format(//,'       Y LOCATION:  ',F8.4,//)
             write(2,1175)
 1175  format(5X,'     X          U          V          P          RO  ',/)
             Do 50 i = 1, n
               write(2,1200) x(j,i),u(j,i),v(j,i),p(j,i),ro(j,i)
 1200          format(5X,F8.4,2X,4(F8.4,2X))
   50        continue
   60      continue
          Close(2)
          return
          end
```

APPENDIX A3: SEAGULL

Description of the Program SEAGULL

The program SEAGULL is a code designed for the analysis of two-dimensional or axisymetric supersonic inviscid flow of an ideal gas. All the discontinuities are treated explicitly. The limitation of the program is that the axial component of the mach number should remain supersonic during the execution. Although originally designed for internal flows, SEAGULL can be used for external flow due to optional input of the lower or upper wall geometry. The geometry for the upper wall and lower wall are assigned in subroutines GEOMB and GEOMC. Descriptions of the input and outputs are given on the following page. The code could also be used to merge several ducts into one analysis.

For the purposes of the propulsion group, the program is used to calculate the flow properties along the forebody of the hypersonic drone. The flow parameters obtained from this program will be used for the boundary layer code EDDYBL to obtain the shape of the boundary layer. Once the boundary layer geometry is known it could be added to the forebody geometry for a better estimation of the flow properties along the forebody.

The input parameters

Steps between output
Number of sharp corners on upper wall and lower wall (10 maximum each),their locations and angles in degrees
Type of the flow (2D or axisymetric)
Mesh points
Geomatry discription
Constant or variable Gamma
Mach number
Distance to end the run
Free stream Pressure, Temperature, Gamma, Inclination in degrees, Mach number, Gas constant
Lower and upper wall temperatures

Output discription

Forces and Moments on the wall and on the R-Z plane
Viscous and Inviscid forces
Heat transfer from upper and lower wall
The pressure, temperature, velocity componant in the R and Z direction, the mach number, the streamline inclination in degrees, total temperature, for each mash point and its R location.

For the five degree cone, the downstream values output from SEAGULL at Mach 10 upstream conditions are:

$M = 8.271$

$P/P_\infty = 3.060$

$RHO/RHO_\infty = 2.139$

From [22], for a five degree cone with no angle of incidence to the freestream and M_∞=10, we have:

$M_\infty = 9.925$

$P/P_\infty = 2.95$

$RHO/RHO_\infty = 1.8033$

A comparison of these values illustrates a limitation of the code; specifically, SEAGULL's downstream values are somewhat in error. Also, SEAGULL shows that the flowfield downstream of the shock decreases in velocity with increasing distance from the nose. These effects are caused by the duct flow modelling that SEAGULL uses. This effect is minimal, however, and the properties on the wall change by less than 5% over the entire forebody if the walls of the duct are kept far apart to minimize the compression caused by the internal modeling of SEAGULL. This introduces some error into the downstream flow properties. This error is unavoidable due to the necessity to model multi-ramp geometries, which was not possible by merely using conical shock tables because the ramps are not subject to uniform freestream conditions.

APPENDIX A4: EDDYBL

PROGRAM EDDYBL

EDDYBL is a fully compressible, two-dimensional or axisymmetric computer program for the calculation of boundary layer properties. The program accounts for mass flux at the body surface, heat flux, pressure and temperature gradients, and both transverse and longitudinal body curvature. The program has the capability to start from a stagnation point and proceed through transition into turbulence. The equations used by the program cannot account, however, for the effects of shock-boundary layer interaction or separated flow. If the program encounters separation, execution terminates at that point, although the data is saved for all calculations prior to that point. Also, the program does not account for gas rarification or it's effects in any way.

The calculation of the boundary layer properties can be made in two ways: using the program's two-equation model or it's multiscale model.[ref. 12-13]. In short, the two equation model uses conservation of mass and momentum in conjunction with an equation for the turbulent mixing energy, and another equation for the turbulent dissipation rate.[ref. 8, p.2]. These last two equations account for the creation and destruction of turbulence.

The multiscale model differs from the two equation model in several ways. Although the multiscale model also uses the conservation of mass and momentum, as well as the same turbulent mixing energy equation, the multiscale model uses a slightly different equation for the turbulent dissipation rate to "predict the effects of plane strain and shear on homogeneous turbulence." [ref. 9, p.4]. The largest difference between the two models lies in the way that they treat the Reynold's Stress tensor, which accounts for vortices and turbulence.

The two-equation model lumps all of the vortices, or "eddies", into one term. The multiscale model lumps the eddies into "large" and "small" eddies. [ref 19, p.3]. This scaling of the turbulence proves to be more accurate than two-equation model. Our applications use the multiscale model exclusively, and so further discussion will be limited to the multiscale model. References 1 through 4 offer a much more complete description of the two models used.

As previously mentioned, EDDYBL is a fully compressible boundary layer code. In addition to the other capabilities previously mentioned, EDDYBL has the capability to start form user-supplied boundary layer properties. That is, if the user knows what the properties of the boundary layer are at a certain point in the flowfield, then computation can begin at that point and there is no need to make calculations for points further upstream. Furthermore this allows restarting EDDYBL from previous runs. In our application, we will use EDDYBL to calculate boundary layer properties to a point where the free stream conditions change. We then restart computation from the old boundary layer properties with the new free stream conditions. In this way we proceed in a piece wise manner along the body in question.

There are many input parameters for EDDYBL. The free stream velocity, static temperature and pressure may be either be input directly or may be calculated by the program itself. The program will calculate the free stream properties based upon the far upstream total pressure, total temperature, mach number and shock wave angle. (EDDYBL uses the Rankine-Hugoniot Relations to calculate the free stream properties downstream of the shock).

The properties of the free stream gas itself are also defined by the user. The ratio of specific heats, the specific gas constant, and both the laminar and turbulent Prandtl numbers must be defined by the user. The turbulent Prandtl number has been determined experimentally to be 0.9 for most flows, but communication with the author indicates that more accurate results are obtained if the turbulent Prandtl number is set to 8/9. The laminar Prandtl number is a function of viscosity, which is in turn a function of temperature. It's value be calculated by the user and input for each free stream condition. Another free stream property that is user-supplied is the free stream turbulence intensity. This value varies from 0.05% for well designed wind tunnels to 100% for turbulent jets. [ref. 15, p.257].

The properties of the surface itself are described by three separate data files. The first data file contains N arclength-pressure pairs that define the static pressure at the body's surface. (The user determines the number of arclength-presssure pairs, N). Specifying the pressure in this manner allows the user to impose pressure gradients upon the boundary layer. EDDYBL uses a cubic spline fit to determine pressures at intermediate points.

The second file defines the thermal properties of the surface. Again, N sets of arc length, temperature and pressure values are specified. Note that only temperature or heat flux need be specified. If temperature is specified, heat flux will be calculated. If heat flux is specified, then temperature will be calculated.

The last data file specifies the body geometry of the surface and the rate of mass addition or removal at the wall. N sets of five numbers define the mass flux and body geometry. Four of the numbers describe the arc length, axial distance, the radius from the center

line, and the local curvature for a given arc length. The fifth number specifies the mass flux at that station.

Finally, within the program itself the user defines the angle that the free stream makes with the center line of the body. Also, the roughness height Reynolds's number is defined to allow for different surface roughnesses.

The grid resolution for the finite difference method is also determined by the user. Initial and final arc lenghts, maximum number of stream wise steps and the initial step size are all defined by the user. The step size between stations will be changed by the program itself as needed to maintain accuracy and conserve time. Execution will be terminated when either the specified arc length has been reached or the program has reached the maximum number of stream wise steps. Also, the user can specify the number of grid points normal to the surface. More points will increase the resolution but will also increase computing time. The number of points normal to the surface remains constant. Also, the user must choose the model to be used. The closure coefficients for the models may also be changed, but the author has shown the default values to perform well when compared to experimental results. [ref. 19,20]. Also, the velocity profile of the boundary layer obeys the Sutherland Viscosity Law, although a power law may be invoked by the user.

Finally, the user must define boundary layer properties if starting from his own predetermined conditions. The coefficient of skin friction, the boundary layer thickness, shape factor, and [illegible] must all be supplied by the user in addition to the parameters mentioned above.

The program outputs boundary layer properties for each stream wise station.(see attached sheet and ref [12], pp.23-24). The output listing is very complete and easily lends itself to comparison with experimental data. Additionally, the program outputs a boundary layer profile at the last station and at any intermediate station requested by the user. It also creates an output file that can be used to restart from the last station's properties.

The program has several basic limitations. First, it is limited to laminar or turbulent, non-rarified boundary layer analysis. As previously mentioned, the program cannot account for separation or shock-boundary layer interaction. Also, free stream values remain constant throughout a given run, and if the free stream is indeed variable then the program must be run in a series of stream wise sections, each section maintaining constant free stream conditions. Finally, the program is limited to two-dimensional analysis, although the effects of stream wise curvature are accounted for in the axisymmetric case.

Program EDDYBL is a product of DCW Industries and has been tested by the author for compressible flows ranging as high as Mach 5 and including the effects of cooled walls and adverse pressure gradients. [19, p.11-13]. Accuracy of the computed values is shown to be within 8% of experimental results.

Despite verification of the program's accuracy, there are a number of factors affecting the program's application to hypersonic boundary layers. Among these are surface roughness and freestream turbulence. Another possibly important aspect which was not considered in this application were real gas effects, which become important at high Mach numbers. The groups original intention was to compare the results of this program with those of another boundary layer program which accounted for real gas effects. This comparison was never accomplished. However, results in literature for high Mach number flows and communication with researchers at NASA indicate that the freestream conditions under consideration are not sufficiently severe to warrant consideration of real gas effects. [16].

APPENDIX: EDDYBL OUTPUT PARAMETERS

The following quantities are printed in the integral parameter portion of Program EDDYBL output.

Name	Symbol/Equation	Definition	Dimensions
BETA	$\bar{\beta}=(2\xi/U_e)dU_e/d\xi$	Pressure gradient parameter	None
CFE	$c_{f_e}=2\tau_w/\rho_e U_e^2$	Skin friction based on edge density	None
CFW	$c_{f_w}=2\tau_w/\rho_w U_e^2$	Skin friction based on wall density	None
D/T	$H=\delta^*/\theta$	Shape factor	None
DELTA	δ	Boundary-layer thickness	ft
DLTAST	δ^*	Displacement thickness	ft
DPEDS	$d(p_e/\rho_\infty U_\infty^2)/d\bar{s}$	Dimensionless pressure gradient	None
DTEDX	$d\bar{T}_e/d\bar{\xi}$	Transformed edge temperature gradient	None
DUEDX	$d\bar{U}_e/d\bar{\xi}$	Transformed edge velocity gradient	None
ECOUNT		Number of points where k < 0	None
EMAX	$\sqrt{\beta^*}(\rho k)_{max}/\tau_w$	Maximum turbulent energy parumeter	None
ES	S	Dimensionless surface dissipation rate	None
ETAEDG	N_e	Mesh point number at B.L. edge	None
HD	$h=q_w/(T_w-T_{aw})$	Heat transfer coefficient	Btu/ft^2/sec/^{o}R
IEDGE	N	Total number of mesh points in B.L.	None
ITRO		Number of iterations for convergence	None
M	m	Streamwise step number	None
ME	M_e	Edge Mach number	None
MUE	μ_e	Edge molecular viscosity	slug/ft/sec
NSKIP	-	Number of points below u = USTOP	None
NSTE	$h/\rho_e U_e C_p$	Stanton number based on edge density	None
NSTW	$h/\rho_w U_e C_p$	Stanton number based on wall density	None
NUE	$Pr_L h s/\mu_e C_p$	Nusselt number based on edge viscosity	None
NUW	$Pr_L h s/\mu_w C_p$	Nusselt number based on wall viscosity	None
PE	p_e	Edge pressure	lb/ft^2
QSD	q_w	Surface heat flux	Btu/ft^2/sec
RE	ρ_e	Edge density	slug/ft^3
REDELT	$Re_{\delta^*}=\rho_e U_e \delta^*/\mu_e$	Displacement thickness Reynolds number	None
RES	$Re_s=\rho_e U_e s/\mu_e$	Arc length Reynolds number	None
RETHET	$Re_\theta=\rho_e U_e \theta/\mu_e$	Momentum thickness Reynolds number	None
RFCTOR	r	Recovery factor	None
RMI	r_o	Body radius	ft
RVWALD	$\rho_w v_w$	Surface mass flux	slug/ft^2/sec
S	s	Arc length	ft
TAUD	τ_w	Surface shear stress	lb/ft^2
TE	T_e	Edge temperature	^{o}R
THETA	θ	Momentum thickness	ft
UE	U_e	Edge velocity	ft/sec
UTAU	u_τ	Friction velocity	ft/sec

Name	Symbol/Equation	Definition	Dimensions
WCOUNT		Number of points where $\omega < 0$	None
XI	$\xi=\int\rho_e U_e \mu_e r_o^{2j} ds$	Transformed streamwise coordinate	None
Z	z	Axial distance	ft

The following quantities are printed in the profiles portion of Program EDDYBL output.

Name	Symbol/Equation	Definition	Dimensions
i	i	Mesh point number	None
y/delta	y/δ	Dimensionless normal distance	None
u/Ue	u/U_e	Dimensionless velocity	None
yplus	$y^+=u_\tau y/\nu_w$	Sublayer distance coordinate	None
uplus	$u^+=u/u_\tau$	Sublayer velocity coordinate	None
k/Ue**2	k/U_e^2	Dimensionless turbulent kinetic energy	None
omega	$\nu_e\omega/U_e^2$	Dimensionless dissipation rate	None
eps/mu	μ_T/μ	Dimensionless eddy viscosity	None
L/delta	$\sqrt{k}/\beta^*/(\omega\delta)$	Dimensionless turbulent length scale	None
uv/tauw	$\langle-\rho u'v'\rangle/\tau_w$	Dimensionless Reynolds shear stress	None
T/Te	T/T_e	Temperature ratio	None

APPENDIX A5: INLET

A computer program entitled "Design of Supersonic Inlets by a Computer Program Incorporating the Method of Characteristics" (Ref. 11), dubbed "Inlet" by the propulsion group, was obtained to aid in the design of the inlet of the scramjet. Inlet is a sophisticated program written in 1968 by Bernhard H. Anderson of the NASA Lewis Research Center in Cleveland, Ohio. Inlet is based on steady, inviscid, irrotational, two-dimensional or axisymmetric flow. Its main solution scheme utilizes the method of characteristics, which was originally developed in 1929 but only practically implemented after the advent of modern computers. The method of characteristics as used in Inlet has its root in two-dimensional potential flow theory. Not only is the potential function, phi, included (phi is actually incorporated into the method of characteristics equations), but the stream function, psi, is also included for determination of the diffuser's physical boundaries by numerical mass flux integration. The oblique shock relations are also extensively utilized to determine the flowfield; hence continuity, momentum, and energy equations are also considered in the calculations. Additional equations incorporated which yield design consideration data are mass flow spillage and additive drag equations. The numerical techniques used by Inlet to solve these equations simultaneously include finite difference techniques, Runge-Kutta numerical integration, and iteration.

Inlet is particularly useful in designing scramjet inlets since it allows the internal boundaries of the cowl or centerbody walls along with freestream conditions to be prescribed. This

results in the calculation of the internal cowl and centerbody wall geometries required for the input flow conditions. A useful application of Inlet is to calculate the internal cowl and centerbody boundaries from given upstream flow conditions and desired downstream conditions at the entrance of the diffuser. This is done by specifying forebody ramp geometry and freestream flow conditions along with desired shock pattern at the cowl lip and internal to the diffuser. Inlet then calculates the geometry required to cancel or reflect the shock at either the cowl or centerbody boundary by using the characteristic equations. Concurrently, Inlet determines the placement of the boundary by considering mass flux integration and performing iterations until the mass flux obtained by the placement of the boundary equals the initial mass flux entering the diffuser. In this manner, the internal boundaries are constructed and printed out as part of the output data. The boundaries can then be used to study the off-design conditions for the scramjet inlet just constructed.

Some important phenomenon to be studied in the next two quarters include the boundary layer, shock wave-boundary layer interaction, and chemical dissociation in the boundary layer. Because inlet does not account for these phenomenon, a comparison of the results obtained from Inlet at high freestream Mach numbers (M>5) with experimental data in that regime will be essential in justifying the use of Inlet for the design of the forebody and diffuser geometry. Such a comparison performed in the Inlet description report (Ref 11) revealed good Inlet results for Mach numbers less then 2.5. However, comparisons at M = 3.85

begin to show deviation between the theoretical and experimental data, probably due to the increased boundary layer effect at this higher Mach number. Since boundary layer effects and shock wave-boundary layer interaction become increasingly more significant at Mach numbers greater than 5, the determination of the extent of this deviation for Mach numbers at the design region is essential if Inlet is to be useful for the final design of the forebody and diffuser. Nonetheless, should deviations prove to be significant, Inlet should at least yield some qualitative guidelines to consider in the final design of the scramjet inlet.

INPUTS

Freestream Conditions

AMO — Free-stream Mach number

GAM — Ratio of specific heats (Use 1.4 for ideal gas)

Ramp Geometry

THETC — Initial ramp angle, radians

BETAE — Estimation of ramp shock angle

ALPHA — Deflection angle of second ramp (measured from tangent of first ramp)

Cowl Specifications

COWLA — Initial interior cowl angle, radians

THETAL — Location of cowl lip relative to spike tip measured from centerline of ramp in radians (Note: THETAL is used only when the cowl contour is unspecified. Under this condition the cowl lip radius is 1.

SPILL — Set SPILL = 0 to locate the cowl at along initial shock wave. Set SPILL = 1.0 to locate the cowl at THETAL.

XCOWL — x-coordinate of cowl lip position (Used when you want to place the cowl lip somewhere besides at the location where the ramp shock wave would intersect it. Use when inlet geometry is known and off-design performance is to be studied. Set XCOWL = 0 to place the cowl lip along the ramp shock wave.)

YCOWL — y-coordinate of cowl lip position (Used when you want to place the cowl lip somewhere besides at the location where the ramp shock wave would intersect it. Use when inlet geometry is known and off-design performance is to be studied. Set YCOWL = 0 to place the cowl lip along the ramp shock wave.)

OUTPUTS

Conditions in the Vicinity of Ramp Oblique Shock

Program outputs:

1. position of point for calculations
2. Mach number
3. angle of flow
4. angle of shock wave
5. ratio of static pressure behind shock to static pressure in front of shock
6. ratio of total pressure behind shock to total pressure in front of shock

Conditions on Ramp Contour

1. x-coordinate of point
2. y-coordinate of point
3. magnitude of velocity vector
4. flow angle
5. x-direction component of the velocity
6. y-direction component of the velocity
7. Mach number
8. ratio of static pressure to freestream total pressure
9. ratio of static pressure to total pressure behind the shock

SPECIFYING COWL GEOMETRY

Cowl contour is specified by third-order polynomial of form

$$Y = R(I,1) + R(I,2)\ X + R(I,3)\ X^2 + R(I,4)\ X^3$$

The coefficients are specified in sets from 1 to NR where NR is an input variable specifying the number of sets of cowl contour coefficients to be read in. Also the starting position where the above equation is in effect must also be specified by the variable COWL(I) which specifies the X-coordinate to impose the specified set of coefficients.

Centerbody Specifications

Similiar to cowl specification, centerbody is express as a third-order polynomial of the form

$$Y = S(I,1) + S(I,2)\ X + S(I,3)\ X^2 + S(I,4)\ X^3$$

The coefficients are specified in sets from 1 to NS where NS is an input variable specifying the number of sets of centerbody contour coefficients to be read in. Also the starting position where the above equation is in effect must also be specified by the variable BODY(I) which specifies the X-coordinate to impose the specified set of coefficients.

Calculation of Cowl or Centerbody Coefficients

When the Cowl or Centerbody coefficients are to be calculated set the corresponding coefficients equal to 0 and instead specify the flow conditions within the inlet by specifying the following input variables:

NTHR — Number of internal isentropic compression sections.

AMT(J) — Final Mach number specified for the end of the J^{th} section, J = 1,NTHR .

THR(J) — Length of J^{th} section.

ANG(J) — Final surface angle (radians) of J^{th} section.

NIS(J) — Number of surface net points within THR(J).

Flowfield Specifications

START — Initial net point spacing parameter for point locations. Flow properties are calculated at each point. (A good initial value for start is 0.050)

DELP — Ratio of angular location of last inital data point to inital shock angle. The program constructs the initial datum line from the point on the surface, BODY (2), to a point in the field whose angular location is DELP times the initial shock angle.

PRINT — Set PRINT = 0 to bypass the output printout for the forebody flow field calculations.
Set PRINT = 1.0 to print flow field calculations.

M — Number of points in flowfield calculations.

Internal Flow

NTHR — Number of internal isentropic conpressions sections.

ISHK — Used for off-design calculations only.
For on-design calculations set ISHK = 1.
For off-design ISHK is index which specifies at which centerbody location BODY (ISHK) the shock wave is canceled.

NSHK — Number of internal shock waves to be computed.
Set NSHK = 1 to cancel cowl lip shock.
NSHK - 1 specifies number of internal shock reflections.

Input Parameters

DELB — Initial increment used in calculation of ramp shock angle (set DELB = 1.4×10^{-4})

DELU1 — Integration increment for conic flow field calculation (Set DELU1 = 1.0×10^{-5})

ERROR — Convergence parameter (Set ERROR = 1.0×10^{-4})

OFF — Set OFF = 0 for on design calculations.
Set OFF = 1.0 for off-design calculations.

NDIM — Set NDIM = 2 for 2-D case.

NR — Number of sets of cowl contour coefficients.

ND — Number of increments in addiditive drag calculations.

Conditions in the flow field

1. x-coordinate of point
2. y-coordinate of point
3. magnitude of velocity vector
4. flow angle
5. x-direction component of the velocity
6. y-direction component of the velocity
7. Mach number
8. ratio of static pressure to freestream total pressure
9. ratio of static pressure to total pressure behind the shock

Conditions in the Vicinity of Cowl Oblique Shock

1. x-coordinate of point
2. y-coordinate of point
3. Mach number
4. flow angle
5. shock wave angle
6. ratio of pressure behind shock to pressure ahead of shock
7. rato of total pressure behind shock to total pressure ahead of shock

Conditions along Cowl Contour Surface

1. x-coordinate
2. y-coordinate
3. magnitude of velocity vector
4. flow angle
5. x-direction component of velocity
6. y-direction component of velocity
7. Mach number

8. ratio of static pressure to freestream total pressure

9. ratio of static pressure to total pressure behind shock

Table of Cowl Coefficients

The program list cowl coefficients along with the x-coordinate position where the coefficients become effective.

Table of Centerbody coefficients

The program list centerbody coefficients along with the x-coordinate position where the coefficients become effective.

APPENDIX A6: CPIPE

Symbols

A	cross section area
C_f	friction coefficient
F	force
h	enthalpy
$\overline{m}$	molecular weight
p	static pressure
q	dynamic pressure
$Q, \dot{q}$	heat flux into control volume
T	temperature
v	velocity
ν	moles of vitiate
w	mass flux
x	axial distance
β	angle between wall and duct centerline
θ	angle
ρ	density
Re	Reynolds number
Pr	Prandtl number
μ	viscosity
γ	ratio of specific heats

Subscripts

a	air
f	fuel
f	friction
q	end of axial step
v	vitiate
w	wall
T	isentropic stagnation
aw	adiabatic wall
∞	ambient condition

APPENDIX CPIPE

Summary

CPIPE is a fortran program written in 1968 by G.Y. Anderson of NASA Langley Research Center. CPIPE is a 1-dimensional, real gas analysis of the combustion of hydrogen in air in a supersonic channel (see Figure A1). CPIPE was originally intended to perform a one step analysis of the entire underbody flowfield, but can be modified to only analyze the combustor region. Given the initial upstream conditions and other inputs (see Table A1), CPIPE outputs the downstream 1-dimensional flow properties. CPIPE allows for several fuel injection points and allows the user to specify the fuel Mach number, stagnation pressure and temperature, and angle at which it is injected. There are several other options available regarding the boundary layer transition point and mixing models used (see Options, Table A1). In addition, CPIPE contains some empirical relations (introduced by Chuck McClinton, NASA Langley Research Center) which approximate the likelihood of autoignition and flameholding.

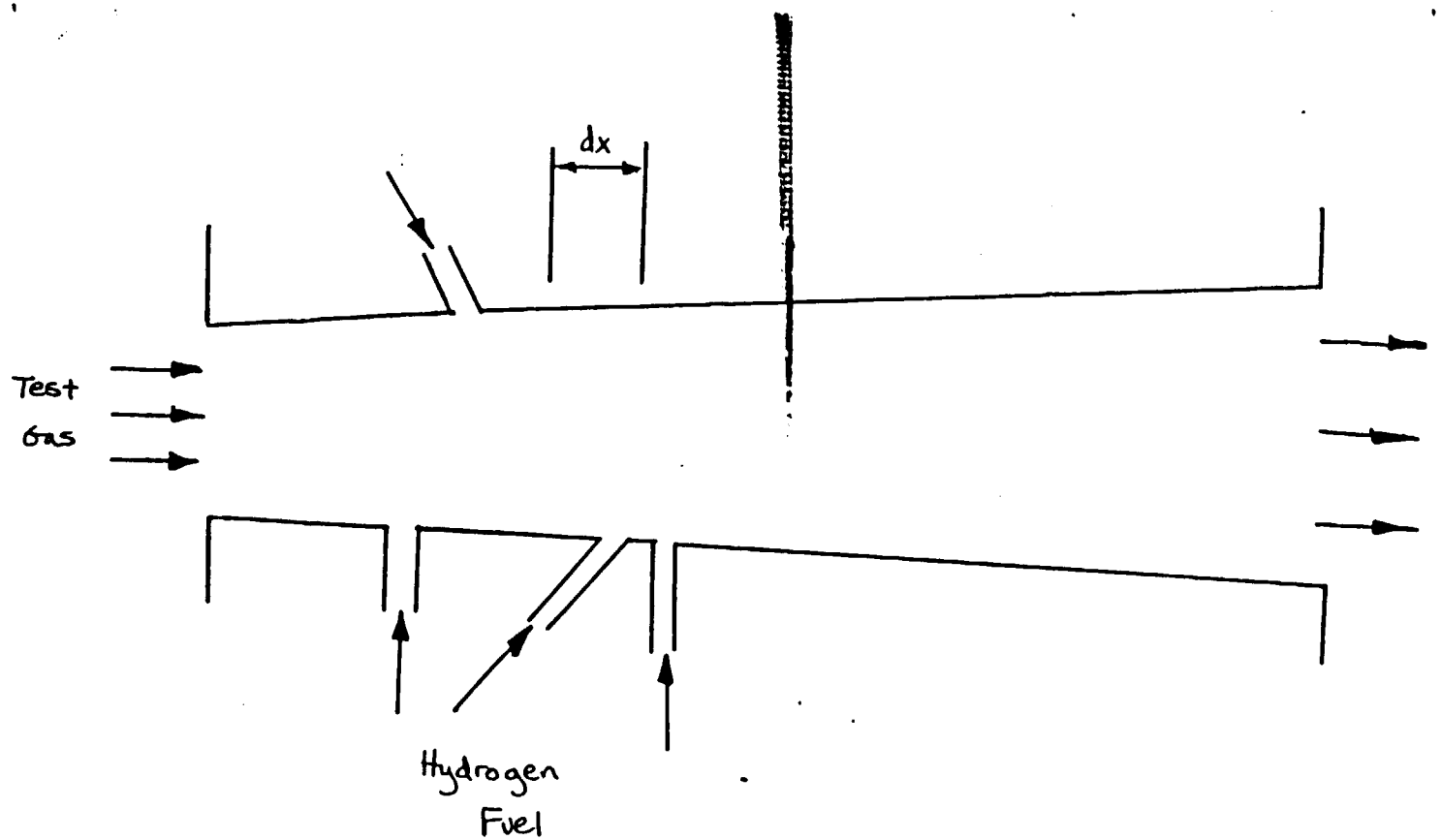

Figure A1 - Idealized one-dimensional supersonic combustor.

Conservation Equations

CPIPE uses the mass, momentum, and energy conservation equations to perform a one step analysis of the flow properties in a supersonic channel. The equations and the control volumes they are applied to are shown explicitly below:

Control Volumes

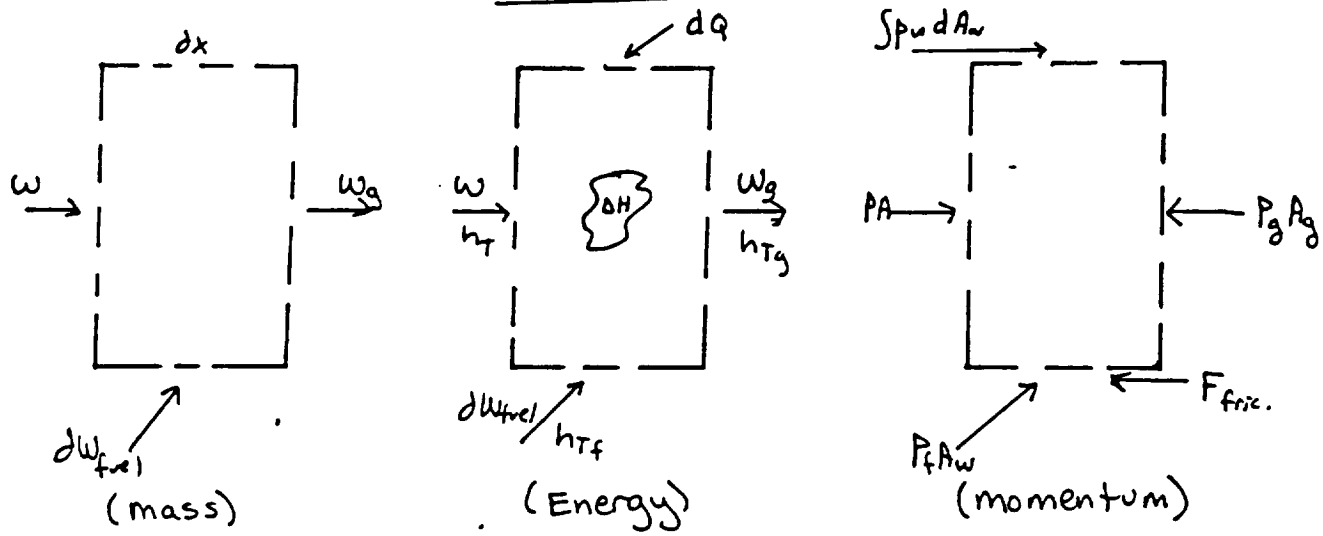

mass: $\omega + dW_f - W_g = 0$

Energy: $\omega h_T + dW_f h_{Tf} + dQ - W_g h_{Tg} = 0$

Momentum: $(PA + WV) + (P_f A_f W \sin\beta + dW_f V_f \cos\theta)$

$$- (P_g A_g + W_g V_g) + \int_{x}^{x_g} p_w \, dA_w - dF_F = 0$$

Temperature

CPIPE performs a 1-dimensional analysis of the wall heating in a supersonic channel. Given the temperature distribution along the wall of the channel, CPIPE will calculate the heat flux. The equations used to calculate the heat flux are shown explicitly below:

Wall heat flux found using Modified Reynolds Analogy:

$$\dot{q}_w = \int_{A_w} \frac{C_f}{2} \rho V (h_{aw} - h_w) \left(\frac{A_r^2}{4}\right)^{1/2} dA_w \qquad (1)$$

C_f - Van Driest skin friction coefficient found from iterative solution of:

$$\frac{0.242}{A\sqrt{C_{f_\infty}}\sqrt{T_w/T_\infty}} \frac{(\sin^{-1}\alpha + \sin^{-1}\beta)}{57.3066} = 0.41 \pm \log_{10} Re_{y_\infty} C_{f_\infty} - \frac{1+2n}{2} \log_{10}\left(\frac{T_w}{T_\infty}\right) \qquad (2)$$

where $\alpha = \frac{2A^2+B}{(B^2+4A^2)^{1/2}}$ $\beta = \frac{B}{(B^2+4A^2)^{1/2}}$ $n = 0.76$

and, $A^2 = \left[\gamma - 1/2\right] \frac{M_\infty^2}{T_w/T_\infty}$ $B = \left[\left\{1 + \left[\gamma - 1/2\right] M_\infty^2\right\} / (T_w/T_\infty)\right] - 1$

$$Re_{y_\infty} = \frac{\rho V l}{\mu}$$

Species Viscosity (Southerlands formula):

$$\mu_i = C_1 \frac{T^{3/2}}{T + C_2} \times 10^{-8} \frac{lb\text{-}s}{ft^2} \qquad \mu = \sum_{i=1}^{N_s} \left\{ \frac{x_i \mu_i}{\sum_{j=1}^{N_s} x_j \phi_{ij}} \right\}$$

where $\phi_{ij} = \frac{\left[1 + \left(\frac{\mu_i}{\mu_j}\right)^{1/2} \left(\frac{\bar{m}_j}{\bar{m}_i}\right)^{1/4}\right]^2}{\sqrt{8}\left(1 + \frac{\bar{m}_i}{\bar{m}_j}\right)^{1/2}}$

Species considered (H_2O, O_2, H_2, N_2)

Adiabatic Wall Enthalpy: $h_{aw} = h + (P_r)^{1/3} \frac{V^2}{2}$

where $(P_r)^{1/3} = \frac{c_p \mu}{K} = \frac{4\gamma}{9\gamma - 5}$

TABLE A1- CPIPE INPUTS

Geometry:

X_o = beginning axial location (m)
X_{max} = end axial location (m)
ΔX = step size (m)
XTRAN = X position where B.L transitions (m)
WID = width of engine (m)
GAP = Nondimensionalizing height of Combustor = 1.0(m)

Distributions:

{TA, XA} = { flow area (m^2), axial location (m)}

{TWP, XWP} = {wetted perimeter (m), axial location (m)}

Upstream Conditions (1-D):

P_o = static pressure (N/m^2)
T_o = static temp. (°K)
~~M_∞ = mach~~
U_∞ = velocity (m/s)

Fuel Injection Parameters: (specify for each injection pt)

{TPHI, XPHI} = {injected equivalence ratio, axial location (m)}

{TPHIR, XPHIR} = {reacted equivalence ratio, axial location (m)}

TTF - Fuel stagnation temp (°K) (1000)

PTF = Fuel stagnation press (N/m^2) (4758000)

MF = Fuel mach number (1.0)

THETA = Fuel injection angle (rad. fr. horizontal) (.78)

BETA = Wall angle at injection (rad.) (0.0)

KF = end of fuel inj. region (cm)

TABLE A1— CPIPE INPUTS (continued)

Temperature:

{Tw, Twx} = {Temperature wall (°K), axial position (m)}

Trank = Temp of fuel in tank (20°K)

Options:

Initial B.L. status: (ALAM1)	1	Laminar B.L. at x_0
	0	Turbulent B.L. " "
	-1	$C_f = q_w = 0$
B.L. Transition cooling: (ALAMTRN)	1	Laminar flow
	0	Turbulent flow
Type of rxn model: (EQUIL)	1	only Mixing Limits Rxn
	0	Chemical Kinetics modeled.

APPENDIX B: HAND CALCUALTIONS

Drag Calculation:

$D = q_\infty C_D S_{ref}$

$S_{ref} = 335\ ft^2$ (based on Hc

$C_D = .05$

$q_\infty = \frac{1}{2}\frac{\rho_\infty}{g} V_\infty^2$

at $M = 10$ alt = 100,000 ft

$\rho_\infty = .0010439\ \frac{lbm}{ft^3}$

$a_\infty = 991.68\ ft/s$

$V_\infty = 9916.8\ ft/s$

$q_\infty = \frac{1}{2}\frac{\rho_\infty}{g} V_\infty^2 = 1588.7\ \frac{lbf}{ft^2}$ (reasonably structural lk

$D = q_\infty C_D S_{ref} = \boxed{26,610.7\ lbf = \text{Drag}}$

Thrust Calculation:

* Need to get newest estimates from SCRAM (Luis)

* Thrust equation: (momentum balance on c.v.)

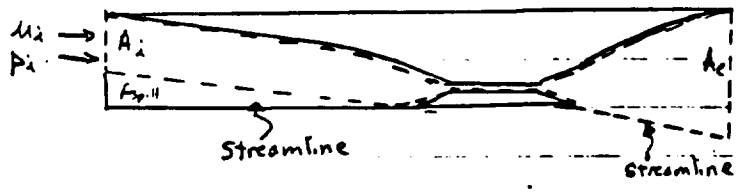

$T = \dot{m}_e u_e - \dot{m}_i u_i + p_e A_e - p_i A_i$ $\quad \dot{m}_e = \rho_e u_e A_e$

$\dot{m}_i = \rho_i u_i A_i$

$T_{effective} = T - D_{spill}$ $\quad D_{spill} = \int_{A_{spill}} p\, dA$

Overall Geometry:

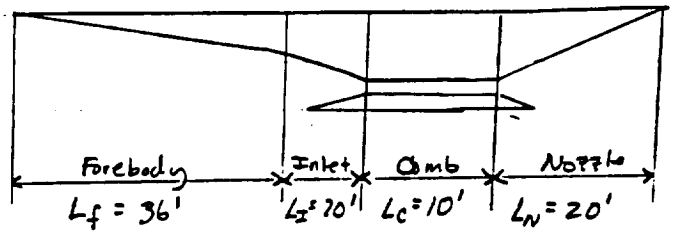

obviously not drawn to scale

Forebody:

FOREBODY	$P_{t2}/P_{t\infty}$	M_2	P_2/P_∞
#1	.7829	7.51	8.97
#3	.8798	7.85	9.17
#11	.7780	7.33	14.63

Design #1:

Ramp angle	5°	5°	3°
Location	0.0	15'	24'

Design #3:

Ramp angle	5°	5°	3°
Location	0.0	18'	27'

By moving ramps aft, ① decrease in stagnation pressure losses (i.e. more efficient), ② decreased magnitude of Mach decrease, ③ increased static pressure gain.

Design #11:

Ramp angle	5°	5°	3°	3°
Location	0.0	18'	27'	31'

Additional ramp ① decreases mach more than #1 (which simply moved ramps forward), ② Stagnation pressure losses are only slightly more than #1 ③ major increase in static pressure gain.

Final configuration → #11
Values of properties at exitplane (36'):

$P/P_\infty = 14.63$ $\quad P_\infty = 23.27\ lbf/ft^2$
$M = 7.33$
$T/T_\infty = 2.1107$ $\quad T_\infty = 408\ °R$
$P_t/P_{t\infty} = 0.778$ (mass averaged value for total pressure only)

INLET: Used Mach 7-4 inlet design (see attached sheets)

From Pete's sheet:

$\frac{A_e}{A_\infty} = 0.133062$ $\quad \frac{P_{te}}{P_{t\infty}} = .77570$

$\frac{A_i}{A_\infty} = 0.360845$ $\quad \frac{P_e}{P_\infty} = 21.1588$ $\quad M_e = 4.0$

$\frac{L_{comb}}{A_\infty} = 6.4$

Setting A_e = 5 inches = .42' $\Rightarrow$ $A_\infty = 3.13'$
$A_i = 1.13'$ (dist cowl lip from body)
$\Rightarrow L_{comb} = 20'$

Use exit conditions from forebody design:

$P_i = 14.63\ (23.27\ \frac{lbf}{ft^2}) = 340.4\ lbf/ft^2$

$\frac{P_e}{P_i} = 21.1588 \Rightarrow P_e = 340.4\ (21.1588) = \underline{7203.3}\ \frac{lbf}{ft^2}$

$\frac{P_{ti}}{P_{t\infty}} = 0.778$ $\quad \frac{P_{te}}{P_{ti}} = .77570 \Rightarrow \frac{P_{ti}}{P_{t\infty}} = \underline{0.604}$

$T_i = 2.1107 \times 408\ °R = \underline{861.16\ °R}$

Since INLET does not estimate temp rise in inlet, we estimated it using oblique shock tables from: J. D. Anderson

Temperature Estimation in INLET:

1st 5° ramp: θ = wedge angle = 5° β = wave angle = 12°

$M_1 = 7.0$ $M_{n,1} = M_1 \sin\beta = 9.455$

$\frac{P_2}{P_1} = 2.232$ $M_{n,2} = .7157$ $\frac{T_2}{T_1} = 1.294$ $\frac{\rho_2}{\rho_1} = 1.793$

$M_2 = \frac{M_{n,2}}{\sin(\beta-\theta)} = 5.87$

$T_2 = \frac{T_2}{T_1} T_1 = 1114.34\ ^\circ R$ $P_2 = \frac{P_2}{P_1} P_1 = 759.86\ lbf/ft^2$

$\rho_2 = \frac{\rho_2}{\rho_1} \rho_1 = 0.010399\ lbm/ft^3$

2nd 5° ramp: $\theta = 5°$ $\beta = 13°$

$M_{n,2} = M_2 \sin\beta = 0.32$ $\frac{P_3}{P_2} = 1.866$ $M_{n,3} = 0.776$

~~$\frac{T_3}{T_2} = 1.204$ $\frac{\rho_2}{\rho_1} = 1.551$~~ $M_3 = \frac{M_{n,3}}{\sin(\beta-\theta)} = 5.57$

$T_3 = 1341.7\ ^\circ R$

$P_3 = 1417.9\ lbf/ft^2$ $\rho_3 = .01613\ lbm/ft^3$

Rest of inlet: We know that the rest of the inlet compresses the flow from M 5.6 -> 4.0, approx. this by one more oblique shock

From Ref: [T. Bertin, M. Smith "Aerodynamics for Engineers" Prentiz-Hall, Inc, New Jersey, 1979]

$M_2 = 4.0$ $M_1 = 5.6$ => wedge angle ~ 16° wave angle ~ 26°

$M_{n,1} = M_1 \sin 26° = 2.45$ $\frac{T_3}{T_2} = 2.088$ $\frac{P_3}{P_2} = 3.273$

$P_3 = .0579\ \frac{lbm}{ft^3}$

$T_3 = 2801.5\ ^\circ R$

To check find P to combustor: $\frac{P_3}{P_2} = 6.836$

$P_3 = 9692.8\ lb/ft^2$ => compare to $P = 7203\ lb/ft^2$

-> Temp guess 13 not bad for rough estimate.

Summary INLET:

Exit conditions: $P_e = 7203.3$ lbf/ft²

$\frac{P_{te}}{P_{t\infty}} = 0.604$

$T_e \cong 2801.5°R$

$M_e = 4.0$

$\rho_e = .0579$ lbm/ft³

$A_e = 5$ inches $= .42'$

Use these as inputs for CPIPE.

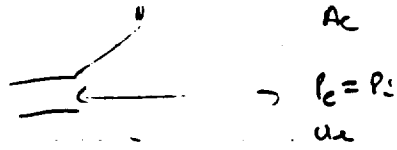

Summary of CPIPE outputs:

$M_e = 2.2986$

$P_e = 17380.0$ lbf/ft²

$T_e = 5596.4°R$

Assumes no stagnation pressure loss across combustor: $\frac{P_{te}}{P_{t\infty}} = 0.604$

$A_e = 6$ inches $= .5'$

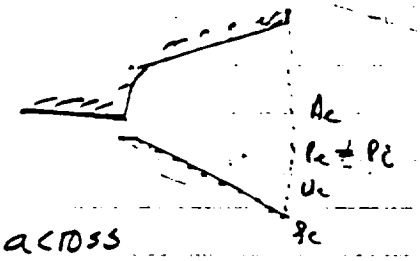

Nozzle: does not work (SEAGULL). If use ideal expansion (i.e. $P_e = P_\infty = 23.27$ lbf/ft²) Should be able to find (from texts) the exit velocity. If ideally expanded, Streamline defining A_e will extend straight from the exit of combustor (see diagram in Thrust Calc). Can find A_i by tracing the streamline from the cowl lip, maintaining the same distance from the forebody (you should not cross any shock waves).

For thrust eqn: $T = \dot{m}_e u_e - \dot{m}_i u_i + P_e A_e - P_i A_i$ $\quad \dot{m}_e = \rho_e u_e A_e$ $\quad \dot{m}_i = \rho_i u_i A_i$

$\rho_i = .0010439$ lbm/ft³

$u_i = 9916.8$ ft/s

$A_i = .7131 - .210'$

$A_{spill} = 21 - 12.3 = 8.7'$

$P_i = 23.27$ lbf/ft² $= P_e$

A_e, u_e } determined above

$P_e = P_i$?

Mass Removal Required to Completely Remove Boundary Layer at 5000

Considering mass removal sufficient to completely remove displacement thickness at 35':

$\delta^* = .136$ ft

$U_e = 9806$ ft/sec

$\rho_e = .0000744$ slug/ft^3

The mass removal rate per unit depth is simply

$\Rightarrow \dot{m} \; \delta^* \rho_e U_e = .0992$ slug/ft sec

Over the width of the forebody $w \cong 7'$

$\Rightarrow \dot{m}_{TOT} \cong .209$ slug/sec

Over the same area, the velocity of the removed mass would need to be

$$v = \frac{\dot{m}_{TOT}}{\rho_e w} = \frac{.208}{.0000744 \cdot 7} \cong 400 \text{ ft/sec}$$

MASS REMOVED ON 5000 : BOUNDARY LAYER SUCTION

APPROXIMATE THE MASS REMOVAL AS , $\dot{m}$ [slug/ft²/s]

$\dot{m}$	z
0	30'
-.0005	33'-40'

$\rho_E = .0000744$ slugs/ft³

WITH A LINEAR APPROXIMATION BETWEEN 30-33'

Thus

$\dot{m}$ per unit depth is

$$\dot{m} = \tfrac{1}{2}(-.0005)(3') + (-.0005)(7')$$

$$\Rightarrow \dot{m} = .00425 \text{ slugs/sec·ft}$$

If suction is to be performed at this rate over the entire width of the forebody prior to the first inlet ramp angle, then

$$\dot{m} = .00425 \cdot W \quad , W = \text{width of forebody} \approx 7'$$

$$\therefore \dot{m}_{TOT} = 7(.00425) =$$

$$\Rightarrow \dot{m}_{TOTAL} = .0298 \text{ slugs/sec}$$

$$\Rightarrow V_{min} = \frac{\dot{m}_{TOT}}{\rho_E W} = 57.2 \text{ ft/sec}$$

ORIGINAL PAGE IS
OF POOR QUALITY

COMPUTER CODES — 19.4 ft DOWNSTREAM MACH = 5.96

ASSUME PITOT STAGE CONSTANT

$$P_{EXIT} = \left[\frac{17380\left[1+\frac{\gamma-1}{2}(2.3)^2\right]}{\left[1+\frac{\gamma-1}{2}(5.96)^2\right]}\right] = 141.74 \text{ lbf/ft}^2$$

WHERE $M_i = 2.3$ & $P_i = 17380$ lbf/ft² AT COMBUSTOR EXIT

CONSEQUENTLY, THE TOTAL TEMPERATURE ALSO STAYS CONSTANT, HENCE FROM ISENTROPIC RELATIONSHIPS:

$$T_{EXIT} = \left[5596.4\,^\circ R\ \frac{1+0.2(2.3)^2}{1+0.2(5.96)^2}\right] = 1415.6\,^\circ.$$

$$a = \sqrt{\gamma RT} = \left[1.4(1716)\text{ lbm}(1415.6)\right]^{1/2} = 1844 \text{ ft/sec}$$

$$u = M_e a = 5.96 \times 1844 = 10990 \text{ ft/sec}.$$

EFFECTIVE NOZZLE EXIT AREA IS DETERMINED BY APPLYING THE CONTINUITY EQUATION.

MASS FLUX AT COMBUSTOR EXIT:

$$\dot{m} = \rho u a = \left[\frac{17380}{1716(5596.4)}\right](2.29)\sqrt{1.4(1716)(5596.4)}\,(0.5)$$

(ρ, u, a)

$$= 7.729 \text{ slug/ft}^3\text{-sec}.$$

$$A = \frac{\dot{m}}{\rho u} = \left[\frac{7.729(1716)(1415.6)}{10990 \times 141.74}\right] = 12.05 \text{ ft}^2 \text{ PER foot SPAN}$$

FINALLY $T = \dot{m}_e u_e - \dot{m}_o u_o + P_e A_e - P_i i_o$

$$= (7.729)(10990)\cos(10^\circ) + 141.74 \times 12.05 - 23.27(7.13)$$
$$- 7.19(9916)^2(.001044)/32$$

$$= 2646 \text{ lb per foot Span}$$

REFERENCES

References

1. Penland, J.A., Hallissy, J.B., and Dillon, J.L. "Aerodynamic Characteristics of a Hypersonic Research Airplane Concept having a 70 degree swept double-delta wing at mach numbers from 0.80 to 1.20, with summary of data from 0.20 to 6.0", NASA TP-1552, December 1979.

2. Anderson, John D., Jr., Fundamentals of Aerodynamics, McGraw-Hill Book Company, Inc., New York, 1984, Chapters 9 and 13.

3. Anderson, John D., Jr., Modern Compressible Flow, McGraw-HillBook Company, Inc., New York, 1982, Chapters 7, 11, and 12.

4. Moretti, G. and Abbett, M., "A Time-Dependent Computational Method for Blunt Body Flows", **AIAA Journal**, v. 4, no. 12, 1966, p. p. 2136-2141.

5. Barnwell, Richard W., "A Time-Dependent Method for Calculating Supersonic Blunt-Body Flow Fields with Sharp Corners and Embedded Shock Waves", NASA TN D-6031, 1970.

6. Barnwell, Richard W., "A Time-Dependent Method for Calculating Supersonic Angle-of-Attack Flow about Axisymmetric Blunt Bodies with Sharp Shoulders and Smooth Nonaxisymmetric Blunt Bodies", NASA TN D-6283, 1971.

7. Masson, B. S., Taylor, T. D., and Foster, R. M., "Application of Gudonov's Method to Blunt-Body Calculations", **AIAA Journal**, v. 7, no. 4,1969,p. p. 694-698.

8. Anderson, John D., Jr., Albacete, L. M., and Winkelmann, A. E., "On Hypersonic Blunt Body Flow Fields Obtained with a Time-Dependent Technique", Naval Ordnance Laboratory, NOLTR 68-129, 1968.

9. No reference.

10. McClinton, C.R., Torrence, M.G., Gooderum, P.B., and Young, I.R. "Nonreactive Mixing Study of a scramjet swept-strut fuel injector", NASA TN D-8069, December 1975.

11. McClinton, C.R., and Torrence, M.G. "Normal Injection of Helium from swept struts into ducted supersonic flow", NASA TM X-72632, January 1975.

12. Billig, F.S., Orth, R.C. and Funk, J.A. "Direct-Connect Tests of a Hydrogen-Fueled Supersonice Combustor" NASA CR-1904, August 1971.

13. Penland, Jim A., Hallisey, James B.,.Piloon, James L., "Aerodynamic Characteristics of a Hypersonic Research Airplane Having a 70 Degree Swept Double Delta Wing at Mach Numbers From 0.8 to 12.0, With Summary of Data From 0.6 to 6.0", NASATP, 552, Langley Research Center, Hampton, Va, 1979.

14. Holman, J. P. Experimental Methods for Engineers, McGraw Hill, New York, 1984.

15. NATO, "Recent Developments in Boundary Layer Research Part 3", AGARDograph, 97, May 1965.

THERMAL MANAGEMENT GROUP

Design of a Combined Impingement and Actively Cooled Panel Concept for a Hypersonic Drone

Group Members:
Virginia Koch
James Marcolesco
Gregory Noffz
Jerry Yen

Faculty Advisor:
Professor A.F. Mills

Abstract

The aim of this paper is to design and compare active cooling systems that met the requirements of a hypersonic drone. The design procedure involved the determination of a flight condition to be studied; justification of the use of an active regenerative cooling system; and, finally, the optimization of the design of such a system. Several computer codes were written to facilitate parametric studies of the design. Two designs are proposed: one utilizing the hydrogen fuel as a coolant, and the other utilizing ethylene glycol as the secondary fluid. Due to weight considerations, the hydrogen design was determined to be preferable.

Table of Contents

1 List of Symbols

a Speed of Sound

c Specific Heat (Btu/lb R)

g Acceleration due to Gravity

h Altitude (Ft.) or Enthalpy(ft^2/sec^2)

k Conductivity

q Total Heat Transfer Rate (Btu/ft^2)

t Time (Sec)

A Area (ft^2)

D Drag = $0.5\rho_\infty V^2 C_D A$

L Lift = $0.5\rho_\infty V^2 C_L A$

M Mach Number = V/a

P Pressure

R Radius

T Temperature

V Flight Velocity (ft/s)

SUBSCRIPTS

B body

d diameter

eq equilibrium

s stagnation

sh shock value

SL sea level value

w wall value

∞ free stream

δ inviscid edge of the boundary layer

SUPERSCRIPTS

- mean value

. derivative with respect to time

SPECIAL SYMBOLS AND CONSTANTS

g gravitational constant at sea level

Le Lewis Number = Pr/Sc

L/D Ratio of lift to drag

Pr Prandtl number

Re Reynolds number

ρ_{sl} sea level density

σ Stefan-Boltzmann constant

GREEK SYMBOLS

ϵ Emissivity

μ Viscosity

ρ Density

2 Introduction

The phenomenon of aerodynamic heating was first experienced on re-entry vehicles, where heating rates on the order of tens of BTU/ft^2s were encountered for relatively short periods of time. In spite of these high heating rates, the short time interval that the vehicles were in the critical regime allowed the problem to be managed with passive systems, such as ablative surfaces or heat sink structures.

Air breathing vehicles, generally experiencing less intense heating rates, tend to be in the critical regimes for much longer periods of time. The aircraft skin does not possess sufficient thermal capacity to act as a heat sink. In addition, requirements for reusablility and turn-around time rule out ablative surfaces.

With these considerations in mind, the aim of the Thermal Management Group was to design a hypersonic drone cooling system suitable for testing candidate National Aerospace Plane (NASP) cooling systems. The hypersonic drone vehicle configuration was the same (see Appendix 5) as that studied by the 1987-88 UCLA Advanced Aeronautics Design Class. The analysis was focused upon the nose region of the drone since the computation of high stagnation point heating rates is simpler and better understood than the heating rates occurring ~~occuring~~ within the engine.

Due to the relatively low heating rates experienced at the drone nose, the use of a heat pipe was unwarranted. Instead, the designed system was based on an actively cooled panel concept. Although the actual thermal design of the NASP nose region would probably make

use of the heat pipe concept, there will exist panels elsewhere that will require an active cooling system. The design presented here, then, is simply a test of that concept. It would be judicious to point out that this thermal design is by no means meant to be directly applicable to the nose of the NASP. Rather, it is the concept of actively cooled panels that is currently under study; the system design just happens to be located at the nose region of the hypersonic drone.

The design procedure involved the determination of a flight condition to be studied; justification of the use of an active regenerative cooling system; and finally, the analysis and optimization of the design of such a system. The aircraft configuration is presented first, followed by a detailed description of the design procedure and results.

3 Determination of Flight Profile and Nose Geometry

To obtain useful data from flight tests, a suitable flight profile was established. In general, the flight condition is governed by two basic parameters: altitude and Mach number. Decreasing altitide will increase air density, resulting in increased heating rates and higher equilibrium temperatures, particularly at high Mach numbers. Also, with an increase in Mach number, specific impulse (ISP) and engine efficiency tend to decrease. Thus, given a range of Mach numbers for scramjet operation (5-12) and a rough estimate of the fuel tank size (8 feet diameter, 40 feet long), an effort was made to determine a flight condition where active cooling was required (due to material limitations), while maximizing the flight time for data collection and experiments.

A code called Hypersonic Equilibrium Temperature and Heat Flux (HETAQ) [See Appendix 2.1] was created to develop a data base of flight conditions. HETAQ varied Mach numbers from 5 to 12, altitudes from 70,000 feet to 115,000 feet, and nose radii from 1 to 6 inches. Lees Approximate Method was used to determine stagnation point heating rates, and an energy balance of the convective heat transfer with radiative cooling produced the skin equilibrium temperature. A simple routine incorporating the thrust equation was used to determine the total flight time available given the geometry of the proposed fuel tank, Mach number, and altitude. The code calculated time to thermal equilibrium for aluminum and titanium noses at each given flight condition. This was necessary to prove that the time required for the craft to reach thermal equilibrium would be less than the cruise flight time.

Once the data base was developed from HETAQ, the group selected a flight condition suitable for the entire design team. Specifically, though a higher Mach number was desirable for the propulsion group, the resulting shorter flight time proved to be incompatible with the Thermal Management Group's aim of achieving steady-state conditions. From the HETAQ data, any speed faster than Mach 9 or 10 would result in the use of too much fuel and thus create undesirable heating rates. Therefore, the speed was set at Mach 10, and the altitude set at 100,000 feet. In addition, the nose radius was set at one inch, since a smaller nose radius results in a higher equilibrium temperature (the temperature that would arise without cooling). The higher temperature was desired to justify the use of an active cooling system. Indeed, the equilibrium temperature for such a configuration is 4000°R, high enough

to require an active cooling system.

In summary, with a flight profile of Mach 10 at 100,000 feet, and with a nose radius of one inch, results from HETAQ determined that the stagnation point and points aft required cooling.

4 Methods for Computing Aerodynamic Heating

In the hypersonic regime, the aircraft endures the most severe heating rates at the stagnation region of the body. A stagnation point is defined as the point on the body where a streamline terminates. The stagnation region differs from the rest of the flow field in that the boundary layer is at its thinnest. A large change in velocity near the stagnation point means a large change in kinetic energy. This lost kinetic energy is converted to thermal energy in the form of stagnation point heating. A thin boundary layer means the flow is at free stream conditions very close to the body. Heat transfer is thus at a maximum where the boundary layer thickness is at a minimum. The larger velocity gradient and the thin boundary layer combine to make the stagnation region the area of critical aerodymnamic heating.

It is important to note that the boundary layer, defined as the region dominated by viscous effects, has a finite thickness at the stagnation point. Thus, the flow properties at the edge of the boundary layer, required by all of the methods discussed below, are the properties behind the bow shock, NOT the stagnation properties.

Heat transfer rates from flat plates subjected to convection are given by equations of

the form

$$\dot{q}_s = h(T_\infty - T_w), \tag{1}$$

where h is the convective heat transfer coefficient. This quantity depends on the Reynold's Number

$$Re = \frac{\rho V L}{\mu}$$

The length from the leading edge, L, is zero at the stagnation point. Therefore, instead of relying on Re as a parameter, the methods discussed use the velocity gradient at the stagnation point.

A method used extensively is the Fay and Riddell Method. Developed in 1959 at Avco, it is accepted as the most accurate formula available, but is also one of the most difficult to use (See Ref. 11). The heat transfer rate is given by

$$\dot{q}_s = \frac{1}{1020 Pr^{0.6}\sqrt{R_o}}(\frac{\rho_w \mu_w}{\rho_s \mu_s})^{0.1}(\rho_s \mu_s V_\infty)^{0.5}(h_s - h_W)(\frac{dV_\delta}{V_\infty d\theta})_s^{0.5}[1 + (Le^m - 1)\frac{h_D}{h_s}] \tag{2}$$

where

Le = Lewis Number = 1.4

m = 0.52 for Equilibrium Boundary Layer Flow

= 0.63 for Frozen Boundary Layer Flow

It is apparent that eqn.(2) is quite complex, particularly since terms such as the enthalpies and the velocity gradient are themselves derived from long equations.

Lees Approximate Method, presented in 1958 (See Ref. 11), resulted in a reasonably accurate (+ or - 12 percent) value for stagnation point heat transfer rate.

$$\dot{q}_s = \frac{1}{\sqrt{R_o}}(15.5)2^{0.5n}(\rho_\infty)^{0.5}(\frac{V_\infty}{1000})^3 \tag{3}$$

For pencil and paper preliminary design, Lees Approximate Method provided the necessary accuracy with the minimum amount of computation and the least chance for error. Lees Approximate Method was also the chosen as the standard method by Hankey (Ref. 11).

Fortunately, the group had access to MINIVER, a software tool that calculates stagnation point heating rates as well as heating rates at other regions. MINIVER utilizes the Fay-Riddell Method among others, depending on the region and flow regime. Between Fay-Riddell, Lees and MINIVER, the group was able to verify results quickly. This practice not only served to increase the group's confidence in the results but also to increase the group's understanding of the physical phenomenon.

So far, stagnation POINT heat transfer rates ($\frac{Btu}{Ft^2 Sec}$) have been discussed. Before one can speak of heat loads ($\frac{Btu}{Sec}$), the heat transfer rates away from the stagnation point must be determined and the frontal area must be known. The heat transfer rate away from the stagnation point is given as a function of theta by

$$\dot{q} = \dot{q}_s(COS\theta)^{3/2} \tag{4}$$

for θ up to 60^o. This correlation is accurate to within seven percent (See Ref.11). Since five degree half angle nose cones are considered appropriate for hypersonic aircraft (See Ref.4), theta varies from 0 to 85 degrees. This range is beyond the sixty degree limit of accuracy, but is adequate for a first order approximation. Using the incremental area as shown Figure 6, the above equation is integrated over theta to give heat transfer ($\frac{Btu}{Sec}$) through the nose. Recall that heat transfer rate PER AREA decreases with an increase in nose radius. However, total heat transfer increases with an increase in nose radius. This is due to the increase in frontal area with larger radii. An optimum would have to be found between the size of the nose radius and and the size of the conical portion of the nose. Correlations exist that give heat transfer rates for flat plates at angles of attack. Using the proper incremental area, these correlations can be integrated to find the total heat transfer to the conical portion of the nose.

5 Mission Selection

The first step involved the derivation of stagnation point heat transfer rates ($\frac{Btu}{ft^2 sec}$) using Lees Approximate Method for various flight conditions. Heat transfer rates were computed in terms of nose radius and wall enthalpy, h_w, given by

$$h_w = 0.234(T_w) + (10)^{-5}(T_w)^2 \tag{5}$$

This allowed designers to vary the important parameters of nose radius and wall tem-

perature at a given flight condition and determine the heat transfer rate. The following is a list of some of the flight conditions examined. Stagnation point heat transfer is given by

$$\dot{q}_s = \frac{X}{\sqrt{R_o}}(1 - \frac{h_w}{Y}) \tag{6}$$

where X and Y are constants FOR THAT FLIGHT CONDITION.

MACH	ALTITUDE	X	Y
6	50000	74.07	777.40
	70000	49.02	782.70
8	50000	175.75	1307.02
	70000	116.19	1315.11
9	100000	93.24	1704.68
10	50000	343.30	1987.30
	70000	226.95	2000.45

A graphical summary of this data is given in Figure 2 for various nose radii and flight conditions. In addition, sample calculations can be found in Appendix 1.

At this point, the worst case must be examined. Provided there exists no active cooling scheme and the structure of the vehicle does not act as a heat sink, the final equilibrium temperature of the nose must be determined. Even if the heat from aerothermal heating is not bled off by a coolant or absorbed by the structure, energy is still lost to the surroundings via radiation. There exists some temperature such that the amount of heat coming in due to convection is exactly equal to the amount of heat leaving due to radiation (See Figure

3). This temperature is called the equilibrium temperature and can be solved for by using the following equation.

$$\dot{q}_s = \epsilon\sigma(T_{w,eq}^4 - T_\infty^4) \tag{7}$$

T_∞ can be taken to be zero and as a first estimate, ϵ, the emissivity, can be taken to be 0.85. For the same flight conditions listed above and a nose radius of four feet, the corresponding equilibrium temperatures are given below.

MACH	ALTITUDE [ft]	EQUILIBRIUM TEMP. [R]
6	50000	2225
	70000	2090
8	50000	3025
	70000	2810
10	50000	3777
	70000	3525

Note that even with such a large and impractical nose radius, the equilibrium temperatures become too high for a conventional material such as aluminum. Therefore, an active cooling system must be designed that can maintain the nose at a reasonable temperature. Figure 4 shows equilibrium temperatures at 100,000 feet as a function of Mach number and nose radius. Note that at our designated flight condition of Mach 10, 100,000 feet the equilibrium wall temperature is about $4500R$.

The next parameter that must be examined is the time required for the nose to reach equilibrium, provided no heat is bled off by a coolant or absorbed by the structure. An approximate energy balance that gives an estimate of time required to reach equilibrium skin temperature is given by

$$\rho C_p V(T_{w,eq} - T_{initial}) = \dot{q}_s A \Delta t - \sigma \epsilon A(T_{w,eq} - T_\infty)\Delta t \tag{8}$$

Assuming an "eggshell" type structure of uniform thickness, times on the order of seconds are required to reach equilibrium (See Figure 5). Aluminum, 1/16" thick takes the longest to reach steady state. In reality, there would exist some support structure behind the shell (spars, ribs, etc.) that would act as a heat sink and lengthen time to equilibrium. However, the craft would have to be accelerated to its target flight condition. As it passes through the lower Mach numbers, it would experience aerothermal heating. Therefore, when the clock "starts", $T_{initial}$ is already greater than the temperature at launch. Despite these complications, it is obvious that a drone at the designated flight condition would easily reach thermal equilibrium within the estimated 5.32 minute burn time.

In summary,

1) There exists several methods, including the code HETAQ, that allow rapid and accurate calculation of stagnation point heat transfer rates.

2) The stagnation point is the area of critical aerodynamic heating.

3) Correlations for heat transfer rates can be integrated over frontal areas to determine

total heat transfer ($\frac{Btu}{Sec}$) for a reasonable first estimate.

4) Heat transfer rates and heat loads at hypersonic speeds are large enough to warrant design of an active cooling system for any vehicle that spends more than even a few seconds in these regimes.

5) Due to propulsion and drag considerations, Mach 10 and 100,000 feet is chosen as the target flight condition.

6) With an estimated flight time of 5.32 minutes at Mach 10, 100,000 feet, the nose of the aircraft should reach thermal equilibrium long before the hydrogen fuel runs out.

6 Analysis and Design of an Active Cooling System

High heating rates at the nose of the drone dictate that the coolant be routed from the tank to the stagnation region and then back along the cone before being routed to the scramjet (See Figure 7). The design is broken up into two parts; impingement cooling and panel cooling. Impingement cooling takes place in the manifold immediately behind the stagnation region where a single jet of coolant impinges on the inside surface of the nose and is then routed into numerous tubes. Panel cooling takes place after the coolant enters the tubes and is modelled by a fin analysis.

Both impingement cooling and panel cooling are modelled in the Actively Cooled Structure Evaluation System (ACSES), a FORTRAN computer program written by the authors.

6.1 Impingement Cooling

A method commonly used to cool the leading edge of a gas-turbine airfoil involves the impingement of a jet of coolant against the leading edge's inside surface. Impingement cooling can also be applied to the nose of the hypersonic research vehicle currently under study by the UCLA Advanced Aeronautics Design Class.

In Ref. 13, Livingood presents Nusselt number correlations determined experimentally for jet impingement upon a concave, semi-hemispherical surface. Since the nose of the hypersonic test vehicle was modelled as a semi-hemisphere, a subroutine program called upon by ACSES utilized these correlations in determining the final fluid bulk temperature

exiting the semi-hemisphere manifold.

The geometrical parameters of the manifold (see Figure 8), including nozzle diameter, d, nose radius, R_n, and distance between the nozzle and the nose inner surface Z_n, were input into the program. These parameters could be varied to optimize the manifold design. The fluid bulk temperature entering the manifold from the nozzle ($T_{b,noz}$), and the coolant mass flow rate through the nozzle, MFR_{noz}, were also input and optimized. Finally, fluid properties for two different coolants were used. The program outputted the fluid bulk temperature exiting the impingement cooling apparatus, $T_{b,out}$. This $T_{b,out}$ value was then returned to the program as the inital coolant temperature entering the active cooling tubes extending aft of the nose.

The procedure used to find $T_{b,out}$ was an iterative one. First, an initial guess was made for $T_{b,out}$. Fluid properties were then calculated based on the film temperature T_{film}:

$$T_{film} = 0.5[T_{w,max} + 0.5(T_{b,noz} + T_{out})], \tag{9}$$

where $T_{w,max}$ was the maximum allowable wall temperature. For the design considered, the nose wall was assumed to be at $T_{w,max}$ for the maximum efficiency of the design. $T_{w,max}$ itself was considered a conservative value since it was taken as half of the material's melting temperature.

The average Nusselt number correlation, Nu_{ave}, for jet impingement on a concave semi-hemisphere, as presented by Livingood (Ref. 13), was used to determine an average heat transfer coefficient h_{ave}. The correlation and the resulting average heat transfer coefficient

are presented below.

$$Nu_{ave} = 2.98 Re^{0.585} (\frac{d}{D})^{1.10} (\frac{Zn}{d})^{-0.007}; \tag{10}$$

$$h_{ave} = \frac{Nu_{ave} k}{d} \tag{11}$$

where,

Re = Reynolds number based on nozzle diameter, d

D = 2 R_n = nose diameter

k = thermal conductivity of the coolant

Once the average heat transfer coefficient was obtained, the total heat transfer into the coolant was evaluated. The coolant heat transfer was equivalent to the aerodynamic stagnation point heating of the nose minus the radiative cooling. Thermal resistivity through the thin-skinned, highly conductive nose was considered negligible in this analysis. Thus, the coolant heat transfer was:

$$q_{coolant} = q_{nose} - q_{radiation} \tag{12}$$

where q_{nose} was a function of the stagnation heat flux as determined by Lees' approximate method of stagnation heating in Hankey's report (Ref. 11), and outlined in Appendix 1. Given the surface area of the nose, the temperature exiting the manifold could be easily determined:

$$q_{coolant} = h_{ave} A_{surf} (T_{b,out} - T_{b,noz}) \tag{13}$$

or,

$$T_{b,out} = \frac{q_{coolant}}{h_{ave} A_{surf}} + T_{b,noz} \tag{14}$$

This $T_{b,out}$ was then compared with the initial guess, and the entire procedure was repeated until the values for $T_{b,out}$ converged.

6.2 Panel Cooling

The coolant tubes were placed equidistant apart on the cone. The distance between the tubes L, was therefore only a function of x, the distance from the manifold. This symmetry of the geometry and the assumed symmetry of the aerodynamic heat load dictated that only one of the coolant panes need be considered. These panels were then divided into slices of width and analyzed accordingly.

fig a.

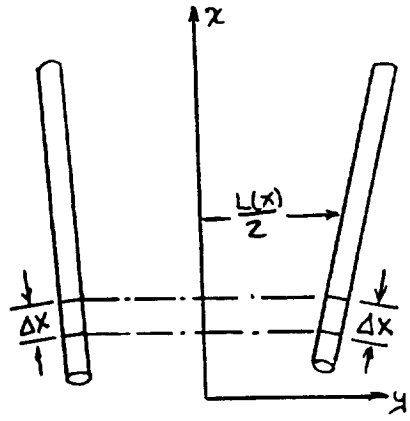

The analysis was divided into three modes of heat transfer: convection from the coolant to the inside wall of the tube; conduction from the inside wall to the outside wall of the tube;

and conduction from the base of the fin through the nose cone wall (which was modeled as a fin). Given an initial coolant fluid temperature, the goal of this analysis was to calculate the maximum temperature of the panel.

6.2.1 Fin Analysis Due to symmetry, coolant temperature at a given x location was independent of the particular tube. This fact implied a temperature profile shown below, with $\frac{\partial T}{\partial y} = 0$ at the midpoint section of the two adjacent tubes.

fig b.

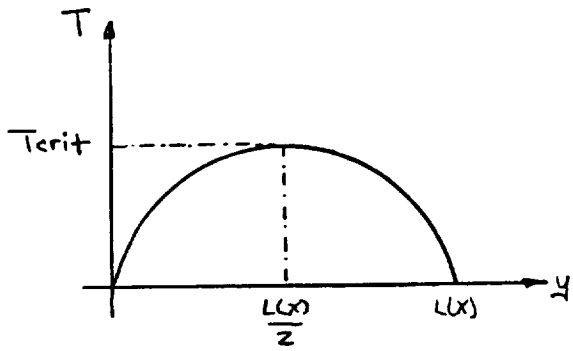

The analysis was then simplified, in that only half of the panel need be modeled by the fin. The fin endpoints were the base of the tube and the midline of the two adjacent tubes. A detailed derivation follows.

fig c.

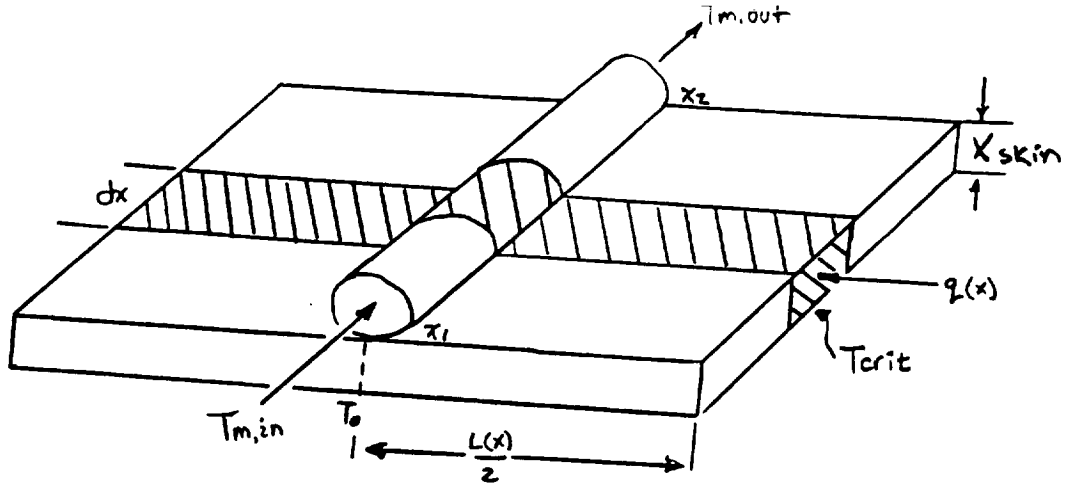

q(x) = Heat flux

X_{skin} = Thickness of skin.

T_o = Base of "fin" temperature.

X_1, X_2 = Station locations: $\Delta x = x_2 - x_1$

Performing an energy balance in the y direction:

•Assume Top surface adiabatic: Temperature and heat flux constant across width Δx

$$qA_c|_y - qA_c|_{y+dy} + q_s P dy = 0 \tag{15}$$

A_c = cross sectional area = $t \cdot \Delta x$

P = exposed perimeter = Δx

•Dividing by dy and using the definition of a derivative and Fourier's Law: $q = -k\frac{\partial T}{\partial y}$ the above equation becomes:

$$kt\frac{\partial^2 T}{\partial y^2} + q_s(x) = 0 \tag{16}$$

•However, it was assumed the temperature did not vary across the width Δx so an ordinary differential equation was obtained (Eqn 17):

$$kt\frac{d^2 T}{dy^2} + q_s(x) = 0 \tag{17}$$

•Boundary conditions:

$$\frac{dT}{dy} = 0 \ldots\ldots y = \frac{L}{2} \tag{18}$$

$$T = T_o \ldots\ldots y = 0 \tag{19}$$

•Integrating twice:

$$T = -\frac{q_s(x)}{2kt} y^2 + C_1 y + C_2 \tag{20}$$

•Applying the boundary conditions, and solving for the constants, Eqn 20 becomes:

$$T = \frac{q_s(x)}{2kt}(y^2 - yL) + T_o \tag{21}$$

Equation 21 applies anywhere along the fin; however, the temperature of interest was the midline temperature of the panel, which was the maximum temperature the panel of skin would reach: $T_{y=\frac{L}{2}} = T_{crit}$

$$T_{crit} = q_s(x)(\frac{L^2}{8kt}) + T_o \tag{22}$$

T_o, the temperature at the base of the fin which was the same as the temperature on the outside wall of the tube, was calculated from the conduction and convection analysis.

6.2.2 Convection The total heat that must be absorbed by the coolant fluid was equal to twice the amount of heat absorbed over the surface area of the fin, as heat was entering the tube from both sides

$$Q = L(x) q_s \Delta x \tag{23}$$

The flow in the tube was turbulent with a high temperature gradient at the wall. Thus a convection correlation given by Incopera and DeWitt(Ref. 9) was used to best fit the conditions.

$$Nu_d = 0.027 Re_d^{4/5} Pr^{1/3} (\frac{\mu}{\mu_s})^{0.14}$$

mu = dynamic viscosity at the mean temperature of the fluid

mu_s = dynamic viscosity at the wall temperature

Re_d = $\frac{Ud}{\nu}$

valid if:

$0.7 \leq Pr \leq 16,700$,

$Re_d \geq 10,000$,

4d $\geq$ 10,

•The heat transfer coefficient can be calculated from the Nusselt number:

$$h = \frac{Nu_d k}{d} \tag{25}$$

•From Newton's Law of Cooling, the temperature of the wall can be calculated:

$$T_{wall} = T_m + \frac{Q}{hA_{xc}} \tag{26}$$

The properties were evaluated at T_m, the bulk mean temperature of the fluid. T_m was calculated by using a heat balance. Knowing an initial $T_{m,in}$, $T(m, out)$ can be calculated:

$$T_{m,out} = \frac{Q}{\dot{m} C_p} + T_{m,in} \tag{27}$$

Therefore, the temperature of the inside wall was now known and could be used in the conduction analysis to calculate the temperature on the outside of the wall of the tube, or T_o, as it was referred to in the fin analysis.

6.2.3 Conduction

fig d.

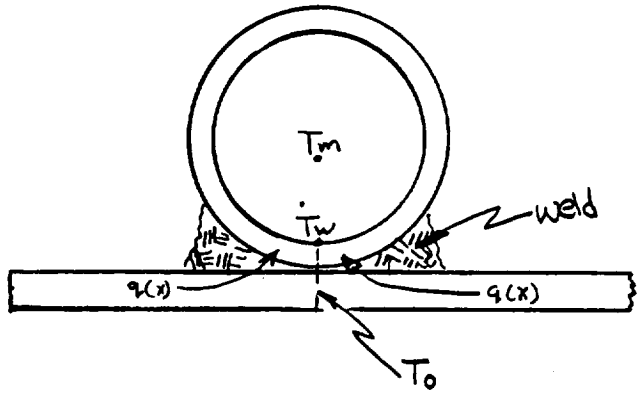

The equation for conduction heat transfer through a plane was used to calculate the outside wall temperature, T_o. The heat was assumed to flow through the bottom of the tube only. A fin analysis of the circumference of the tube demonstrated a rapid decrease in wall temperature after approximately 30 percent of the diameter. Because the tube was welded to the nose wall, additional heat transfer would occur. Thus, 50 percent

of the surface area was chosen as the effective area of conduction.

$$A_{cond} = \frac{d\pi\Delta x}{2} \tag{28}$$

Treating the tube as a flat plate of thickness x_{tube}, and thermal conductivity k_{tube}, the heat rate is:

$$Q = \frac{k_{tube}}{x_{tube}} A_{cond}(T_o - T_{wall}) \tag{29}$$

This equation can be solved for T_o

$$T_o = \frac{Q x_{tube}}{k_{tube} A_{cond}} + T_{wall} \tag{30}$$

The conduction heat transfer and the convection heat transfer equations were combined into a thermal resistance network. Conservation of energy implied the heat rates, Q, used in equations (26) and (29) must be equal.

network

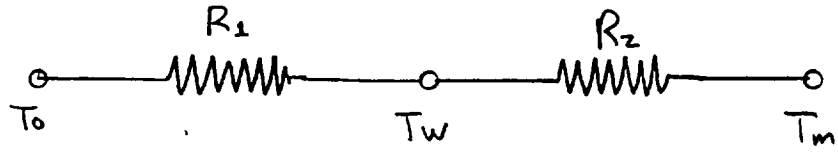

$$R_1 = \frac{x_{tube}}{k_{tube} A_{cond}} \tag{31}$$

$$R_2 = \frac{1}{hA_{xc}} \tag{32}$$

$$T_o = Q(\frac{1}{hA_{cross}} + \frac{x_{tube}}{k_{tube}A_{cond}}) + T_m \tag{33}$$

Finally, T_o can be calculated from eqn. (33) and T_{crit} from eqn. (22). The objective of the design was to keep T_{crit} less than the maximum allowable temperature for the nose cone material, T_{max}.

7 Results/Discussion

Two design configurations were evaluated. One utilized liquid hydrogen as the coolant and the other a 30 percent aqueous glycol solution. The hydrogen configuration was composed of supercritical hydrogen flowing directly from a highly pressurized fuel tank to the active cooling system design. The hydrogen was then diverted back to the scramjet engine. The ethylene glycol design consisted of glycol circulating through a closed loop system including a pump, a heat exchanger, and the active cooling system design.

Both the designs were formulated with three common constraints in mind: the critical temperature was to remain less than the maximum allowable material temperature; the coolant velocity was to be less than the fluid speed of sound; and the pressure loss was to be kept as small as possible. A description of the specific constraints applied to each design is presented below.

The critical wall temperature for both designs was set at 1000 K. This corresponded to half the melting temperature of the wall material, molybdenum. This constraint was the most critical for both designs.

In the hydrogen design, the constraint placed upon fluid velocity was the most restrictive. The highest value of fluid velocity occurred in the nozzle entering the manifold. The fluid temperature in the nozzle was assumed to be equal to 20 K. The speed of sound of supercritical hydrogen was then found to be 1675 m/s (Appendix 4). The pressure of the hydrogen stored in the fuel tank was assumed to be approximately 3000 psi. It was decided to set the maximum allowable pressure to twenty-five percent or 750 psi.

Similarly, the glycol design constraints were determined. The speed of sound was 1644 m/s (Ref. 6), and the maximum pressure loss was assumed to be about 700 psi, to limit the size of the pump required. An additional constraint placed on the glycol design involved the temperature range of the coolant. The freezing point of a 30 percent aqueous

glycol solution is 257 K; this temperature was chosen as the minimum coolant temperature. The maximum coolant temperature was chosen to be 420 K (Ref. 6).

Once given the design constraints, various parametric studies were performed and several observations were made. In order to decrease the pressure loss, large tubes or smaller coolant mass flow rates were needed. However, with a smaller mass flow rate, the nose temperature increased and more tube branching was required. The larger the tube size, the less efficient was the heat transfer in the tube. Hence the critical wall temperature increased with increasing tube size.

7.1 Final Designs

Liquid Hydrogen Coolant Final Design:

After parametrically varying mass flow rate and tube geometry, the liquid hydrogen design converged upon the following configuration (see Appendix 3.1):

mass flow rate : 3.5 kg/s

Tube diameter : 4.88 mm

wall thickness : 2mm

initial number of tubes : 24

Branching locations : 0.225 m, 0.875 m, 2.1m, 3.55 m

Coolant velocities are kept well within the sonic range in both the impingement nozzle (806 m/s) and the tubes (281m/s). System pressure loss is also kept to a minimum of about 150 psi. Outlet coolant temperature is 703 K. Therefore, all of the previously mentioned constraints were satisfied.

Increasing tube size would lower the pressure drop even more for the same mass flow rate. However, the fewer number of tubes allowed would result in the critical temperature being exceeded. Hence, 4.88 mm diameter tubes are the largest standard tubing that can be used with out fear of the craft exceeding the critical temperature.

30 Percent Aqueous Glycol Solution Final Design:

The critical aspect about the glycol coolant design was minimizing temperatures near the stagnation region. This was accomplished by using small tube sizes and as many tubes as allowed by the geometry. Since the density of this coolant is much larger than that of liquid hydrogen, and since the glycol flows in a closed system with a heat exchanger, high mass flow rates could also be used to minimize initial wall temperatures. This, however, created large pressure losses which would have to be overcome with a powerful pumping system.

The following configuration was determined to best satisfy the design constraints on wall critical temperature and coolant pressure loss (see Appendix 3.2):

mass flow rate : 150 kg/s

Tube diameter : 6.5mm

wall thickness : 2.5mm

initial number of tubes : 20

Branching locations : 0.1m, 0.75m, 1.9m, 4.35m

The velocity of the coolant remains within the sonic limit both in the impingement nozzle (953 m/s) and the tubes (224 m/s). The outlet temperature of the glycol solution is 418 K. The pressure loss in the system is relatively high (1422 psi). Therefore, all of the constraints were satisfied save that of pressure loss.

This high pressure loss was found to be unavoidable. In order to keep the critical wall temperature below 1000 K at all stations, a high mass flow rate and a thick skin were required. Since weight is a critical issue in any aircraft design, the 2.5 mm wall thickness was judged to be as thick as desired. Taking all of the above into consideration, a compromise on the pressure loss was required. This resulted in a pressure loss 722 psi greater than the imposed design constraint.

Because the ethylene glycol design required a heat exchanger, a preliminary heat exchanger analysis was performed in which heat transfer coefficients of liquid hydrogen and glycol were compared. Given a tubular counter-flow heat exchanger, calculations were performed (listed in Appendix 1.5), and it was determined that the heat transfer coefficient for the liquid hydrogen was only about two to three times smaller than that of the ethylene glycol, given similar conditions. Thus, a configuration of bare concentric tubes could be used without fins on the inner tube extending out into the liquid hydrogen. If the proposed ethylene glycol design was chosen as the preferable design, the next step then would be to utilize software capable of designing such a heat exchanger.

7.2 Comparison of the Two Designs

The liquid hydrogen design met all of the design constraints with a satisfactory margin of safety, whereas the ethylene glycol design failed to meet the pressure constraint, and met the temperature constraint with a very low margin of safety. In addition, the ethylene glycol design required a heat exchanger and a large pump, as well as a greater skin thickness, all of which add considerably to the weight of the drone vehicle. Therefore, the liquid hydrogen design was deemed the better of the two.

One concern about the liquid hydrogen design is safety. In particular, a leak may prove to be disastrous for such a highly pressurized system of hydrogen. Because this will be placed on an unmanned drone vehicle, weight considerations dictated this small compromise in safety. In application to the NASP, however, appropriate safety measures could be taken to insure against such an occurrence.

8 Summary

Given an existing configuration, the authors determined a suitable flight condition for a hypersonic drone that would require some form of active cooling scheme and provide the propulsion group with an adequate challenge. The flight condition chosen was Mach 10 at 100,000 feet. The authors wrote a FORTRAN program called HETAQ (Hypersonic Equilibrium Temperature and Heat Flux) that parametrically varied Mach and altitude while computing equilibrium temperatures, heat fluxes and flight times for each flight condition.

Heating rates for regions aft of the stagnation point were derived for the chosen flight condition. An active cooling configuration was determined and consisted of coolant impinging on the inside of the skin at the stagnation region and then being routed through numerous tubes running back along the inside of the nose cone.

The authors wrote ACSES (Actively Cooled Structure Evaluation System), a FORTRAN program that allows the user to vary tube and manifold geometry, mass flow rate, and coolant to observe what effect these parameters have on critical temperature, coolant temperature, and pressure loss.

A design for liquid hydrogen coolant was formulated that optimized pressure loss and mass flow rate, given imposed design constraints. A design for ethylene glycol was also formulated. The hydrogen design was deemed the better of the two for the drone vehicle, based on weight considerations.

9 The Bibliography

References

1. "Aerodynamic Preliminary Analysis System (APAS)." NASA-Langley.

2. Average Heat-Transfer Characteristics of a Row of Circular Air Jets Impinging on a Concave Surface." NASA TM X-2657. 1972.

3. Bowers, Albion and Illif, Kenneth W. "A Generic Hypersonic Aerodynamic Model Example (GHAME)." NASA Ames-Dryden. A Proposed NASA TM. September 1987.

4. Bowers, Al. NASA Ames-Dryden.

5. Chupp, R., Helms, H., McFadden, P., and Brown, T. "Evaluation of Internal Heat-Transfer Coefficients for Impingement-Cooled Turbine Airfoils." J. Aircraft V 16, No.3, May-June 1969, pp 203-208.

6. CRC Handbook of Tables for Applied Engineering Science, 2nd Edition. Bolz, R.E. and Ture, G.L., CRC Press Inc; Cleveland,1973.

7. Hydrogen: Its Technology and Implications. Cox,K.E. and Williamson, K.D.. CRC Press; Cleveland, 1975.

8. DeJarnette, Fred R. and McNeil, F. "A Review of some Approximate Methods Used in Aerodynamic Heating Analysis." J. Thermophysics, Vol 1 no 1 (January 1987).

9. Fundamentals of Heat and Mass Transfer. Incopera, Frank and DeWitt, David. John Wiley and Sons; New York, 1985.

10. Gentry, E. and Douglas, S. "Hypersonic Arbitrary Body Program", McDonnell Douglas Corporation.

11. Hankey, Wilbur L., Jr, Neumann, Richard 1Lt. USAF, and Flynn, Evard. "Design Procedures for Computing Aerodynamic Heating at Hypersonic Speeds." Flight Dynamics Laboratory, Wright-Patterson AFB. June 1960.

12. Liepmann, H.W. and Roshko, A. "Elements of Gas Dynamics." CalTech. John Wiley. 1952.

13. Livingood, John and Gauntner, James. "Heat-Transfer Characteristics of a Single Circular Jet Impinging on a Concave Semihemispherical Surface." NASA TM X-2859. August 1973.

14. Local Heat Transfer Characteristics of a Row of Circular Air Jets Impinging on a Concave Semicylindrical Surface." NASA TN D-7127. January 1973.

15. Nowak, R.J., and Kelly, H.N.. "Actively Cooled Airframe Structures for High Speed Flight", J. Aircraft, v 14, no. 3, March 1977, p.p. 244-250.

16. Trauber, M., Menees, g., and Adelman, H. "Aerothermodynamics of Transatmospheric Vehicles." J. Aircraft, Vol 14 No 3 (March 1977).

17. Penland, et al. "Aerodynamic Characteristics of a Hypersonic Research Airplane Con-

cept Having a 70 Degree Swept Double-Delta Wing at Mach Numbers from 0.80 to 1.20 with Summary of Data from 0.2 to 6.0." NASA Langley Research Center, VA. NASA TP-1552 (1979).

18. Sova, G., and Divan, P. "Aerodynamic Preliminary Analysis System II." North American Aircraft Operations, Rockwell International.

19. vanDriest,

E.R. "The Problem of Aerodynamic Heating." Aeronautical Engineering Review, October 1956).

10 Figures

Figure 1

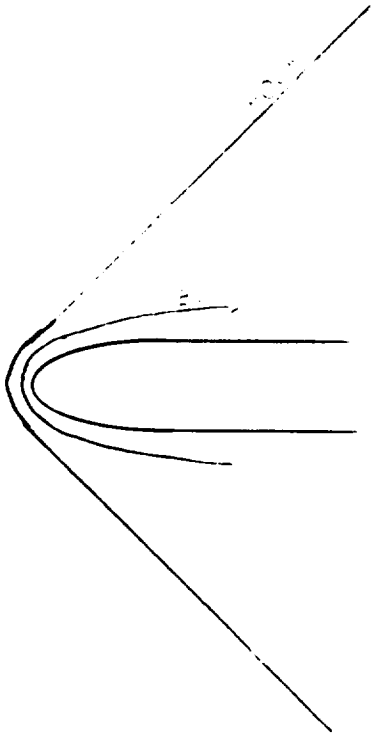

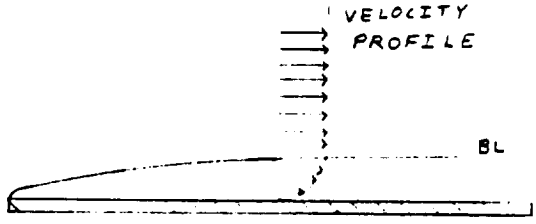

ORIGINAL PAGE IS
OF POOR QUALITY

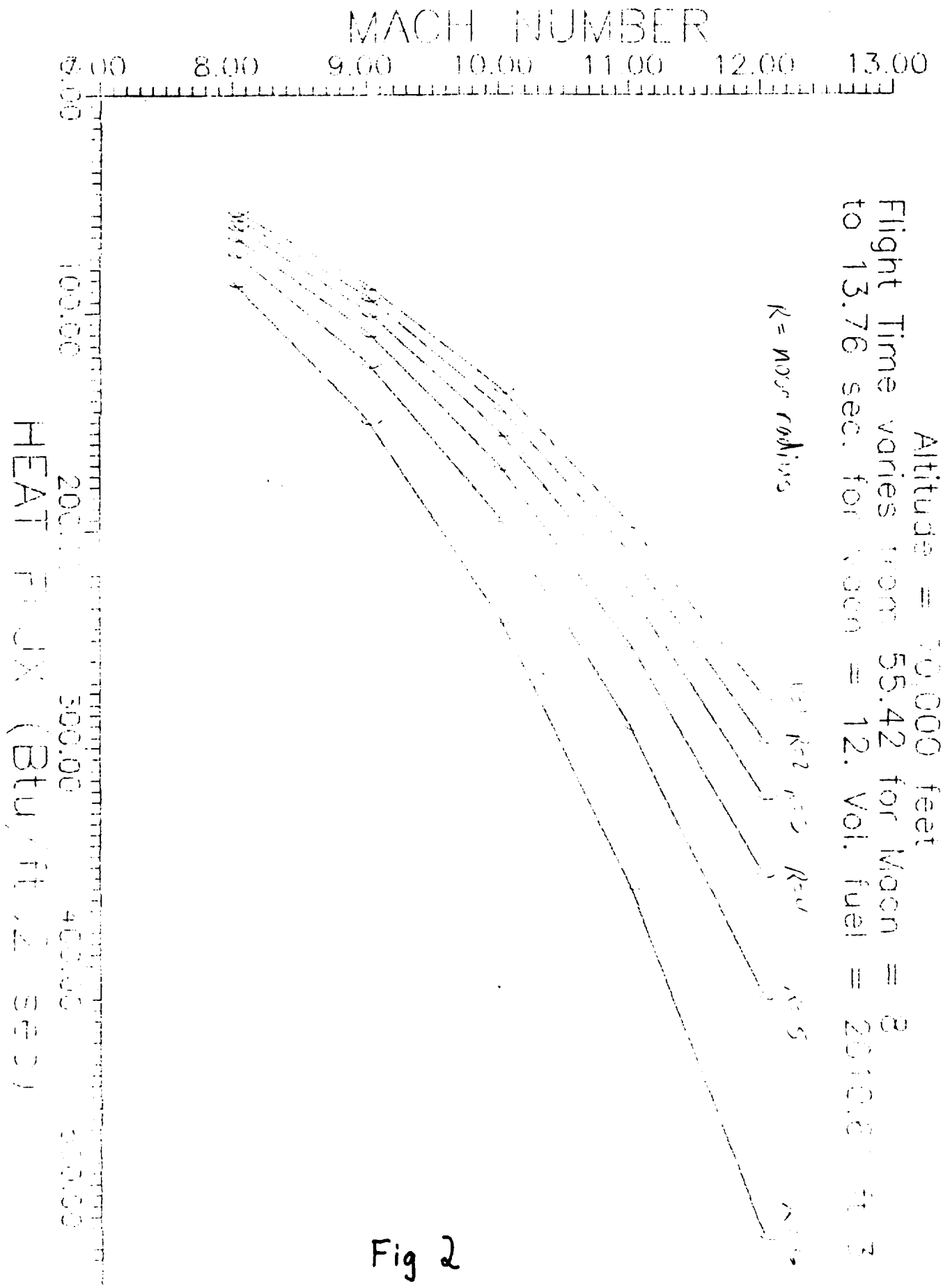

Fig 2

Skin Equilibrium Temperature Calculation

Energy balance on skin assuming no heat transfer through back-face:

convective heat transfer = radiative heat transfer

$$q_s A = q_r A$$

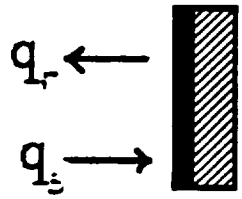

$$q_s A = \varepsilon \sigma A \left(T_{w,eq}^4 - T_\infty^4 \right)$$

q_s = heat flux at stagnation point from Lees approximate method

A = area

ε = emissivity of material

σ = Boltzmann constant

$T_{w,eq}$ = equilibrium wall temperature

T_∞ = ambient air temperature

$T_{w,eq}$ was calculated as a function of altitude, Mach number and nose radius to obtain a data base

Fig 3

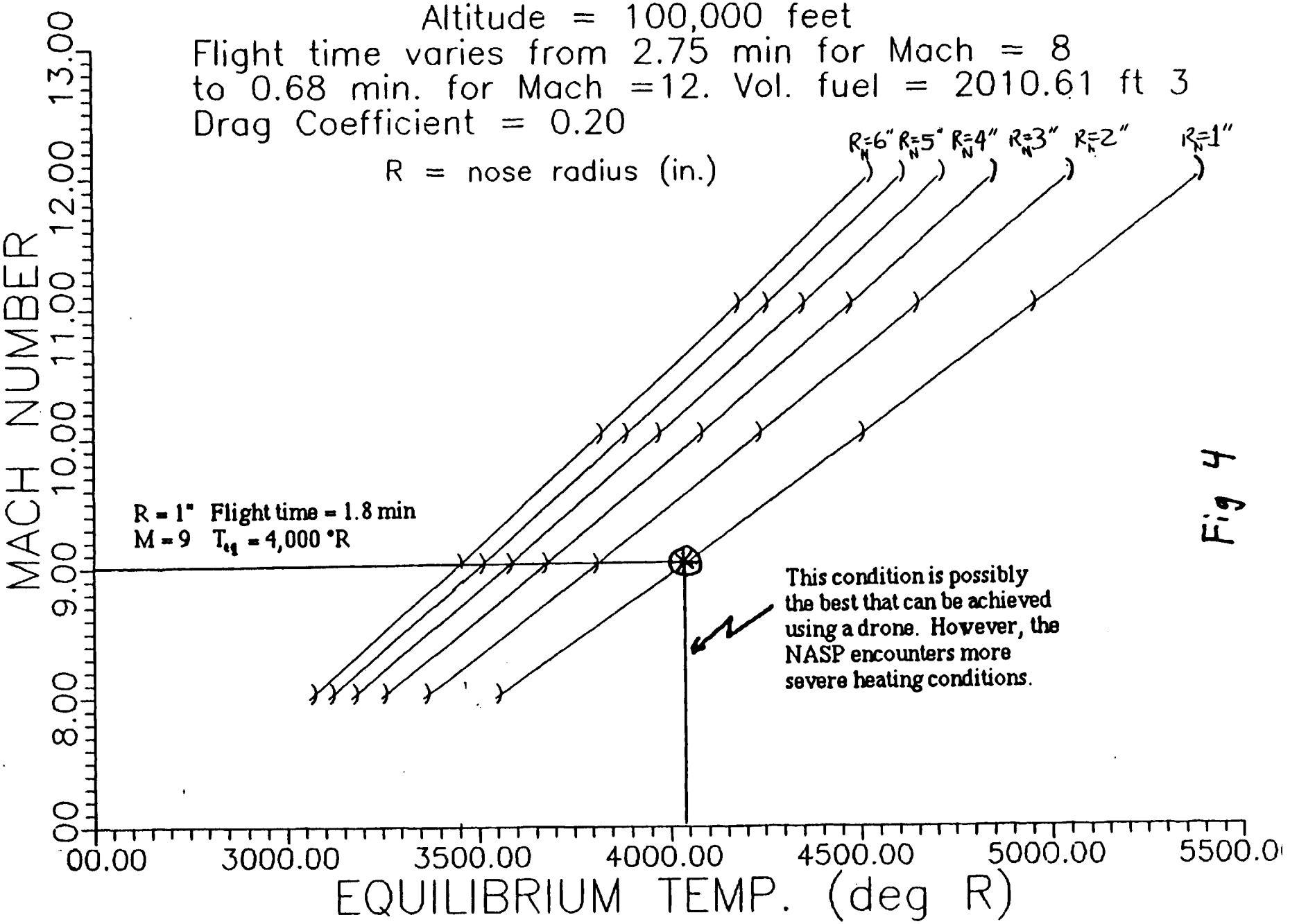
Altitude = 100,000 feet
Flight time varies from 2.75 min for Mach = 8
to 0.68 min. for Mach =12. Vol. fuel = 2010.61 ft 3
Drag Coefficient = 0.20
R = nose radius (in.)
R_N=6" R_N=5" R_N=4" R_N=3" R_N=2" R_N=1"
R = 1" Flight time = 1.8 min
M = 9 T_eq = 4,000 °R
This condition is possibly the best that can be achieved using a drone. However, the NASP encounters more severe heating conditions.
MACH NUMBER
8.00 9.00 10.00 11.00 12.00 13.00
00.00 3000.00 3500.00 4000.00 4500.00 5000.00 5500.0
EQUILIBRIUM TEMP. (deg R)

Fig 4

Time to Skin Equilibrium Temperature Calculation

Approximate energy balance to give an estimate of the flight time required to achieve the equilibrium skin temp.

$$\rho CV(T_{w,eq} - T_{initial}) =$$

$$q_s A \Delta t - \sigma \varepsilon A (T_{w,eq} - T_{\infty}) \Delta t$$

Some sample materials
at 100,000 ft; Mach 9; radius = 1"
flight time = 1.8 min

	Skin Thickness	
	1 mm	1/16"
Aluminum:	3.8 sec	6.0 sec
Titanium:	2.7 sec	4.3 sec

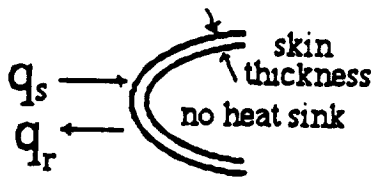

$q_s = q_r$

Fig 5

Heating Rates For Noses of Various Radii

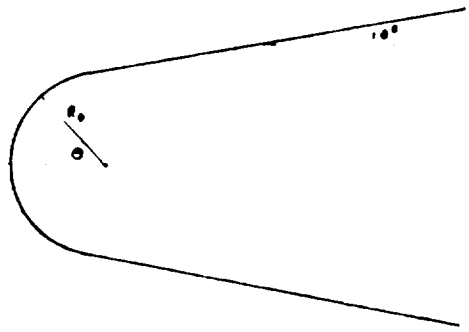

$0 \le \theta \le 80°$

$\dot{q} = \dot{q}_s (\cos\theta)^{3/2}$

$q = \dot{q} \cdot (\text{Area})$

Incremental Area $dA = 2\pi R_o \sin\theta \, d\theta$

$$q_{nose} = \int_0^{80°} \dot{q}_s (\cos\theta)^{3/2} \cdot 2 \cdot \pi \cdot R_o \sin\theta \, d\theta$$

$$\boxed{q_{nose} = \dot{q}_s \cdot R_o \cdot (2.4816)}$$

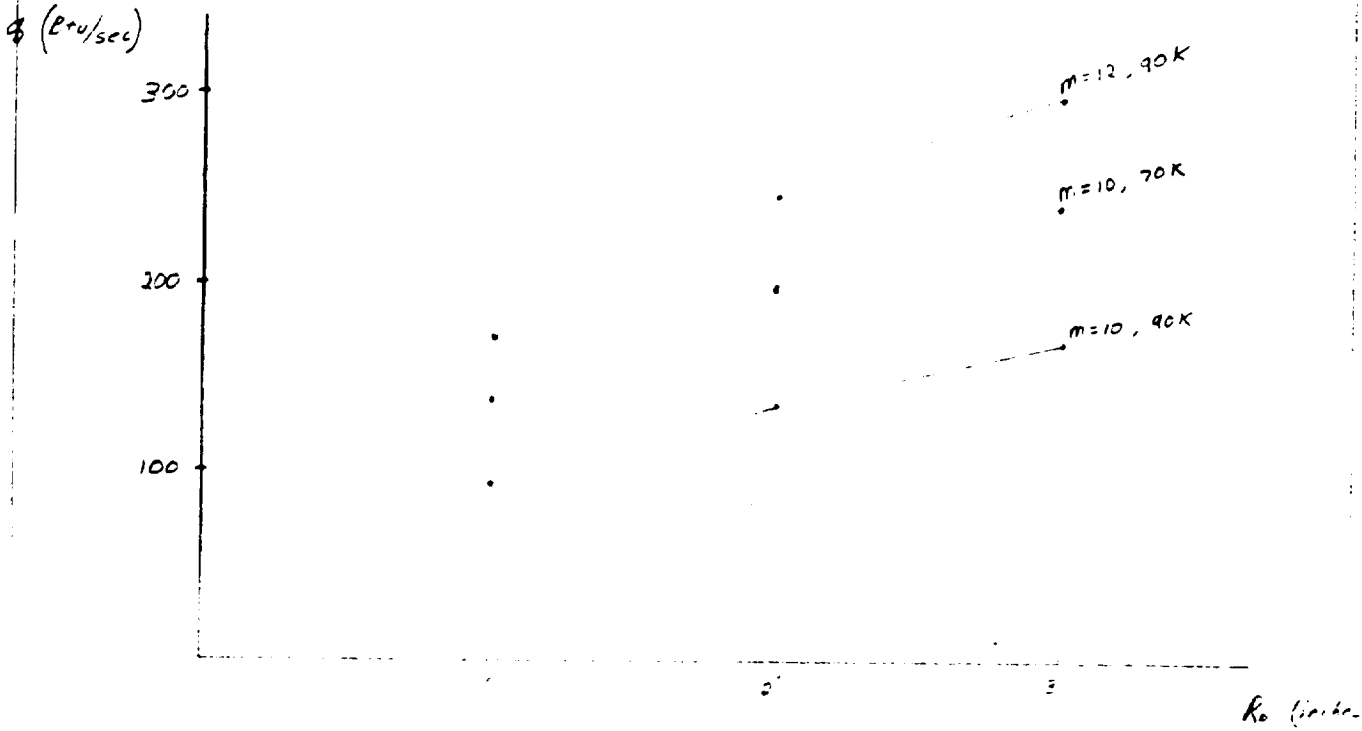

Fig 6

Combined Impingement and Actively Cooled Panel Concept for the Drone Nose:

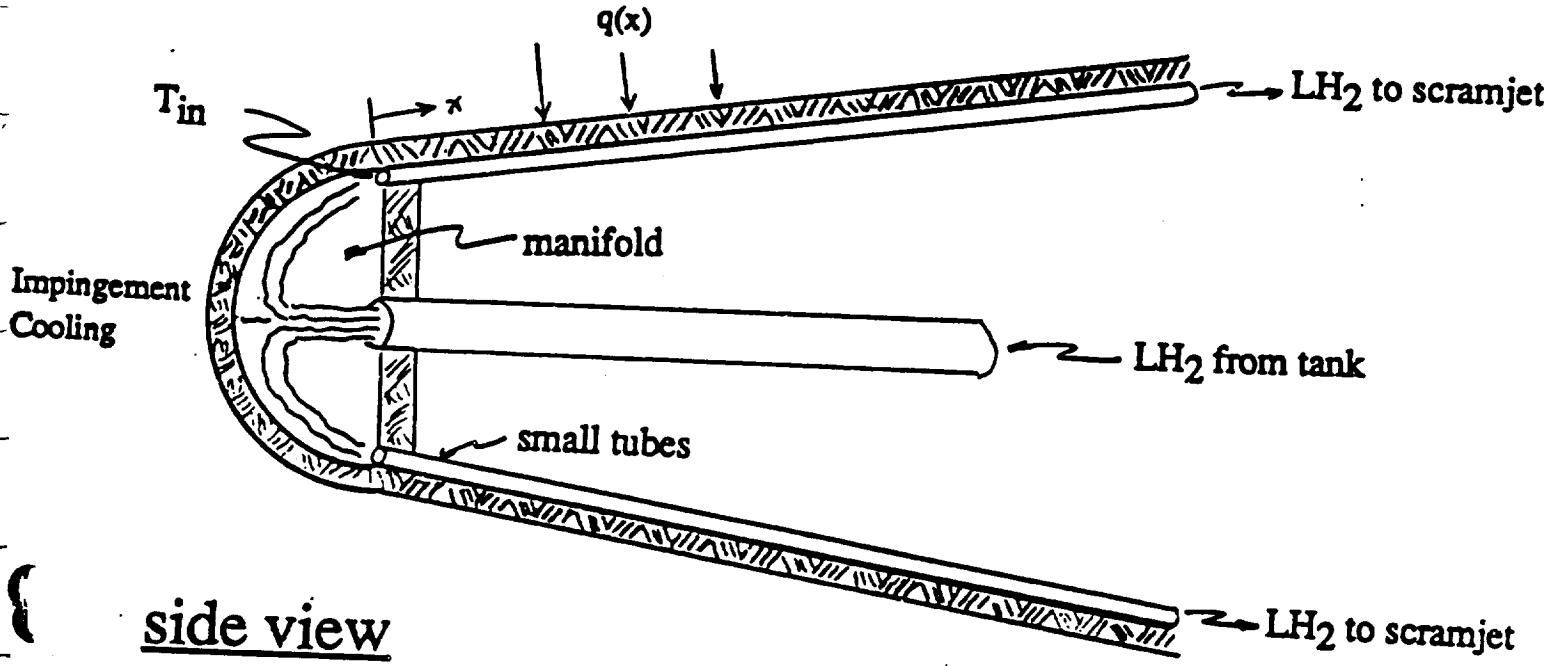

side view

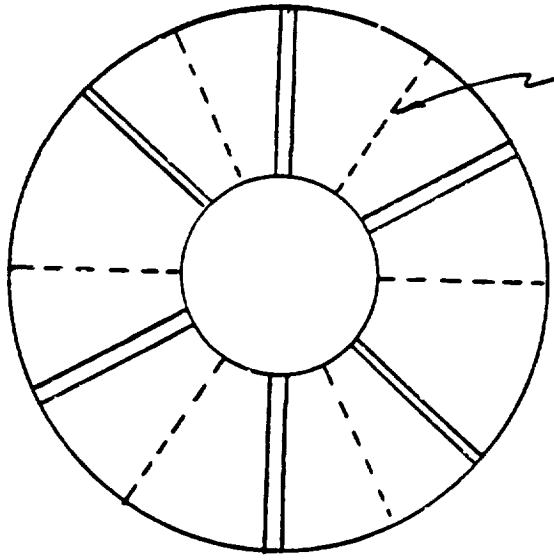

end view

* Maximum skin temperature is midway between coolant tubes

* Tubes welded to skin chosen to simplify fabrication

Fig 7

Impingement cooling at nose

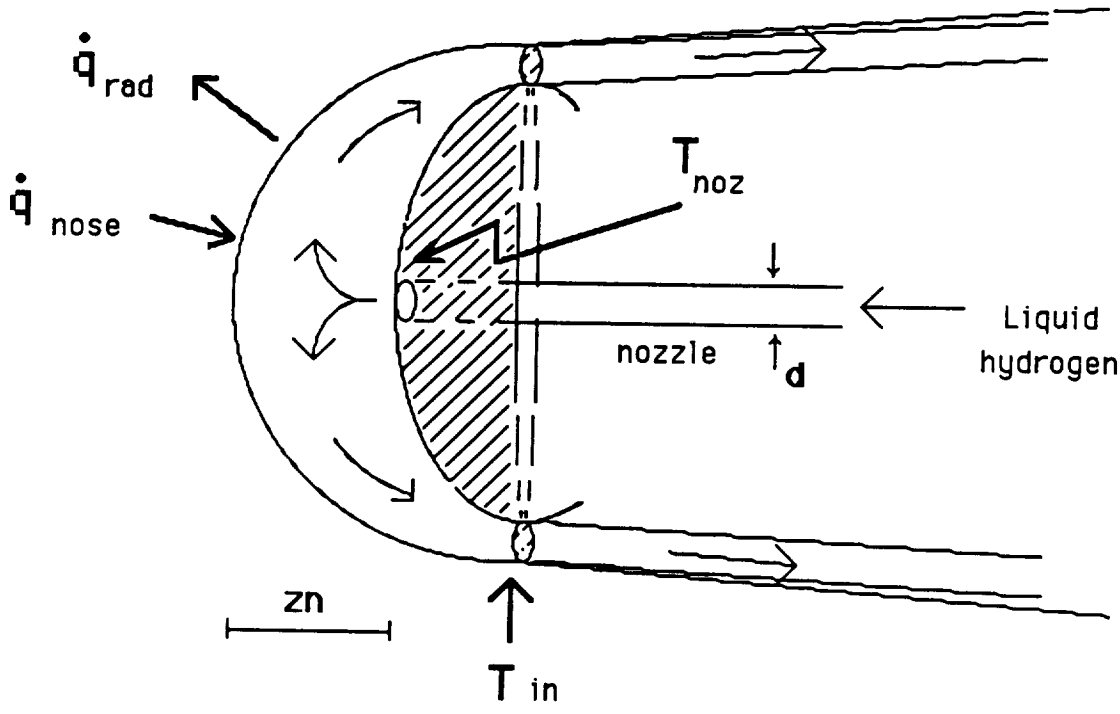

- **Livingood's correlation for $\overline{Nu}$ = f(Re, geometry)**

$$\overline{Nu} = 2.98\,(Re)^{0.585}\left(\frac{d}{D}\right)^{1.10}\left(\frac{zn}{d}\right)^{-0.007}$$

D = hemisphere diameter
zn = nozzle exit - to - target separation
d = nozzle diameter

- **Average heat transfer coefficient, $\overline{h} = \dfrac{\overline{Nu} * k}{d}$**

- **$(Tin - Tnoz) = \dfrac{\dot{q}_{nose} - \dot{q}_{rad}}{area * \overline{h}}$**

Fig 8

Appendix 1: Sample calculations

Appendix 1.1: Stagnation Point Heating

(Lees' Approximate Method)

$M = 6 \quad A = 70000$ ft (Lee's Approx)

$$V_\infty = 6(976) = 5856 \text{ ft/sec}$$

$$\rho_\infty = \rho_{SL} \exp(-h/23700) = 2.378\times10^{-4} \exp(-70000/23700)$$

$$= 1.24\times10^{-4} \text{ lb sec}^2/\text{ft}^4$$

$$h_s = h_c = .25 T_\infty + V_\infty^2/50100$$

$$= .25(460-67) + 5856^2/50100$$

$$= 782.73 \text{ Btu/lb}$$

$$\dot{q} = 21.92 (\rho_\infty^{.5}) \frac{1}{\sqrt{R_n}} \left(\frac{V_\infty}{1000}\right)^3 \left(1 - \frac{h_w}{h_s}\right)$$

$$\dot{q} = 21.92 (1.24\times10^{-4})^{.5} \frac{1}{\sqrt{R_n}} \left(\frac{5856}{1000}\right)^3 \left(1 - \frac{h_w}{782.73}\right)$$

$$\boxed{\dot{q} = \frac{49.02}{\sqrt{R_n}} \left(1 - \frac{h_w}{782.7}\right)} \quad \text{Btu/ft}^2\cdot\text{sec}$$

Equilibrium Temp for $R_n = 4$

$$h_w = .234 T_w + 1\times10^{-5} T_w^2$$

$$\dot{q}_{conv} = \dot{q}_{rad}$$

$$24.5 = .03131 h_w + .85(4.81\times10^{-13}) T_w^4$$

$$24.5 = .007327 T_w + 3.131\times10^{-7} T_w^2 + 4.0885\times10^{-13} T_w^4$$

Say $T_w = 1500°R$ $\quad 24.5 \neq 13.76$

Say $T_w = 2000°R$ $\quad 24.5 \cong 22.45$

Say $T_w = 2050°R$ $\quad 24.5 \cong 23.55$

Say $T_w = 2100°R$ $\quad 24.5 \cong 24.71$

$$\boxed{T_w \text{ @ Equilibrium} \cong 2090°R}$$

$M = 8$, $Alt = 70000$

$V_\infty = 8(976) = 7808$ ft/sec

$\rho_\infty = \rho_{SL} \exp(-h/23700)$

$= (2.378 \times 10^{-3}$ lb sec^2/ft$^4) \exp(-70000/23700)$

$= 1.24 \times 10^{-4}$ lb sec^2/ft^4

$$\dot{q} = 21.92 \sqrt{\rho_\infty} \cdot \frac{1}{\sqrt{R_o}} \left(\frac{V_\infty}{1000}\right)^3 \left(1 - \frac{h_w}{h_s}\right)$$

$$= 21.92 \sqrt{1.24 \times 10^{-4}} \cdot \frac{1}{\sqrt{R_o}} \left(\frac{7808}{1000}\right)^3 \left(1 - \frac{h_w}{h_s}\right)$$

$h_s = h_e = .25 T_\infty + V_\infty^2/50100$

$h_s = .25(460-67) + 7808^2/50100$

$h_s = 1315.11$ Btu/lb

$$\boxed{\dot{q} = \frac{116.19}{\sqrt{R_o}} \left(1 - \frac{h_w}{1315.11}\right)} \quad \text{Btu/ft}^2\text{ sec}$$

Equilibrium Wall Temp

$\dot{q}_{conv} = \dot{q}_{rad}$ for $R_o = 4$

$58.09 = .04417\, h_w + .85 (4.81 \times 10^{-13}) T_w^4$ $\quad h_w = .234 T_w + 1 \times 10^{-5} T_w$

$58.09 = .010337\, T_w + 4.417 \times 10^{-7} T_w^2 + 4.0885 \times 10^{-8} T_w^4$

Say $T_w = 2000°R$ $\quad 58.09 \neq 28.98$

Say $T_w = 2800°R$ $\quad 58.09 \cong 57.53$

$$\boxed{T_w \cong 2810°R}$$

$M = 10$, $Alt = 70k$ (Lee's Approx)

$$V_\infty = 10(976) = 9760 \text{ ft/sec}$$

$$\rho_\infty = (2.378 \times 10^{-3} \text{ lb sec}^2/\text{ft}^4) \exp(-70000/23700)$$

$$= 1.24 \times 10^{-4} \text{ lb sec}^2/\text{ft}^4$$

$$\dot{q} = 21.92 (1.24 \times 10^{-4})^{.5} \frac{1}{\sqrt{R_n}} \left(\frac{9760}{1000}\right)^3 \left(1 - \frac{h_w}{h_s}\right)$$

$$h_s = .25 T_\infty + U_\infty^2/50100$$

$$= .25(460 - 67) + 9760^2/50100$$

$$= 2000 \text{ Btu/lb}$$

$$\boxed{\dot{q} = \frac{226.95}{\sqrt{R_n}} \left(1 - \frac{h_w}{2000}\right)}$$

Equilibrium Temperature

$\dot{q}_{conv} = \dot{q}_{rad}$

$R = 4$ ft

$$\frac{226.95}{\sqrt{4}} \left(1 - \frac{h_w}{2000}\right) = .85(4.81 \times 10^{-13}) T_w^4$$

$$113.47 = .05673 h_w + 4.0885 \times 10^{-13} T_w^4$$

$$113.47 = .01327 T_w + 5.673 \times 10^{-7} T_w^2 + 4.0885 \times 10^{-13} T_w^4$$

Say	$T_w = 2000°R$	$113.47 \neq 35.35$
Say	$T_w = 3000°R$	$113.47 \neq 78.03$
Say	$T_w = 4500°R$	$113.47 \neq 238.8$
Say	$T_w = 3580°R$	$113 \doteq 108$
Say	$T_w = 3550°R$	$113 \doteq 119$

Equilibrium: $\boxed{T_{wall} \doteq 3525°R}$

$M = 6$ $\quad Alt = 50000$ ft

ORIGINAL PAGE IS OF POOR QUALITY

$$a = \sqrt{\gamma R T} = \sqrt{1.4(1731.3)(460 - 69.7)}$$

$$= 973 \text{ ft/sec}$$

$$V_\infty = 6(973) = 5836 \text{ ft/sec}$$

$$\rho_\infty = \rho_{SL} \exp(-h/23700) = 2.378 \times 10^{-3} \cdot \exp(-50000/23700)$$

$$= 2.89 \times 10^{-4} \text{ lb sec}^2/\text{ft}^4$$

$$h_s = h_c = .25 T_\infty + V_\infty^2/50100$$

$$= .25(460 - 69.7) + 5836^2/50100$$

$$= 777.4 \text{ Btu/lb}$$

$$\dot{q} = 21.92 \frac{1}{\sqrt{R_o}} \cdot (\rho_\infty^{.5}) \cdot \left(\frac{V_\infty}{1000}\right)^3 \left(1 - \frac{h_w}{h_s}\right)$$

$$\dot{q} = 21.92 \frac{1}{\sqrt{R_o}} \cdot \left(2.89 \times 10^{-4}\right)^{-.5} \left(\frac{5836}{1000}\right)^3 \left(1 - \frac{h_w}{777.4}\right)$$

$$\boxed{\dot{q} = \frac{74.07}{\sqrt{R_o}} \left(1 - \frac{h_w}{777.4}\right)} \quad \text{Btu/ft}^2\text{.sec}$$

Equilibrium Wall Temp $\quad h_w = .234 T_w + 1 \times 10^{-5} T_w^2$

$R_o = 4$

$$37.03 = .047638 h_w + .85 (4.81 \times 10^{-13}) T_w^4$$

$$37.03 = .01114 T_w + 4.764 \times 10^{-7} T_w^2 + 4.0885 \times 10^{-13} T_w^4$$

Say $T_w = 2000$ °R $\quad 37.03 \neq 30.72$

Say $T_w = 2300$ °R $\quad 37.03 \neq 39.58$

Say $T_w = 2250$ °R $\quad 37.03 \doteq 37.95$

$$\boxed{T_w \doteq 2225 \text{ °R}}$$

$M = 8$ Alt = 50000 ft

$V_\infty = 8(973) = 7784$ ft/sec

$\rho_\infty = 2.84 \times 10^{-4}$

$h_s = .25 T_\infty + V_\infty^2/50100$

$= .25(460 - 69.7) + 7784^2/50100$

$= 1307$ Btu/lb

$$\dot{q} = 21.92 \cdot \rho_\infty^{.5} \cdot \frac{1}{\sqrt{R_o}} \cdot \left(\frac{V_\infty}{1000}\right)^3 \left(1 - \frac{h_w}{h_s}\right)$$

$$= 21.92 \left(2.84 \times 10^{-4}\right)^{.5} \frac{1}{\sqrt{R_o}} \left(\frac{7784}{1000}\right)^3 \left(1 - \frac{h_w}{1307}\right)$$

$$\boxed{\dot{q} = \frac{175.75}{\sqrt{R_o}} \left(1 - \frac{h_w}{1307}\right)} \quad \text{Btu/ft}^2 \cdot \text{sec}$$

Equilibrium Wall Temp for $R_o = 4$

$h_w = .234 T_w + 1 \times 10^{-5} T_w^2$

$87.87 = .06723 h_w + .85(4.81 \times 10^{-13}) T_w^4$

$87.87 = .01573 T_w + 6.723 \times 10^{-7} T_w^2 + 4.0885 \times 10^{-13} T_w^4$

Say $T_w = 3000°R$ $\quad 87.87 \neq 85.27$

Say $T_w = 3050°R$ $\quad 87.87 \neq 89.61$

$$\boxed{T_w \cong 3025°R}$$

$M = 10$ $Alt = 50000$ ft

$V_\infty = 9730$

$\rho_\infty = 2.89 \times 10^{-4}$ lb sec^2/ft^4

$h_s = .25(460 - 69.7) + 9730^2/50100$

$= 1987.3$ Btu/lb

$$\dot{q} = 21.92 \left(2.89 \times 10^{-4}\right)^{.5} \frac{1}{\sqrt{R_o}} \left(\frac{9730}{1000}\right)^3 \left(1 - \frac{h_w}{1987.3}\right)$$

$$\boxed{\dot{q} = \frac{343.3}{\sqrt{R_o}} \left(1 - \frac{h_w}{1987.3}\right) \text{ Btu/ft}^2\text{-sec}}$$

Equilibrium Temp $R = 4/4$

$h_w = .234 T_w + 1 \times 10^{-5} T_w^2$

$\dot{q}_{conv} = \dot{q}_{rad}$

$$171.63 = .0202 T_w + \left(8.6363 \times 10^{-7}\right) T_w^2 + \left(4.0885 \times 10^{-13}\right) T_w^4$$

Say $T_w = 3000°R$ $171.63 \neq 101.48$

Say $T_w = 4000°R$ $171.63 \neq 199.3$

Say $T_w = 3600°R$ $171.63 \neq 152.6$

Say $T_w = 3800°R$ $171.63 \cong 174.48$

Say $T_w = 3780°R$ $171.63 \cong 172.1$

$$\boxed{T_w \cong 3777°R}$$

M = 9	100 K	1/2/68

100 K $T\,^{\circ}F = -51.098$

$\rho = .0109971$ atm

Density ratio = .013960

$a = \sqrt{\gamma R T} = \sqrt{1.4(1731.3)(460 - 51.098)}$

$= 995$ ft/sec

$V_\infty = 9(995) = 8960$ ft/sec

$\rho_\infty = \rho_{SL} \exp(-h/23700) = .2378 \times 10^{-3} \cdot \exp\left(\frac{-100000}{23700}\right)$

$= 3.497 \times 10^{-5}$ $\frac{lb\ sec^2}{ft^4}$

$h_0 = h_e = .25\,T_\infty + V_\infty^2/50100$

$= .25(409) + 8960^2/50100$

$= 1704.677$

$\dot{q} = 21.92 \frac{1}{\sqrt{R_0}} \cdot \rho_\infty^{.5} \cdot \left(\frac{V_\infty}{1000}\right)^3 \left(1 - \frac{h_w}{h_s}\right)$

$\frac{21.92}{\sqrt{R_0}} \cdot \left(3.497 \times 10^{-5}\right)^{.5} 719.323 \left(1 - \frac{h_w}{h_s}\right)$

$\dot{q} = \frac{93.242}{\sqrt{R_0}} \left(1 - \frac{h_w}{1704.677}\right)$

Appendix 1.2: Heating Rate Away From Stagnation Point

Calculations For Heating Rate Away From Stagnation Point:

$$\dot{q} = \dot{q}_s (\cos\theta)^{3/2}$$ for θ up to 60° (7% accuracy)

For this aircraft, nose will be a 10° half angle cone. Therefore, θ will vary between 0 and 80°. Use the above formula anyway.

$M = 10$ $\quad$ $70\,k$ $\quad$ $T_{equil} = 3525°R$

Lee's Method yields

$$\dot{q}_s = \frac{226.95}{\sqrt{R_o}}\left(1 - \frac{h_w}{2000}\right)$$

Melting Point of Steel: $1810°K = 3258°R$

$\Rightarrow$ Assume Wall Temperature = $\underline{1200°R}$

$$h_w = .234\,T_w + 1\times10^{-5}\,T_w^2$$

$$= .234(1200) + 1\times10^{-5}(1200^2) = 295.2 \text{ Btu/lb}$$

$$\Rightarrow \quad \dot{q}_s = \frac{226.95}{\sqrt{R_o}}\left(1 - \frac{295.2}{2000}\right)$$

$$\boxed{\dot{q}_s = 193.45/\sqrt{R_o}} \quad \text{Btu/ft}^2\text{-sec}$$

Compute heat loads for various nose radii

$R_c = 1'' = 1/12$ ft

$$\dot{q}_s = 193.45/\sqrt{1/12} = 670 \text{ Btu/ft}^2\text{.sec}$$

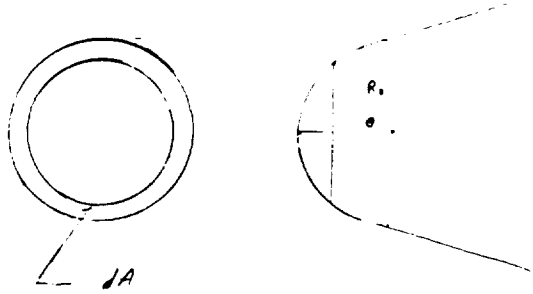

$q = \dot{q} \cdot \text{Area}$

Incremental Area $dA = 2\pi R_c \sin\theta \cdot d\theta$

$$q_{nose} = \int_0^{80^\circ} \dot{q}_s (\cos\theta)^{3/2} \cdot 2\pi R_c \sin\theta \, d\theta$$

$$q_{nose} = 350.81 \int_0^{80^\circ} (\cos\theta)^{3/2} \sin\theta \, d\theta$$

$u = \cos\theta \qquad du = -\sin\theta \, d\theta$

$$\int (\cos\theta)^{3/2} \sin\theta \, d\theta = -\int u^{3/2} \, du$$

$$= -\frac{2u^{5/2}}{5} + C$$

$$q_{nose} = -350.81 \left(\frac{2}{5}\right) \cdot (\cos\theta)^{5/2} \Big|_0^{80^\circ}$$

$$q_{nose} = -140.32 \left[(\cos 80^\circ)^{5/2} - \cos 0^{5/2}\right]$$

$$q_{nose} = \underline{138.55 \text{ Btu/sec}}$$

Fig 6

$R_o = 2'' = 1/6$ ft

$\dot{q}_s = 193.45/\sqrt{1/6} = 473.8$ Btu/ft^2.sec

$q = \dot{q} \cdot Area$

$$q_{nose} = \int_0^{80°} \dot{q}_s (\cos\theta)^{3/2} \cdot 2\pi \cdot R_o \sin\theta \, d\theta$$

$$q_{nose} = -\dot{q}_s 2\pi R_o \frac{2}{5}\left[(\cos\theta)^{5/2}\right]_0^{80°}$$

$$q_{nose} = -198.48\left[(\cos 80°)^{5/2} - 1\right]$$

$q_{nose} = 196$ Btu/sec

$R_o = 3'' = 1/4$ ft

$$\dot{q}_s = q_s 2\pi R_o \frac{2}{5}(.98743)$$

$$\dot{q}_s = (193.45/\sqrt{1/4}) \cdot 2\pi (1/4)(\tfrac{2}{5})(.98743)$$

$\dot{q}_s = 240$ Btu/sec

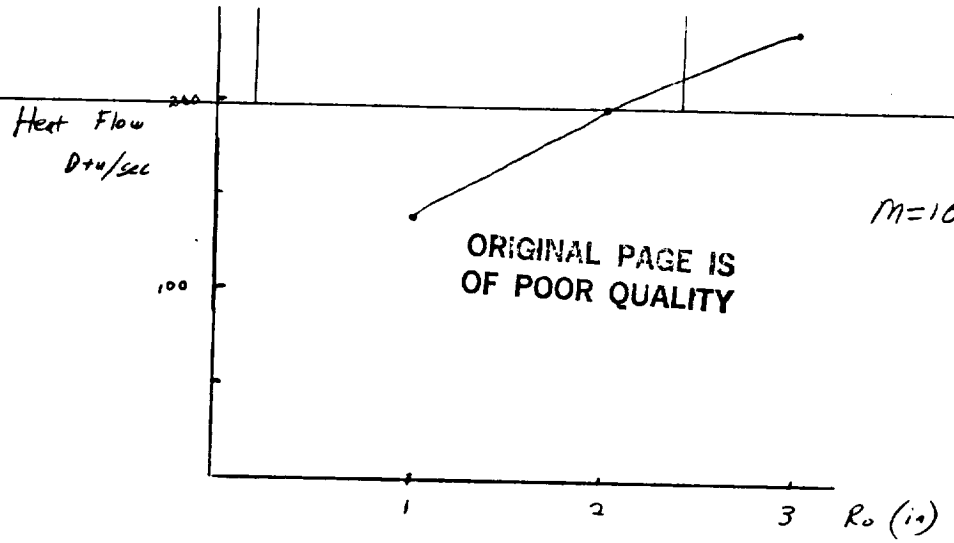

M=10 70 k

M = 10 90 k

$$a = \sqrt{\gamma R T} = \sqrt{(1.4)(1731.3)(460 - 56.53)}$$

$$a = 988.9 \text{ ft/sec}$$

$$V_\infty = 9889 \text{ ft/sec}$$

$$\rho_\infty = \rho_{SL} \cdot \exp(-h/23700) = 2.378 \times 10^{-3} \cdot \exp(-90000/23700)$$

$$= 5.333 \times 10^{-5} \quad lb\ sec^2/ft^4$$

$$h_s = h_e = .25 T_w + V_\infty^2/50100$$

$$= .25(460 - 56.53) + 9889^2/50100$$

$$= 2053 \text{ Btu/lb}$$

$$\dot{q}_s = 21.92 \frac{1}{\sqrt{R_o}} \cdot (\rho_\infty)^{.5} \cdot \left(\frac{V_\infty}{1000}\right)^3 \left(1 - \frac{h_w}{h_s}\right)$$

$$\dot{q}_s = \frac{21.92}{\sqrt{R_o}} \cdot (5.333 \times 10^{-5})^{.5} \left(\frac{9889}{1000}\right)^3 \left(1 - \frac{h_w}{2053}\right)$$

$$\boxed{\dot{q}_s = \frac{154.8}{\sqrt{R_o}} \left(1 - \frac{h_w}{2053}\right)}$$

Wall temp = 1200° R

h_w = 295.2 Btu/lb

ORIGINAL PAGE IS
OF POOR QUALITY

$$\dot{q}_s = \frac{154.8}{\sqrt{R_o}}\left(1 - \frac{295.2}{2053}\right)$$

$$\boxed{\dot{q}_s = 132.54/\sqrt{R_o}}$$

R_o = 1" = 1/12 ft

$$\dot{q}_s = 132.54/\sqrt{1/12} = 459 \text{ Btu/ft}^2\text{-sec}$$

$$\dot{q}_{nose} = \dot{q}_s \cdot 2 \cdot \pi (R_o) \frac{2}{5} (.98743)$$

$$q_{nose} = 459 \cdot 2 \cdot \pi (1/12) \frac{2}{5} (.98743)$$

$$q_{nose} = \underline{94.95 \text{ Btu/sec}}$$

R_o = 2" = 1/6 ft

$$\dot{q}_s = 132.54/\sqrt{1/6} = 324.6 \text{ Btu/ft}^2\text{-sec}$$

$$q_{nose} = 324.6 \cdot 2 \cdot \pi (1/6) \frac{2}{5} (.98743)$$

$$= \underline{134 \text{ Btu/sec}}$$

R_o = 3" = 1/4 ft

$$\dot{q}_s = 132.54/\sqrt{.25} = 268 \text{ Btu/ft}^2\text{-sec}$$

$$q_{nose} = 268 \cdot 2 \cdot \pi (1/4) \frac{2}{5} (.98743)$$

$$= \underline{167 \text{ Btu/sec}}$$

G-24

$M = 12$ $\quad$ 90K

$V_\infty = 12\,(988.9) = 11867$ ft/sec

$e_\infty = 5.333 \times 10^{-5}$

$h_s = h_e = .25\,T_\infty + V_\infty^2/50100$

$= .25(460 - 5653) + 11867^2/50100$

$= 2912$ Btu/lb

$$\dot{q}_s = \frac{21.92}{\sqrt{R_o}} \left(5.333 \times 10^{-5}\right)^{.5} \left(\frac{11867}{1000}\right)^3 \left(1 - \frac{h_w}{2912}\right)$$

$$\dot{q}_s = \frac{267.5}{\sqrt{R_o}} \left(1 - \frac{h_w}{2912}\right)$$

For $T_w = 1200\,°R$

$h_w = 295.2$ Btu/lb

$$\dot{q}_s = \frac{267}{\sqrt{R_o}} \left(1 - \frac{295.2}{2912}\right)$$

$$\boxed{\dot{q}_s = 240/\sqrt{R_o}}$$

$R_o = 1'' = 1/12$ ft

$\dot{q}_s = 240/\sqrt{1/12} = 831$ Btu/ft²·sec

$q_{nose} = 831\, R_o\, (2.4816)$

$q_{nose} = 172$ Btu/sec

$R_o = 2'' = 1/6$ ft

$\dot{q}_s = 240/\sqrt{1/6} = 588$ Btu/ft²·sec

$q_{nose} = 588 \cdot R_o\, (2.4816) = 243$ Btu/sec

$R_o = 3'' = 1/4$ ft

$q_s = 240/\sqrt{.25} = 480$ Btu/ft²sec

$q_{nose} = 480\ R_o\ (2.4816) = 298$ Btu/sec

Appendix 1.3: Heating rates for Noses of Various Radii

Heating Rates For Noses of Various Radii

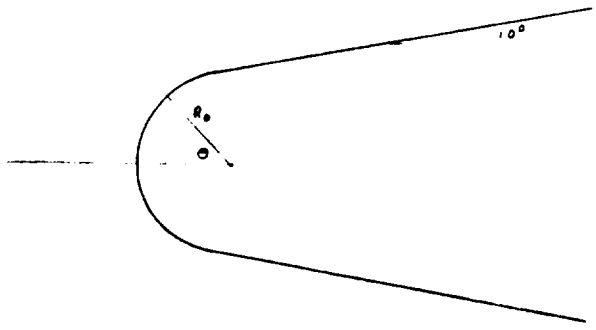

$0 \le \theta \le 80°$

$\dot{q} = \dot{q}_s (\cos\theta)^{3/2}$

$q = \dot{q} \cdot (\text{Area})$

Incremental Area $dA = 2\pi R_o \sin\theta \, d\theta$

$$q_{nose} = \int_0^{80°} \dot{q}_s (\cos\theta)^{3/2} \cdot 2 \cdot \pi \cdot R_o \sin\theta \, d\theta$$

$$\boxed{q_{nose} = \dot{q}_s \cdot R_o \cdot (2.4816)}$$

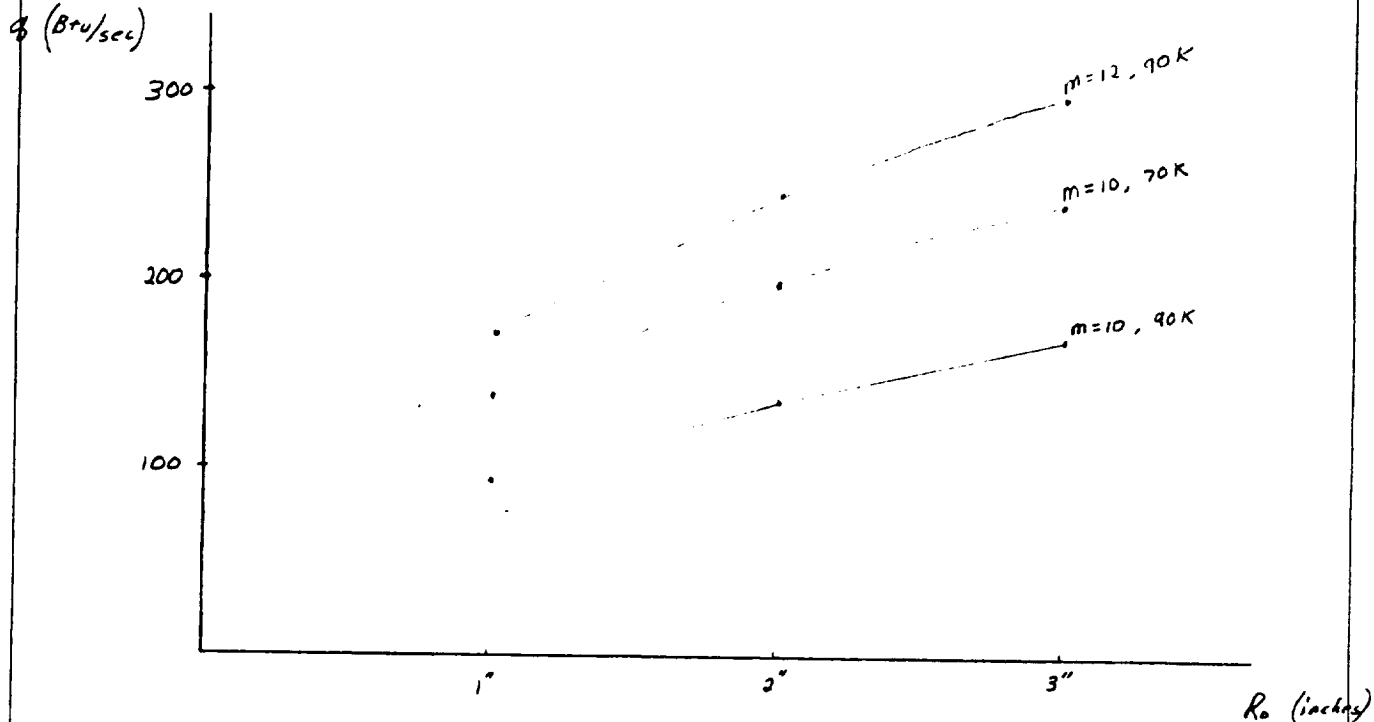

Appendix 1.4: Equilibrium Temperature Calculation

T_∞, h_e ← h_w, T_w

Lee's Approx. Method

$$\dot{q}_s\sqrt{R_0} = \left[1 - \frac{h_w}{h_s}\right]\left[15.5 \cdot Z^{(0.5)n} (\rho_\infty)^{0.5} \left(\frac{U_\infty}{10000}\right)^3\right]$$

where: $h_w = T_w(0.234 + 0.01\frac{T_w}{1000})$; $h_e = h_s = 0.25 T_\infty + \frac{U_\infty^2}{50 \cdot 32}$ (Btu/lb)

$$\dot{q}_s = \epsilon\sigma\left[T_w^4 - T_\infty^4\right]$$

$$\dot{q}_s\sqrt{R_0} = \left[1 - \frac{T_w(0.234 + 1\times10^{-5} T_w)}{0.25 T_\infty + \frac{V_\infty^2}{32 \cdot 2}}\right]\left[2.192031\times10^{-8}\rho_\infty^{0.5}(V_\infty)^3\right]$$

alt = 70,000 ft

$T_\infty = 392.97$ °R

$\rho_\infty = 1.376\times10^{-4}$ slugs/ft³

Mach = 8

$V_\infty = 7768.4$ ft/sec

$$\dot{q}_s\sqrt{R_0} = 120.5454 - 0.02165(T_w) - 9.2529\times10^{-7} T_w^2 \quad (II)$$

alt = 115,000 ft

$T_\infty = 427.55$ °R

$\rho_\infty = 1.552\times10^{-5}$ slugs/ft³

Mach = 8

$V_\infty = 8103.2$ ft/sec

$$\dot{q}_s\sqrt{R_0} = 46.35949 - 7.65793\times10^{-3}(T_w) - 3.27262\times10^{-7}(T_w)^2 \quad (I)$$

No. of Sol. (I) = (II) = 0

$$\left(\dot{q}_s\sqrt{R_0}\right) = \sqrt{R_0}\,\epsilon\sigma\left[T_w^4 - T_\infty^4\right]$$

$\epsilon = 0.85$ (emissivity) ; $\sigma = 4.81\times10^{-13}\left(\frac{\text{Btu}}{\text{ft}^2\,\text{sec}\,°\text{R}^4}\right)$

(1) $120.5454 - 0.02165(T_w) - 9.2528 \times 10^{-7}(T_w)^2 = \sqrt{R_s}\,\epsilon\sigma\left(T_w^4 - T_\infty^4\right)$

$$\sqrt{R_s}\left(T_w^4 - T_\infty^4\right) = 2.9454 \times 10^{14} - 5.29534 \times 10^{9}(T_\infty) - 2.26313 \times 10^{9} T_\infty^2$$

$$T_w^4 = \frac{1}{\sqrt{R_s}}\left[2.9454 \times 10^{14} - 5.29534 \times 10^{9}(T_\infty) - 2.26313 \times 10^{9} T_\infty^2\right]$$

$T_w = 2932.20512\ ^\circ R = 2364.20612\ ^\circ F$

$R_s = 4'$ @ 70,000 ft from Fig 5

$\dot{q}_s = \epsilon\sigma\left[T_w^4 - T_\infty^4\right] = 26\ \frac{BTU}{ft^2\,sec}$

$$46.38949 - 7.65793 \times 10^{-3} T_w - 3.27262 \times 10^{-7} (T_w)^2 = \sqrt{R_0}\, \epsilon\sigma \left(T_w^4 - T_\infty^4\right) \times \phi$$

$$T_w^4 = \left[1.13463 \times 10^{14} - 1.97301 \times 10^{10} T_w - 9.00445 \times 10^{5} T_w^2\right] \left[\frac{1}{\sqrt{R_0}}\right]$$

(Heating) $\Rightarrow T_w = 2381.35459\,^\circ R = 1921.4\,^\circ F$

@ $R_0 = 4'$; 115000' @ Mach 5

$$\dot{q}_c = \epsilon\sigma(T_w^4 - T_\infty^4) = 13.13 \ \frac{BTU}{ft^2 sec}$$

Appendix 1.5: Preliminary Heat Exchanger Analysis

HEAT EXCHANGER

CONFIGURATION

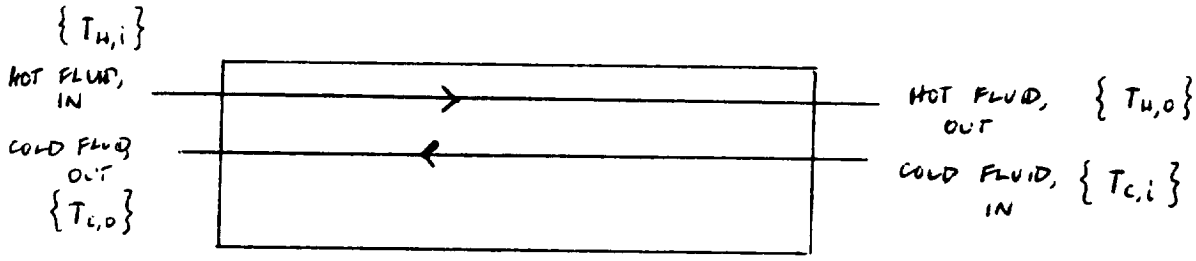

HOT FLUID : GLYCOL

COLD FLUID: HYDROGEN

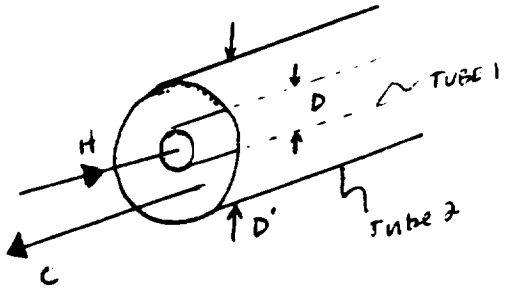

QUESTION: ARE FINS REQUIRED ON TUBE 1?

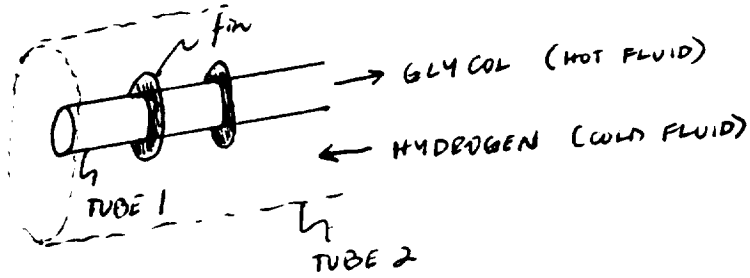

ORIGINAL PAGE IS
OF POOR QUALITY

PROPERTIES

H_2 (≈ 250 K)	30% Glycol (300 K)
$C_p = 15300$ J/kgK	$C_p = 4041$ J/kgK
$\mu = 77 \times 10^{-7}$ kg/m·s	$\mu = 940.6 \times 10^{-7}$ kg/m·s
$k = 180 \times 10^{-3}$ W/mK	$k = 509.9 \times 10^{-3}$ W/mK
$P_r = .69$	$P_r = 0.745$

RELATIONS

$$Re_D = \frac{4\dot{m}}{\mu \pi D}$$

$$Pr = \frac{\mu C_p}{k}$$

(Ref. 4)

$$Nu_D = 0.023\, Re_D^{0.8}\, Pr^{0.33}, \quad Re_D > 2300,\ Pr > 0.5 \quad \text{(TURB. FLOW)}$$

$$Nu_D = 3.65 + \frac{0.065\,(D/L)\,Re_D\,Pr}{1 + 0.04\left[(D/L)\,Re_D\,Pr\right]^{2/3}}, \quad \text{(LAMINAR FLOW)}$$

$$h_D = \frac{Nu_D\, k}{D}$$

CALCULATIONS

First, an energy balance is performed, where the heat exchanger is assumed to be 100% effective — that is, $T_{c,o} = T_{H,i}$:

$$\dot{m}_H C_{P_H} (T_{H,i} - T_{H,o}) = \dot{m}_c C_{P_c} (T_{c,o} - T_{c,i})$$

$$\frac{\dot{m}_H}{\dot{m}_c} = \frac{C_{P_c} (T_{c,o} - T_{c,i})}{C_{P_H} (T_{H,i} - T_{H,o})}$$

Substituting values:

$$\frac{\dot{m}_H}{\dot{m}_c} = \frac{5200 (500-20)}{4041 (500-300)} = 9.025$$

Thus, this ratio of mass flow rates is required for 100% effectiveness. If this heat exchanger is required to be quite effective, say 80% effective, then

$$\frac{\dot{m}_H}{\dot{m}_c} \Rightarrow .80 (9.025) = 7.22$$

TUBE FLOW & LAM. FLOW

If $\dot{m}_c$ is chosen, then

$\dot{m}_c = .001$ kg/s $\qquad\qquad \dot{m}_H = .00722$ kg/s

Also, $D = .010$ m, $D_h = \frac{4(\text{Area})}{\text{Perimeter}} = D' - D$;
if $D' = .020$m, then $D_h = .010$ m also, simplifying this analysis.

Results are listed, in which Nusselt number correlations were used to calculate heat transfer coefficients.

TUBE

→ $\dot{m}_c$ = .001 kg/s — $\dot{m}_H$ = .00732 kg/s

Re_{D_n} = 16535.6 — Re_D = 9800

Nu_{D_n} = 48.103 — Nu_D = 32.45

h_c = 865.85 W/m^2K — h_H = 1654.5 W/m^2K

$\frac{h_H}{h_c}$ = 1.9

→ $\dot{m}_c$ = .01 kg/s — $\dot{m}_H$ = .0722 kg/s

Re_{D_n} = 165356.0 — Re_D = 97737

Nu_{D_n} = 303.85 — Nu_D = 204.9

h_c = 5469.3 — h_H = 10448

$\frac{h_H}{h_c}$ = 1.9

LAM

→ $\dot{m}_c$ = .0001 kg/s — $\dot{m}_H$ = .0007 kg/s

Re_{D_n} = 1653.55 — Re_D = 947.59

Nu_{D_n} = 4.264 — Nu_D = 4.05

h_c = 76.76 — h_H = 206.5

$\frac{h_H}{h_c}$ = 2.7

Thus, h_{H/h_c} is only about 2 to 3, which means that h_c (h of Hydrogen) is only 2 to 3 times smaller than h_H (h of glycol). Thus, fins are probably not necessary for Tube 1.

→ = selected parameter

Appendix 2: Computer Codes

Appendix 2.1.1: HETAQ Description

HETAQ Manual:

We used Lees Approximate Method in HETAQ because it quickly and accurately determined stagnation point heating rates. From there, obtaining the skin equilibrium temperatures for varying flight conditions was just a matter of equating two equations and solving for the unknown.

Using the simple energy balance equation:

convective heat transfer = radiative heat transfer

$$q_s = q_r$$

the convective heat transfer q_s is identical to the radiative heat transfer q_r. So we can now equate q_s with the radiative heat expression:

$$q_s = q_r = \epsilon\sigma(T_{wall}^4 - T_\infty^4)$$

Now, equating the expression of q_s from Lees Approximate Method with that from the radiative expression and solving for the unknown wall temperature T_{wall} gives a fourth order equation with which Newton's Method was used, iterating to solve T_{wall} with the HETAQ code.

Due to the limitations of fuel it was necessary to determine how long it would take for the nose to reach its equilibrium temperature. If it is longer than the calculated flight time, then the data obtained is in the transient region, and possibly not as valuable as data

taken at a cruise equilibrium temperature. Therefore, this time calculation was a valuable step in ~~determing~~ determining what the proposed flight condition would be.

In calculating the time it took for the skin to reach this equilibrium temperature, an approximate energy balance was used to give an estimate of the flight time required:

$$\rho CV(T_{w,eq} - T_{initial}) = \dot{q}_s A\Delta t - \sigma\epsilon A(T_{w,eq} - T_\infty)\Delta t$$

This equation assumes that the nose piece is a simple thin skin structure (no heat sink) which is actively cooled to the desired wall temperature–to be determined by the material's thermal properties. The time needed to reach equilibrium is quite short for the materials we analyzed. Using a thin titanium skin around 1 mm thick would only require a time of 1.8 minutes. This should leave enough time for equilibrium data to be taken.

Here is a summary of the process used. Calculate what the stagnation point heating rates will be using Lees Approximate Method. Then, determine what the skin equilibrium temperature will be, using the $q_s = q_r$ energy balance equation. Now, in order to show that there will be a heating problem, if the equilibrium temperature is greater than the limiting temperature of the nose material, active cooling must be used. To determine how much cooling will be necessary, set the wall temperature at the limiting material temperature and use Lees Approximate Method to determine

$$q_s = q_r + q_{cool}$$

where q_{cool} is the cooling rate to be determined by the active cooling system.

Appendix 2.1.2: HETAQ Data

HETAQ DATA

2 JAN 85

Tank: contains oxygen

Tank: contains nitrogen = 4.41 lb-ft^3
Tank: length = 40 ft diameter = 8 ft
Fuel: volume = 2010.7 ft^3 weight = 5886.9378 lbs
CD = .7 Fuselage area = 805 ft^2

Altitude = 100000 ft

Mach = 5

Radius = 1 inches

Nose equil temp = 3543.21 R q = 64.36 btu / ft^2 sec

Steady state reached		1 mm	1/16" (1.59 mm)
	= aluminum:	5.45 sec	8.65 sec
	= titanium:	3.92 sec	6.22 sec

Flight computed at: ISP = 2350 sec Thrust = 126297.86 lbs
Fuel flow rate = 53.74 lb/sec
Flight time = 1e5.35 sec 2.75 min

Radius = 2 inches

Nose equil temp = 3356.46 R q = 51.42 btu / ft^2 sec

Steady state reached		1 mm	1/16" (1.59 mm)
	= aluminum:	6.34 sec	10.07 sec
	= titanium:	4.59 sec	7.34 sec

Flight computed at: ISP = 2350 sec Thrust = 126297.86 lbs
Fuel flow rate = 53.74 lb/sec
Flight time = 1e5.35 sec 2.75 min

Radius = 3 inches

Nose equil temp = 3247.27 R q = 45.44 btu / ft^2 sec

Steady state reached		mm	1/16" (1.59 mm)
	= aluminum:	6.94 sec	11.05 sec
	= titanium:	5.01 sec	7.95 sec

Flight computed at: ISP = 2350 sec Thrust = 126297.86 lbs
Fuel flow rate = 53.74 lb/sec
Flight time = 1e5.35 sec 2.75 min

Radius = 4 inches

Nose equil temp = 3169.86 R q = 41.24 btu / ft^2 sec

Steady state reached		1 mm	1/16" (1.59 mm)
	= aluminum:	7.46 sec	11.84 sec
	= titanium:	5.37 sec	8.52 sec

Flight computed at: ISP = 2350 sec Thrust = 126297.86 lbs
Fuel flow rate = 53.74 lb/sec
Flight time = 1e5.35 sec 2.75 min

Radius = 5 inches

Nose equil temp = 3108.74 R q = 38.18 btu / ft^2 sec

Steady state reached	1 mm	1/16" (1.59 mm)
Aluminum:	7.69 sec	12.8 sec
Titanium:	7.55 sec	8.99 sec

[illegible]

F = Flow rate = 53.74 lb/sec
Flight time = 1e5.35 sec 2.75 min

Radius = 4 inches

Nose axial temp = 3058.47 R q = 35.93 btu / ft^2 sec

Steady state reached	1 mm	1/16" (1.59 mm)
Aluminum:	8.24 sec	13.08 sec
Titanium:	5.97 sec	9.41 sec

Flight conditions: ISP = 2350 sec Thrust = 126297.6e lbs
Fuel flow rate = 53.74 lb/sec
Flight time = 1e5.35 sec 2.75 min

Proposed Flight Condition

Mach = 6

Radius = 1 inches

Nose axial temp = 4024.48 R q = 107.25 btu / ft^2 sec

Steady state reached	1 mm	1/16" (1.59 mm)
Aluminum:	3.73 sec	6.01 sec
Titanium:	2.72 sec	4.32 sec

Flight conditions: ISP = 1e66 sec Thrust = 159845.73 lbs
Fuel flow rate = 80.4 lb/sec
Flight time = 1e.51 sec 1.84 min

Radius = 2 inches

Nose axial temp = 3727.66 R q = 88.17 btu / ft^2 sec

Steady state reached	1 mm	1/16" (1.59 mm)
Aluminum:	4.47 sec	7.09 sec
Titanium:	3.31 sec	5.3 sec

Flight conditions: ISP = 1966 sec Thrust = 159845.73 lbs
Fuel flow rate = 80.4 lb/sec
Flight time = 110.82 sec 1.84 min

Radius = 3 inches

Nose axial temp = 3e65.59 R q = 73.81 btu / ft^2 sec

Steady state reached	1 mm	1/16" (1.59 mm)
Aluminum:	4.94 sec	7.85 sec
Titanium:	3.65 sec	5.84 sec

Flight conditions: ISP = 1966 sec Thrust = 159845.73 lbs
Fuel flow rate = 80.4 lb/sec
Flight time = 110.82 sec 1.84 min

Radius = 4 inches

Nose axial temp = 3672.11 R q = 66.5e btu / ft^2 sec

Steady state reached	1 mm	1/16" (1.59 mm)
Aluminum:	5.32 sec	8.44 sec
Titanium:	3.92 sec	6.07 sec

Flight conditions: ISP = 1988 sec Tmrust = 159845.73 lbs
Fuel flow rate = 80.4 lb/sec
Flight time = 110.52 sec 1.84 min

Radius = 5 inches

Nose equil temp = 3500.01 R q = 61.38 btu / ft^2 sec

Steady state reached	1 mr	1/16" (1.59 mm)
Aluminum:	5.63 sec	8.95 sec
Titanium:	4.05 sec	6.44 sec

Flight conditions: ISP = 1988 sec Tmrust = 159845.73 lbs
Fuel flow rate = 80.4 lb/sec
Flight time = 110.52 sec 1.84 min

Radius = 6 inches

Nose equil temp = 3441.41 R q = 57.34 btu / ft^2 sec

Steady state reached	1 mr	1/16" (1.59 mm)
Aluminum:	5.91 sec	9.39 sec
Titanium:	4.25 sec	6.75 sec

Flight conditions: ISP = 1988 sec Tmrust = 159845.73 lbs
Fuel flow rate = 80.4 lb/sec
Flight time = 110.52 sec 1.84 min

Radius = 7 inches

Nose equil temp = 3381.24 R q = 166.5 btu / ft^2 sec

Steady state reached	1 mr	1/16" (1.59 mm)
Aluminum:	2.76 sec	4.38 sec
Titanium:	1.98 sec	3.15 sec

Flight conditions: ISP = 1775 sec Tmrust = 197340.41 lbs
Fuel flow rate = 111.17 lb/sec
Flight time = 79.93 sec 1.33 min

Radius = 8 inches

Nose equil temp = 4105.23 R q = 130.31 btu / ft^2 sec

Steady state reached	1 mr	1/16" (1.59 mm)
Aluminum:	3.24 sec	5.13 sec
Titanium:	2.32 sec	3.68 sec

Flight conditions: ISP = 1775 sec Tmrust = 197340.41 lbs
Fuel flow rate = 111.17 lb/sec
Flight time = 79.93 sec 1.33 min

Radius = 9 inches

Nose equil temp = 4079.19 R q = 112.27 btu / ft^2 sec

Steady state reached	1 mr	1/16" (1.59 mm)
Aluminum:	3.55 sec	5.62 sec
Titanium:	2.61 sec	4.16 sec

Flight conditions: ISP = 1775 sec Tmrust = 197340.41 lbs
Fuel flow rate = 111.17 lb/sec
Flight time = 79.93 sec 1.33 min

Radius = 4 inches

Nose equil temp = 3952.28 R q = 100.77 btu / ft^2 sec

Steady state reached	mm	1/16" (1.59 mm)
Aluminum:	3.95 sec	6.29 sec
Titanium:	2.89 sec	4.52 sec

Flight conditions: ISP = 1779 sec Thrust = 197340.41 lbs
Fuel flow rate = 111.17 lb/sec
Flight time = 79.93 sec 1.33 min

Radius = 3 inches

Nose equil temp = 3878.66 R q = 93.55 btu / ft^2 sec

Steady state reached	mm	1/16" (1.59 mm)
Aluminum:	4.21 sec	6.68 sec
Titanium:	3.08 sec	4.8 sec

Flight conditions: ISP = 1779 sec Thrust = 197340.41 lbs
Fuel flow rate = 111.17 lb/sec
Flight time = 79.93 sec 1.33 min

Radius = 4 inches

Nose equil temp = 3811.24 R q = 86.21 btu / ft^2 sec

Steady state reached	mm	1/16" 1.59 mm)
Aluminum:	4.47 sec	7.02 sec
Titanium:	3.19 sec	5.05 sec

Flight conditions: ISP = 1779 sec Thrust = 197340.41 lbs
Fuel flow rate = 111.17 lb/sec
Flight time = 79.93 sec 1.33 min

Radius = 3 inches

Nose equil temp = 3744.33 R q = 79.44 btu / ft^2 sec

Steady state reached	mm	1/16" (1.59 mm)
Aluminum:	3.79 sec	3.33 sec
Titanium:	1.8 sec	3.34 sec

Flight conditions: ISP = 1483 sec Thrust = 238781.9 lbs
Fuel flow rate = 160.47 lb/sec
Flight time = 55.56 sec .93 min

Radius = 2 inches

Nose equil temp = 3620.03 R q = 69.61 btu / ft^2 sec

Steady state reached	mm	1/16" (1.59 mm
Aluminum:	3.51 sec	3.99 sec
Titanium:	1.61 sec	3.37 sec

Flight conditions: ISP = 1483 sec Thrust = 238781.9 lbs
Fuel flow rate = 160.47 lb/sec
Flight time = 55.56 sec .93 min

Radius = 1 inches

Nose equil temp = 3443.98 R q = 162.38 btu / ft^2 sec

**ORIGINAL PAGE IS
OF POOR QUALITY**

Steady state reached	1 mm	1/16" (1.59 mm)
Aluminum:	2.51 sec	4.46 sec
Titanium:	2.02 sec	3.21 sec

Flight condition one: ISP = 1488 sec Thrust = 238781.9 lbs
Fuel flow rate = 160.47 lb/sec
Flight time = 55.38 sec .92 min

4

Adiabatic temp = 4141.87 R q = 145.16 btu / ft^2 sec

Steady state reached	1 mm	1/16" (1.59 mm)
Aluminum:	3.05 sec	4.84 sec
Titanium:	2.19 sec	3.46 sec

Flight condition one: ISP = 1488 sec Thrust = 238781.9 lbs
Fuel flow rate = 160.47 lb/sec
Flight time = 55.38 sec .92 min

Radius = 0 inches
Nose equilibrium temp = 4146.51 R q = 133.95 btu / ft^2 sec

Steady state reached	1 mm	1/16" (1.59 mm)
Aluminum:	3.35 sec	5.15 sec
Titanium:	2.33 sec	3.71 sec

Flight condition one: ISP = 1488 sec Thrust = 238781.9 lbs
Fuel flow rate = 160.47 lb/sec
Flight time = 55.38 sec .92 min

Radius = 0.5 inches
Nose equilibrium temp = 4170.21 R q = 133.65 btu / ft^2 sec

Steady state reached	1 mm	1/16" (1.59 mm)
Aluminum:	3.41 sec	5.43 sec
Titanium:	2.46 sec	3.9 sec

Flight condition one: ISP = 1488 sec Thrust = 238781.9 lbs
Fuel flow rate = 160.47 lb/sec
Flight time = 55.38 sec .92 min

Mach = 6.0
Radius = 1 inches
Nose equilibrium temp = 3387.87 R q = 344.83 btu / ft^2 sec

Steady state reached	1 mm	1/16" (1.59 mm)
Aluminum:	1.63 sec	2.59 sec
Titanium:	1.17 sec	1.86 sec

Flight condition three: ISP = 1313 sec Thrust = 334170.2 lbs
Fuel flow rate = 254.43 lb/sec
Flight time = 41.16 sec .68 min

Radius = 2 inches
Nose equilibrium temp = 3143.27 R q = 254.49 btu / ft^2 sec

Steady state reached	1 mm	1/16" (1.59 mm)
Aluminum:	1.98 sec	3.14 sec
Titanium:	1.42 sec	2.26 sec

E.C

Flight conditions: ISP = 1313 sec Thrust = 284170.2 lbs
Fuel flow rate = 216.42 lb/sec
Flight time = 41.06 sec .68 min

Rad ius = 3 inches

Nose equil temp = 4846.34 R q = 225.53 btu / ft^2 sec

Steady state reached	1 mm	1/16" (1.59 mm)
Aluminum:	2.32 sec	3.52 sec
Titanium:	1.58 sec	2.53 sec

Flight conditions: ISP = 1313 sec Thrust = 284170.2 lbs
Fuel flow rate = 216.42 lb/sec
Flight time = 41.06 sec .68 min

Radius = 4 inches

Nose equil temp = 4706.05 R q = 201.04 btu / ft^2 sec

Steady state reached	1 mm	1/16" (1.59 mm)
Aluminum:	2.41 sec	3.68 sec
Titanium:	1.73 sec	2.78 sec

Flight conditions: ISP = 1313 sec Thrust = 284170.2 lbs
Fuel flow rate = 216.42 lb/sec
Flight time = 41.06 sec .68 min

Radius = 5 inches

Nose equil temp = 4604.06 R q = 183.7 btu / ft^2 sec

Steady state reached	1 mm	1/16" (1.59 mm
Aluminum:	2.57 sec	4.09 sec
Titanium:	1.85 sec	2.94 sec

Flight conditions: ISP = 1313 sec Thrust = 284170.2 lbs
Fuel flow rate = 216.42 lb/sec
Flight time = 41.06 sec .68 min

Radius = 6 inches

Nose equil temp = 4514.3 R q = 170.54 btu / ft^2 sec

Steady state reached	1 mm	1/16" (1.59 mm
Aluminum:	2.71 sec	4.31 sec
Titanium:	1.95 sec	3.1 sec

Flight conditions: ISP = 1313 sec Thrust = 284170.2 lbs
Fuel flow rate = 216.42 lb/sec
Flight time = 41.06 sec .68 min

Appendix 2.1.3: HETAQ Results

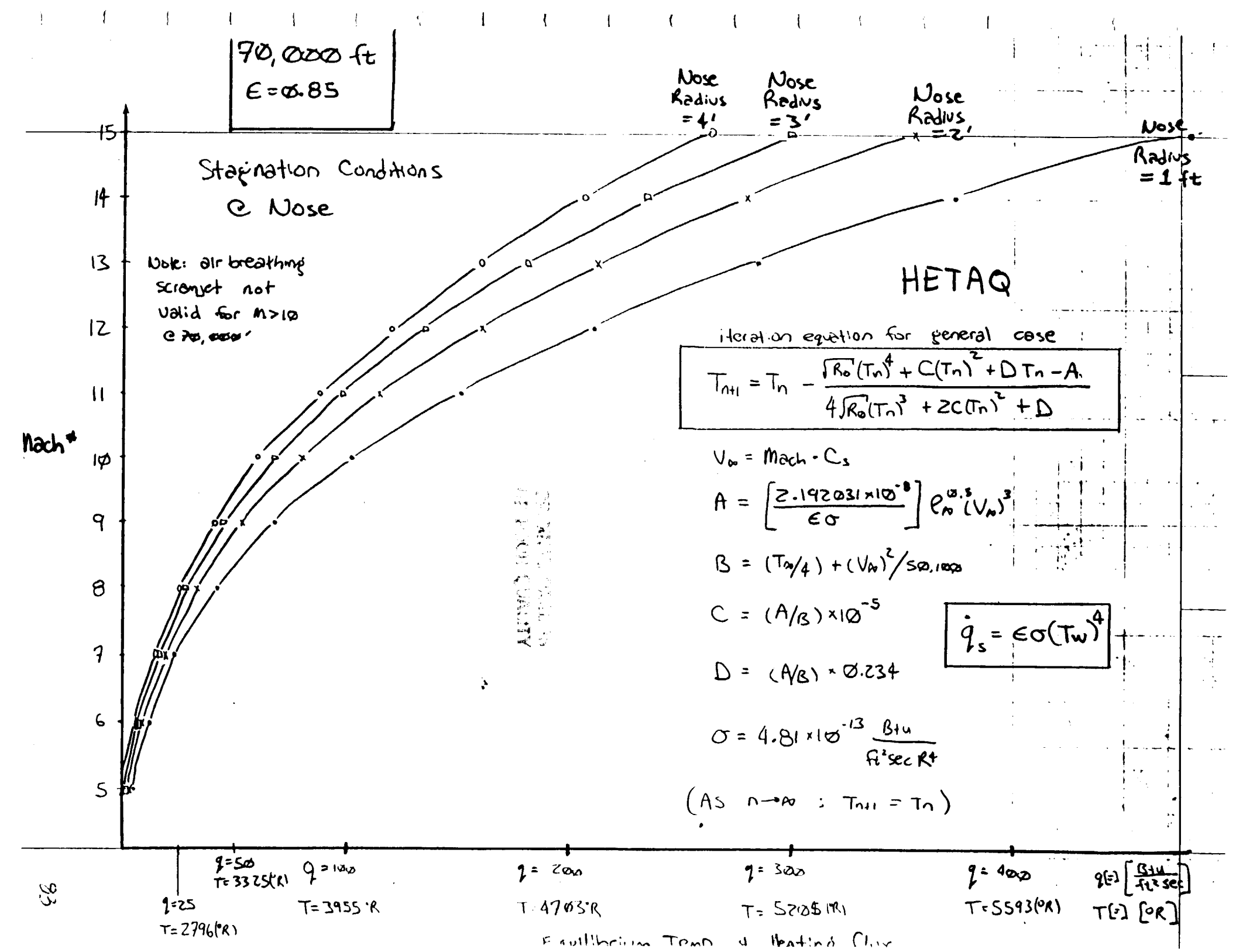
70,000 ft
ε = 0.85
Nose Radius = 4'
Nose Radius = 3'
Nose Radius = 2'
Nose Radius = 1 ft
Stagnation Conditions @ Nose
Note: air breathing scramjet not valid for M > 10 @ 70,000'
HETAQ
iteration equation for general case
$T_{n+1} = T_n - \frac{\sqrt{R_0}(T_n)^4 + C(T_n)^2 + D T_n - A}{4\sqrt{R_0}(T_n)^3 + 2C(T_n)^2 + D}$
$V_\infty = \text{Mach} \cdot C_s$
$A = \left[\frac{2.192031 \times 10^{-8}}{\epsilon\sigma}\right] \rho_\infty^{10.5} (V_\infty)^3$
$B = (T_\infty/4) + (V_\infty)^2/50,000$
$C = (A/B) \times 10^{-5}$
$D = (A/B) \times 0.234$
$\sigma = 4.81 \times 10^{-13} \frac{Btu}{ft^2 sec\, R^4}$
(As $n \to \infty$; $T_{n+1} = T_n$)
$\dot{q}_s = \epsilon\sigma(T_w)^4$
Mach#
15
14
13
12
11
10
9
8
7
6
5
q=25
T=2796(°R)
q=500
T=3325(°R)
q=1000
T=3955°R
q=2000
T=4703°R
q=3000
T=5210$(°R)
q=4000
T=5593(°R)
q[=] [Btu/ft² sec]
T[=] [°R]
Equilibrium Temp. & Heating Curve

1000,0000 ft
$\epsilon = 0.85$

HETAQ.DATA

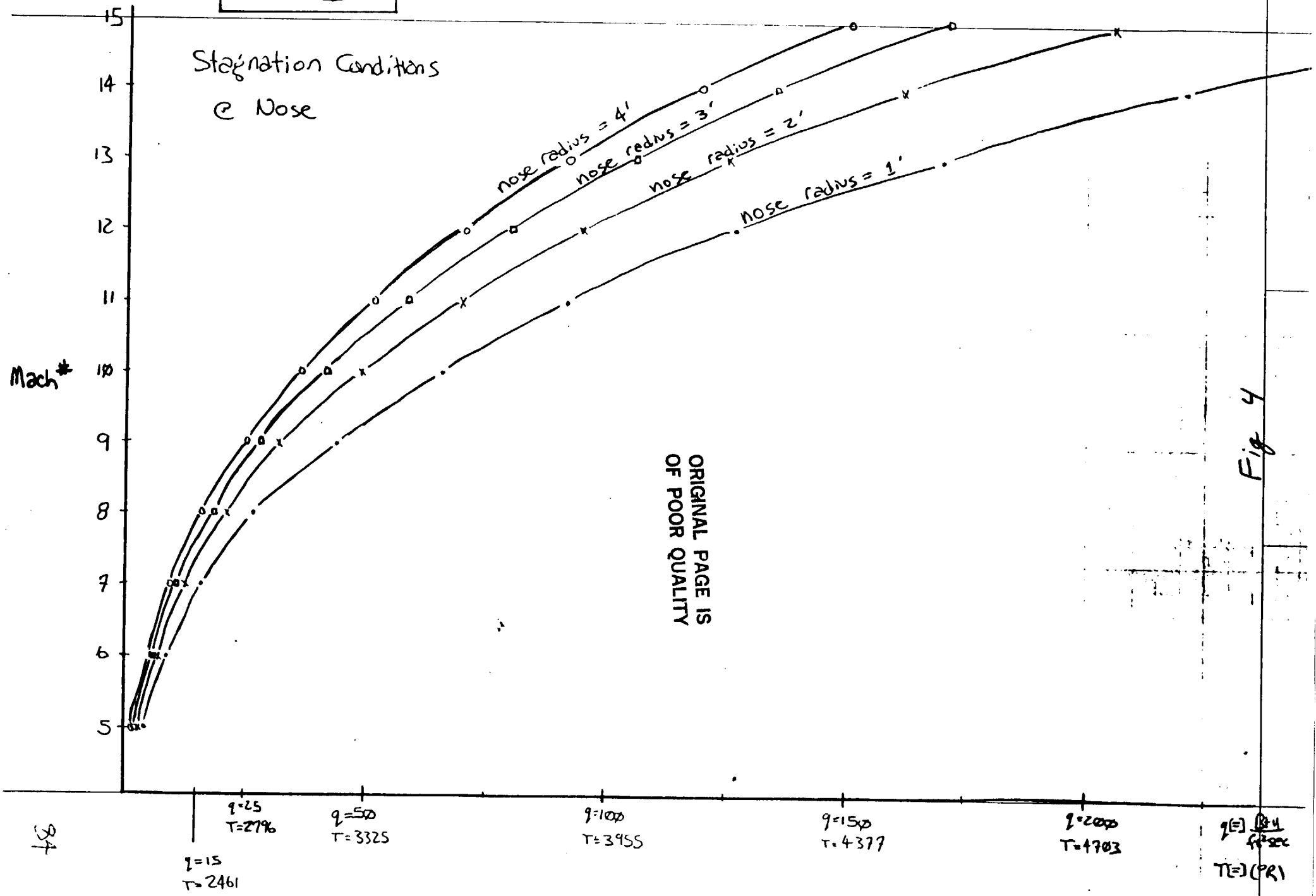

Fig 4

115,000 ft
$\epsilon = 0.85$

HETAQ.DATA

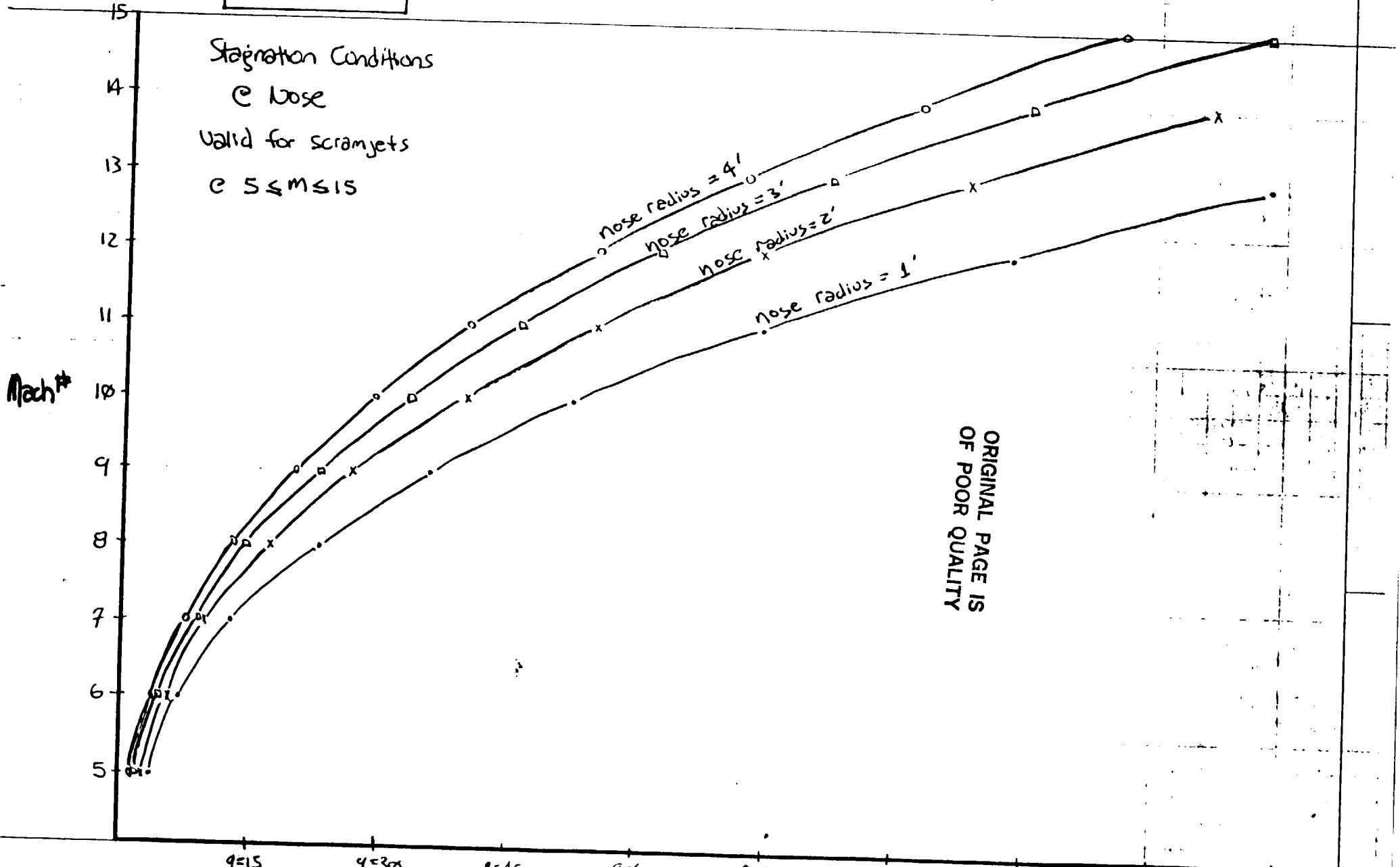

Appendix 2.1.4: HETAQ Code Listing

]hetaq

ORIGINAL PAGE IS OF POOR QUALITY

]
]LIST

```
  1  DIM T(4,12,6),Q(4,12,6),FL(4,12,6),TR(4,12,6),T1(4,12,6),T2(4,12,6),I
     SP(12),TS(4,12,6,4)
  2  TEXT : HOME : READ N: FOR I = 1 TO N: READ Z(I),RO(I),TI(I),CS(I): NEXT
     I: REM  READ IN DATA...ALT (FT), DENSITY (SLUGS/FT^3), TEMP INFINITY
     (R), SPEED OF SOUND (FT/SEC)
  4  READ NUM: FOR I = 1 TO NUM: READ M$(I),CP(I),DNS(I),TH(I): NEXT : REM
     READ IN  MATERIAL PROPERTIES
  5  FOR I = 8 TO 12: READ ISP(I): NEXT : REM  ISP FOR MACH #
  6 E = 0.85:S = 4.81E - 13:PI = 3.141592654:S0 = 605: REM SET SIGMA, EMMI
    SSIVITY, PI, PLAN FORM AREA (FT^2)
  7 Z = 0.01: REM  ACCURACY SETTING
  8 DI = 8:L = 40:CD = 0.20:HD = 4.42: REM set dimensions of tank, drag co
    eff, density of liq hydrogen
  9 VOL = PI * ((DI / 2)  2) * L:WH = HD * VOL: REM vol, weight of H2 in
    ft^3, Lb
 10  PRINT : PRINT "(A)utomatic calculation   or   (M)anual?  ":: INPUT I
    $: IF I$ = "M" OR I$ = "m" THEN 2000
 97  REM
 98  REM      VARY PARAMETERS
 99  REM
 1[illegible]  FOR I = 4 TO 4
 1[illegible]  FOR M = 8 TO 12: REM  MACH NUMBER
 1[illegible]  FOR K = 1 TO 6: REM RADIUS IN INCHES
 2[illegible] R =  SQR (K / 12)
210 CS = CS(I)
220 TI = TI(I)
230 RO = RO(I)
240 ISP = ISP(M)
500  GOSUB 5000: GOSUB 10000: GOSUB 30000
600 T(I,M,K) =  INT (100 * T) / 100:Q(I,M,K) =  INT (100 * Q) / 100
610  FOR L = 1 TO NUM:TS(I,M,K,L) =  INT (100 * DNS(L) * CP(L) * TH(L) *
    (T(I,M,K) - 500) / Q(I,M,K)) / 100: NEXT L
620 FL(I,M,K) =  INT (100 * FL) / 100:TR(I,M,K) =  INT (100 * TR) / 100:
    REM  FL= FUEL FLOW, TR = THRUST
6[illegible] T1(I,M,K) = T1:T2(I,M,K) = T2
[illegible] NEXT [illegible]
997  REM
998  REM    SAVE DATA TO DISK
999  REM
1000  PRINT  CHR$ (4):"OPEN HETAQ.DATA"
1010  PRINT  CHR$ (4):"WRITE HETAQ.DATA"
1050  PRINT "Initial conditions:": PRINT : PRINT "Density of hydrogen =
   ":HD:" lb/ft^3"; SPC( 3):"Tank:  length = ":L:" ft          Diameter
   = ":DI:" ft"
1060  PRINT "Fuel:  Volume = ":VOL:" ft^3": SPC( 5):"Weight = ";WH
1070  PRINT "Cd = ";CD; SPC( 3):"Plan form area = ":S0:" ft^2"
[illegible]  PRINT
1[illegible]  FOR I = 4 TO 4
[illegible]  PRINT : PRINT : PRINT "Altitude = ":Z(I):" ft"
1200  FOR M = 8 TO 12
```

ORIGINAL PAGE IS
OF POOR QUALITY

```
1900  PRINT "Mach = ";M
1900  FOR K = 1 TO 6
1900  PRINT "Radius = ";K;" inches"
1900  PRINT "Nose equil temp = ";T(I,M,K);" R"; SPC( 3);"q = ";
      Q(I,M,K);" btu / ft^2 sec"
1710  PRINT : PRINT "Steady state reached        1 mm        1/
      16"; CHR$ (34);" (1.59 mm)"
1720  PRINT "M$(1);": "; SPC( 5);TS(I,M,K,1);" sec"; SPC( 8);TS
      (I,M,K,2);" sec"
1730  PRINT "M$(3);": "; SPC( 5);TS(I,M,K,3);" sec"; SPC( 8);TS
      (I,M,K,4);" sec"
1800  REM  FLIGHT CONDITIONS
1810  PRINT : PRINT "Flight conditions:  ISP = ";ISP(M);" sec
      Thrust = ";TR(I,M,K);" lbs"
1820  PRINT "Fuel flow rate = ";FL(I,M,K);" lb/sec": PRINT
      29);"Flight time = ";T1(I,M,K);" sec   Flight time = ";T2(I,M,K);" m
      in"
1890  NEXT K,M,I
1900  PRINT CHR$ (4);"CLOSE HETAQ.DATA"
1901  END
1997  REM
1998  REM   DO MANUAL CALCULATIONS
2000  REM
2010  PRINT : PRINT : INPUT "Mach number = ";M
2050  INPUT "Density = ";RO
2070  INPUT "Speed of sound = ";CS
2090  INPUT "T(infinity) = ";TI
2100  INPUT "Nose radius = (in ft)";K:R =  SQR (K)
2110 ISP = ISP(M)
2200  GOSUB 5000: GOSUB 10000: GOSUB 30000
2205  PRINT "Initial conditions:": PRINT : PRINT "Density of hydrogen =
      ";HD;" lb/ft^3": SPC( 3);"Tank: length = ";L;" ft Diameter = ";DI;"
      ft"
2206  PRINT "Fuel volume = ";VOL;" ft^3"; SPC( 5);"Fuel weight = ";WH
2207  PRINT "Cd = ";CD: SPC( 5);"Plan form area = ";SO;" ft^2": PRINT
2210  FOR L = 1 TO NUM:TM(L) =  INT (100 * DNS(L) * CP(L) * TH(L) * (T -
      500) / Q) / 100: NEXT L
2300  PRINT : PRINT : PRINT "Equilibrium temp = ";T;" R": PRINT "Heating
      rate = ";Q;" btu / ft^2 sec"
2310  PRINT : PRINT  SPC( 5): Steady state reached        1 mm        1/
      16"; CHR$ (34);" (1.59 mm)"
2320  PRINT  SPC( 20);M$(1);": "; SPC( 5);TM(1);" sec"; SPC( 8);TM(2);"
      sec"
2330  PRINT  SPC( 19);M$(3);": "; SPC( 5);TM(3);" sec"; SPC( 8);TM(4);"
      sec"
2400  REM  FLIGHT CONDITIONS
2410  PRINT : PRINT  SPC( 9);"Flight conditions:  ISP = ";ISP;" sec   Th
      rust = ";TR;" lbs"
2420  PRINT  SPC( 29);"Fuel flow rate = ";FL;" lb/sec": PRINT  SPC( 29);
      "Flight time = ";T1;" sec   Flight time = ";T2;" min"
2500  GOTO 2010
4997  REM
4998  REM    CALCULATE COEFFICIENTS
4999  REM
5000 V = M * CS:A = (2.192031E - 8) * ( SQR (RO)) * (V * V * V) / (E * S
      )
5010 B = (TI / 4) + (V * V) / 50100:C = (A / B) * 1E - 5
5020 D = (A / B) * 0.234
5030  REM  M = MACH #: CS = SPEED OF SOUND (FT/SEC): V = VINFINITY (FT/S
      EC): RO = DENSITY AT ALTITUDE: TI = TEMP INFINITY (R): S [=] BTU/FT^
```

```
    2 SEC R^4
5040  RETURN
9998  REM
9999  REM     DO ITERATION CALCULATION
10000  REM
10100 T = 2500
10500 X = T - ((R * T * T * T * T) + (C * T * T) + (D * T) - A) / ((4 *
    R * T * T * T) + (2 * C * T * T) + D)
10800  IF ( ABS (T - X) > Z) THEN T = X: GOTO 10500
10900 Q = E * S * T * T * T * T
11000  RETURN
29999  REM
30000  REM     DO  THRUST  CALCULATIONS
30001  REM
30010 TR = CD * 0.5 * RO * V * V * SO: REM  THRUST EQN
30020 FL = TR / ISP: REM   FLOW RATE (FT^3 / SEC)
30050 T1 =  INT (100 * WH / FL) / 100:T2 =  INT (100 * T1 / 60) / 100: REM
    FLIGHT TIME IN SEC AND MIN
31000  RETURN
49997  REM
49998  REM     ATMOSPHERIC DATA
49999  REM
50000  DATA 5.70000,1.3761E-4,392.97,971.05
50010  DATA   80000.8.445E-5,398.46,977.81
50020  DATA   90000,5.2173E-5,403.95,984.54
50030  DATA  100000,3.320E-5,409.17,991.2
50040  DATA  110000.2.01E-5.419.87.1003.8
60000  DATA  4,"Aluminum",0.208.169,3.281E-3,"Aluminum",0.208,169,5.208E
    -3
60010  DATA  "Magnesium".0.232.109.3.281E-3,"Magnesium",0.232,109,5.208E
    -3
61000  DATA  2350.1988.1775.1488.1313
```

Appendix 2.2.1: ACSES Description

This program integrates the theories of conduction, convection, and fin analysis discussed already. Its main objective is to provide a first approximation in the design of a combined impingement and actively cooled panel concept for the drone nose. The code allows the user to vary tube/nose geometry and material/coolant properties with which it uses to calculate the critical skin temperature distribution, total pressure loss, and exiting coolant temperature.

The design constraint is that the skin of the nose never exceed a maximum allowable temperature. A branching routine is incorporated in the program to help avoid this, but at the expense of an appreciable pressure loss. Thus the task is to find a design that limits the abount of branching necessary to keep the skin temperature below this maximum value and the pressure losses at a minimum.

ACSES requires the following input parameters:

- Number of coolant tubes (tubes)
- Maximum distance back on nose to be analyzed [m]
- Number of stations (subdivisions) for iteration of properties (xnum)
- Coolant tube inner diameter (dtube [mm])
- Thickness of coolant tubes (xtube [mm])
- Friction factor of coolant tubes (f)
- Radius of the nose cone (rnose [mm])
- Skin thickness of nose cone (xskin [mm])
- Skin limiting temperature (tmax [K])
- Mass flow rate of coolant into the manifold (mfr0 [kg/s])
- Impingement nozzle inner diameter (nozd [mm])
- Distance from nozzle exit to impingement on back of nose wall (zn [mm])

- Choice of coolant (liquid hydrogen, water glycol solution (50%), Therminol 60)
- Initial coolant temperature (tman [K])

ACSES gives the following as output:

- The location of each required branch
- At each station along the nose cone:
  -- Surface heat flux (qmm [W/m^2])
  -- Bulk mixing temperature of coolant (tmav [k])
  -- Inside tube wall temperature (tw [K])
  -- Base of tube temperature (t0 [K])
  -- Local Reynolds number
  -- Pressure loss (pressl [Pa])
- Final results
  -- Exiting coolant temperature (tmo [K])
  -- Total pressure loss (ploss [PA], [psi], [atm])
  -- Outlet tube mass flow rate (mfr [kg/s])
  -- Total number of branches

Assumptions:

- The properties of the tube and skin materials were evaluated near their maximum allowable temperatures, tmax, and taken as constant along the entire nose cone region. Since the properties don't vary too greatly at these temperatures, a constant value serves as a good approximation.
- Nonaccelerating, level-cruise at Mach 10, 100,000 feet. This flight profile allows ACSES to calculate the stagnation point heating rate and use it to determine the heat flux at any point along the nose.

- Each tube branch is perfect and occurs over a negligible distance. Pressure and frictional losses are neglected as well.
- Coolant properties vary greatly along entire nose region but are taken to be constant over each differential station. They are evaluated at the mean bulk temperature (Tmo - Tmi) / 2 and iterated to within 1 degree accuracy.
- Tubes start at hemisphere of nose cap and extend back radially.
- The distance that the heat transfer across the coolant tubes occurs is taken to be 50% of the tube circumference. This approximation is valid due to the fin effect of the tube shell. Analysis shows that the wall temperature decreases to the coolant temperature within 15% of the circumference. The other 35% of the circumference approximates the heat transfer through the solder that welds the tube to the nose skin.
- Radiation off the nose and away from the inside wall have been neglected. Calculations show that it contributes less than 1% of the total heat flux.

Equations:

After the input of the parameters, the program goes through a set of equations to calculate the output. The order is as follows:

- Find the coolant temperature exiting the manifold
- Calculate nose and wall enthalpy to be used in heat flux calculation

h =

- Start at first station

-- Calculate heat flux

q =

-- Calculate distance between two tubes

L =

-- Iterate on energy balance to find temperature leaving station

--- Evaluate Cp at Tm

--- Find temperature leaving station

Tmo =

--- Recalculate mean bulk temperatue

Tm = Tmi + Tmo / 2

--- Check with first guess, if not within 1 degree, iterate again

-- Evaluate coolant properties at new mean bulk temperature

-- Calculate Prandtl, Reynolds, and Nusselt numbers:

Pr =

Re =

Nu =

from turbulent inner flow correlation valid for Re greater than and 0.7 < Pr < 13000 and ..... Viscosity is evaluated at mean bulk temperature and at wall temperature.

-- Calculate heat transfer coefficient between inner wall and coolant

h =

-- Calculate thermal resistance network

R1 = R2 =

-- Wall temperature of tube from convection of coolant is used to evaluate viscosity of coolant--iterate to within 1 degree as before.

tw = tmav + (qm * R1)

-- Find base of fin temperature from conduction through tube wall

t0 = tw + (qm * R2)

-- Find critical wall temperature using the base of fin temperature with the fin analysis

Tcrit = t0 + (qmm * (L ^ 2) / (8 * kskin * xskin))

-- If tcrit > tmax branch

--- double the number of tubes

--- half the mass flow rate

-- Evaluate pressure loss along the station. Total pressure loss is found from the sum of each station loss.

ploss =

-- Print out calculations to an output file

-- Continue the analysis with the next station

- Print out results

-- Total pressure loss

-- Final coolant exiting temperature

Limitations of ACSES:

The program only permits the design of a welded tube system. This configuration was chosen because of its ease to manufacture. The analysis also assumes a uniform heat distribution along the skin which in reality, might have several "hot spots" due to surface irregularities. This could be potentially disasterous because the existing design has no way of knowing where these hot spots are or any way to divert coolant to cool them off. If the temperature exceeded critical limits, the skin loses its structural integrety. This in turn would cause the cooling system to fail and allow temperatures to reach equilibrium and burn through the skin, destroying the drone. Currently under investigation are ways of discouraging the formation of hot spots--possibly by applying a thin ceramic layer on the outside of the nose.

Advantages of ACSES:

The program is a quick and relatively simple way to initiate the design of an actively cooled nose cone. The assumptions and correlations used in the code are accurate for the purposes they are serving and were easily integrated into the analysis. ACSES provides the means for a first approximation on what might otherwise be a series of tedious calculations. Due to the interactive nature of the program, many different cases varying in geometry, coolant choice, and materials can be run and compared in a short amount of time.

In the future, ACSES can be modified to provide the thermal design of the leading edge of the drone as well. Correlations would be needed for the given wing geometry which express the heat flux along the leading edge. The code would also have to allow for variable mass flow rates with multiple impindgements along the span.

Appendix 2.2.2: ACSES Listing

— Final Code —
5 June 88

```
C-----------------------------------------------------------------------
C
C       A C S E S :  Actively Cooled Structure Evaluation System
C
C       Ginger Koch, James Marcolesco, Greg Noffz, Jerry Yen
C
C       Version: 5.24.88
C
C-----------------------------------------------------------------------
C
C       I N P U T  P A R A M E T E R S :
C       ================================
C
C       tubes    =  number of tubes
C       dtube    =  tube inner diameter, input [mm], converted to [m]
C       xtube    =  thickness of tube, input [mm], converted to [m]
C       xskin    =  skin thickness, input [mm], converted to [m]
C       xnum     =  number of stations
C       mfr0     =  mass flow rate of coolant into manifold [kg/s]
C       nozd     =  impingement nozzle inner diameter [m]
C       choice   =  choice of coolant
C       prnt     =  1) short print   2) long print
C
C-----------------------------------------------------------------------
C
C       C O N S T A N T  P A R A M E T E R S :
C       ======================================
C
C       rnose    =  radius of nose cone [m]
C       alpha    =  cone angle, convert from degrees to radians
C       h        =  maximum distence back from nose analyzed [m]
C       zn       =  impingement nozzle distance [m]
C       tmax     =  meterial limiting temperature [K]
C                =  1000 [K] for molybdenum
C       tmaxr    =  1800 [R] for molybdenum
C       tman     =  temperature of coolant into manifold [K]
C       pi       =  3.141592654
C       f        =  friction factor of coolant tubes
C       kskin    =  thermal conductivity of nose [W/mK]
C                     evaluated at tmax for material
C                     103.77 for molybdenum at Tmax
C       ktube    =  thermal conductivity of the tube wall [W/mK]
C                =  29.4 [W/mK] for Cupronickel 30%
C
C
C       Commercial Tubing Sizes:
C
C       ID      OD      Thickness   gage    max number
C       [mm]    [in]      [mm]              for 1" nose
C       ==========================================
C       1.68    1/8       0.76      A         50
C       3.24    3/16      0.76      A         33
C       4.88    1/4       0.76      A         25
C       3.92    1/4       1.24      18        25
C       6.32    5/16      0.81      21A       20
C
C       Cupronickel 70% Cu  30% Ni  Wrought
C       yield strength: 57,000 [psi] 393 [MPa]
C       tensile strength: 60,000 [psi] 414 [MPa]
C       melting temperature: 1500 [K]
C       specific gravity: 8.95
```

```
c       Nozzle Tubing Sizes:

c       ID      OD      Thickness   gage
c       [mm]    [in]      [mm]
c       ============================
c       11.08   1/2       0.81        21A
c        9.40   1/2       1.65        16
c       14.12   5/8       0.89        20A
c       17.32   3/4       0.89        20A
c
c-----------------------------------------------------------------------
c
c       D E P E N D E N T  P A R A M E T E R S :
c       =======================================
c
c       tcin     =  coolant temperature exiting manifold
c                     and entering tubes = tk1 [K]
c       tfcal    =  temporary tfilm calculation [K]
c       tmav     =  bulk mixing temperature of coolant, used
c                     to evaluate properties [K]
c       t0       =  base of fin temperature [K]
c       tw       =  temperature inside tube wall [K]
c       tcrit    =  midline critical temperature [K]
c       tmi,tmo  =  mean fluid temperature at station k, in and out [K]
c       tout     =  final fluid exiting temperature [K]
c       mfr      =  mass flow rate in one tube [kg/s]
c       nvel     =  nozzle velocity [m/s]
c       tvel     =  tube velocity [m/s]
c       q        =  total heat at dx surf in terms of enthalpy from free
c                     stream conditions [W]
c       qm       =  [W/m]
c       qmm      =  [W/m^2]
c       choice   =  choice of coolant
c       ro       =  density of coolant from curve fit [kg/m^3]
c       mu       =  dynamic viscosity of coolant from curve fit [kg/m^3]
c       muw      =  dynamic viscosity of collant at wall temp
c       cp       =  specific heat of coolant from curve fit [J/kgK]
c       pr       =  Prandtl number of coolant from curve fit
c       re       =  Reynolds number of coolant
c       nu       =  Nusselt number of coolant from correlation
c       hnose    =  nose enthalpy
c       hwall    =  wall enthalpy
c       hx       =  local heat transfer coefficient for turbulent flow
c                     correlation at station x [W/m^2K]
c       kfluid   =  thermal conductivity of fluid from curve fit [W/mK]
c       ploss    =  system pressure loss [?]
c       pressl   =  dummy variable, piecewise pressure loss
c       L        =  distance between tubes at distance x [m]
c       k        =  position number, k = 2, xnum
c       x1,x2    =  distance back from manifold of next and previous
c                     station = (k-1) * h / xnum [m]
c       dx       =  distance between stations (x2 - x1) [m]
c       areah    =  area that heat transfer takes place across tube
c       areas    =  area that conduction takes place across skin
c
c       nbr      =  number of branches
c       xbr      =  distance back of each branch
c       br       =  flag that branching has occurred
```

```
c-----------------------------------------------------------------------
c
c       C O O L A N T   P R O P E R T Y   S U B R O U T I N E S :
c       =========================================================
c
c       thcond(choice,tmav,kfluid) thermal cond at tfilm, kh [W/mK]
c
c       specht(choice,tmav,cp)     specific heat at tfilm, cp [J/kgK]
c
c       dynv(choice,tmav,mu)       dynamic viscosity at tfilm, tw
c                                       mu [kg/(m)(sec)]
c
c       dense(choice,tmav,ro)      density at tfilm, exponential fit,
c                                       ro [kg/m^3]
c
c       fit(choice,tmav,e,answer) curve fit routines
c
c-----------------------------------------------------------------------
c
c       M A I N   P R O G R A M :
c       =========================
c
c
c234567
      program main
        integer xnum, tubes, flag, numtub, choice, nbr, br
        real h,mfr0,mfr,kfluid,kskin,ktube,hx,nu,L,hnose,hwall,f,
     *       nozd,nvel,dtube,mu,muw,xbr,max

c-----------------------------------------------------------------------
c
c       R E A D   I N   I N P U T   D A T A :
c       =====================================
c
c-----------------------------------------------------------------------

        open(2,file='acses.in')
          read(2,1400) rnose,alpha,zn
 1400     format(4f10.5)
          read(2,1401) tmax,tmaxr,kskin,emiss,ktube,epslon
 1401     format(6f10.3)
        close(2)

        pi = 3.141592654
        ploss = 0.

  100   format(/)
  200   format(//)
        print *,' Parameter input:'
        write (0,100)
        print *,' Coolants:  [1] liquid hydrogen '
        print *,'            [2] water-glycol solution (30%) '
        print *,'            [3] Therminol 60 '
        print *,' Input coolant choice ---------------> '
        read *, choice
        print *,' Minimum coolant temperatures: '
        print *,'        [1]  12 K   '
        print *,'        [2] 270 K   '
        print *,'        [3] 250 K   '
        print *,' Input initial coolant temp [K] -----> '
```

```
      read *, tman
      print *,' Input tube diameter [mm] ----------> '
      read *, dtube
      dtube = dtube / 1000
      print *,' Input tube thickness [mm] ----------> '
      read *, xtube
      xtube = xtube / 1000
      max = 2 * pi * rnose / (dtube + (2*xtube))
      print *,' For given geometry, # tubes < ',max
      print *,' Input number of tubes --------------> '
      read *, tubes

      print *,' Input wall thickness [mm] ----------> '
      read *, xskin
      xskin = xskin / 1000
      print *,' Max distance back on cone [m] ------> '
      read *, h
      print *,' Input number of stations -----------> '
      read *, kmax
      print *,' Input coolant mass flow rate [kg/s] --> '
      read *, mf2
      print *,' Impingement nozzle diameter [mm] ---> '
      read *, dnozz
      dnozz = dnozz / 1000
      print *,' 0) Short print    1) Long print ------> '
      read *, ifmt
      write (6,10)

C-----------------------------------------------------------------------
C
C     C O M P U T E  N O S E  W A L L  E N T A L P Y :
C     ================================================
C
C-----------------------------------------------------------------------

      hnose = (0.234 * tmaxr) + (0.00001 * tmaxr ** 2.)
      hwall = hnose
      rnose1 = rnose * 3.2808
      c1=9.792*(rnose1**(-.3))*alpha*(2080.-hnose)
     *  /(2080.-(3.6667*hwall))

C-----------------------------------------------------------------------
C
C                F I N D  C O O L A N T  T E M P
C                ===============================
C               E X I T I N G  I M P I N G E M E N T :
C               =======================================
C
C-----------------------------------------------------------------------
```

```
                epslon)
        tmi = tcin
        tmav = 1.2 * tmi
        tw = 10. * tmi

        x1 = 0.
        dx = h / xnum
        br = 0
        nbr = 0
        numtub = tubes
        rad = alpha * 2 * pi / 360
        f = 0.008
        mfr = mfr0 /  numtub
        xh =  pi * dtube / 2.
        xs =  pi * dtube / 2.
        call dense(choice,tmi,ro)

        nvel = (4*mfr0) / (ro * pi * (nozd ** 2))
        tvel = (4*mfr)  / (ro * pi * (dtube ** 2))

        open(5,file = 'acsee.out')
        open(10,file = 'plot.qs')
        open(11,file = 'plot.tm')
        open(12,file = 'plot.tcr')
        write (5,1008)
        write (5,1009)
        if (print.eq.1) then
          write (*,1008)
          write (*,1009)
        endif

c-------------------------------------------------------------------------
c       S T A T I O N  C A L C U L A T I O N S :
c       =======================================
c
c       main routine to calculate tmi,tmo at each (dx) station
c       to a distance h away from manifold, xnum times.
c       limits of integration are x1,x2
c
c-------------------------------------------------------------------------

        do 10 k = 2, xnum
          x2 = k * dx

          L = (2. * pi / numtub) * (x2 * sin(rad) + rnose)

c
c         Conversion factor from Btu/s ftsqrd to Watts/msqrd
c         is 11352.8855
c
c
          qmm = 11352.8855* c1 * (x2 ** (-0.2))

          qm  = L * qmm

          q = qm * dx

          if (prnt.eq.0) write (*,1510) k,x2
10        format(3X,I3,'    x  =  ',F5.2)

          if (br.eq.1) then
            br = 0
            if (prnt.eq.0) write (*,1011) nbr
          endif
```

```
c-----------------------------------------------------------------------
c
c        I T E R A T I O N :
c        ===================
c
c-----------------------------------------------------------------------

  600   call specht(choice,tmav,cp)

        tmo = tmi + (q / (mfr * cp))

        titer = (tmo + tmi) / 2

        if (abs(titer - tmav).gt.epslon) then
          tmav = titer
          go to 600
        endif

  700   call thcond(choice,tmav,kfluid)
        call dynv(choice,tmav,mu)
        call dynv(choice,tw,muw)
        call dense(choice,tmav,ro)
        pr = mu * cp / kfluid
        re = 4 * mfr / (pi * mu * dtube)
        nu = (0.027*re**0.8)*((mu/muw)**.14)*(pr**(1/3))
        hx = kfluid * nu / dtube

        r1 = 1 / (hx * xh)
        twiter = tmav + (qm  * r1)

        if (abs(twiter - tw).gt.epslon) then
          tw = twiter
          goto 700
        endif

        r2 = xtube / (ktube * xh)
        t0 =  tw + (qm * r2)

        tcrit = t0 + (qmm * (L ** 2) / (8 * kskin * xskin))

        press1 = (8*f*dx*(mfr**2))/((pi**2)*ro*(dtube**5))
        ploss = ploss + press1


        if (tcrit.ge.(0.95 * tmax)) then
          br = 1
          nbr = nbr + 1
          xbr = x2
          numtub = tubes * (2 ** nbr)
          mfr = mfr0 / numtub
        endif


 1008   format ('  #      x:      qs:     tmav:      press:      ',
     *           'tw:       t0:      tcrit:     Re:')
 1009   format ('        [m]    [W/m^2]     [K]      [Pa]        ',
     *           '[K]       [K]       [K]',/)
        write (5,1010) k,x2,qmm,tmav,press1,tw,t0,tcrit,re
```

```
      write (10,1015) x2, qmm
      write (11,1015) x2, tmav
      write (12,1015) x2, tcrit
1015  format (e15.4,1x,e15.4)

      if (prnt.eq.1) then
        write (*,1010) k,x2,qmm,tmav,pressl,tw,t0,tcrit,re
      endif

1010  format (i4,1x,f5.3,1x,e8.3,1x,e8.3,1x,e8.3,1x,
     *  e8.3,1x,e8.3,1x,e8.3,1x,e8.3)

      if (br.eq.1) then
        write (5,1011) nbr

        if (prnt.eq.1) write (*,1011) nbr
1011    format (/,'----> branch # ',i4,' <----',/)

      endif

      tmi = tmo
      x1 = x2

 10   continue


c-----------------------------------------------------------------------
c
c     P R I N T  O U T  R E S U L T S :
c     ================================
c
c-----------------------------------------------------------------------

      write (5,100)
      write (5,1020)

      if (prnt.eq.1) then
        write (*,100)
        write (*,1020)
      endif

1020  format(////////////////////,' Results and initial parameters:',/)
      if (choice.eq.1) then
        write (5,1050)

        if (prnt.eq.1) write (*,1050)

1050    format ('  Coolant considered:   Liquid hydrogen',/)
      elseif (choice.eq.2) then
            write (5,1060)

            if (prnt.eq.1) write (*,1060)

1060        format ('  Coolant considered:   Water/glycol solution
     .(30%)',/)
      else
            write (5,1070)

            if (prnt.eq.1) write (*,1070)

1070        format ('  Coolant considered:   Therminol 60',/)
      endif

      write (5,1110) tcin
1110  format ('  Temperature exiting manifold = ',e10.4,' [K]')
      write (5,1120) tmo
```

```
1120    format (' Initial exiting temperature = ',e10.4,' [K]')
        write (5,1130) ploss, (ploss * 1.4504e-4), (ploss/101350)
1130    format ('          System pressure loss = ',e10.4,' [Pa]  ',
     *          e10.4,' [psi]', f8.2, ' atm')
        write (5,1140) tubes
1140    format ('       Initial number of tubes = ',i4)
        write (5,1150) (dtube * 1000)
1150    format ('                  Tube diameter = ',f5.2,' [mm]')
        write (5,1160) (xtube * 1000)
1160    format ('                  Tube thickness = ',f5.2,' [mm]')
        write (5,1170) (rnose * 1000)
1170    format ('                    Nose radius = ',f4.1,' [mm]')
        write (5,1180) (xskin * 1000)
1180    format ('                   Wall thickness = ',f4.1,' [mm]')
        write (5,1190) alpha
1190    format ('                 Cone half angle = ',f4.1,' [deg]')
        write (5,1200) mfr0
1200    format ('         Nozzle mass flow rate = ',f9.4,' [kg/s]')
        write (5,1202) nvel
1202    format (' Velocity of coolant in nozzle = ',f8.3,' [m/s]')
        write (5,1204) mfr
1204    format ('    Outlet tube mass flow rate = ',f7.4,' [kg/s]')
        write (5,1206) tvel
1206    format (' Outlet vel of coolant in tubes = ',f8.3,' [m/s]')
        write (5,1208) (zn * 1000)
1208    format ('   Impingement target distance = ',f4.1,' [mm]')
        write (5,1210) (nozd * 1000)
1210    format ('   Impingement nozzle diameter = ',f5.2,' [mm]')
        write (5,1215) nbr
1215    format ('             Number of branches = ',i4)
        write (5,1220) tmax
1220    format (' Limiting material temperature = ',f5.0,' [K]')
      close(5)
      close(10)
      close(11)
      close(12)
      if (prnt.eq.1) then
        write (*,1110) tcin
        write (*,1120) tmo
        write (*,1130) ploss, (ploss * 1.450e-4), (ploss/101350)
        write (*,1140) tubes
        write (*,1150) (dtube * 1000)
        write (*,1160) (xtube * 1000)
        write (*,1170) (rnose * 1000)
        write (*,1180) (xskin * 1000)
        write (*,1190) alpha
        write (*,1200) mfr0
        write (*,1202) nvel
        write (*,1204) mfr
        write (*,1206) tvel
        write (*,1208) (zn * 1000)
        write (*,1210) (nozd * 1000)
        write (*,1215) nbr
        write (*,1220) tmax
      endif
      end

C
C*********************** SUBROUTINE MANI ******************************
C
C                Jerry Yen                          version 5.26.88
C
C     Variable description
C       pi, sigma ... constants
C       theta ... angle from nose tip of semihemisphere to back end of
C           manifold (deg)
```

```
C       area ... surface area of semihemisphere from theta = 0 to 80
C            degrees (m^2)
C       rnose ... nose radius (m)
C       hwall ... wall enthalpy (English units)
C         (All temperatures are in degrees Kelvin)
C       tbnoz ... temperature of fluid entering manifold from nozzle
C       twmax ... maximum allowable wall temperature
C       tbin ... fluid bulk temperature exiting manifold (entering tubes)
C       tbin1 ... guess for tbin (used in iteration)
C       tfilmn, tfilm ... film temperature at which properties are evaluated
C       ttube ... tube wall temperature
C       nozd ... nozzle diameter (m)
C       reyn ... Reynolds number based on nozzle diameter and nozzle exit
C            velocity
C       zn ... nozzle-to-target separation distance (m)
C       emiss ... radiative emissivity of wall
C       dtarg ... hemisphere diameter (m)
C       qstag, qrad, qnose ... stagnation, radiative, and nose heat
C            fluxes (English units)
C       nuavg ... average Nusselt number based on correlation
C       k ... thermal conductivity of fluid (W*m/K)
C       htc ... heat transfer coefficient of fluid ((W*m^2)/K)
C       diff ... used in iteration
C       mfrnoz ... mass flow rate at nozzle (kg/s)
C
C     Inputs required:  TBNOZ, TWMAX, NOZD, RNOSE, MFRNOZ,
C        ZN, EMISS
C
C     Output:  TBIN
C
      Subroutine MAN1(choice,tbnoz,twmax,nozd,rnose,mfrnoz,zn,emiss,
                      ttube,tbin,epslon)
      Real  tbnoz,twmax,twmax1,nozd,rnose,rnose1,reyn,zn,emiss,ttube,
           tbin,pi,sigma,theta,area,hwall,qstag,qrad,qnose,mfrnoz,
           nuavg,tbin1,tfilmn,k,htc,diff,tfilm,epslon
       Integer choice
C
C     Variables independent of fluid temperature are calculated
C          and converted into SI units
C
           pi = 3.141592654
           sigma = 5.67E-08
           theta = 85.0 * (pi/180.0)
C
C     "...1" quantities represent English units in use; note that hwall
C       and qstag are both in English units.  They are converted into
C       mks units in qnose by .2931.
C
           rnose1 = rnose * (3.281)
           dtarg = rnose * 2.0
           area =   2.0 * pi * (rnose**2) * (1.0 - COS(theta))
           twmax1 = twmax * 1.8
           hwall = 0.234 * twmax1 + 1.0E-05 * (twmax1**2)
           qstag = ((128.0/(SQRT(rnose1))) * (1.0 - (hwall/2080)))
           qstag = qstag * 3600.
           qrad = emiss * sigma * (twmax**4) * area
           qnose = qstag * rnose1 * 2.4816 * .2931
C
C     Correlation is only good for ZN/NOZD . le . 7.0
C
           tfilm = 0.5 * (ttube + tbnoz)
           call dynv(choice, tfilm, visc)
           reyn = (4.0 * mfrnoz)/(pi * visc * nozd)
20         if ((zn/nozd).le.7.0) then
              nuavg = 2.98 * (reyn**0.585) * ((nozd/dtarg)**1.10) *
                      ((zn/nozd)**(-0.007))
```

```
            else
               write(6,1000)
 1000          format(//,' **** NOTE:  ZN/NOZD  is  greater  than  7****',
     .    /,' (ZN = nozzle-to-target separation distance;  NOZD = nozzle
     .diameter)',/,' Please re-input data:  ZN, NOZD  =    ')
               read* , zn,nozd
               go to 20
            endif

C     Now we iterate for TBIN (temperature of the fluid exiting the
C       manifold)
C
            tbin = 1.1*tbnoz
     10     tbin1 = tbin
            tfilmn = 0.5 * (0.5 * (tbin1 + tbnoz) + 0.5 * twmax)
            call  THCOND(choice, tfilmn, k)
            htc = (nuavg * k)/nozd
            tbin = tbnoz + ((qnose - qrad)/(area * htc))
            diff = ABS(tbin - tbin1)
C
C     Can change the next line for a more precise & time-consuming
C      iteration
C
            if (diff.gt.epslon) go to 10
            return
            end

c-----------------------------------------------------------------------
c
c                C O O L A N T   P R O P E R T I E S:
c                ====================================
c              S U B R O U T I N E S / C U R V E  F I T :
c              ==========================================
c-----------------------------------------------------------------------

       subroutine thcond(choice,tmav,k)
         real k,lk,a1(10),a2(2),a3(2),tmav
         integer choice
         data a2
     *        /.44874,3.1929e-4/
         data a3
     *        /0.16381,-8.329e-4/

         if (choice.eq.1) then
            a = 1.6030e+02
            b = -0.64379
            c = 4.1102e-03
            d = -7.679e-06
            e = 6.2779e-09
            f = -1.819e-12

            k = a+(b*tmav)+(c*(tmav**2))+(d*(tmav**3))+(e*(tmav**4))+
     .           (f*(tmav**5))
            k = k * 1e-03
         elseif (choice.eq.2) then
            call fit4(tmav, a2, k)
         else
            call fit4(tmav,a3,k)

         endif
       return
       end

       subroutine specht(choice,tmav,cp)
         real a1(10),b(10),a2(2),a3(2),tmav,cp
```

```
      integer choice
      data a2
*          /3.6511E03,2.5361E-04/

      if (choice.eq.1) then
           a = 5.9055e+03
           bb = 1.4564E+02
           c = -0.78868
           d = 1.8103e-03
           e = -1.835e-06
           f = 6.7750e-10

           Cp = a+(bb*tmav)+(c*(tmav**2))+(d*(tmav**3))+(e*(tmav**4))+
     .          (f*(tmav**5))

      elseif (choice.eq.2) then
          if (tmav.lt.280.) then
             cp = 3930.
             return
          else
             call fit4(tmav,a2,cp)
          endif
      else

          CP = 36.2858 * (Tmav ** 0.6687)

      endif
      return
      end


      subroutine dynv(choice,tmav,mu)
        real mu,visc,a1(10),a2(2),a3(2)
        integer choice
        data a2
*          /14.945,-0.02994/
       data a3
*          /1.018e5,-2.07e-2/
        if (choice.eq.1) then
           a = 2.0053e+02
           b = -1.30242
           c = 3.5588e-03
           d = -3.205e-06
           e = 9.3978e-10

           mu = a+(b*tmav)+(c*(tmav**2))+(d*(tmav**3))+(e*(tmav**4))
           mu = mu * 1.0E-07
           return
        elseif (choice.eq.2) then
            call fit4(tmav, a2, mu)
            return
        else
            if (tmav.le.300) then
              mu = 10 * 2.7355e37 * (tmav ** (-16.5512))
            else
              call fit4(tmav,a3,mu)
              mu = 2.674e9 * (tmav ** (-4.7321))
            endif
        endif
      return
      end


      subroutine dense(choice,tmav,ro)
        real a2(2), a3(8), ro, tmav
        integer choice
```

ORIGINAL PAGE IS
OF POOR QUALITY

```
      data a2
     *   /1.1719E3,-4.142E-04/

         if (choice.eq.1) then
            a = 1.0374e+02
            b = -0.9265
            c = 3.7198e-03
            d = -7.189e-06
            e = 6.5313e-09
            f = -2.235e-12

            ro = a+(b*tmav)+(c*(tmav**2))+(d*(tmav**3))+(e*(tmav**4))+
                 (f*(tmav**5))

            return

         elseif (choice.eq.2) then
                call fit4(tmav,a2,ro)
         else

           RO= 1173.0803 - (0.5093 * Tmav) - (2.795E-04 * (Tmav ** 2))

         endif
       return
       end

         subroutine fit4(tmav,a,answer)
            real tmav, a(2), answer
            answer = a(1) * (2.718281828 ** (a(2) * tmav))
         return
         end
```

ORIGINAL PAGE IS
OF POOR QUALITY

Appendix 3: Design Results

Appendix 3.1: Hydrogen Design

$\dot{m} = 3.5$ kg/s Final LH2 Design

#	x: [m]	qs: [W/m^2]	tmav: [K]	press: [Pa]	tw: [K]	t0: [K]	tcrit: [K]	Re:
2	0.050	.832E+07	.149E+03	.451E+05	.197E+03	.415E+03	.719E+03	.504E+07
3	0.075	.767E+07	.149E+03	.451E+05	.197E+03	.413E+03	.736E+03	.504E+07
4	0.100	.724E+07	.150E+03	.456E+05	.198E+03	.416E+03	.764E+03	.508E+07
5	0.125	.693E+07	.150E+03	.456E+05	.198E+03	.420E+03	.797E+03	.508E+07
6	0.150	.668E+07	.152E+03	.461E+05	.201E+03	.428E+03	.836E+03	.512E+07
7	0.175	.648E+07	.152E+03	.461E+05	.202E+03	.434E+03	.876E+03	.512E+07
8	0.200	.631E+07	.153E+03	.467E+05	.204E+03	.443E+03	.920E+03	.517E+07
9	0.225	.616E+07	.153E+03	.467E+05	.206E+03	.450E+03	.966E+03	.517E+07
----> branch # 1 <-----								
10	0.250	.603E+07	.155E+03	.118E+05	.201E+03	.327E+03	.466E+03	.261E+07
11	0.275	.592E+07	.155E+03	.118E+05	.203E+03	.332E+03	.480E+03	.261E+07
12	0.300	.582E+07	.156E+03	.120E+05	.205E+03	.337E+03	.497E+03	.264E+07
13	0.325	.572E+07	.156E+03	.120E+05	.206E+03	.342E+03	.513E+03	.264E+07
14	0.350	.564E+07	.158E+03	.121E+05	.209E+03	.348E+03	.530E+03	.266E+07
15	0.375	.556E+07	.158E+03	.121E+05	.210E+03	.353E+03	.546E+03	.266E+07
16	0.400	.549E+07	.160E+03	.123E+05	.213E+03	.359E+03	.565E+03	.269E+07
17	0.425	.542E+07	.160E+03	.123E+05	.214E+03	.363E+03	.582E+03	.269E+07
18	0.450	.536E+07	.162E+03	.125E+05	.217E+03	.369E+03	.601E+03	.272E+07
19	0.475	.530E+07	.163E+03	.126E+05	.218E+03	.375E+03	.619E+03	.274E+07
20	0.500	.525E+07	.164E+03	.127E+05	.220E+03	.380E+03	.638E+03	.275E+07
21	0.525	.520E+07	.165E+03	.128E+05	.222E+03	.386E+03	.657E+03	.277E+07
22	0.550	.515E+07	.166E+03	.129E+05	.224E+03	.391E+03	.677E+03	.278E+07
23	0.575	.511E+07	.167E+03	.130E+05	.226E+03	.396E+03	.697E+03	.280E+07
24	0.600	.506E+07	.169E+03	.131E+05	.228E+03	.402E+03	.717E+03	.282E+07
25	0.625	.502E+07	.170E+03	.132E+05	.230E+03	.407E+03	.738E+03	.284E+07
26	0.650	.498E+07	.171E+03	.133E+05	.232E+03	.412E+03	.759E+03	.285E+07
27	0.675	.494E+07	.172E+03	.134E+05	.234E+03	.418E+03	.780E+03	.287E+07
28	0.700	.491E+07	.173E+03	.135E+05	.236E+03	.423E+03	.801E+03	.289E+07
29	0.725	.487E+07	.175E+03	.137E+05	.238E+03	.428E+03	.823E+03	.291E+07
30	0.750	.484E+07	.176E+03	.138E+05	.240E+03	.434E+03	.845E+03	.293E+07
31	0.775	.481E+07	.177E+03	.139E+05	.242E+03	.439E+03	.868E+03	.295E+07
32	0.800	.478E+07	.179E+03	.140E+05	.244E+03	.444E+03	.891E+03	.297E+07
33	0.825	.475E+07	.180E+03	.141E+05	.246E+03	.450E+03	.914E+03	.298E+07
34	0.850	.472E+07	.181E+03	.143E+05	.248E+03	.455E+03	.937E+03	.300E+07
35	0.875	.469E+07	.183E+03	.144E+05	.250E+03	.460E+03	.961E+03	.302E+07
----> branch # 2 <-----								
36	0.900	.467E+07	.184E+03	.363E+04	.243E+03	.350E+03	.480E+03	.152E+07
37	0.925	.464E+07	.185E+03	.367E+04	.245E+03	.353E+03	.488E+03	.153E+07
38	0.950	.462E+07	.187E+03	.370E+04	.247E+03	.357E+03	.497E+03	.154E+07
39	0.975	.459E+07	.188E+03	.374E+04	.249E+03	.361E+03	.505E+03	.155E+07
40	1.000	.457E+07	.190E+03	.377E+04	.251E+03	.364E+03	.514E+03	.156E+07
41	1.025	.455E+07	.191E+03	.381E+04	.253E+03	.368E+03	.522E+03	.157E+07
42	1.050	.453E+07	.193E+03	.384E+04	.254E+03	.371E+03	.531E+03	.159E+07
43	1.075	.451E+07	.195E+03	.388E+04	.256E+03	.375E+03	.540E+03	.160E+07
44	1.100	.448E+07	.196E+03	.391E+04	.258E+03	.378E+03	.549E+03	.161E+07
45	1.125	.446E+07	.198E+03	.395E+04	.260E+03	.382E+03	.558E+03	.162E+07
46	1.150	.445E+07	.199E+03	.399E+04	.262E+03	.386E+03	.567E+03	.163E+07
47	1.175	.443E+07	.201E+03	.402E+04	.264E+03	.389E+03	.576E+03	.164E+07
48	1.200	.441E+07	.203E+03	.406E+04	.266E+03	.393E+03	.585E+03	.165E+07
9	1.225	.439E+07	.204E+03	.410E+04	.268E+03	.396E+03	.594E+03	.166E+07
50	1.250	.437E+07	.206E+03	.414E+04	.270E+03	.400E+03	.604E+03	.167E+07
51	1.275	.435E+07	.208E+03	.418E+04	.272E+03	.404E+03	.613E+03	.168E+07
52	1.300	.434E+07	.210E+03	.422E+04	.274E+03	.407E+03	.623E+03	.169E+07
53	1.325	.432E+07	.211E+03	.425E+04	.277E+03	.411E+03	.632E+03	.170E+07
54	1.350	.430E+07	.213E+03	.429E+04	.279E+03	.415E+03	.642E+03	.171E+07
55	1.375	.429E+07	.215E+03	.433E+04	.281E+03	.418E+03	.652E+03	.172E+07

57	1.425	.426E+07	.219E+03	.441E+04	.285E+03	.426E+03	.671E+03	.174E+07
58	1.450	.424E+07	.221E+03	.445E+04	.287E+03	.429E+03	.681E+03	.175E+07
59	1.475	.423E+07	.223E+03	.449E+04	.289E+03	.433E+03	.692E+03	.176E+07
60	1.500	.422E+07	.225E+03	.453E+04	.291E+03	.437E+03	.702E+03	.177E+07
61	1.525	.420E+07	.227E+03	.457E+04	.294E+03	.440E+03	.712E+03	.178E+07
62	1.550	.419E+07	.229E+03	.461E+04	.296E+03	.444E+03	.722E+03	.179E+07
63	1.575	.417E+07	.231E+03	.465E+04	.298E+03	.448E+03	.733E+03	.180E+07
64	1.600	.416E+07	.233E+03	.469E+04	.300E+03	.452E+03	.743E+03	.181E+07
65	1.625	.415E+07	.235E+03	.472E+04	.303E+03	.456E+03	.754E+03	.182E+07
66	1.650	.414E+07	.237E+03	.476E+04	.305E+03	.459E+03	.765E+03	.183E+07
67	1.675	.412E+07	.239E+03	.480E+04	.307E+03	.463E+03	.776E+03	.183E+07
68	1.700	.411E+07	.241E+03	.484E+04	.310E+03	.467E+03	.787E+03	.184E+07
69	1.725	.410E+07	.243E+03	.488E+04	.312E+03	.471E+03	.798E+03	.185E+07
70	1.750	.409E+07	.245E+03	.491E+04	.314E+03	.475E+03	.809E+03	.185E+07
71	1.775	.408E+07	.248E+03	.495E+04	.317E+03	.479E+03	.820E+03	.186E+07
72	1.800	.406E+07	.250E+03	.499E+04	.319E+03	.483E+03	.831E+03	.187E+07
73	1.825	.405E+07	.252E+03	.502E+04	.322E+03	.487E+03	.843E+03	.187E+07
74	1.850	.404E+07	.254E+03	.506E+04	.324E+03	.491E+03	.854E+03	.188E+07
75	1.875	.403E+07	.257E+03	.509E+04	.327E+03	.495E+03	.866E+03	.188E+07
76	1.900	.402E+07	.259E+03	.513E+04	.329E+03	.499E+03	.877E+03	.188E+07
77	1.925	.401E+07	.261E+03	.516E+04	.332E+03	.503E+03	.889E+03	.189E+07
78	1.950	.400E+07	.264E+03	.519E+04	.335E+03	.507E+03	.901E+03	.189E+07
79	1.975	.399E+07	.266E+03	.522E+04	.337E+03	.511E+03	.913E+03	.189E+07
80	2.000	.398E+07	.269E+03	.526E+04	.340E+03	.515E+03	.925E+03	.189E+07
81	2.025	.397E+07	.271E+03	.529E+04	.343E+03	.520E+03	.937E+03	.189E+07
82	2.050	.396E+07	.273E+03	.532E+04	.346E+03	.524E+03	.949E+03	.189E+07
83	2.075	.395E+07	.276E+03	.535E+04	.348E+03	.528E+03	.962E+03	.189E+07

ORIGINAL PAGE IS
OF POOR QUALITY

----> branch # 3 <----

84	2.100	.394E+07	.279E+03	.134E+04	.342E+03	.433E+03	.543E+03	.946E+06
85	2.125	.393E+07	.281E+03	.135E+04	.344E+03	.436E+03	.548E+03	.945E+06
86	2.150	.392E+07	.284E+03	.136E+04	.347E+03	.439E+03	.554E+03	.944E+06
87	2.175	.391E+07	.286E+03	.136E+04	.350E+03	.443E+03	.560E+03	.943E+06
88	2.200	.390E+07	.289E+03	.137E+04	.353E+03	.447E+03	.566E+03	.941E+06
89	2.225	.390E+07	.292E+03	.138E+04	.356E+03	.450E+03	.571E+03	.939E+06
90	2.250	.389E+07	.294E+03	.138E+04	.359E+03	.454E+03	.577E+03	.936E+06
91	2.275	.388E+07	.297E+03	.139E+04	.362E+03	.458E+03	.583E+03	.933E+06
92	2.300	.387E+07	.300E+03	.140E+04	.365E+03	.462E+03	.589E+03	.930E+06
93	2.325	.386E+07	.302E+03	.140E+04	.369E+03	.466E+03	.595E+03	.926E+06
94	2.350	.385E+07	.305E+03	.141E+04	.372E+03	.470E+03	.601E+03	.922E+06
95	2.375	.384E+07	.308E+03	.141E+04	.375E+03	.474E+03	.608E+03	.918E+06
96	2.400	.384E+07	.311E+03	.142E+04	.378E+03	.478E+03	.614E+03	.914E+06
97	2.425	.383E+07	.314E+03	.142E+04	.382E+03	.482E+03	.620E+03	.909E+06
98	2.450	.382E+07	.317E+03	.143E+04	.385E+03	.486E+03	.626E+03	.904E+06
99	2.475	.381E+07	.320E+03	.143E+04	.388E+03	.490E+03	.633E+03	.898E+06
100	2.500	.381E+07	.322E+03	.144E+04	.392E+03	.494E+03	.639E+03	.892E+06
101	2.525	.380E+07	.325E+03	.144E+04	.395E+03	.498E+03	.646E+03	.886E+06
102	2.550	.379E+07	.328E+03	.145E+04	.399E+03	.502E+03	.652E+03	.880E+06
103	2.575	.378E+07	.331E+03	.145E+04	.402E+03	.507E+03	.659E+03	.874E+06
104	2.600	.378E+07	.334E+03	.145E+04	.406E+03	.511E+03	.666E+03	.867E+06
105	2.625	.377E+07	.338E+03	.146E+04	.410E+03	.515E+03	.672E+03	.860E+06
106	2.650	.376E+07	.341E+03	.146E+04	.413E+03	.520E+03	.679E+03	.853E+06
107	2.675	.375E+07	.344E+03	.147E+04	.417E+03	.524E+03	.686E+03	.845E+06
108	2.700	.375E+07	.347E+03	.147E+04	.421E+03	.529E+03	.693E+03	.837E+06
109	2.725	.374E+07	.350E+03	.148E+04	.425E+03	.533E+03	.700E+03	.830E+06
110	2.750	.373E+07	.353E+03	.148E+04	.428E+03	.538E+03	.707E+03	.822E+06
111	2.775	.373E+07	.356E+03	.149E+04	.432E+03	.542E+03	.714E+03	.813E+06
112	2.800	.372E+07	.360E+03	.149E+04	.436E+03	.547E+03	.721E+03	.805E+06
113	2.825	.371E+07	.363E+03	.149E+04	.440E+03	.552E+03	.728E+03	.797E+06
114	2.850	.371E+07	.366E+03	.150E+04	.444E+03	.556E+03	.736E+03	.788E+06
115	2.875	.370E+07	.369E+03	.150E+04	.448E+03	.561E+03	.743E+03	.780E+06
116	2.900	.369E+07	.373E+03	.151E+04	.452E+03	.566E+03	.750E+03	.771E+06
117	2.925	.369E+07	.376E+03	.151E+04	.457E+03	.571E+03	.758E+03	.762E+06
118	2.950	.369E+07	.380E+03	.152E+04	.461E+03	.576E+03	.765E+03	.753E+06
119	2.975	.368E+07	.383E+03	.152E+04	.465E+03	.581E+03	.773E+03	.744E+06

120	3.000	.367E+07	.386E+03	.153E+04	.469E+03	.585E+03	.780E+03	.736E+06
121	3.025	.366E+07	.390E+03	.154E+04	.474E+03	.590E+03	.788E+03	.727E+06
122	3.050	.366E+07	.393E+03	.154E+04	.478E+03	.596E+03	.796E+03	.718E+06
123	3.075	.365E+07	.397E+03	.155E+04	.482E+03	.601E+03	.803E+03	.709E+06
124	3.100	.365E+07	.400E+03	.155E+04	.487E+03	.606E+03	.811E+03	.700E+06
125	3.125	.364E+07	.404E+03	.156E+04	.491E+03	.611E+03	.819E+03	.691E+06
126	3.150	.363E+07	.407E+03	.157E+04	.496E+03	.616E+03	.827E+03	.682E+06
127	3.175	.363E+07	.411E+03	.158E+04	.500E+03	.621E+03	.835E+03	.673E+06
128	3.200	.362E+07	.414E+03	.158E+04	.505E+03	.626E+03	.843E+03	.664E+06
129	3.225	.362E+07	.418E+03	.159E+04	.509E+03	.632E+03	.851E+03	.656E+06
130	3.250	.361E+07	.422E+03	.160E+04	.514E+03	.637E+03	.859E+03	.647E+06
131	3.275	.361E+07	.425E+03	.161E+04	.519E+03	.642E+03	.867E+03	.638E+06
132	3.300	.360E+07	.429E+03	.162E+04	.523E+03	.648E+03	.875E+03	.630E+06
133	3.325	.359E+07	.433E+03	.163E+04	.528E+03	.653E+03	.883E+03	.622E+06
134	3.350	.359E+07	.436E+03	.164E+04	.533E+03	.659E+03	.892E+03	.613E+06
135	3.375	.358E+07	.440E+03	.165E+04	.538E+03	.664E+03	.900E+03	.605E+06
136	3.400	.358E+07	.444E+03	.166E+04	.542E+03	.669E+03	.908E+03	.597E+06
137	3.425	.357E+07	.447E+03	.167E+04	.547E+03	.675E+03	.917E+03	.589E+06
138	3.450	.357E+07	.451E+03	.169E+04	.552E+03	.681E+03	.925E+03	.581E+06
139	3.475	.356E+07	.455E+03	.170E+04	.557E+03	.686E+03	.934E+03	.573E+06
140	3.500	.356E+07	.459E+03	.171E+04	.562E+03	.692E+03	.942E+03	.565E+06
141	3.525	.355E+07	.462E+03	.173E+04	.567E+03	.697E+03	.951E+03	.558E+06

----> branch # 4 <-----

142	3.550	.355E+07	.466E+03	.436E+03	.558E+03	.624E+03	.688E+03	.275E+06
143	3.575	.354E+07	.470E+03	.440E+03	.562E+03	.628E+03	.693E+03	.271E+06
144	3.600	.354E+07	.474E+03	.444E+03	.567E+03	.633E+03	.699E+03	.268E+06
145	3.625	.353E+07	.478E+03	.449E+03	.572E+03	.639E+03	.705E+03	.264E+06
146	3.650	.353E+07	.481E+03	.453E+03	.577E+03	.644E+03	.711E+03	.261E+06
147	3.675	.352E+07	.485E+03	.458E+03	.582E+03	.649E+03	.717E+03	.257E+06
148	3.700	.352E+07	.489E+03	.462E+03	.587E+03	.654E+03	.723E+03	.254E+06
149	3.725	.351E+07	.493E+03	.468E+03	.592E+03	.660E+03	.729E+03	.251E+06
150	3.750	.351E+07	.497E+03	.474E+03	.597E+03	.665E+03	.735E+03	.247E+06
151	3.775	.350E+07	.501E+03	.479E+03	.602E+03	.670E+03	.741E+03	.244E+06
152	3.800	.350E+07	.505E+03	.485E+03	.607E+03	.675E+03	.747E+03	.241E+06
153	3.825	.350E+07	.508E+03	.491E+03	.611E+03	.681E+03	.753E+03	.238E+06
154	3.850	.349E+07	.512E+03	.498E+03	.616E+03	.686E+03	.759E+03	.235E+06
155	3.875	.349E+07	.516E+03	.504E+03	.621E+03	.691E+03	.765E+03	.232E+06
156	3.900	.348E+07	.520E+03	.511E+03	.627E+03	.697E+03	.772E+03	.229E+06
157	3.925	.348E+07	.524E+03	.518E+03	.632E+03	.702E+03	.778E+03	.226E+06
158	3.950	.347E+07	.528E+03	.526E+03	.637E+03	.707E+03	.784E+03	.224E+06
159	3.975	.347E+07	.532E+03	.533E+03	.642E+03	.713E+03	.790E+03	.221E+06
160	4.000	.346E+07	.536E+03	.541E+03	.647E+03	.718E+03	.796E+03	.218E+06
161	4.025	.346E+07	.540E+03	.550E+03	.652E+03	.724E+03	.802E+03	.216E+06
162	4.050	.346E+07	.544E+03	.558E+03	.657E+03	.729E+03	.809E+03	.213E+06
163	4.075	.345E+07	.548E+03	.567E+03	.662E+03	.734E+03	.815E+03	.211E+06
164	4.100	.345E+07	.552E+03	.577E+03	.667E+03	.740E+03	.821E+03	.208E+06
165	4.125	.344E+07	.556E+03	.586E+03	.672E+03	.745E+03	.827E+03	.206E+06
166	4.150	.344E+07	.560E+03	.596E+03	.677E+03	.751E+03	.834E+03	.204E+06
167	4.175	.343E+07	.564E+03	.607E+03	.682E+03	.756E+03	.840E+03	.201E+06
168	4.200	.343E+07	.568E+03	.618E+03	.687E+03	.761E+03	.846E+03	.199E+06
169	4.225	.343E+07	.572E+03	.629E+03	.692E+03	.767E+03	.852E+03	.197E+06
170	4.250	.342E+07	.576E+03	.640E+03	.698E+03	.772E+03	.859E+03	.195E+06
171	4.275	.342E+07	.580E+03	.652E+03	.703E+03	.778E+03	.865E+03	.193E+06
172	4.300	.341E+07	.584E+03	.664E+03	.708E+03	.783E+03	.871E+03	.191E+06
173	4.325	.341E+07	.588E+03	.677E+03	.713E+03	.789E+03	.878E+03	.189E+06
174	4.350	.341E+07	.592E+03	.689E+03	.718E+03	.794E+03	.884E+03	.187E+06
175	4.375	.340E+07	.596E+03	.703E+03	.723E+03	.800E+03	.890E+03	.185E+06
176	4.400	.340E+07	.600E+03	.716E+03	.728E+03	.805E+03	.897E+03	.183E+06
177	4.425	.339E+07	.605E+03	.730E+03	.733E+03	.810E+03	.903E+03	.181E+06
178	4.450	.339E+07	.609E+03	.745E+03	.739E+03	.816E+03	.909E+03	.179E+06
179	4.475	.339E+07	.613E+03	.759E+03	.744E+03	.821E+03	.916E+03	.178E+06
180	4.500	.338E+07	.617E+03	.774E+03	.749E+03	.827E+03	.922E+03	.176E+06
181	4.525	.338E+07	.621E+03	.790E+03	.754E+03	.832E+03	.928E+03	.174E+06

183	4.575	.337E+07	.629E+03	.821E+03	.764E+03	.843E+03	.941E+03	.171E+06
184	4.600	.337E+07	.633E+03	.837E+03	.769E+03	.849E+03	.947E+03	.170E+06
185	4.625	.337E+07	.638E+03	.853E+03	.775E+03	.854E+03	.954E+03	.168E+06

----> branch # 5 <----

36	4.650	.336E+07	.642E+03	.217E+03	.762E+03	.802E+03	.827E+03	.833E+05
37	4.675	.336E+07	.646E+03	.221E+03	.766E+03	.807E+03	.832E+03	.826E+05
188	4.700	.335E+07	.650E+03	.225E+03	.772E+03	.812E+03	.837E+03	.819E+05
189	4.725	.335E+07	.654E+03	.229E+03	.777E+03	.817E+03	.843E+03	.812E+05
190	4.750	.335E+07	.659E+03	.233E+03	.782E+03	.822E+03	.848E+03	.805E+05
191	4.775	.334E+07	.663E+03	.237E+03	.787E+03	.827E+03	.854E+03	.799E+05
192	4.800	.334E+07	.667E+03	.241E+03	.792E+03	.833E+03	.859E+03	.792E+05
193	4.825	.334E+07	.671E+03	.245E+03	.797E+03	.838E+03	.864E+03	.786E+05
194	4.850	.333E+07	.676E+03	.248E+03	.802E+03	.843E+03	.870E+03	.780E+05
195	4.875	.333E+07	.680E+03	.252E+03	.807E+03	.848E+03	.875E+03	.774E+05
196	4.900	.333E+07	.684E+03	.255E+03	.812E+03	.853E+03	.881E+03	.768E+05
197	4.925	.332E+07	.689E+03	.258E+03	.817E+03	.859E+03	.886E+03	.762E+05
198	4.950	.332E+07	.693E+03	.261E+03	.822E+03	.864E+03	.892E+03	.757E+05
199	4.975	.332E+07	.697E+03	.263E+03	.827E+03	.869E+03	.897E+03	.751E+05
200	5.000	.331E+07	.702E+03	.266E+03	.832E+03	.874E+03	.903E+03	.746E+05

ORIGINAL PAGE IS
OF POOR QUALITY

Results and initial parameters:

Coolant considered: Liquid hydrogen

Temperature exiting manifold = 0.1482E+03 [K]
Final exiting temperature = 0.7039E+03 [K]
System pressure loss = 0.1038E+07 [Pa] 0.1505E+03 [psi] 10.24 atm
Initial number of tubes = 24
Tube diameter = 4.88 [mm]
Tube thickness = 0.76 [mm]
Nose radius = 25.4 [mm]
Wall thickness = 2.0 [mm]
Cone half angle = 5.0 [deg]
Nozzle mass flow rate = 3.5000 [kg/s]
Velocity of coolant in nozzle = 806.279 [m/s]
Outlet tube mass flow rate = 0.0046 [kg/s]
Outlet vel of coolant in tubes = 281.257 [m/s]
Impingement target distance = 25.4 [mm]
Impingement nozzle diameter = 14.12 [mm]
Number of branches = 5
Limiting material temperature = 1000. [K]

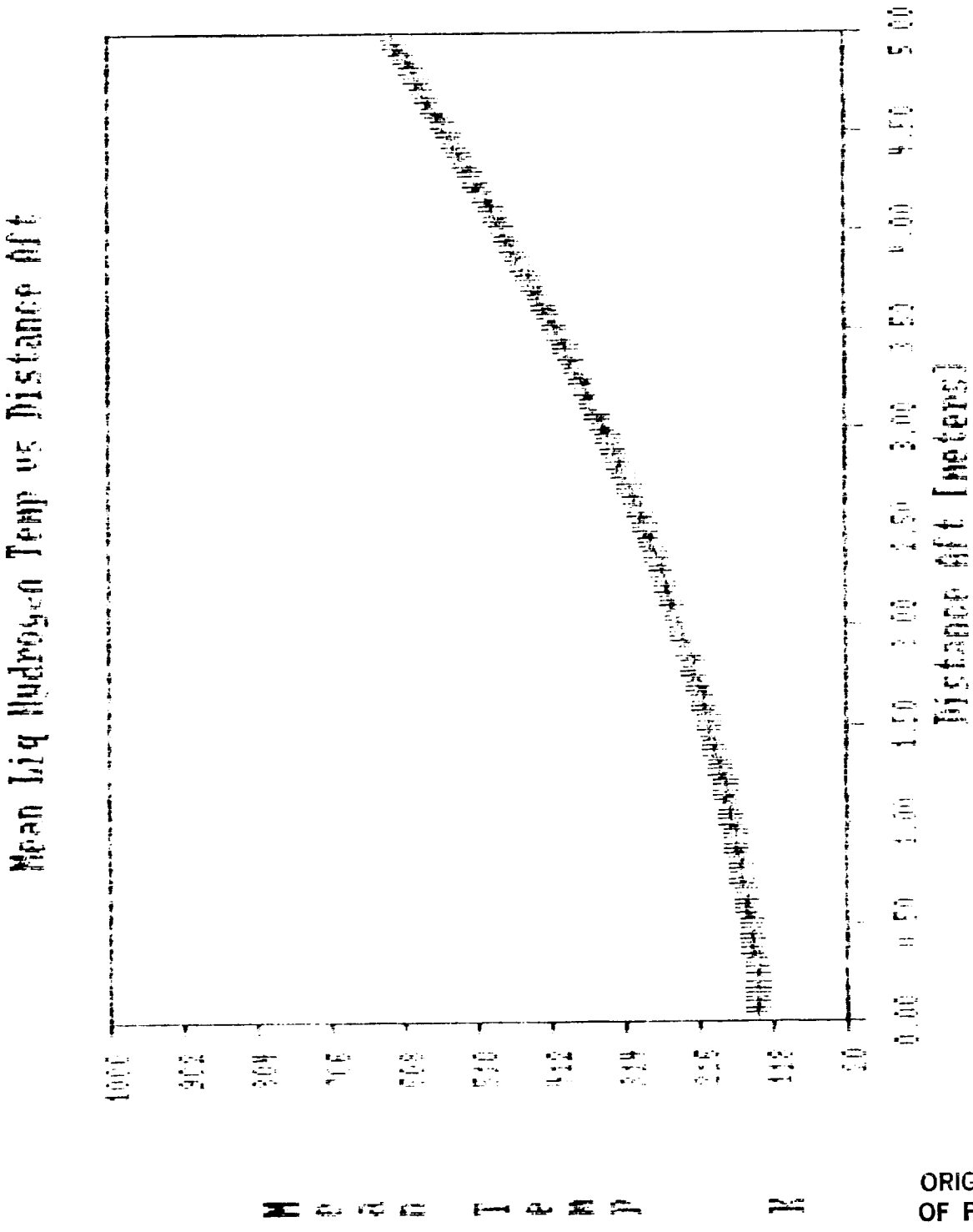

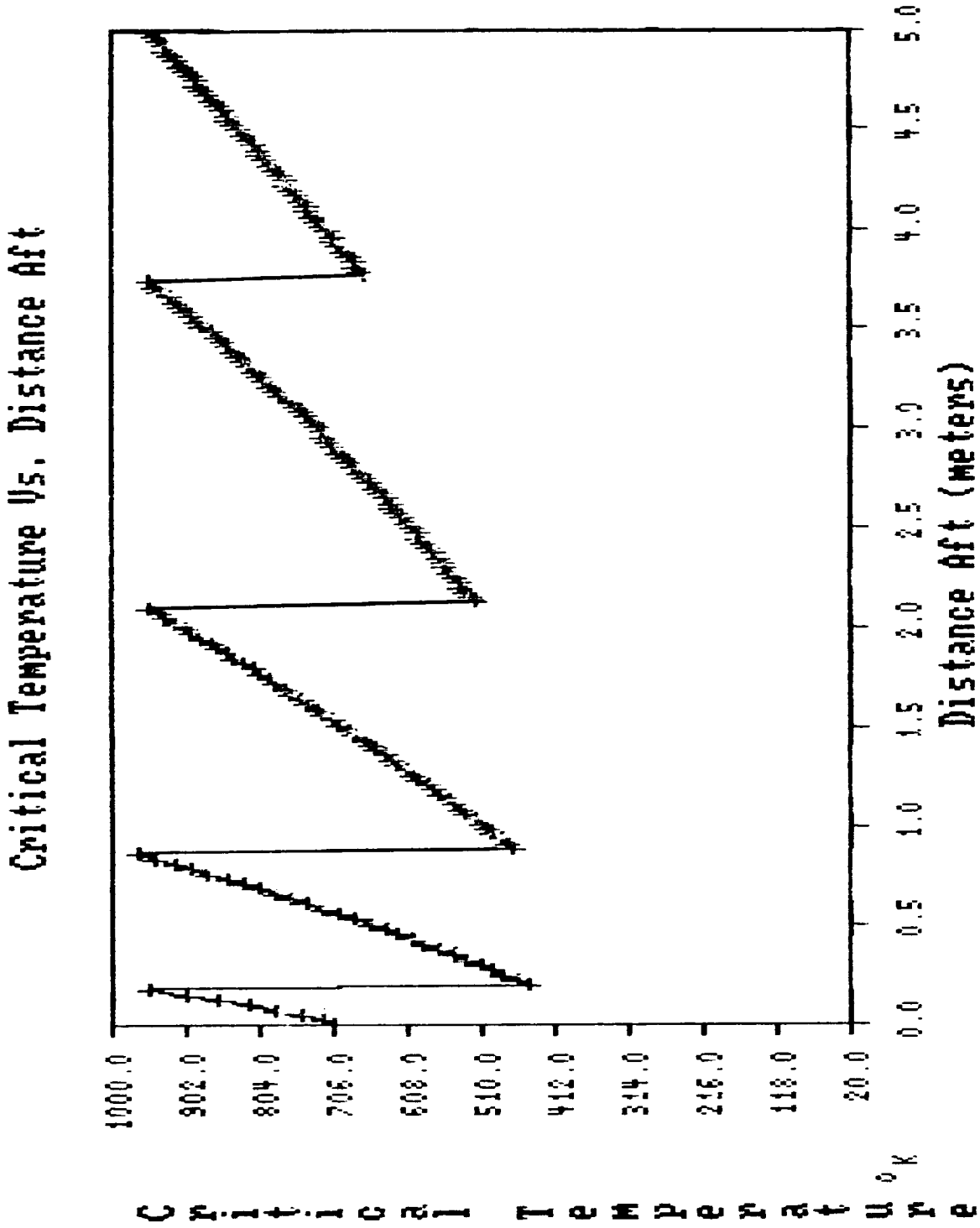

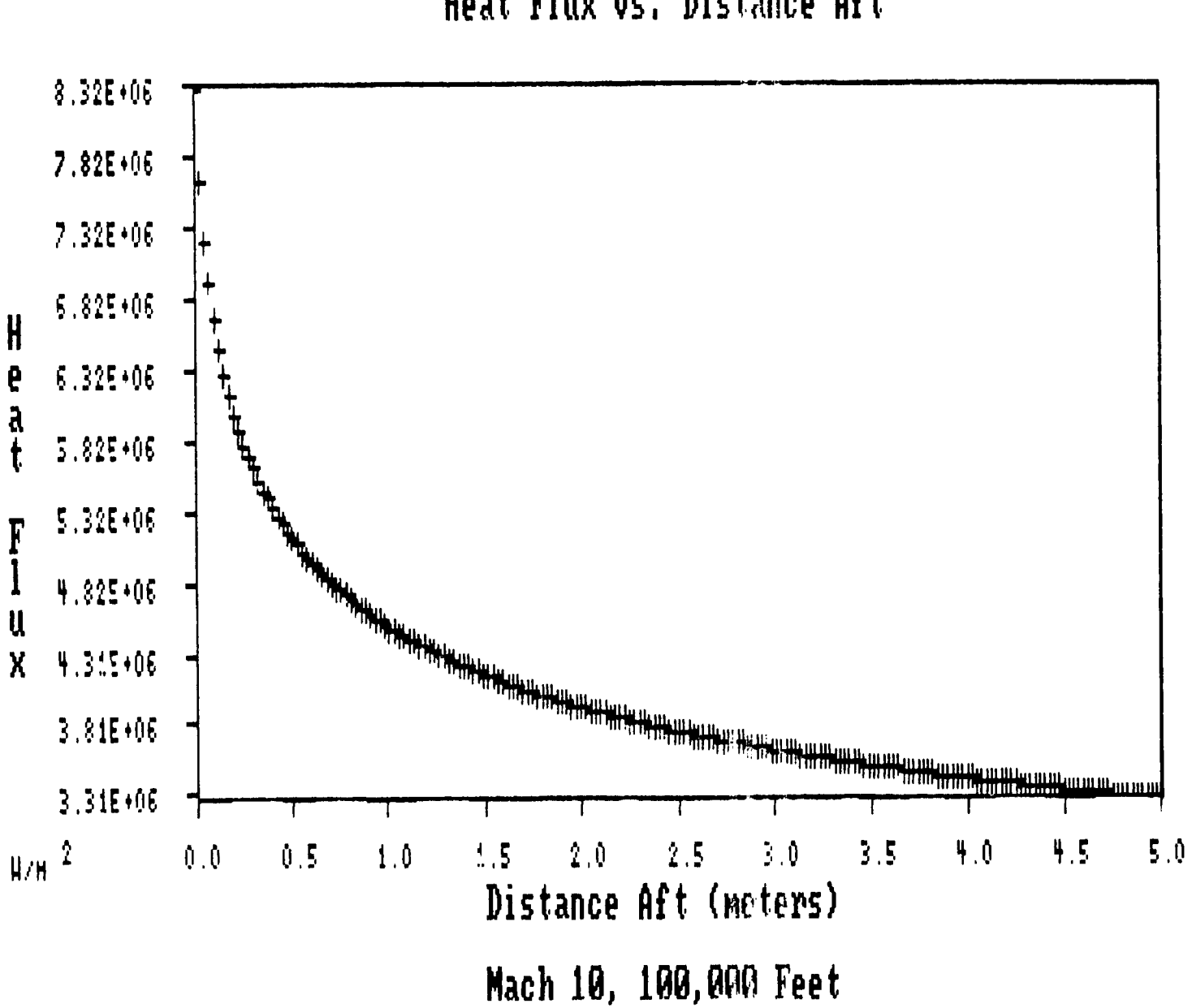
Heat Flux Vs. Distance Aft
8.32E+06
7.82E+06
7.32E+06
6.82E+06
6.32E+06
5.82E+06
5.32E+06
4.82E+06
4.31E+06
3.81E+06
3.31E+06
Heat Flux
W/M 2
0.0
0.5
1.0
1.5
2.0
2.5
3.0
3.5
4.0
4.5
5.0
Distance Aft (meters)
Mach 10, 100,000 Feet

Densi[illegible] of Liquid Hydrogen

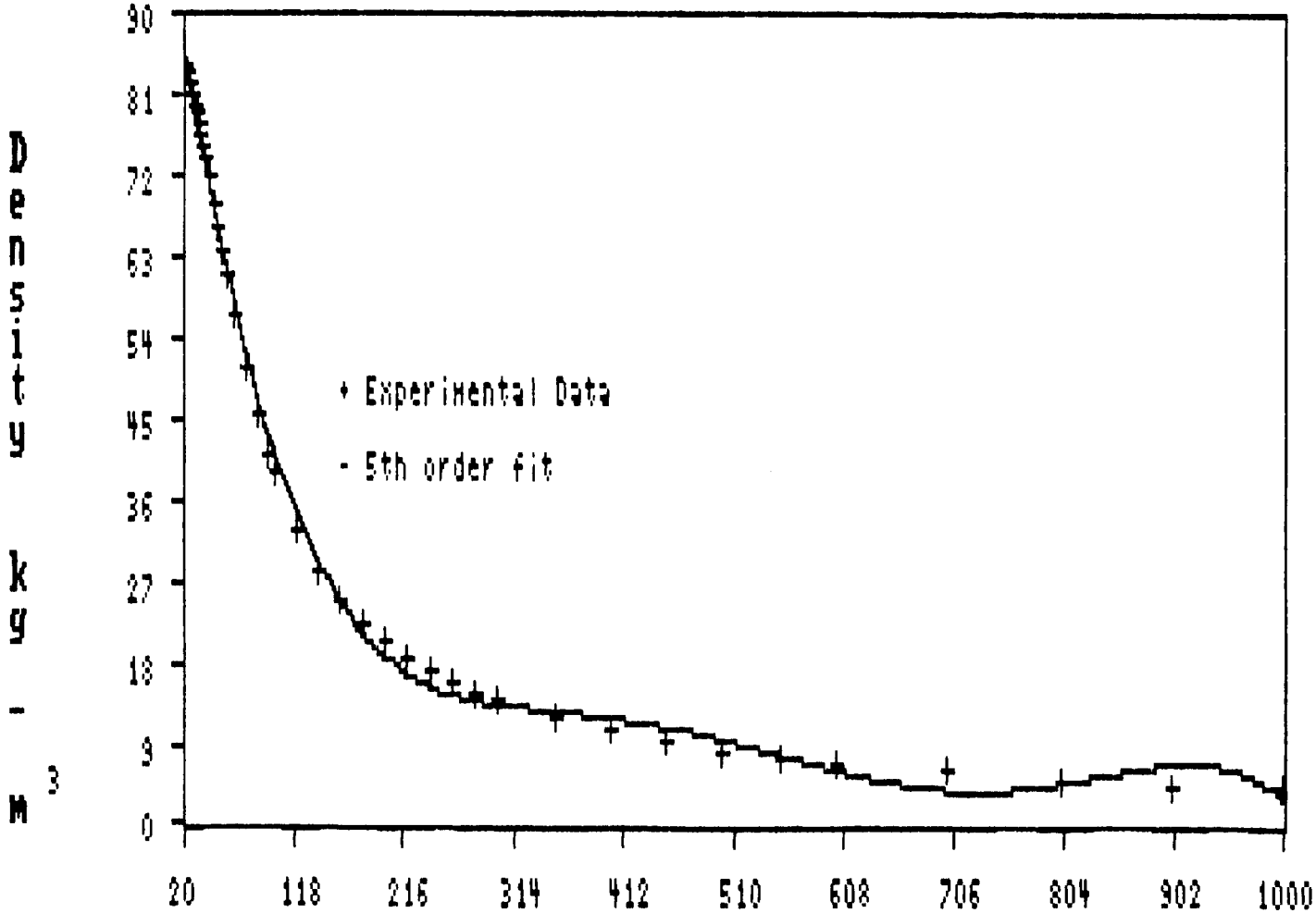

$y = a + bx + cx^2 + dx^3 + ex^4 + fx^5$

a = 1.0374 E+02
b = -0.9265
c = 3.7198 E-03
d = -7.189 E-06
e = 6.5313 E-09
f = -2.235 E-12

Values fit for 20 MPa Isobar

Thermal Conductivity of Liq Hydrogen

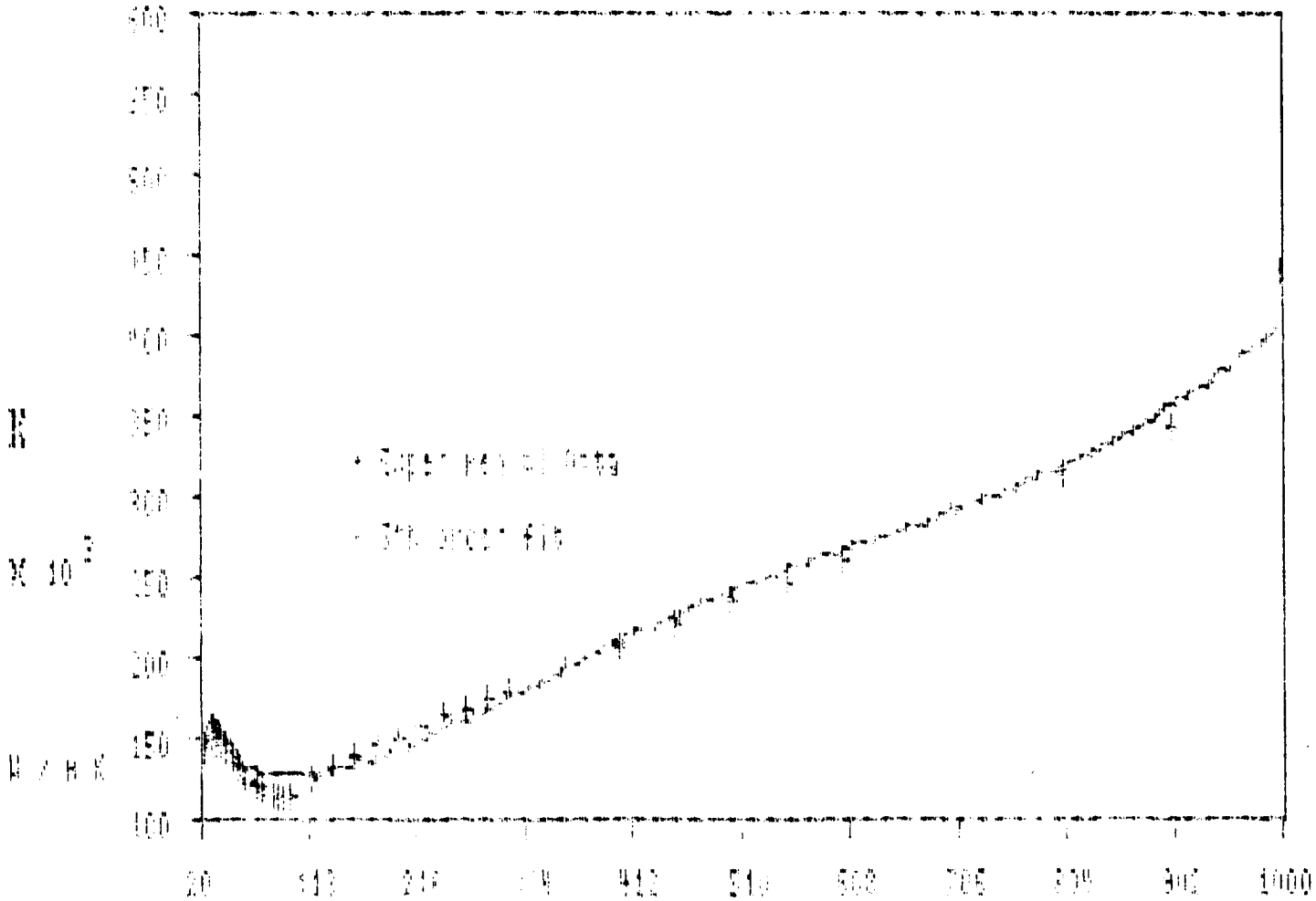

$y = a + bx + cx^2 + dx^3 + ex^4 + fx^5$

a = 1.6030 E+02
b = -0.64379
c = 4.1102E-03
d = -7.679 E-06
e = 6.2779E-09
f = -1.819 E-12 ($K = y * E-03$)

Values fit for 20 MPa Isobar

021

Specific Heat ... Liquid Hydrogen

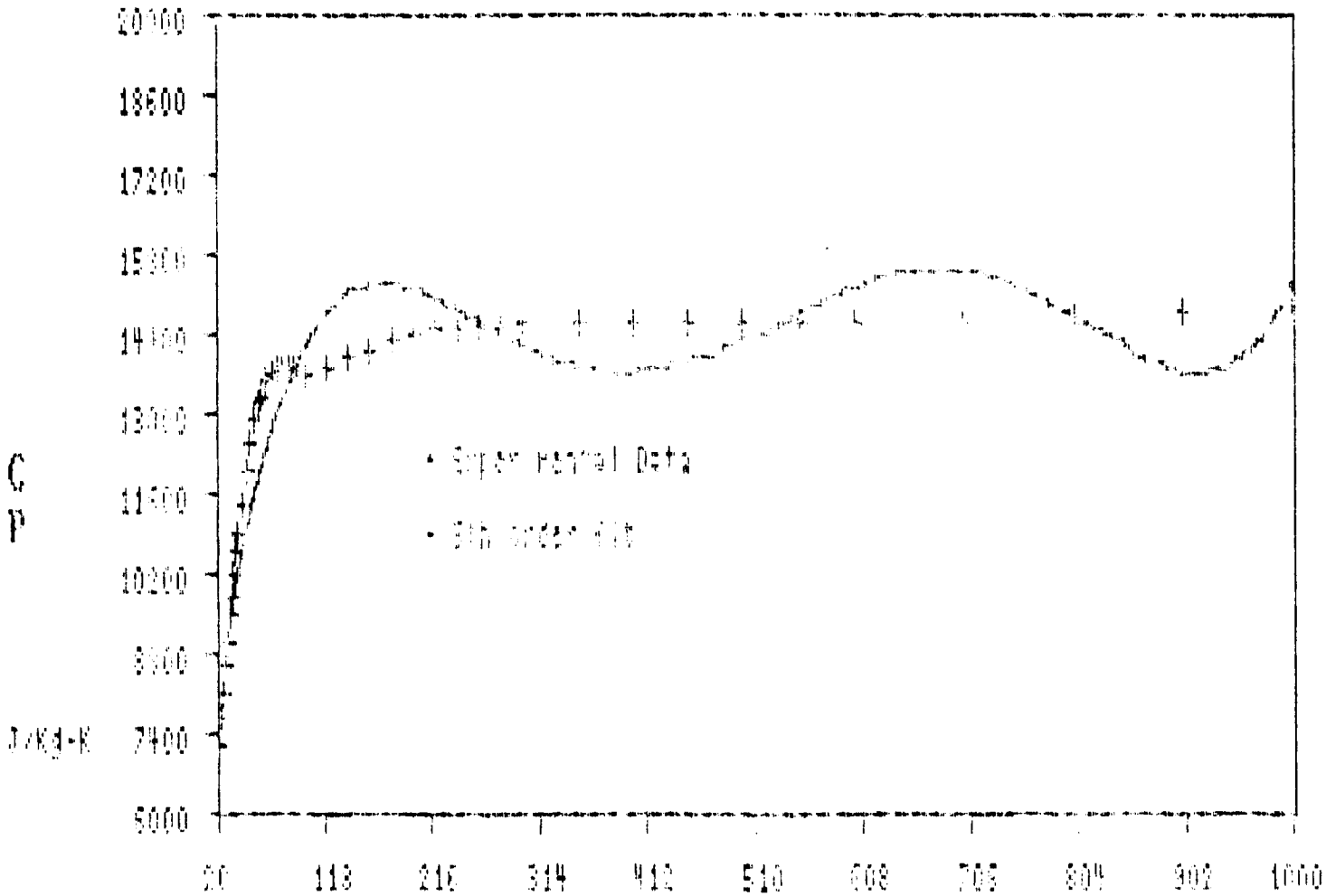

$y = a + bx + cx^2 + dx^3 + ex^4 + fx^5$

a = 5.9055E+03
b = 1.4564E+02
c = -0.78868
d = 1.8103E-03
e = -1.835E-06
f = 6.7750E-10

Values fit for 20 MPa Isobar

ORIGINAL PAGE IS
OF POOR QUALITY

Appendix 3.2: Ethylene Glycol Design

Ethylene Glycol $\dot{m}$=150 kg/s

#	x: [m]	qs: [W/m^2]	t-max: [K]	press: [Pa]	tw: [K]	t0: [K]	tcrit: [K]	Re:
2	0.100	.724E+07	.371E+03	.156E+07	.384E+03	.565E+03	.966E+03	.654E+07
------> branch # 1 <------								
3	0.150	.668E+07	.371E+03	.591E+06	.382E+03	.476E+03	.594E+03	.327E+07
4	0.200	.631E+07	.371E+03	.391E+06	.382E+03	.461E+03	.618E+03	.327E+07
5	0.250	.603E+07	.371E+03	.391E+06	.383E+03	.457E+03	.647E+03	.327E+07
6	0.300	.582E+07	.371E+03	.391E+06	.383E+03	.493E+03	.677E+03	.327E+07
7	0.350	.564E+07	.371E+03	.391E+06	.384E+03	.500E+03	.709E+03	.327E+07
8	0.400	.549E+07	.371E+03	.391E+06	.384E+03	.506E+03	.743E+03	.327E+07
9	0.450	.535E+07	.372E+03	.391E+06	.386E+03	.513E+03	.780E+03	.338E+07
10	0.500	.525E+07	.372E+03	.391E+06	.387E+03	.519E+03	.816E+03	.338E+07
11	0.550	.515E+07	.372E+03	.391E+06	.388E+03	.526E+03	.855E+03	.338E+07
12	0.600	.506E+07	.372E+03	.391E+06	.388E+03	.532E+03	.895E+03	.338E+07
13	0.650	.498E+07	.372E+03	.391E+06	.389E+03	.539E+03	.937E+03	.338E+07
14	0.700	.491E+07	.373E+03	.391E+06	.390E+03	.545E+03	.981E+03	.348E+07
------> branch # 2 <------								
15	0.750	.483E+07	.373E+03	.978E+05	.388E+03	.469E+03	.587E+03	.174E+07
16	0.800	.478E+07	.374E+03	.978E+05	.389E+03	.472E+03	.600E+03	.174E+07
17	0.850	.472E+07	.373E+03	.978E+05	.389E+03	.475E+03	.614E+03	.174E+07
18	0.900	.467E+07	.373E+03	.978E+05	.389E+03	.478E+03	.628E+03	.174E+07
19	0.950	.462E+07	.374E+03	.979E+05	.391E+03	.482E+03	.643E+03	.180E+07
20	1.000	.457E+07	.374E+03	.979E+05	.391E+03	.485E+03	.659E+03	.180E+07
21	1.050	.453E+07	.374E+03	.979E+05	.391E+03	.489E+03	.675E+03	.180E+07
22	1.100	.448E+07	.374E+03	.979E+05	.392E+03	.492E+03	.692E+03	.180E+07
23	1.150	.445E+07	.375E+03	.979E+05	.394E+03	.496E+03	.709E+03	.186E+07
24	1.200	.441E+07	.375E+03	.979E+05	.394E+03	.499E+03	.726E+03	.186E+07
25	1.250	.437E+07	.375E+03	.979E+05	.394E+03	.503E+03	.736E+03	.186E+07
26	1.300	.434E+07	.375E+03	.979E+05	.395E+03	.505E+03	.752E+03	.186E+07
27	1.350	.430E+07	.377E+03	.980E+05	.396E+03	.509E+03	.771E+03	.193E+07
28	1.400	.427E+07	.377E+03	.981E+05	.396E+03	.511E+03	.787E+03	.193E+07
29	1.450	.424E+07	.377E+03	.980E+05	.396E+03	.514E+03	.805E+03	.193E+07
30	1.500	.422E+07	.377E+03	.980E+05	.397E+03	.516E+03	.823E+03	.193E+07
31	1.550	.419E+07	.378E+03	.980E+05	.398E+03	.521E+03	.842E+03	.201E+07
32	1.600	.416E+07	.378E+03	.980E+05	.398E+03	.524E+03	.860E+03	.201E+07
33	1.650	.414E+07	.378E+03	.980E+05	.398E+03	.527E+03	.878E+03	.201E+07
34	1.700	.411E+07	.379E+03	.981E+05	.400E+03	.531E+03	.899E+03	.208E+07
35	1.750	.409E+07	.379E+03	.981E+05	.400E+03	.533E+03	.916E+03	.208E+07
36	1.800	.406E+07	.379E+03	.981E+05	.400E+03	.536E+03	.934E+03	.208E+07
37	1.850	.404E+07	.380E+03	.981E+05	.402E+03	.540E+03	.958E+03	.215E+07
------> branch # 3 <------								
38	1.900	.402E+07	.380E+03	.245E+05	.399E+03	.470E+03	.579E+03	.108E+07
39	1.950	.400E+07	.380E+03	.245E+05	.399E+03	.471E+03	.584E+03	.108E+07
40	2.000	.398E+07	.381E+03	.245E+05	.401E+03	.474E+03	.592E+03	.112E+07
41	2.050	.396E+07	.381E+03	.245E+05	.401E+03	.475E+03	.597E+03	.112E+07
42	2.100	.394E+07	.381E+03	.245E+05	.401E+03	.476E+03	.603E+03	.112E+07
43	2.150	.392E+07	.382E+03	.246E+05	.402E+03	.479E+03	.611E+03	.116E+07
44	2.200	.390E+07	.383E+03	.246E+05	.402E+03	.480E+03	.617E+03	.116E+07
45	2.250	.389E+07	.383E+03	.246E+05	.402E+03	.481E+03	.623E+03	.116E+07
46	2.300	.387E+07	.384E+03	.246E+05	.404E+03	.484E+03	.631E+03	.121E+07
47	2.350	.385E+07	.384E+03	.246E+05	.404E+03	.485E+03	.637E+03	.121E+07
48	2.400	.384E+07	.384E+03	.246E+05	.404E+03	.486E+03	.643E+03	.121E+07
49	2.450	.382E+07	.385E+03	.246E+05	.406E+03	.489E+03	.651E+03	.126E+07
50	2.500	.381E+07	.385E+03	.246E+05	.406E+03	.490E+03	.658E+03	.126E+07
51	2.550	.379E+07	.385E+03	.246E+05	.406E+03	.492E+03	.664E+03	.126E+07

54	2.700	.375E+07	.388E+03	.246E+05	.407E+03	.497E+03	.686E+03	.135E+07
55	2.750	.373E+07	.388E+03	.246E+05	.409E+03	.499E+03	.694E+03	.135E+07
56	2.800	.372E+07	.389E+03	.246E+05	.408E+03	.500E+03	.701E+03	.140E+07
57	2.850	.371E+07	.389E+03	.246E+05	.409E+03	.502E+03	.709E+03	.140E+07
58	2.900	.369E+07	.390E+03	.246E+05	.409E+03	.504E+03	.716E+03	.144E+07
59	2.950	.368E+07	.390E+03	.246E+05	.411E+03	.506E+03	.724E+03	.144E+07
60	3.000	.367E+07	.391E+03	.246E+05	.411E+03	.507E+03	.731E+03	.149E+07
61	3.050	.366E+07	.391E+03	.246E+05	.412E+03	.509E+03	.740E+03	.149E+07
62	3.100	.365E+07	.392E+03	.247E+05	.412E+03	.510E+03	.747E+03	.154E+07
63	3.150	.363E+07	.392E+03	.247E+05	.413E+03	.512E+03	.755E+03	.154E+07
64	3.200	.362E+07	.393E+03	.247E+05	.413E+03	.514E+03	.763E+03	.159E+07
65	3.250	.361E+07	.393E+03	.247E+05	.414E+03	.516E+03	.771E+03	.159E+07
66	3.300	.360E+07	.394E+03	.247E+05	.414E+03	.517E+03	.779E+03	.165E+07
67	3.350	.359E+07	.394E+03	.247E+05	.415E+03	.519E+03	.788E+03	.165E+07
68	3.400	.358E+07	.395E+03	.247E+05	.415E+03	.520E+03	.795E+03	.171E+07
69	3.450	.357E+07	.395E+03	.247E+05	.416E+03	.522E+03	.804E+03	.171E+07
70	3.500	.356E+07	.396E+03	.247E+05	.416E+03	.523E+03	.812E+03	.177E+07
71	3.550	.355E+07	.397E+03	.247E+05	.417E+03	.526E+03	.821E+03	.177E+07
72	3.600	.354E+07	.398E+03	.247E+05	.417E+03	.527E+03	.829E+03	.184E+07
73	3.650	.353E+07	.398E+03	.247E+05	.418E+03	.529E+03	.838E+03	.184E+07
74	3.700	.352E+07	.399E+03	.247E+05	.418E+03	.530E+03	.846E+03	.191E+07
75	3.750	.351E+07	.399E+03	.247E+05	.419E+03	.532E+03	.856E+03	.191E+07
76	3.800	.350E+07	.400E+03	.247E+05	.419E+03	.533E+03	.864E+03	.198E+07
77	3.850	.349E+07	.400E+03	.247E+05	.420E+03	.535E+03	.873E+03	.198E+07
78	3.900	.348E+07	.402E+03	.248E+05	.420E+03	.536E+03	.882E+03	.206E+07
79	3.950	.347E+07	.402E+03	.248E+05	.421E+03	.537E+03	.891E+03	.206E+07
80	4.000	.346E+07	.403E+03	.248E+05	.421E+03	.540E+03	.900E+03	.214E+07
81	4.050	.345E+07	.403E+03	.248E+05	.422E+03	.542E+03	.909E+03	.214E+07
82	4.100	.344E+07	.404E+03	.248E+05	.422E+03	.543E+03	.918E+03	.223E+07
83	4.150	.343E+07	.404E+03	.248E+05	.423E+03	.545E+03	.928E+03	.223E+07
84	4.200	.342E+07	.405E+03	.249E+05	.423E+03	.546E+03	.937E+03	.233E+07
85	4.250	.341E+07	.405E+03	.249E+05	.424E+03	.548E+03	.947E+03	.233E+07
86	4.300	.340E+07	.406E+03	.249E+05	.424E+03	.549E+03	.956E+03	.243E+07

87	4.350	.339E+07	.407E+03	.620E+04	.425E+03	.486E+03	.590E+03	.121E+07
88	4.400	.338E+07	.407E+03	.621E+04	.424E+03	.488E+03	.593E+03	.127E+07
89	4.450	.338E+07	.408E+03	.621E+04	.424E+03	.488E+03	.596E+03	.127E+07
90	4.500	.337E+07	.410E+03	.621E+04	.425E+03	.490E+03	.600E+03	.132E+07
91	4.550	.336E+07	.410E+03	.621E+04	.425E+03	.491E+03	.603E+03	.132E+07
92	4.600	.335E+07	.411E+03	.621E+04	.427E+03	.492E+03	.606E+03	.138E+07
93	4.650	.334E+07	.412E+03	.621E+04	.427E+03	.493E+03	.609E+03	.138E+07
94	4.700	.333E+07	.413E+03	.622E+04	.428E+03	.495E+03	.613E+03	.144E+07
95	4.750	.332E+07	.413E+03	.622E+04	.428E+03	.495E+03	.615E+03	.144E+07
96	4.800	.331E+07	.415E+03	.622E+04	.429E+03	.497E+03	.619E+03	.151E+07
97	4.850	.330E+07	.415E+03	.622E+04	.429E+03	.497E+03	.622E+03	.151E+07
98	4.900	.330E+07	.416E+03	.622E+04	.430E+03	.499E+03	.626E+03	.158E+07
99	4.950	.329E+07	.416E+03	.622E+04	.430E+03	.501E+03	.628E+03	.158E+07
100	5.000	.328E+07	.418E+03	.623E+04	.432E+03	.502E+03	.632E+03	.166E+07

ORIGINAL PAGE IS OF POOR QUALITY

Results and initial parameters:

Coolant considered: Water/glycol solution (50%)

Temperature exiting manifold	= 0.3708E+03 [K]
Final exiting temperature	= 0.4181E+03 [K]
System pressure loss	= 0.9805E+07 [Pa] 0.1422E+04 [psi] 96.75 a
Initial number of tubes	= 80
Tube diameter	= 6.50 [mm]
Tube thickness	= 0.70 [mm]
Nose radius	= 25.4 [mm]
Wall thickness	= 2.5 [mm]
Cone half angle	= 5.0 [deg]
Nozzle mass flow rate	= 150.0000 [kg/s]
Velocity of coolant in nozzle	= 953.126 [m/s]
Outlet tube mass flow rate	= 0.4687 [kg/s]
Outlet vel of coolant in tubes	= 224.686 [m/s]
Impingement target distance	= 25.4 [mm]
Impingement nozzle diameter	= 14.12 [mm]
Number of branches	= 4
Limiting material temperature	= 1000. [K]

Appendix 4: Hydrogen properties

Table 4.12 (continued)
THERMODYNAMIC PROPERTIES OF NORMAL HYDROGEN

20.68 MPA ISOBAR

TEMPERATURE DEG. K	VOLUME CU M/KG	ISOTHERM DERIVATIVE CU M-MPA/KG	ISOCHORE DERIVATIVE MPA/K	INTERNAL ENERGY KJ/KG-K	ENTHALPY KJ/KG	ENTROPY KJ/KG-K	CV KJ / KG-K	CP	VELOCITY OF SOUND M/S
* 19.368	0.01169	2.2344	1.894	236.2	470.8	14.482	5.38	6.88	1668
20	0.01173	2.2848	1.894	239.7	474.4	14.786	5.47	6.97	1675
21	0.01180	2.1564	1.893	245.4	481.5	15.054	5.68	7.22	1667
22	0.01187	2.1087	1.890	251.3	488.6	15.396	5.72	7.47	1659
23	0.01195	2.0611	1.887	257.4	496.4	15.734	5.83	7.71	1651
24	0.01203	2.0136	1.882	263.7	504.2	16.068	5.93	7.95	1642
25	0.01210	1.9664	1.875	270.2	512.3	16.397	6.03	8.18	1634
26	0.01219	1.9195	1.868	276.9	520.6	16.728	6.11	8.41	1625
27	0.01227	1.8731	1.860	283.8	529.1	17.062	6.20	8.63	1615
28	0.01236	1.8274	1.851	290.8	537.9	17.359	6.28	8.86	1606
29	0.01245	1.7797	1.844	298.8	546.9	17.675	6.35	9.10	1597
30	0.01254	1.7369	1.832	305.3	556.1	17.987	6.41	9.30	1588
31	0.01263	1.6937	1.819	312.8	565.5	18.295	6.47	9.51	1577
32	0.01273	1.6468	1.806	320.5	575.1	18.606	6.53	9.71	1566
33	0.01283	1.6088	0.9921	328.3	584.9	18.902	6.58	9.90	1556
34	0.01293	1.5685	0.9777	336.2	594.9	19.201	6.63	10.09	1546
35	0.01304	1.5277	0.9636	344.3	605.1	19.496	6.67	10.28	1535
36	0.01315	1.4861	0.9483	352.5	615.4	19.789	6.71	10.46	1523
37	0.01326	1.4494	0.9331	360.8	626.0	20.078	6.75	10.66	1513
38	0.01337	1.4146	0.9177	369.3	636.8	20.365	6.78	10.82	1503
39	0.01349	1.3793	0.9019	377.8	647.7	20.648	6.80	10.99	1493
40	0.01361	1.3444	0.8859	386.5	658.7	20.928	6.82	11.15	1482
42	0.01386	1.2803	0.8533	404.1	681.3	21.479	6.85	11.44	1462
44	0.01412	1.2218	0.8206	422.0	704.5	22.018	6.89	11.73	1442
46	0.01440	1.1649	0.7880	439.8	727.7	22.534	6.95	12.03	1428
48	0.01468	1.1145	0.7558	458.4	752.1	23.051	6.99	12.38	1408
50	0.01498	1.0671	0.7242	477.2	776.9	23.558	7.03	12.54	1388
52	0.01529	1.0229	0.6935	496.3	802.2	24.055	7.05	12.77	1361
54	0.01562	0.9819	0.6636	515.6	828.0	24.541	7.07	12.98	1342
56	0.01595	0.9463	0.6346	535.3	854.3	25.021	7.08	13.15	1325
58	0.01630	0.9139	0.6067	554.8	880.8	25.486	7.08	13.29	1318
60	0.01666	0.8863	0.5803	574.3	907.5	25.938	7.07	13.48	1296
65	0.01760	0.8298	0.5197	623.1	975.1	27.018	7.07	13.62	1265
70	0.01868	0.7893	0.4671	671.6	1043.6	28.034	7.07	13.76	1239
75	0.01964	0.7626	0.4216	719.7	1112.6	28.987	7.09	13.84	1228
80	0.02073	0.7461	0.3823	767.3	1181.9	29.881	7.13	13.87	1208
85	0.02184	0.7398	0.3486	814.4	1251.1	30.721	7.20	13.85	1193
90	0.02297	0.7396	0.3195	860.9	1320.3	31.513	7.28	13.83	1186
95	0.02412	0.7444	0.2943	907.1	1389.4	32.268	7.37	13.88	1181
100	0.02527	0.7532	0.2725	953.0	1458.3	32.966	7.48	13.77	1178
120	0.02990	0.8101	0.2896	1138.8	1735.9	35.496	8.06	13.88	1181
140	0.03451	0.8842	0.1702	1324.5	2014.7	37.645	8.57	14.03	1283
160	0.03906	0.9669	0.1432	1515.4	2296.6	39.525	9.01	14.19	1234
180	0.04355	1.0521	0.1235	1710.5	2581.4	41.203	9.37	14.32	1268
200	0.04796	1.1390	0.1087	1908.4	2868.7	42.717	9.66	14.43	1304
220	0.05233	1.2245	0.0978	2111.4	3157.9	44.095	9.88	14.51	1341
240	0.05664	1.3105	0.0896	2315.6	3448.5	45.359	10.05	14.56	1378
260	0.06091	1.3950	0.0830	2521.6	3739.8	46.526	10.17	14.59	1415
280	0.06514	1.4793	0.0775	2728.6	4031.5	47.606	10.26	14.68	1451
300	0.06951	1.5696	0.0686	2939.8	4329.2	48.624	10.33	14.78	1495
350	0.08005	1.7808	0.0583	3463.2	5064.3	50.892	10.41	14.69	1585
400	0.09053	1.9889	0.0507	3987.9	5790.4	52.852	10.43	14.67	1672
450	0.10095	2.1960	0.0449	4512.2	6531.3	54.578	10.44	14.64	1755
500	0.11135	2.4040	0.0403	5035.9	7262.8	56.119	10.44	14.62	1835
550	0.12172	2.6108	0.0365	5559.1	7993.5	57.512	10.45	14.61	1911
600	0.13208	2.8173	0.0334	6082.8	8724.3	58.781	10.46	14.61	1984
700	0.15277	3.2299	0.0286	7131.7	10187.8	61.039	10.51	14.65	2122
800	0.17343	3.6420	0.0250	8187.1	11655.7	63.042	10.59	14.72	2256
900	0.19408	4.0541	0.0222	9252.5	13134.8	64.741	10.71	14.84	2378
1000	0.21472	4.4660	0.0200	10331.0	14625.4	66.310	10.87	15.00	2482
1200	0.25599	5.2899	0.0167	12543.3	17663.8	69.060	11.25	15.37	2669
1400	0.29724	6.1139	0.0143	14837.2	20782.8	71.478	11.68	15.88	2826
1600	0.33849	6.9388	0.0125	17216.3	23986.1	73.616	12.12	16.24	2949
1800	0.37974	7.7622	0.0111	19680.9	27275.7	75.547	12.55	16.67	3211
2000	0.42100	8.5865	0.0100	22232.7	30652.7	77.337	12.97	17.18	3364
2500	0.52456	10.6475	0.0080	29048.8	39548.8	81.283	14.48	18.69	3706
3000	0.63076	12.7087	0.0067	37055.1	49670.3	84.983	17.77	22.33	3996

* TWO-PHASE BOUNDARY

Table 4.12 (continued)

THERMODYNAMIC PROPERTIES OF NORMAL HYDROGEN

90 MPA ISOBAR

TEMPERATURE DEG. K	DENSITY KG/CU M	V(DH/DU)$_P$ KJ/KG	V(DP/DU)$_V$ MPA-CU M/KJ X 10^2	-V(DP/DV)$_T$ MPA	(DV/DT)/V 1/DEG. K	THERMAL CONDUCTIVITY W/K-M X 10^3	VISCOSITY KG/M-S X 10^7	THERMAL DIFFUSIVITY SQ M/HR	DIELECTRIC CONSTANT	PRANDTL NUMBER
* 19.368	85.9433	1188.4	0.23748	191.1415	0.00572	130.46	377.62	0.00001	1.20181	1.9648
20	85.2277	1196.5	0.23652	187.8418	0.00582	133.83	353.32	0.00001	1.20064	1.8393
21	84.7262	1207.5	0.23521	182.7804	0.00590	139.12	321.84	0.00002	1.27889	1.6666
22	84.2142	1216.9	0.22624	177.5827	0.00614	143.52	294.22	0.00002	1.27786	1.5318
23	83.6821	1224.6	0.22258	172.4978	0.00638	147.16	271.67	0.00002	1.27520	1.4241
24	83.1599	1231.8	0.21916	167.4527	0.00646	150.15	252.58	0.00002	1.27331	1.3378
25	82.6479	1236.8	0.21594	162.4598	0.00662	152.56	236.83	0.00001	1.27138	1.2657
26	82.0662	1240.2	0.21286	157.5209	0.00678	154.47	221.76	0.00001	1.26942	1.2072
27	81.5054	1243.8	0.20984	152.6787	0.00694	155.94	209.29	0.00000	1.26743	1.1589
28	80.9546	1246.6	0.20687	147.8964	0.00710	157.06	198.32	0.00079	1.26541	1.1185
29	80.3861	1246.2	0.20469	142.9994	0.00738	157.84	188.54	0.00078	1.26334	1.0864
30	79.7683	1246.6	0.20186	138.5345	0.00745	158.37	179.85	0.00077	1.26125	1.0564
31	79.1617	1250.3	0.19908	134.0749	0.00760	158.67	172.05	0.00076	1.25914	1.0347
32	78.5658	1249.8	0.19628	129.4586	0.00777	157.59	165.02	0.00074	1.25700	1.0171
33	77.9419	1251.6	0.19346	125.0936	0.00791	156.98	158.65	0.00073	1.25483	1.0008
34	77.3228	1251.9	0.19062	121.2015	0.00806	156.38	152.86	0.00072	1.25265	0.9870
35	76.6946	1251.8	0.18826	117.1683	0.00822	155.51	147.55	0.00071	1.25044	0.9756
36	76.0619	1248.7	0.18579	113.0376	0.00839	154.64	142.68	0.00070	1.24822	0.9666
37	75.4195	1248.2	0.18338	109.3153	0.00854	153.68	138.17	0.00069	1.24597	0.9579
38	74.7739	1247.5	0.18109	105.7719	0.00868	152.68	134.08	0.00068	1.24370	0.9508
39	74.1217	1245.4	0.17893	102.2326	0.00882	151.62	130.13	0.00067	1.24142	0.9438
40	73.4653	1242.7	0.17682	98.7645	0.00897	150.52	126.52	0.00066	1.23912	0.9369
42	72.1398	1236.5	0.17261	92.3572	0.00924	148.28	119.99	0.00065	1.23450	0.9266
44	70.8011	1235.4	0.16832	86.4468	0.00949	145.81	114.23	0.00063	1.22984	0.9186
46	69.4518	1235.3	0.16338	80.9877	0.00974	143.42	109.10	0.00062	1.22515	0.9152
48	68.0978	1234.6	0.15876	75.8978	0.00996	141.05	104.58	0.00061	1.22045	0.9118
50	66.7399	1233.4	0.15447	71.2196	0.01017	138.73	100.35	0.00060	1.21576	0.9073
52	65.3829	1231.7	0.15049	66.8821	0.01037	136.48	96.59	0.00059	1.21109	0.9039
54	64.0286	1229.6	0.14656	62.8668	0.01056	134.31	93.17	0.00058	1.20643	0.9004
56	62.6829	1228.9	0.14295	59.3154	0.01078	132.23	90.06	0.00058	1.20181	0.8954
58	61.3466	1227.7	0.13971	56.0628	0.01082	130.25	87.22	0.00058	1.19724	0.8897
60	60.0202	1226.7	0.13665	53.2057	0.01091	128.55	84.63	0.00058	1.19274	0.8823
65	56.8213	1235.9	0.12944	47.1405	0.01102	125.23	79.15	0.00058	1.18185	0.8688
70	53.7734	1250.6	0.12286	42.4454	0.01100	122.23	74.67	0.00059	1.17155	0.8438
75	50.8183	1274.2	0.11675	38.8224	0.01086	119.46	71.57	0.00061	1.16194	0.8291
80	48.2479	1305.7	0.11107	36.0881	0.01062	116.91	69.88	0.00063	1.15305	0.8194
85	45.7912	1346.4	0.10578	33.8776	0.01029	116.51	67.25	0.00066	1.14488	0.7996
	43.5352	1393.9	0.10084	32.2081	0.00992	116.11	65.95	0.00069	1.13742	0.7855
	41.4668	1447.1	0.09632	30.8672	0.00953	115.78	64.87	0.00073	1.13061	0.7755
	39.5742	1506.3	0.09212	29.8888	0.00914	116.07	64.04	0.00077	1.12448	0.7546
	33.4477	1793.6	0.07778	27.8944	0.00774	127.13	68.24	0.00099	1.10447	0.7447
140	28.9793	2112.2	0.06855	25.6237	0.00664	134.29	70.44	0.00119	1.09088	0.7359
160	25.6815	2452.6	0.06207	24.7531	0.00578	140.53	72.14	0.00139	1.07938	0.7282
180	22.9647	2801.5	0.05735	24.1615	0.00511	146.57	73.83	0.00160	1.07093	0.7215
200	20.6486	3153.1	0.05396	23.7458	0.00458	152.56	75.64	0.00183	1.06425	0.7154
220	19.1188	3508.9	0.05136	23.4818	0.00415	158.55	77.58	0.00206	1.05878	0.7101
240	17.6549	3864.4	0.04940	23.1363	0.00379	164.46	79.64	0.00230	1.05422	0.7052
260	16.4175	4178.8	0.04788	22.9819	0.00349	170.28	81.79	0.00256	1.05035	0.7009
280	15.3589	4588.9	0.04669	22.7879	0.00324	176.82	84.83	0.00283	1.04703	0.6968
300	14.3862	4823.8	0.04633	22.5803	0.00305	181.67	86.33	0.00309	1.04403	0.6906
350	12.4914	5688.9	0.04488	22.2353	0.00262	195.58	92.27	0.00363	1.03815	0.6836
400	11.0468	6356.5	0.04468	21.9788	0.00231	209.87	98.38	0.00465	1.03368	0.6902
450	9.9858	7099.3	0.04361	21.7611	0.00206	222.51	104.97	0.00592	1.03017	0.6879
500	9.0811	7840.9	0.04294	21.5987	0.00186	236.81	110.78	0.00647	1.02732	0.6864
550	8.2157	8579.4	0.04256	21.4496	0.00170	249.46	116.98	0.00748	1.02497	0.6852
600	7.5713	9322.1	0.04223	21.3309	0.00157	262.92	123.15	0.00855	1.02308	0.6845
700	6.4468	10823.3	0.04168	21.1426	0.00135	289.96	135.33	0.01089	1.01986	0.6836
800	5.7568	12362.2	0.04096	21.0882	0.00119	317.33	147.27	0.01346	1.01748	0.6833
900	5.1525	13953.4	0.04025	20.8686	0.00106	345.23	158.95	0.01625	1.01561	0.6834
1000	4.6572	15605.7	0.03948	20.7994	0.00096	448.56	170.38	0.02270	1.01418	0.6881
1200	3.9065	19075.7	0.03789	20.6651	0.00081	511.88	192.51	0.03063	1.01182	0.6791
1400	3.3643	22776.3	0.03631	20.5698	0.00069	583.17	213.76	0.03948	1.01017	0.6793
1600	2.9548	26662.8	0.03487	20.4971	0.00061	656.24	234.24	0.04923	1.00893	0.6798
1800	2.6334	30691.6	0.03360	20.4489	0.00054	729.67	254.05	0.05986	1.00796	0.6802
2000	2.3753	34905.7	0.03243	20.3953	0.00049	686.38	273.27	0.07147	1.00717	0.6799
2500	1.9064	47448.9	0.02995	20.2979	0.00039	1056.83	319.24	0.10648	1.00576	0.6645
3000	1.5894	67546.4	0.02365	20.1484	0.00033	1571.85	363.54	0.15972	1.00478	0.5160

* TWO-PHASE BOUNDARY

Appendix 5: Hypersonic Cruise Vehicle Configuration

Appendix 5:

Hypersonic Cruise Vehicle (HCV) Configuration (written by Lura Kern)

It was determined early in Winter Quarter 1988 that the Advanced Aeronautics Design Group (AAD) needed a unifying concept for the design of the hypersonic drone. This was accomplished by choosing a configuration that had been researched extensively at NASA Langley Research Center in the late 1970's. The advantage of a single tested configuration for the entire class is clear: each group would base their designs on the same vehicle, with the same restrictions applying to all three groups, thereby forcing greater interaction among the groups.

The configuration chosen by the AAD students was a 70 degree swept delta wing design conceived by NASA Langley engineers. It was a hypersonic research airplane concept, and has been dubbed the Hypersonic Cruise Vehicle (HCV) by the AAD students. Figure 1 shows the HCV as it was originally conceived. The HCV was designed to be air-launched from a B-52 at Mach 0.8 and rocket-accelerated up to a cruise speed of Mach 7 by four liquid hydrogen rocket motors mounted in the base. At this point, the scramjets would be ignited and the vehicle would cruise until burn-out, at which point it would return to base for an unpowered landing. A detailed description of the HCV's configuration is given in Figure 2. In developing the HCV design, a wind tunnel model was built, and performance characteristics of the model were collected and tabulated in Reference 1. The geometric characteristics of the model are tabulated in Table 1. The scaling for the model was 0.021 of the size conceived for the actual HCV.

The first step in adapting the HCV for the purpose of a hypersonic drone was to size it according to the needs of the class. This included calculating the amount of fuel required to go from the air-launch speed to cruise speed. From that, size and weight necessary for the fuel requirements were determined . In order to do this, it became necessary to determine a means of air-launch. The B-52 has size and weight constraints consisting of a 24-ft. wing span limit, a 9-foot fuselage

height limit, and a gross weight restriction of 70,000 pounds. This limits the size of the drone considerably and, in order to reach Mach 10, it was found that the weight limit was exceeded. Alternatives were then examined. The 747 and B-1 aircraft were determined to be viable options for the air-launch.

Therefore, the HCV is a basis upon which each group can build their design. It gives the Flight Systems group the geometry and spacing of the vehicle so that they can determine which sensors and how many are required in certain places. This would result in a more detailed and more exact design. The Thermal Management group can determine critical areas on the HCV that would require cooling. They can change the design within certain reasonable limits to satisfy their cooling system design. A definite configuration for the the drone gives the Propulsion group a starting point on the design of the underbelly for the vehicle; that is, a first iteration could be performed from which they refined their design to achieve an optimum configuration.

FLIGHT SYSTEMS GROUP

Group Members:
Alan Beck
Erik Berg
Aileen H. Honka
Mike Tsirulnikov
Eugene Wang
S. Willet
Ching Yu

Faculty Advisor:
Professor N. Levan

Introduction

Composing one third of the UCLA AAD program is the Flight Systems Group. The purpose of this group is to design, find, and adapt the necessary sensors and determine methods of integrating these sensors with the structure of the proposed drone envisioned by the class. The sensors to be designed are to complement the unique needs of the Propulsion and Thermal Management Groups.

The hypersonic flight regime in which the drone is designed to be flown and tested makes the design of the vehicle and its systems particularly challenging. The extremely high speed environment will lead to a host of problems, including high temperatures, pressures, and static and dynamic loads. From the viewpoint of sensor systems, many of the classic methods are inadequate in this region. For example, because of the huge heat fluxes, external probes are not usually feasible. Instead, non-intrusive methods need to be examined.

The parameters to be measured that were studied by the group were determined by the needs of the other two groups. These include temperature, pressure, flow constituents and concentrations, velocity, and skin friction. Sensors were designed from such diverse fields as quantum electronics, semiconductors, and fiber optics. The sensors researched originated from a variety of environments, from medical laboratories, to experimental laboratories, and our own class members.

This report will now detail the various sensors researched, developed, and adapted by the Flight Systems Group for the hypersonic drone design. The report begins with the very flexible and powerful sensor system called CARS. Next are two conceptual designs for shock-wave and pressure sensors, followed by a fiber optic pressure sensor. A hydrogen-concentration sensor realized using a modified semiconductor device, and a device using a sapphire diaphragm. The final sensor detailed is a laboratory sensor for measuring skin friction such as that encountered in the combustor of the scramjet.

Coherent Anti-Stokes Raman Spectroscopy

Coherent Anti-Stokes spectroscopy, or CARS, is a laser technique which is capable of measuring velocity, temperature, and constituents of gaseous flow. This is done by measuring the returning characteristics of emitted laser light from the molecules.

The range of these parameters (velocity, temperature, pressure, and species concentration) vary under specific conditions. Available data reveal as follows:

A. Temperature and Pressure (in N2 gas)

In N2 gas, measurement error is estimated to be less than 1.5% in time-averaged measurements, and from 3% to 6% for instantaneous measurements, over a wide range of temperature and pressure.

B. Species Concentration

Species concentration sensitivity is greater than 1% to 5%, over a limited range of concentration (0.5% to 20.% depending upon the species). Usually, this is sufficient for practical combustion systems.

C. Velocity

Velocity of a flow constituent, or species, is determined from the Doppler shift of the returning beam, and hence, is subject to the limitations in range of detection possible for this type of frequency shift, if any.

D. Pressure

Though pressure is probably better dealt with using Inverse Raman Spectroscopy (IRS), a CARS system may be capable of measuring variations of pressure in a flow.

The accuracy of the CARS measurements depends largely on the prevailing conditions, the type of CARS used, and the method of processing the CARS data. However, good accuracy of readings under conditions of interest to the Flight Systems Group have been obtained:

"The velocity in a supersonic jet flow has been measured using Continuous Wave CARS and agrees to within 4 percent of the calculated value." (ref. 8).

The dimensions of the CARS apparatus, i.e. its size and weight, depend upon the type of laser used, as well as the geometry of the optics technique used to generate and process the CARS signal. The laser can be made fairly small, thus, it would not have as much influence on the size of the CARS set-up as the rest of the apparatus. A reasonable estimate for the area of the entire set-up 3 ft by 2.5 ft. The entire system size does not seem to be a rigid factor, however, since laser technology is moving toward smaller, and smaller, optical equipment.

The weight should not be more than a few pounds for the laser, and a little more for the optics that direct the beam, excluding any anti-vibrational equipment necessary for the implementation of any sort of laser measurement system on board the drone.

Power consumption (excluding the computer analysis power drain) would depend upon the number and type of lasers used. The supersonic jet flow measurements mentioned previously were taken with a 100 mW laser.

The CARS measurement rate varies with the type of CARS, and the laser pulse frequency used. At least one type of CARS can be used for continuous measurement. This requires a continuous-wave laser instead of a pulsed laser.

Whatever type of laser is used would definitely require an active cooling system, as very high power would be used.

Finally, we consider the placement and distribution of the system. The laser would be inside of the drone in a cooled area. For measuring wide areas of flow, a rotating platform would enable one CARS set-up to suffice. Or, alternatively, more than one clear window could be installed, and the emerging CARS beam re-directed through any of these temperature-resistant quartz windows. (Fig. 1)

CARS has several advantages that make it a good sensor for the drone. For instance, CARS will perform a few types of measurements at once, is generally non-intrusive, and the beam is not damaged by intensive heat. It is possible that CARS need not

have any apparatus to reflect the beam back from the medium it measures. This is due to the fact that the molecules in the medium, themselves, generate a laser-like beam.

The limitations of the CARS technique depends on which type of CARS is used. Some types work well in high pressure, turbulent flow, while others will not work under those same conditions. Most of the major limitations of CARS are a result of pressure gradient problems (the beam is refracted by pressure gradients, resulting in "beam steering" problems).

CARS will satisfy the needs and specifications of the Propulsion and Thermal Management groups. For example, in the air flow boundary layer outside of the drone, refraction and reflection ("beam steering") could possibly be used to our advantage. This is because the return beam is reflected/refracted back exactly in the same path. CARS spectra, and some geometry, can give us temperature and boundary layer data.

CARS can also measure flow constituents in the combustor nozzle, the mixing rate and turbulence of the fuel, and the concentration of elements downstream and upstream of ignition.

The most important aspect of CARS is the Raman effect. Laser light has a single frequency and phase quality. When light of a particular frequency hits a molecule, it emits a laser-like beam with the same qualities of the original beam, except that the emitted light is shifted by a frequency that is unique to that particular molecule or atom. This phenomenon is known as the Raman effect.

When this light hits another molecule of the same type, the probability of the molecule emitting a Raman shifted beam, originally low, greatly increases. The effect is amplified as the beam traverses through a sample of these molecules.

The beam is returned either by a reflecting apparatus at the other end, or by some technique that directs the beam back towards the source. The intensity, phase, and rotational direction of the beam and its spectrum gives information regarding temperature, concentration, and pressure of the molecules hit by the laser. Most of this information is determined by comparing the beam spectrum

to some theoretical or reference spectrum. Velocity is measured by noting the Doppler shift in the returning beam frequency.

Coherent Anti-Stokes Raman Spectroscopy, or CARS, is a laser spectroscopy technique. Spectroscopy is the study of spectra obtained from a spectroscope. A spectrocope is an apparatus that takes incoming light and by using a prism or diffraction grating forms a spectrum by separating the various wavelengths of the light into bands of varying intensity. The wavelength of a particular band can be determined from calculations using the position where the band occurs in the spectrum. How well these bands are distinguished from one another determines the resolution of the spectrum.

In CARS, two or more lasers are combined using a method called Optical Wave-Mixing to generate a single laser beam. This beam has a frequency that molecules in a media will resonate when hit. The enhanced beam that results from the molecule is the CARS beam or signal. This resonant response is the result of the Raman effect discussed earlier. Spectral analysis of the returning CARS signal can reveal information about the temperature, species concentration, pressure, and velocity of the molecules that it originates from.

The two or more beams that are optically wave-mixed are subject to certain requirements. For example, in two-laser CARS one laser is chosen to be the "pump" laser. The other laser is known as the "Stokes" laser because its frequency is shifted in the "red" direction of the electromagnetic spectrum with respect to the pump laser. The Stokes frequency is not fixed, and can take on different values.

The wave-mixed beam goes through the medium to be examined and results in a CARS beam and frequency. This is the "Anti-Stokes" beam, because its frequency is twice the pump frequency less the Stokes frequency. It is shifted towards the blue end of the electromagnetic spectrum with respect to the pump beam.

There are two types of Stokes lasers used in CARS methods: narrowband and broadband. These two ways of generating the Stokes frequency separates CARS into two groups which are named

according to the laser used. Narrowband (also known as "scanning") CARS builds the CARS spectra piece by piece by "tuning" the laser to a small range of Stokes frequencies, taking a measurement for each different frequency. This type of CARS is generally restricted to steady-state flow.

Broadband CARS, in contrast, will generate a complete spectrum for a given range of the Stokes frequency in one measurement. While a narrowband laser will output only a very narrow range of frequencies, a broadband laser outputs a wide range of frequencies. This type of CARS is necessary when measuring "randomly time-varying flows", since the sample could change from one point in time to the next.

Both scanning and broadband CARS usually examine only one species in a sample at a given time. There is a method that is capable of measuring all of the major constituents in a flow simultaneously. It is called Dual Broadband CARS. This method seems to hold the most promise to fulfill the sensor requirements for the hypersonic drone.

Dual Broadband CARS is one of a group of CARS techniques that utilize more than one pump and/or Stokes lasers to create the CARS beam. These are multi-frequency (multi-color) methods, since each laser operates at its own frequency. This method also contains the most potential for high pressure measurements which are expected for the combustor of the drone.

Alan C. Eckbreth and Torger J. Anderson, of United Technologies Research Center developed Dual Broadband CARS. "The technique employs two independent broadband Stokes sources in combination with a pump laser. In addition to the two-color wave-mixing processes between the pump and Stokes lasers, spectrally resolved CARS is produced in a three-color process from species whose Raman resonances correspond to the frequency difference of the two broadband sources. CARS is thus derived from a large number of species simultaneously removing the nominal limitations of CARS to interrogate only one constituent at a time." (Ref. 4)

For the Flight Systems Group purposes, the process of two and three color wave mixing is not so important as is the fact that two

broadband Stokes sources are used with a pump laser. The result is the capability to measure more than one species in a sample at a time.

In the article "Multi-Color CARS for Simultaneous Measurements of Multiple Combustion Species", Eckbreth and Anderson outline three other multi-color techniques as well as rotational/vibrational CARS methods. They are Dual Broadband, Dual Stokes, Dual Pump, Dual Pump-Stokes CARS, Pure Rotational and Combined Rotational/vibrational CARS .

Dual Stokes and Dual Pump CARS are used primarily for measuring two flow constituents at once. Measuring three or more are theoretically possible, but the application is too complicated to be practical. Both of these approaches result in simpler CARS signal detection schemes.

Dual Pump-Stokes CARS is interesting because the Stokes bandwidth can be made very narrow. In hydrogen air combustion, this method can then "track the appearance of H2O product in the reaction". This means that it could keep track of how much fuel is burned in the drones' scramjets.

Pure Rotational CARS is known for its high accuracy in measuring temperatures below 1000 K, even at high pressures. This method is difficult to apply. It uses the rotational approach on Dual Broadband CARS, making it simpler to implement. The advantages of this is the elimination of a Stokes laser, no calibration for the pump laser, and the pump frequency can be arbitrarily chosen for maximum power output.

Combined Vibrational/Rotational CARS combines Vibrational CARS with Rotational CARS. The result is a method that will measure two constituents at once over a very wide range of temperatures.

After considering the assets of all the CARS techniques, Dual Broadband CARS looks like the most promising as a sensor for the hypersonic drone. The major drawback is that there will be a loss of signal intensity in the CARS beam as compared to "regular" CARS. "Due to the increase of the CARS signal with increasing pressure, Dual Broadband CARS should be capable of single pulse

measurements of the major constituents at elevated pressures typical of gas turbines, internal combustion engines, and burning propellants. Furthermore, in Dual Broadband CARS, a beneficial spectral averaging may occur resulting in improved single pulse spectral quality". It is also noted that "dual Broadband CARS may be restricted, particularly for dynamic measurements, to elevated pressure combustion applications. Signal decrease accompanying broadband sources is compensated by ...scaling... with density". (Ref. 5,6)

This suggests that the use of Dual Broadband CARS in the high pressure scramjet engines to monitor the temperature, velocity, and species concentration of the flow there. A remote sensing system is possible for measuring velocity, pressure, and temperature outside of the drone as well.

To summarize, several CARS diagrams have been included. One of these is a "typical" CARS system, and also a configuration for measuring the after-burn of jet engine exhausts. After primarily examining the needs of the Propulsion Group , Dual Broadband CARS was selected as the method most capable of fulfilling them.

CARS Supporting Optics System

Having decided upon which type of CARS to implement, the manner which this was to be done remained to be developed. The following optics arrangement was designed to make the most of the CARS laser spectroscopy system as applied in the scramjet combustor. (Fig 2.)

The first is a result of our desire to check flow patterns in the scramjet in several areas. The optics arrangement is capable of achieving this goal because it uses the idea of one CARS system directed out of many windows.

The second way the optics arrangement optimizes the CARS system is by making the most of the available laser power coming from the optically wave-mixed CARS beam. This beam is split up between these windows in terms of fractions of the original beam pulse(s), as opposed to dividing a single pulse of the beam between all of the windows simultaneously.

The third way is that the CARS system is physically connected to a single, outer structure. This minimizes the effect of the aircraft's vibrations on the data , since all of the components of the optics system will vibrate relative to the drone and not each other. Further, the system may operate at such high speeds (picosecond pulses, for example) that , in comparison, any aircraft-related vibration would be insignificant. More precisely, if pulses are generated fast enough, data could possibly be gathered between one vibration and the next.

Thus, we hope to achieve a system capable of mapping at least part of the scramjet combustor flow, with a minimum amount of power loss, and in the most accurate way possible.

The way the CARS supporting optics system (CARS S.O.S.) operates is rather complicated. The CARS beam is generated in a separate system that is housed inside the main structure of the CARS S.O.S. As this beam comes out of the generating system, it goes through an aperture (marked "A" in the figure) and into the Supporting Optics System. As it travels horizontally into the system, the beam is directed to the first rotating shaft beam

splitter (marked "C") by a totally reflecting mirror ("B"). On this shaft, and on the second , tilted axis shaft below it, are disks which both allow the transmission and reflection of the beam. These disks are designed such that the beam will reflect off each one , in succession, for a predetermined pulse length, L. This pulse length is determined by the amount of reflecting disk that is cut away in the disks between it and the laser aperture. For a cut away length of circumference, d , assuming the laser beam traces this circumference, a pulse will be generated of length,

$$L = (c * d)/(Pi * r * f)$$

where:

r= distance of beam from disk's center

c= the speed of light in a vacuum

f= the frequency of rotation of the shaft about its axis.

Note that the pulse length is dependent on the distance of the beam from the center of disk and not necessarily on the radius of the disk. The radius of the disk only determines the maximum r. This makes the optical design quite a tricky geometry problem, since the radius of a disk depends on the position of the disk on its shaft relative to the incoming beam, the horizontal spacing of the windows, and the amount of room between the horizontal and tilted axis rotating shafts. Thus, the pulse length may be changed by change in axis frequency, but the other parameters are fixed by geometrical requirements.

Once the CARS beam is split into a pulse by the horizontal shaft arrangement of disks, the pulse travels to its reflecting horizontal disk which directs it to the appropriate second, tilted axis shaft disk. These tilted axis shaft disks, also, alternately reflect and pass the beam pulse -- only these reflect the pulse down through a collimating lens (of 300 mm in focal length) and through one of the temperature - resistant quartz windows into the scramjet combustor. There, a CARS signal is generated by the specific,excited molecules, and travels directly up to the tilted shaft disk which first reflected it down. As soon as the pulse is over and the CARS laser is blocked from the reflecting horizontal

disk's view, the tilted shaft disk allows the beam to travel straight up to an optical detector.

If the pulse is long, since the CARS stimulated molecule beam is approximately instantaneously generated, an additional detector may be placed around the aperture of the original beam to collect any overlapping signal that occurs during the pulse generation. Any overlap could then be routed to the appropriate spectral analysis channel. It is possible to use this same system with an entirely reflecting second shaft and one photodetector at the CARS beam aperture . However, having separate photodetectors for each pulse has the possible advantage of easier signal separation at high pulse frequencies and faster electronic processing of the almost continuous wave of CARS returning pulses.

Note that only one pulse will be reflected up from the scramjet at any moment, in either case. Hence, one spectrograph and computer, operating continuously, could receive all of the data. It may, however, take more than one computer to store ,analyze, and process the information at the speed required.

Note, also, that other means could have been used to make the division of the CARS beam between the windows much simpler, but with a considerable power loss increase. Beam splitters which partially reflect and transmit simultaneously, could have been used to split the original beam. But such beam splitters, used twice in succession, would have reduced the outgoing beam intensity to 25% of the original CARS beam.

However, in return for conserving power and the other optimization inherent in its design, the proposed Supporting Optics System has its own particular drawbacks. First, the size of the optics system in very much dependent on the spacing of the windows and number of windows used. A fixed amount of space is necessary to contain the spinning disks and to make sure that the two spinning shafts do not collide with one another.

Also, more power is consumed than in a stationary optics set-up, since power must be supplied to the shaft rotary motors. Further, the very fast rotation of the shafts would generate heat, which would add to the overall problem of cooling the CARS.

Lastly, such a system would be more prone to mechanical failure than a stationary system using half-reflecting/ half-transmitting mirrors.

In summary, however, even with these drawbacks (increased power consumption, greater cooling requirements, and possible mechanical failure), the proposed optics arrangement for the application of CARS in the drone's scramjet combustor should be able fulfill the requirements it was designed to to a satisfactory degree. It will allow the measurement of combustor flow characteristics in several different areas in the combustor, provide the maximum possible power to these measurements (and, hence, the more accurate results), and minimize the effects of any aircraft-related vibration.

The next two devices described are different than the other sensors. Both use novel pulse-laser techniques that were designed conceptually from scratch. Thus, there is considerable ambiguity as to the actual feasibility of the devices since neither the dollar cost nor any available substitutes have been considered. Design is strictly conceptual that can be used as a springboard for further research.

An Optical Pressure Sensor

This device (shown in Fig. 3) uses a Michelson-type interferometric technique to measure the displacement of a material, such as quartz or graphite, under the load of substantial pressure. The sensor does so by an arrangement of thin aluminum mirrors of proper reflectivities embedded in the bulk material through which a laser beam is launched. Fringes are formed as pressure displaces the upper mirror downward towards the laser source. These fringes are then counted and the measure of bulk material displacement under the external load is then calculated. Through accurate calibration or theory, the displacement of the mirror, which moves in parallel with the bulk material it is embedded in, is related to the pressure the bulk is exposed to. Therefore such a device is useful in measuring pressures exceeding ordinary pressure sensors, pressure as high as the bulk material can withstand while still retaining its elastic properties. Outside dynamic pressure anywhere on the surface of a hypersonic airplane can be measured with such a device. The data can be sampled at rates above 100 KHz (limited only by the propagation delays of the associated electronics).

This device suffers from noise that results from all mirrors being displaced simultaneously from pressure. One way of correcting this noise-like effect is by inserting a soft buffer layer between the upper mirror and the lower part of the device.

Multiple Shock-Wave Sensor

The operation of the device is dependent of the shock wave creating a boundary layer. The differing physical properties of abrupt pressure and temperature changes across the boundary layer leading to a spatial discontinuity in the index of refraction. A laser beam can be reflected off of the shock wave because of the index discontinuity.

Due to the high hypersonic speeds, the shock waves will "hug" the plane, being nearly horizontal with respect to the surface. A pulsed laser beam is launched upward at right angles to the surface of the drone into the air (as shown in Fig. 4). The laser beam will be partially reflected upon each impact with each shock wave that it encounters. By detecting the back-scattered beam, its intensity-time profile can be used to predict the locations of the shock waves away from the plane. Knowledge of the appropriate permeability coefficient is needed in the calculation of the shock wave distance. This can be easily obtained with a simple in-flight measurement.

Noise from various sources such as the beam oscillating between two shock waves and beam-steering may be mis-interpreted for a shock wave. The high temperatures and the near-plasma environment outside make the device difficult to design. It is difficult to single out only the intensity peaks produced by scattering the beam from a shock wave front, effectively rejecting noise contributions. Beam steering effect can lead to significant errors in the measurements due to the turbulent environment expected.

The velocity of the drone can be conceivably predicted from the angle the shock wave makes with the fuselage. By scanning the shock wave with the arrangement described above, such an angle can be computed. Combined with the altitude of the drone, and other basic parameters, the velocity can be predicted.

Fiber Optic Pressure Sensor

Fiber optics are currently being used in the measurement of many quantities, such as temperature, acceleration, velocity, electric and/or magnetic fields, fluid levels and acoustic waves. In the measurement of these parameters, the fiber plays either an active or passive role; active when the fiber itself is the sensing element and passive when the fiber simply transmits information from the sensing element. The device considered here is a pressure sensor in which the fiber takes an active role in the measurement.

The sensor is a flattened hollow cylinder about which is wrapped an optical fiber. At one end of the fiber is a source, an AlGaAs LED with a power consumption of the order of milliwatts. At the other end is a detector, a Si PIN photodiode. the pressure differential between the inside of the cylindrical cavity and the outside of it causes the radius of curvature of the flattened section to decrease from infinity to some finite value. As this radius decreases further, there is a corresponding approximately exponential increases in the attenuation of the intensity of light that reaches the detector. The light attenuation at the curved ends is constant and is taken into account when calibrating the device. The amount of light reaching the detector is therefore a function of the pressure difference between the inside and outside of the cavity. The outside of the cavity could be another cavity at a reference pressure, or a cavity in which the pressure can be varied to increase the range of measurement of the device. See figure 5 for a picture of the fiber optic pressure sensor. (ref. 12)

This sensor can be adapted to a high temperature environment by constructing the cylindrical cavity from titanium and threading the approximately 100 micron diameter fibers through tubes welded to the outside of the cylinder. Water or the liquid hydrogen on board would be pumped through these tubes to keep the fibers at a relatively constant temperature. In this way the device can be located near the surface of the inside walls of the engine or the nose of the craft for a flush air data system to optimize the pressure propagation delay time. The source and detector would be located

away from the high temperatures, fibers of course being used to transmit light to the sensor. In this way, real time measurement of pressures on the surface of the aircraft or inside the engine could be made.

The theoretical sensitivity of this device is given by the following equation:

$$S=(1/I)(dI/dP)= S_{opt}\, a^3 (1- \mu^2/eh^3)\, \beta^2 \, (\beta + 12/\pi)/(\beta + \pi)$$

where I=intensity reaching detector

p=pressure

S_{opt} = normalized optical sensitivity for a constant length L of fiber bent to radius R. (ref. 7)

This device will use single-mode fibers rather than multi-mode fibers which were used in the Wright experiment (ref. 20) because of the vibrations of the multi-mode fibers encountered during flight would effect the electromagnetic power propagation and thus pressure measurement. Two advantages are gained, however, with the use of single-mode fibers. First the sensitivity, S_{opt} is an order of magnitude greater, 20 compared to 2. Secondly, with single mode-fibers is proportional to the number of half turns the fiber makes around the flattened cylinder. so that the use of titanium, with two orders of magnitude greater Young's modulus than the epoxy resin of the Wright experiment, causing a two orders of magnitude decrease in the sensitivity can be compensated for with increased half turns of the fiber. Since is already an order of magnitude larger, two extra half turns brings the sensitivity of this device into the range of the Wright experiment, S=8*/bar (1 bar = 100 kPa).

The dynamic range of the epoxy resin cylinder was tested for 200 kPa. This range could, of course, be extended with the use of the titanium cylinder.

MOSFET Hydrogen Concentration Senducer

Hydrogen flow concentration inside the combustor of the SCRAMJET is a very important parameter to be measured because it is related to the rate of combustion, the energy consumption, and the engine efficiency. The sensors used in the are relatively big and intrusive. The MOSFET hydrogen concentration senducer (ref. 3) has many advantages such as small size, low power consumption, high sensitivity, fast response, and relatively non-intrusiveness.

A senducer is a sensor and a transducer combination which senses physical quantities and then converts them through chemical parameters into electrical signals. The acronym, MOSFET, stands for Metal-Oxide-Semiconductor Field-Effect Transistor. It is a four-terminal device as shown in Figure 6.

The operation of a MOSFET is controlled by a vertical action and a horizontal action. The gate-bulk potential difference V_{GB} sets up a capacitive effect which adjusts the amount of carriers (in our case, electrons) in the conducting channel. There will be carriers in the channel if, and only if, the gate-bulk potential is greater than, or equal to, the threshold voltage V_T. This is the vertical action. The horizontal action is controlled by the potential difference applied between the drain and the source V_{DS}. Current flows from the drain to the source if vertical action causes carriers to be present in the conducting channel. Depending on the value of V_{DS}, there are two regions of operation--the linear region and the saturated region. The linear region occurs if $V_{DS} \leq V_{GS} - V_T$ and the saturated region occurs if $V_{DS} \geq V_{GS} - V_T$. The drain current equations are given by:

$$I_D = \mu(W/L)C_{OX}\,[V_{DS}\,(V_{GS} - V_T) - V_{DS}^2/2] \quad \text{linear region}$$

$$I_D = (1/2)(W/L)C_{OX}\,(V_{GS} - V_T)2 \quad \text{saturated region}$$

Where μ = mobility of electrons

W/L = gate width / gate length

C_{OX} = permeability / thickness of SiO_2

Notice that the current in the linear region is less than the current in the saturated region and thus a MOSFET operating in the linear region consumes less power. Also, the fact that the current

in the linear region depends on V_{DS} makes the linear region more flexible for out design.

In our design, the gate material used is palladium (Pd) instead of polysilicon used in microelectronic devices. Palladium, when in contact with hydrogen flow, acts as a catalyst for H_2 ionization t give $2H^+$. This H^+ diffuses into the thin SiO_2 layer to give a charge difference ΔQ. A ΔQ changes the threshold voltage V_T. If at $\Delta Q = 0$, $V_T = V_{TO}$, then $V_T = V_{TO} - V_T = \Delta Q/C_{OX}$. Now, if we substitute $V_T = V_{TO} - \Delta Q/C_{OX}$ into the linear region I_D equation, we have:

$$I_D = \mu(W/L)C_{OX}[V_{DS}\Delta Q/C_{OX} + V_{DS}(V_{GS} - V_{TO} - V_{DS}/2)]$$

Notice that for a particular V_{DS}, I_D is linearly related to ΔQ with a slope equal to $\mu(W/L)V_{DS}$ and the plot is shown in Figure 7.

The senducers can be embedded in the walls of the combustor. The advantage is that although the sensor cannot stand high temperatures, we need not worry about heating effects because the combustor walls will be actively cooled regardless of the presence of the MOSFET senducers.

Note that we can use platinum instead of palladium as the gate material. However, since they act the same for our purpose and that platinum is much more expensive than palladium, palladium is obviously a better choice.

The senducer has the advantage of small size--approximately 10^{-15} m^3, low power consumption on the order of 0.1mW, fast response time on the order of a few nanoseconds, and high sensitivity to H_2 concentration variation because molecular relaxation takes only a fraction of a nanosecond.

To ensure accuracy, each senducer should be calibrated individually because of the doping variations and difference in threshold voltages. However, if all the senducers are made on the same silicon wafer, this calibration problem can be greatly simplified.

Sapphire Diaphragm for Pressure and Temperature Measurement

A sapphire diaphragm approximately an inch in diameter is placed flush with the aircraft's skin. Pressure measurement with this device is based on the photoelastic effect. Light from an LED source is linearly polarized 45 degrees relative to the surface of the diaphragm and passed across the diameter of it. As pressure is applied to the surface, the linearly polarized light becomes elliptically polarized due to the photo-elastic effect. A second polarizer , again placed at 45 degrees relative to the surface, filters out the elliptically polarized light at the opposite end of the diaphragm. The degree to which the linearly polarized light is attenuated is thus a function of pressure. The accuracy of this device can be increased by using two LED sources and alternately polarizing them +45 degrees and -45 degrees relative to the surface, therefore, obtaining four outputs. The resulting four outputs can then be averaged. Temperature measurement with this device is based on blackbody radiation. As the temperature of a substance increases the amount of radiation emitted increases and the wavelength at which it is emitted decreases. The relation that describes this phenomena is Planck's equation. (ref. 17,18)

Since sapphire is not an ideal blackbody, the above relation must be multiplied by the emissivity of sapphire, 0.15, which is an indication of the degree to which it approaches the ideal blackbody.

Sapphire was the material of choice for several reasons. First and foremost is its high temperature properties. Its melting point is 2030 degrees Celsius with its maximum normal use temperature at 1950 degrees Celsius. It is unaffected by oxidizing and reducing atmospheres at elevated temperatures. Its crystalline structure, trigonal, is identical to that of alpha-quartz which was used in the photoelastic experiments. The tested range of quartz was 10 MPa with a 0.07% accuracy. There is no reason to believe that sapphire would be any less. It is a low power consumption device; the LED's are 100mW sources. And finally, since the diaphragm is flush with

the surface there is no need to wait for the pressure wave to propagate down a tube to the pressure sensor located inside the aircraft.

The Dual-Laser-Beam Skin Friction Interferometer

The skin friction sensor, using a non-intrusive double-laser-beam oil viscosity balance technique, was developed by Monson and Higuchi (ref. 14). Two out-of-phase laser beams, reflected from an oil film, gives alternative constructive and destructive interferences. The number of fringes, and thus the rate of change of the oil film over a given time span, can be precisely computed in terms of the known laser wavelength. The skin friction is related to the rate of change of thickness of the flowing oil film. The oil film used is silicon oil since it has a wide range of viscosity, a relative insensitiveness to temperature, a low surface tension, and a very low vapor pressure. The following paragraphs give a brief outline of its operation and characteristics.

Figure 8 shows the configuration of this device. A He-Ne laser beam is generated. The laser beam is expanded by a telescope, linearly polarized, and passed through a neutral density filter to reduce the beam power level to a value that avoids excessive oil heating. The beam is then split into two, using a interferometric flat. One of the beams is rotated by 90^{o} by the half-wave retardation plate, and both beams are focused on the oil film. The reflected beams are separated by a polarization beam splitter and focused on a photodiode after passing them through polarizers and narrow band interference filters at the detectors for additional noise reductions. The interference patterns are then analyzed to give skin friction.

This device is very accurate and inexpensive. It can be used in three-dimensional laminar or turbulent flow. It is only slightly intrusive and can be used at various points on the combustor surface.

The only problem occurs when there are dust particles in the oil. A dust particle exactly at a beam focal point could cause erratic interferometer behavior. A large dust particle just ahead of a beam focal point could locally perturb either the oil, or the oil flow,

enough to influence the skin friction measurement, but could not be detected on the interferometer record.

Conclusion

This ends the report for the Flight Systems Group. The sensor system design was approached with an integration with the Propulsion and Thermal Management groups. The challenging environment and the variety of needed measurements called for a equally large variety of sensors from differing backgrounds and applications. These innovative designs should provide an interesting testbed for the sensor systems on the hypersonic drone.

Bibliography

1. Barlow, A. and Payne, D., "The Stress-Optic Effect in Optical Fibers", IEEE Journal of Quantum Electronics, Vol. QE-19, 1983, p. 834.

2. Beheim, G. and Anthan, D.J., "Fiber-Optic Photoelastic Pressure Sensor with Fiber-Loss Compensation", Optical Society of America Vol. 12, p. 220, 1987.

3. D'Amico, A., "Chemical Senducers", Optical Fiber Sensors, A. N. Chester, et. al. ed., Martinus Nijhoff : Dordrecht, 1987.

4. Eckbreth, Alan C. and Anderson, Torger J., "Multi-Color CARS for Simultaneous Measurements of Multiple Combustion Species ", Laser Applications to Chemical Dynamics, Vol. 72, pp.34-41, SPIE: San Diego, 1987.

5. Eckbreth, Alan C. and Anderson, Torger J., "Dual Broadband CARS for Simulataneous, Multiple Species Measurements", Applied Optics, Vol.24, No. 16, pp 2731-2736, 15 August 1985.

6. Eckbreth, Alan C. and Anderson, Torger J., "Dual Broadband USED CARS", Applied Optics, Vol. 25, No. 10, pp. 1534-1536, 15 May 1986.

7. Gambling, W.A., Matsumura, H., Ragdale, C.M., and Sammut, R.A., "Measurement of Radiation Loss in Curved Single-Mode Fibers", Microwaves, Optics, and Acoustics, Vol. 2, p. 134, 1978.

8. Gustafson, E.K., McDaniel, J.C., and Byer, R.L., "CARS Measurements of Velocity in a Supersonic Jet", IEEE Journal of Quantum Electronics, Vol. QE-17, No. 12, pp. 2258-2259, December 1981.

9. Harvey, Albert B., Fleming, James W., and Barnes, William T., Jr., "Applications of Nonlinear Raman Techniques", Laser Spectroscopy for Sensitive Detection, Vol. 286, SPIE: San Diego, 1981.

10. Hecht, Jeff, The Laser Guidebook, McGraw-Hill Book Company: New York, 1986.

11. Jastrzebski, Z., The Nature and Properties of Engineering Materials, John Wiley and Sons: New York, 1987.

12. Martens, G., "Measurement of Pressure by Photoelastic Effects", Sensors and Actuators, Vol. 6, p. 181, 1984.

13. Miller, J., Titanium: A Materials Survey, U.S. Government Printing Office: Washington, 1957.

14. Monson, D.J. and Higuchi, H., "Skin Friction Measurements by a New Non-Intrusive Double Laser-Beam Oil Viscosity Balance Technique", AIAA Journal, Vol. 19, pp. 739-44, 1981.

15. Olson, Dennies Lee, A Multiplexed Platinum Resistance Thermometer, UCLA Master's Thesis, 1979.

16. Price, R.B., Advanced Instrumentation for Aero Engine Components, Advisory Group for Aerospace Research and Development: Neuilly-Sur-Seine, France, 1986.

17. Tai, Shuichi, Kyuma, Kazuo, and Nunoshita, Masahiro, "Fiber-Optic Acceleration Sensor Based on the Photoelastic Effect", Applied Optics, Vol. 22, p. 1771, 1983.

18. Spillman, W.B., Jr., "Multimode Fiber-Optic Accelerometer Based on the Photoelastic Effect", Applied Optics, Vol. 21, p. 2653, 1982.

19. Stafsudd, Oscar M., Vice Chairman UCLA Electrical Engineering Department, 1988.

20. Wright, O.B., Largeau, D., "Fibre-Optic and Differential Pressure Sensor", Journal of Physics E, Vol. 20, p. 46-51, Jan 1987.

Coherent Anti-Stokes Raman Spectroscopy (CARS)

Schematic CARS Layout

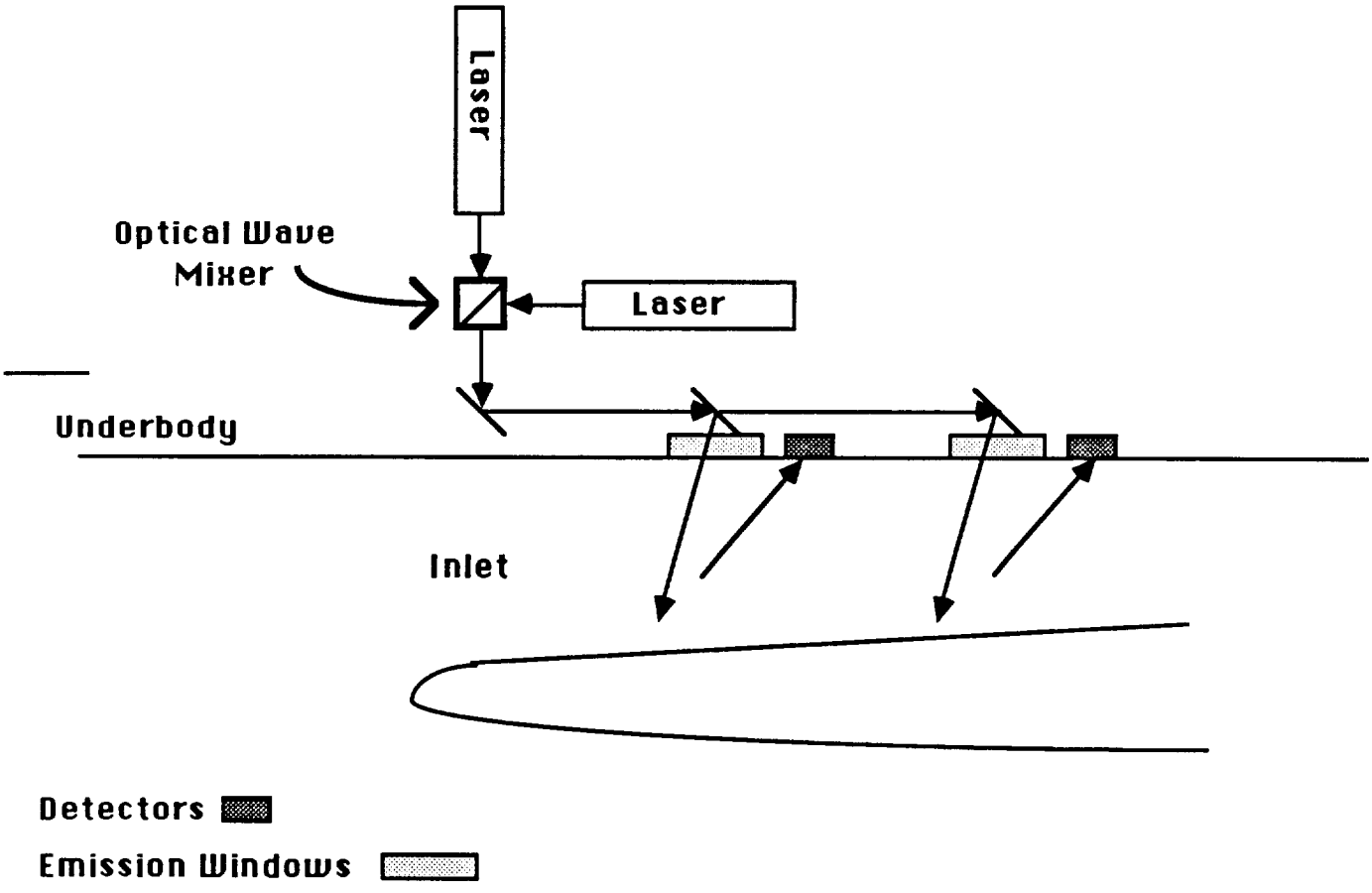

Figure 1

CARS Scanning Setup

Figure 2.

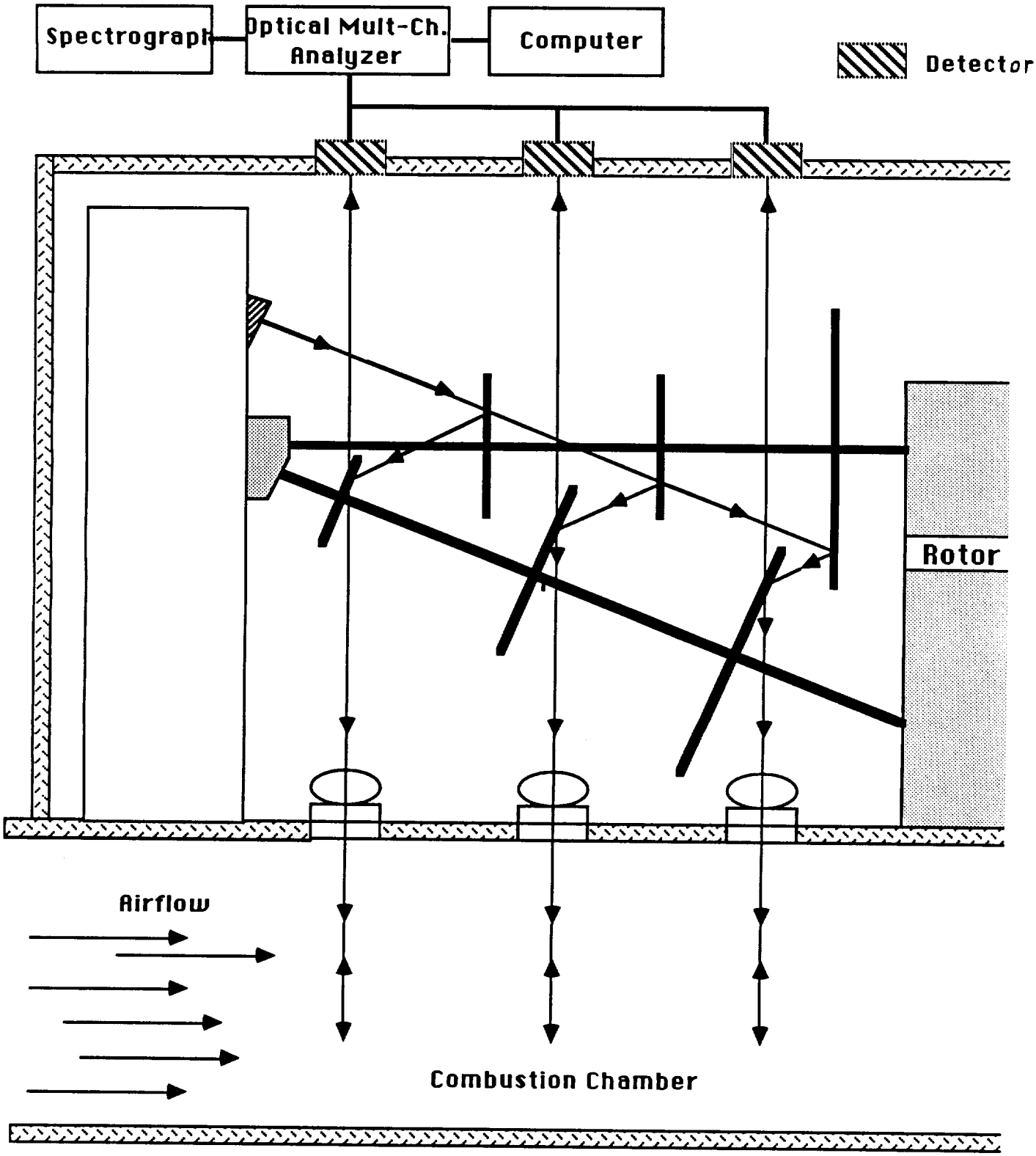

Interferometric Pressure Detector

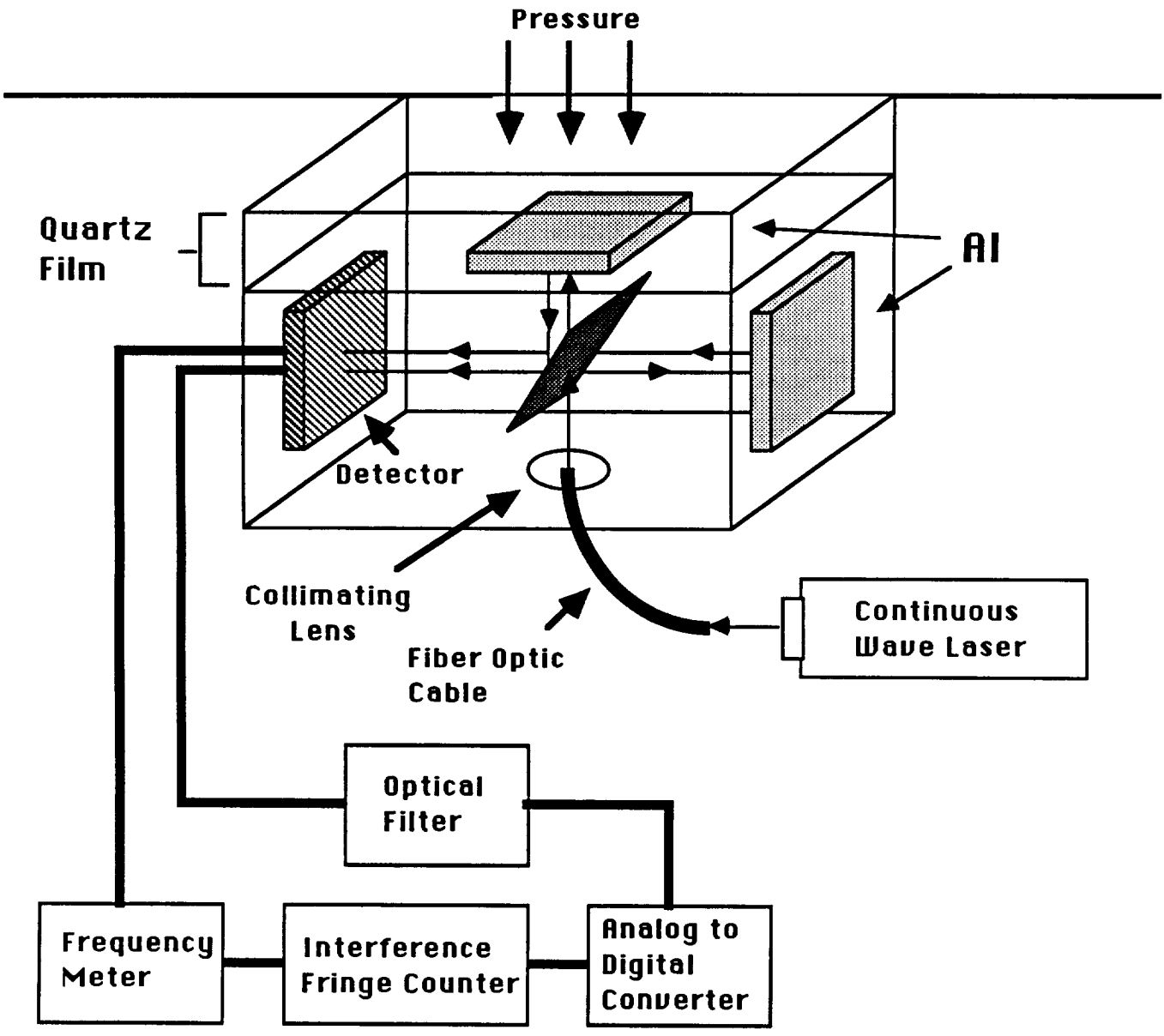

Figure 3

Multiple
Shock Wave Sensor

Figure 4

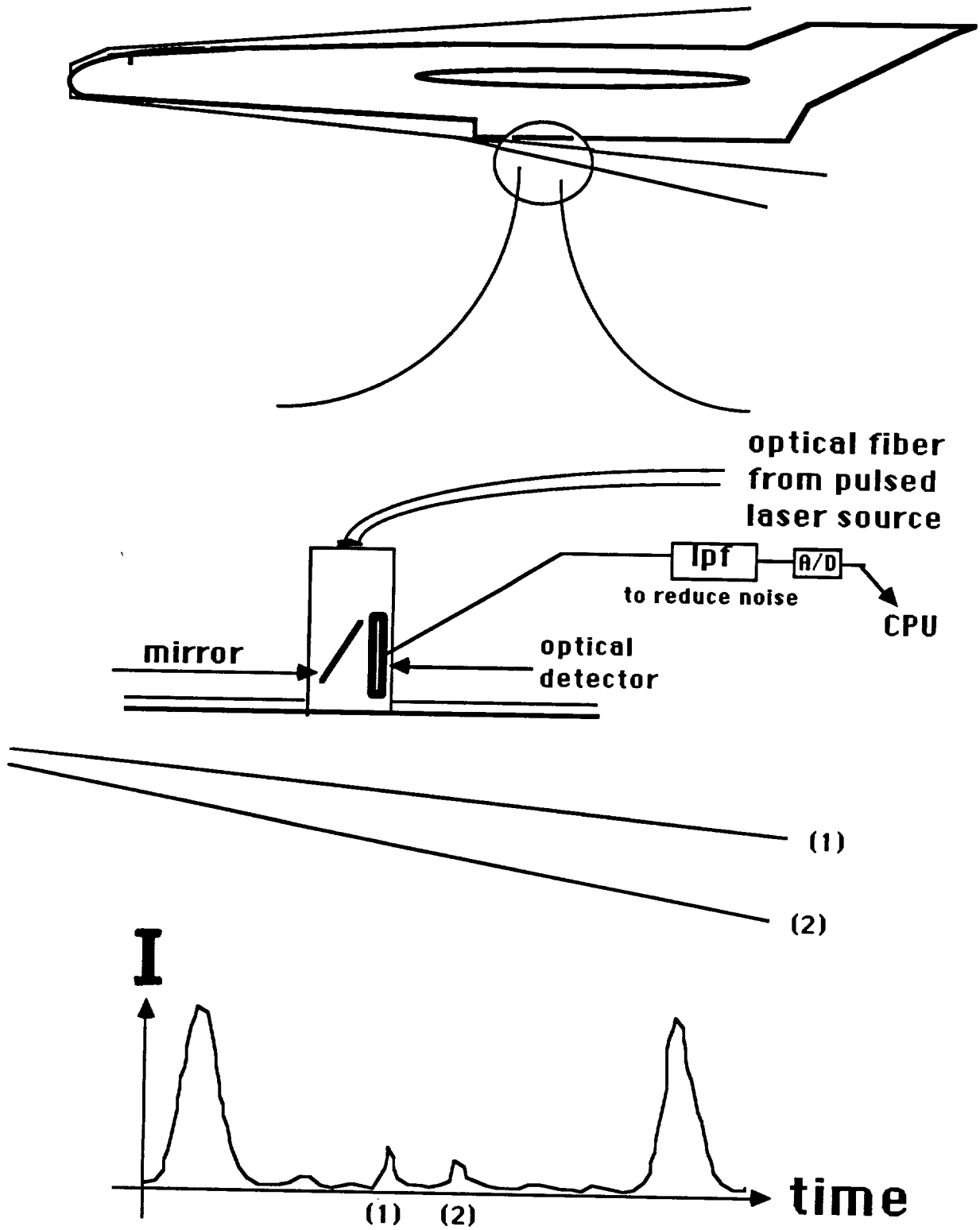

Optical Fiber Pressure Sensor

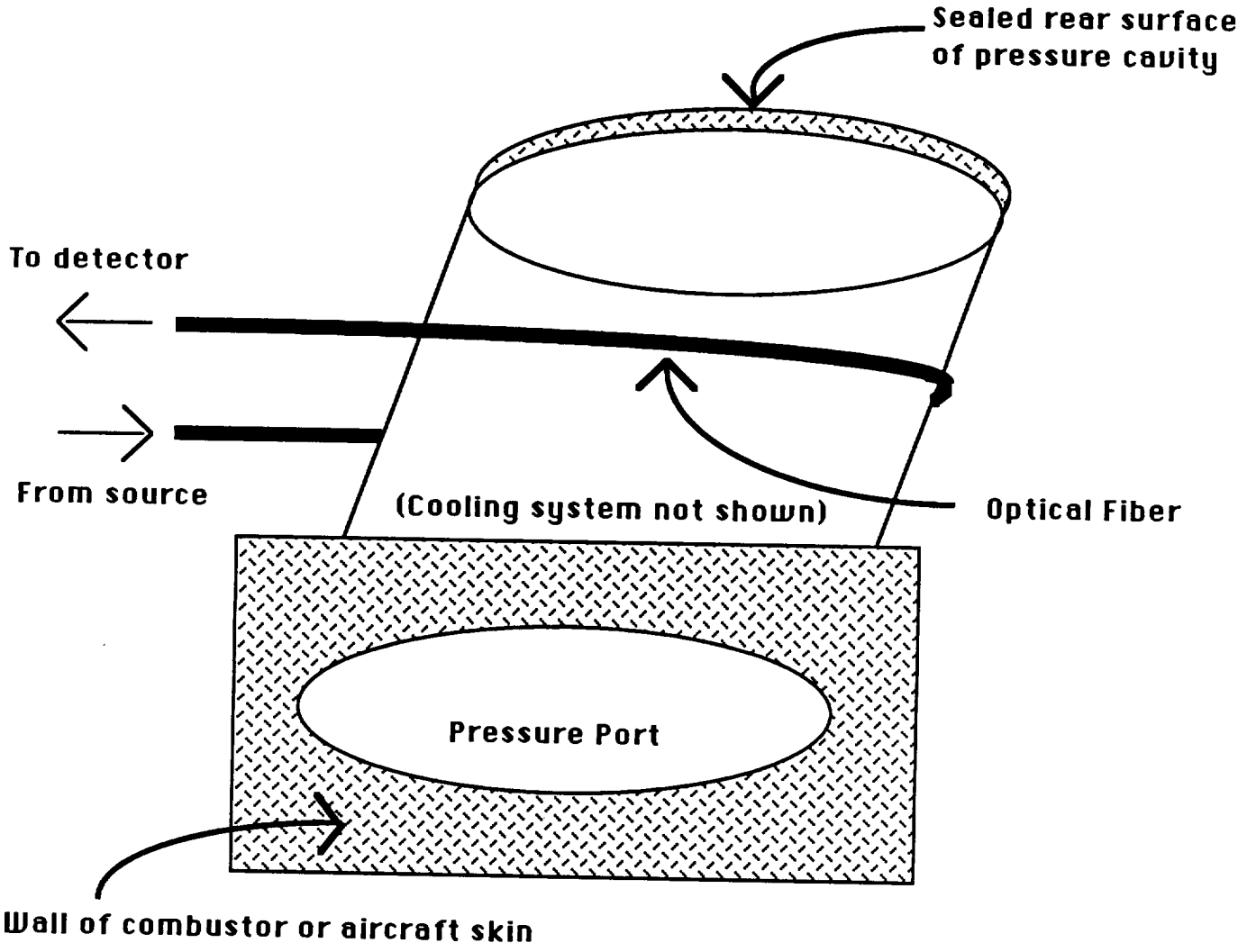

Figure 5

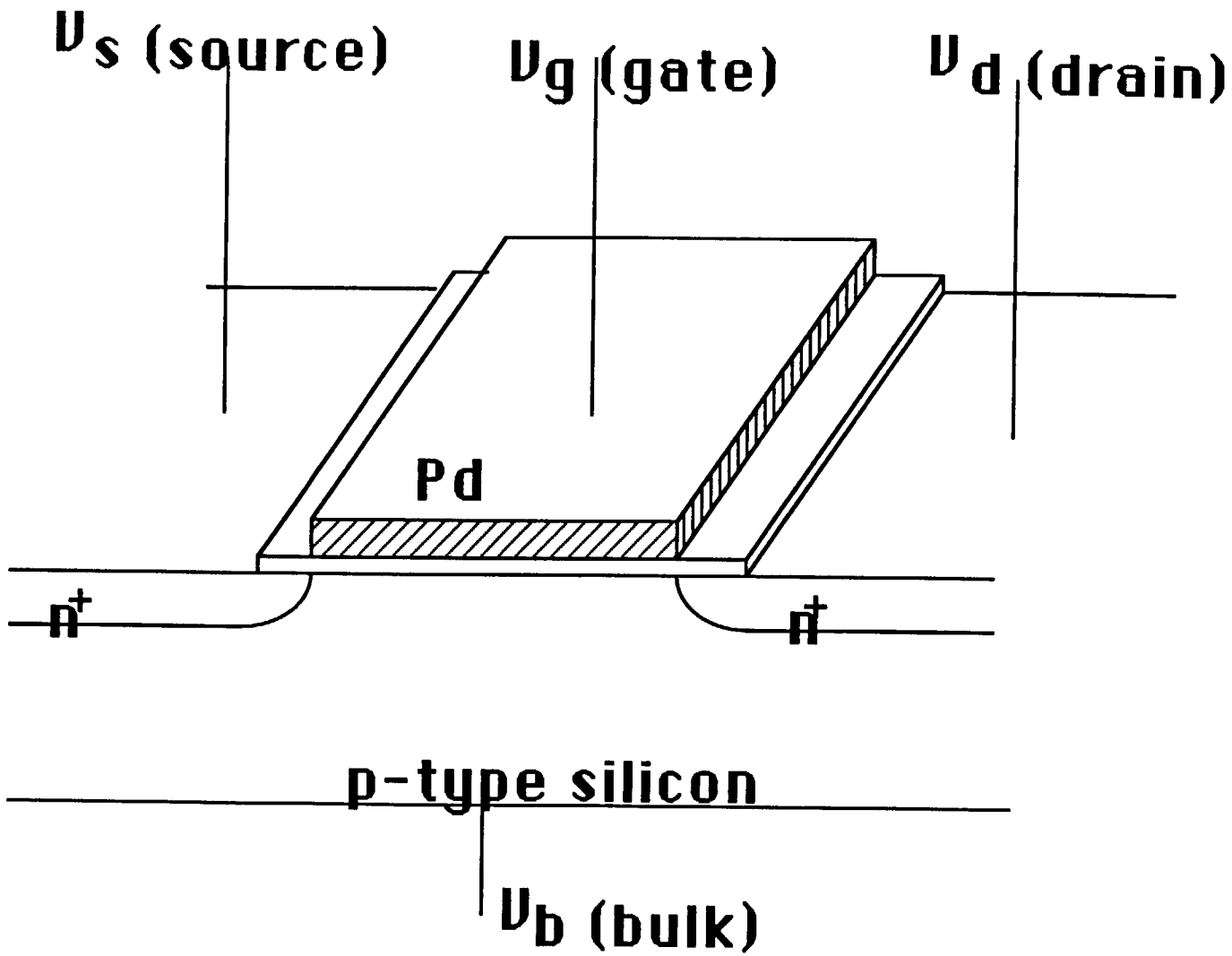

The structure of a MOSFET

Figure 6

Hydrogen MOSFET Characteristics

$$I = \mu (W / L) [(V_{DS}^* \Delta Q) + V_{DS}^* C_{OX}(V_{GS} - V_{TO} - V_{DS}) / 2]$$

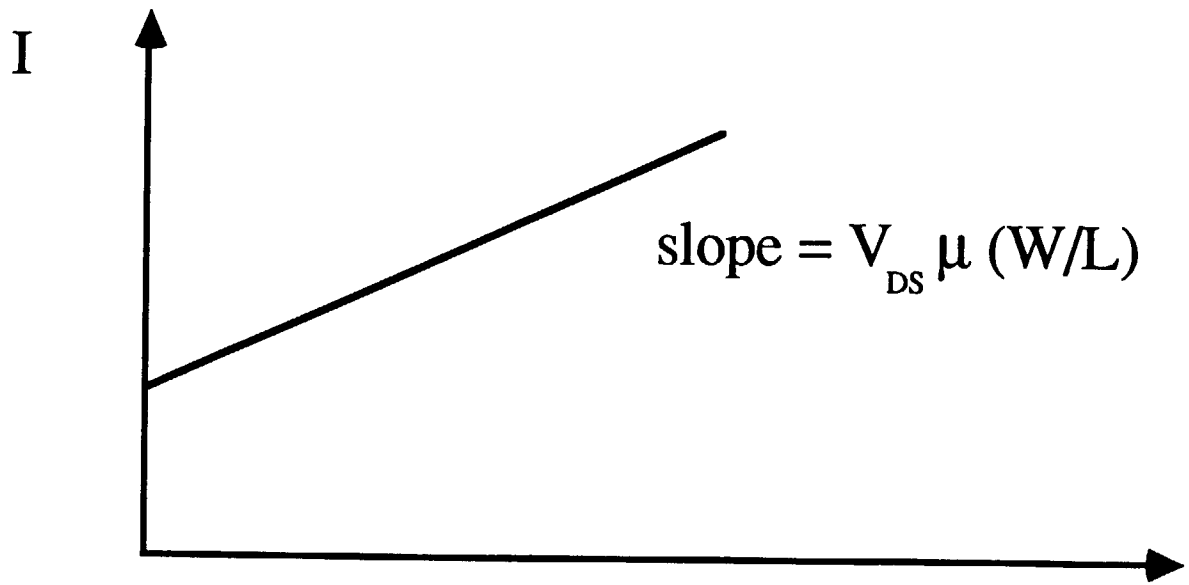

Figure 7

Dual-Laser-Beam Skin Friction Interferometer

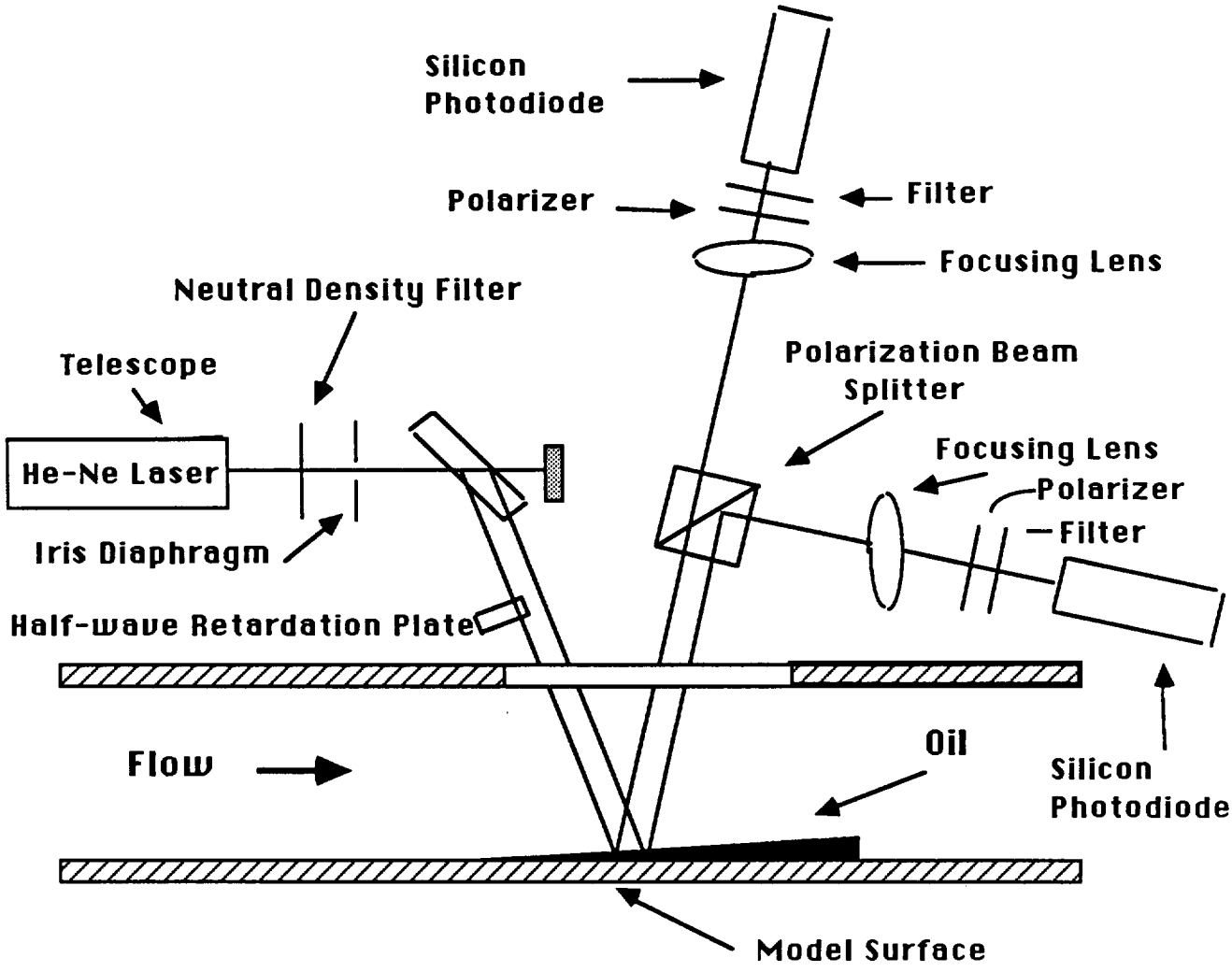

Figure 8